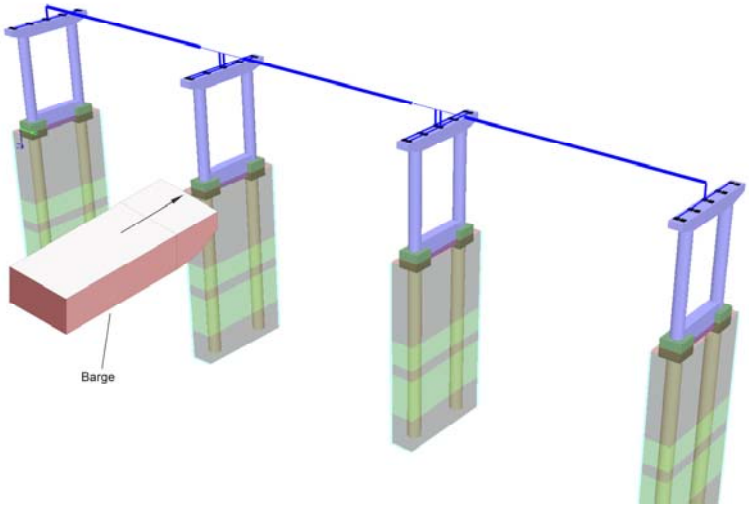

Development of FB-MultiPier Dynamic Vessel-Collision Analysis Models, Phase 2

July 2014

FINAL REPORT

BRIDGE SOFTWARE INSTITUTE

Sponsor:
Florida Department of Transportation (FDOT)

Project Manager:
Sam Fallaha, P.E.

Principal Investigator:
Jae H. Chung, Ph.D.

BSI Development Team:
Michael T. Davidson, Ph.D.
Clinton J. Monari
Henry Bollmann, P.E.
Anand Patil, E.I., M.S.

Address:
Bridge Software Institute (BSI)
Engineering School of Sustainable Infrastructure and Environment (ESSIE)
University of Florida (UF)
1949 Stadium Rd. Room 365
Gainesville FL 32611

Contract:
FDOT Contract No. BDV31-977-17
UF Project No. 00113885

DISCLAIMER

The opinions, findings, and conclusions expressed in this publication are those of the authors and not necessarily those of the State of Florida Department of Transportation. Utilization of FB-MultiPier and Coupled Vessel Impact Analysis (CVIA) is not recommended in conjunction with calculations of the Probability of Collapse (PC) and the Probability of Aberrancy (PA) terms in the current AASHTO LRFD. Within this context, PC term values (which could potentially be greater in value than those predicted using the current AASHTO formulation) and PA term values (which could be potentially be less in value than those predicted using the current AASHTO formulation) may be necessary in forming reasonable, overall estimates of Annual Frequency of Collapse (AF).

SI (MODERN METRIC) CONVERSION FACTORS (from FHWA)

APPROXIMATE CONVERSIONS TO SI UNITS

SYMBOL	WHEN YOU KNOW	MULTIPLY BY	TO FIND	SYMBOL
LENGTH				
in	inches	25.4	millimeters	mm
ft	feet	0.305	meters	m
yd	yards	0.914	meters	m
mi	miles	1.61	kilometers	km

SYMBOL	WHEN YOU KNOW	MULTIPLY BY	TO FIND	SYMBOL
AREA				
in^2	square inches	645.2	square millimeters	mm^2
ft^2	square feet	0.093	square meters	m^2
yd^2	square yard	0.836	square meters	m^2
mi^2	square miles	2.59	square kilometers	km^2

SYMBOL	WHEN YOU KNOW	MULTIPLY BY	TO FIND	SYMBOL
VOLUME				
fl oz	fluid ounces	29.57	milliliters	mL
ft^3	cubic feet	0.028	cubic meters	m^3
yd^3	cubic yards	0.765	cubic meters	m^3
NOTE: volumes greater than 1,000 L shall be shown in m^3				

SYMBOL	WHEN YOU KNOW	MULTIPLY BY	TO FIND	SYMBOL
MASS				
oz	ounces	28.35	grams	g
lb	pounds	0.454	kilograms	kg
T	short tons (2,000 lb)	0.907	megagrams (or "metric ton")	Mg (or "t")

SYMBOL	WHEN YOU KNOW	MULTIPLY BY	TO FIND	SYMBOL
TEMPERATURE (exact degrees)				
ºF	Fahrenheit	5 (F-32)/9 or (F-32)/1.8	Celsius	ºC

SYMBOL	WHEN YOU KNOW	MULTIPLY BY	TO FIND	SYMBOL
ILLUMINATION				
fc	foot-candles	10.76	lux	lx
fl	foot-Lamberts	3.426	candela/m^2	cd/m^2

SYMBOL	WHEN YOU KNOW	MULTIPLY BY	TO FIND	SYMBOL
FORCE and PRESSURE or STRESS				
lbf	pound force	4.45	newtons	N
kips	kips	4,448.22	newtons	N
lbf/in^2	pound force per square inch	6.89	kilopascals	kPa
ksi	kips per square inch	6,894.76	kilopascals	kPa
tsf	tons (short) per square foot	95.67	kilopascals	kPa
pcf	pound force per cubic foot	156.967	newtons per cubic meter	N/m^3

APPROXIMATE CONVERSIONS TO SI UNITS

SYMBOL	WHEN YOU KNOW	MULTIPLY BY	TO FIND	SYMBOL
		LENGTH		
mm	millimeters	0.039	inches	in
m	meters	3.28	feet	ft
m	meters	1.09	yards	yd
km	kilometers	0.621	miles	mi

SYMBOL	WHEN YOU KNOW	MULTIPLY BY	TO FIND	SYMBOL
		AREA		
mm^2	square millimeters	0.0016	square inches	in^2
m^2	square meters	10.764	square feet	ft^2
m^2	square meters	1.195	square yards	yd^2
ha	hectares	2.47	acres	ac
km^2	square kilometers	0.386	square miles	mi^2

SYMBOL	WHEN YOU KNOW	MULTIPLY BY	TO FIND	SYMBOL
		VOLUME		
mL	milliliters	0.034	fluid ounces	fl oz
L	liters	0.264	gallons	gal
m^3	cubic meters	35.314	cubic feet	ft^3
m^3	cubic meters	1.307	cubic yards	yd^3

SYMBOL	WHEN YOU KNOW	MULTIPLY BY	TO FIND	SYMBOL
		MASS		
g	grams	0.035	ounces	oz
kg	kilograms	2.202	pounds	lb
Mg (or "t")	megagrams (or "metric ton")	1.103	short tons (2,000 lb)	T

SYMBOL	WHEN YOU KNOW	MULTIPLY BY	TO FIND	SYMBOL
		TEMPERATURE (exact degrees)		
ºC	Celsius	1.8C+32	Fahrenheit	ºF

SYMBOL	WHEN YOU KNOW	MULTIPLY BY	TO FIND	SYMBOL
		ILLUMINATION		
lx	lux	0.0929	foot-candles	fc
cd/m^2	candela/m^2	0.2919	foot-Lamberts	fl

SYMBOL	WHEN YOU KNOW	MULTIPLY BY	TO FIND	SYMBOL
		FORCE and PRESSURE or STRESS		
N	newtons	0.225	pound force	lbf
N	newtons	0.000224809	kips	kips
kPa	kilopascals	0.145	pound force per square inch	lbf/in^2
kPa	kilopascals	0.000145	kips per square inch	ksi
kPa	kilopascals	0.000145038	kips per square inch	ksi
N/m^3	newtons per cubic meter	0.0104526	pound force per cubic foot	pcf

*SI is the symbol for International System of Units. Appropriate rounding should be made to comply with Section 4 of ASTM E380. (Revised March 2003)

1. Report No.	2. Government Accession No.	3. Recipient's Catalog No.
4. Title and Subtitle Development of FB-MultiPier Dynamic Vessel-Collision Analysis Models, Phase 2		5. Report Date July 2014 6. Performing Organization Code
7. Author(s) Chung, J. H., Davidson, M. T., Monari, C. J., Bollmann, H. T., and Patil, A.		8. Performing Organization Report No.
9. Performing Organization Name and Address Bridge Software Institute University of Florida 1949 Stadium Rd. Room 365 P.O. Box 116580 Gainesville, FL 32611		10. Work Unit No. (TRAIS) 11. Contract or Grant No. BDV-31977-17
12. Sponsoring Agency Name and Address Florida Department of Transportation 605 Suwannee Street, MS 30 Tallahassee, FL 32399		13. Type of Report and Period Covered Final Report 3/1/2014 - 7/31/2014 14. Sponsoring Agency Code
15. Supplementary Notes		

16. Abstract

Massive waterway vessels such as barges regularly transit navigable waterways in the U.S. During passages that fall within the vicinity of bridge structures, vessels may (under extreme circumstances) deviate from the intended vessel transit path. A vessel that has become aberrant may subsequently collide with any nearby bridge substructure components (e.g., piers). When vessel-bridge collisions occur, large lateral dynamic forces are exerted upon the impacted bridge substructure component. The occurrence of collision-induced bridge failures has led to requirements for the design of bridges for vessel collision in the U.S. Over the past decade, significant advances have been made by a group of researchers and engineers at the University of Florida (UF), in collaboration with the Florida Department of Transportation (FDOT), toward the development of design-oriented vessel bridge collision analysis techniques. Based on these collective efforts, the current project was undertaken to implement computationally-efficient numerical modeling capabilities in the bridge finite element analysis software FB-MultiPier (FBMP) for use in calculations of impact design loads and predictions of bridge response. Contained in this report is detailed documentation of the graphical and analytical FBMP development of a simplified bridge modeling technique and a numerically efficient nonlinear dynamic vessel collision analysis technique. The newly implemented software features have been validated from a correctness of coding standpoint, and the predictive capabilities of the features have been demonstrated. By making use of the validated FBMP new features, bridge engineers can rapidly produce and conveniently quantify vessel collision analysis results that account for dynamic phenomena.

17. Key Words	18. Distribution Statement
Finite element analysis, structural dynamics, bridge software, vessel collision	No restrictions.

19. Security Classif. (of this report)	20. Security Classif. (of this page)	21. No. of Pages	22. Price
Unclassified	Unclassified	207	

ACKNOWLEDGEMENTS

The authors would like to thank the Florida Department of Transportation (FDOT) for providing the funding that made this project possible.

EXECUTIVE SUMMARY

Massive vessels such as ships and barges regularly make passages along navigable U.S. waterways. In the vicinity of waterway-spanning structures such as bridges, waterborne vessels generally follow specified vessel transit paths to facilitate safe passage beneath said structures. However, for any of a multitude of reasons, vessels may occasionally deviate from the intended vessel transit path. Consequently, when extreme deviations from vessel-transit paths occur, vessels can potentially collide with waterway structural components such as bridge substructures (e.g., piers). When collisions occur between in-transit vessels and structures such as bridge piers, large lateral forces are generated throughout the impacted bridge substructure component, where significant inertial (dynamic) forces can develop. Thus, aberrant vessels pose significant risks to bridge structures in navigable waterways, and accordingly, phenomena associated with vessel-bridge collisions are typically taken into consideration in bridge design and analysis applications.

Over the past ten years, a group of University of Florida researchers and engineers in collaboration with the Florida Department of Transportation (FDOT) have made significant advances toward the development of design-oriented vessel-bridge collision analysis techniques. Based on these collective advances, development and implementation efforts have been undertaken to implement computationally-efficient numerical modeling capabilities in the bridge finite element analysis software FB-MultiPier (FBMP) for use in calculations of impact design loads and predictions of bridge response. In the following report, new capabilities of FBMP are presented with the intent of providing engineers in practice with a straightforward means of conducting advanced nonlinear vessel-collision analysis using simplified bridge modeling techniques.

The work detailed below focused on developing and implementing algorithms in FBMP that make use of efficient response calculations. Using a phenomenological approach, bridge structural behavior has been represented within the context of nonlinear dynamic analysis through coupled vessel-pier and pier-soil interactions. Further, per the implementation efforts, highly complex numerically-based system responses can be captured using a simplified bridge modeling approach. In particular, a simplified bridge modeling technique has been incorporated into FBMP, where the technique captures the major characteristics of full-bridge behavior, but only requires the presence of a pier of interest and the spans adjacent to said pier.

Complementary to the calculation efficiencies, the implemented numerical tools maintain robustness in predicting impacted bridge response within reasonable margins of error. Since bridge-soil response to vessel collision can be highly nonlinear, an implementation approach was undertaken to ensure that finite element models remain capable of undergoing solution convergence when phenomena such as cracking and crushing of structural members occur. The newly developed tools are housed within the powerful FBMP pier analysis model, which has been available for several years. In turn, the new features of FBMP facilitate straightforward utilization of advanced nonlinear dynamic analysis in bridge design applications.

TABLE OF CONTENTS

LIST OF FIGURES

LIST OF TABLES

Tables Page

CHAPTER 1
INTRODUCTION

1.1 Introduction

Massive waterway vessels such as ships and barges regularly transit navigable waterways in the U.S. While in-transit near bridge structures, vessels generally follow specified vessel transit paths, which provide passive guidance for vessels and vessel groups. Generally, vessels remain within the vessel transit paths. Consequently, incidents such as unintentional grounding incidents are avoided, In addition, by maintaining intended transit paths, vessels can navigate safely beneath bridges that span waterways. However, in the course of passing within the vicinity of bridge structures located in navigable waterways, vessels may (under extreme circumstances) deviate from the intended vessel transit path. As a result, vessels may collide with bridge substructure components (e.g., piers). When vessel-bridge collisions occur, large lateral forces are exerted upon the impacted bridge substructure component. Because the vessel collision forces are generated over relatively short periods of time (over a matter of seconds), significant inertial forces can develop throughout the impacted structure, and result in the generation of additional structural demands. Thus, aberrant vessels pose significant risks to bridge structures in navigable waterways, and accordingly, the phenomena related to vessel-bridge collisions are typically taken into consideration in bridge design and analysis applications.

Over the past decade, significant advances have been made by a group of researchers and engineers at the University of Florida, in collaboration with the Florida Department of Transportation (FDOT), toward the development of design-oriented vessel-bridge collision analysis techniques. Based on these collective efforts, this work was undertaken to implement computationally-efficient numerical modeling capabilities in the bridge finite element analysis software FB-MultiPier (FBMP) for use in calculations of impact design loads and predictions of bridge response. In the following, new capabilities of FBMP are presented with the intent of providing engineers in practice with a straightforward means of conducting advanced nonlinear vessel-collision analysis using simplified bridge modeling techniques.

1.2 Motivation

When subjected to very small static loads, bridge pier structures behave linearly and elastically. Beyond certain thresholds of structure demand, such as those associated with extreme event loading (including vessel collision loading), bridge pier response can include cracking of pier columns and piles in tension, crushing in compression, and other highly nonlinear behavior. These complex structural behaviors are further complicated by erratic soil behavior, which must be represented in nonlinear soil-structure interaction analyses. To capture this coupled vessel-structure and soil-structure behavior for analysis purposes, three-dimensional (3D) high-fidelity finite element analysis (FEA) representations have shown great potential; however, the modeling of complex pier structure geometries founded in soil is still not feasible for large-scale structural analyses in design practice. Additionally, dynamic (time-history) analysis of bridge structural models at any appreciable level of fidelity correlates positively with high computational cost. This correlation holds true not only with respect to hardware requirements (i.e., to maintain speed of computation) but also with respect to the generation of cumbersomely large datasets of

numerical response. Excessively large datasets, in turn, bring forth the need for extensive post-processing efforts, as pertinent response quantities are sought out (e.g., maximum through-time pier column shears).

In response to this need, the present work has focused on developing new numerical models in FBMP that make use of efficient response calculations. These tools are also capable of predicting impacted bridge response within reasonable margins of error. Further, these tools are based on pioneering experimental and numerical studies, which have been conducted by a research team at the University of Florida (UF), and sponsored by the FDOT, since 2003. Using a phenomenological approach, in which bridge structural behavior is represented within the medium of nonlinear dynamic phenomena, extensive analytical work has been conducted to establish the basis of nonlinear dynamic analysis that encompasses coupled vessel-pier and pier-soil interactions (Consolazio and Davidson, 2008). Based on the UF research findings, and given the significant computational resources that are available to designers (where such resources facilitate the modeling of multiple-pier structures), development of a vessel collision analysis tool has become feasible. In addition to having a model that adequately represents coupled system behavior (e.g., vessel-pier, soil-structure), the finite element procedures used to analyze reinforced concrete structures must be reliable and efficient. Since bridge-soil response to vessel collision can be highly nonlinear, the iterative schemes used in implicit dynamic solutions of finite element models must remain capable of undergoing solution convergence when phenomena such as cracking and crushing of structural members take place. A powerful pier analysis model has been available in FBMP (Chung 2014a) for several years, and has been used widely in numerous bridge design and analysis applications. There are no other bridge software tools currently available that are sufficiently robust and efficient to the extent that both constitutive and kinematic nonlinear behavior can be assessed, in a design setting, under arbitrary loading conditions (e.g., quasi-static and dynamic conditions). Consequently, the current work was carried out to develop vessel collision and bridge modeling capabilities that are amenable for use in design applications and to incorporate them into FBMP, which is currently being used in practical, large-scale analyses.

1.3 Implementation-Specific Objectives

From an implementation standpoint, there were two primary objectives associated with the work completed. The first implementation-specific objective pertained to the development and programming of a robust, simplified bridge modeling technique in FBMP. The second objective pertained to the development and programming of numerically-efficient nonlinear dynamic vessel collision analysis models. Those tasks carried out to implement the simplified bridge modeling tool for use in vessel-collision analysis are detailed in Chapter 2 (with emphasis on GUI development) and Chapter 3 (with emphasis on engine development). So as to contextualize the of-interest bridge modeling and vessel collision analysis techniques, summary background discussion is provided in Sec. 1.3.1 and Sec. 1.3.2, respectively.

1.3.1 Simplified Bridge Modeling

When vessel-bridge collisions occur, stiffness and mass dependent superstructure restraint can result in significant portions of the impact load being transferred from the impacted pier to the superstructure. Hence, additional insight into impacted bridge response can be gained by accounting for the influence of adjacent non-impacted piers and spans for vessel-bridge collision analyses. However, conducting and post-processing dynamic analyses for multiple-pier, multiple-span bridge models can rapidly become infeasible to practicing bridge engineers. Alternatively, bridge piers of interest can be analyzed in a numerically efficient manner using an equivalent one-pier two-span (OPTS) bridge model.

The OPTS model simplification procedure involves reducing a multiple-pier, multiple-span bridge model (Fig. 1.3.1) to an equivalent pier model with concentrated stiffnesses and masses connected at the distant ends of each of two retained spans (Fig. 1.3.2). The concentrated stiffnesses are formed using stiffness condensation (e.g., flexibility matrix inversion) for each of the left and right portions of the full bridge model, which are excluded from the OPTS model. The lumped masses are formed by simply lumping each of the half-span masses. A further simplification is made by negating off-diagonal stiffness terms at each condensed stiffness location, resulting in a set of independent springs and lumped masses at each end of the OPTS model (as denoted in Fig. 1.3.2). This simplified modeling technique was previously verified to accurately predict pier structural responses relative to corresponding full-bridge structural response predictions (Consolazio et al., 2008).

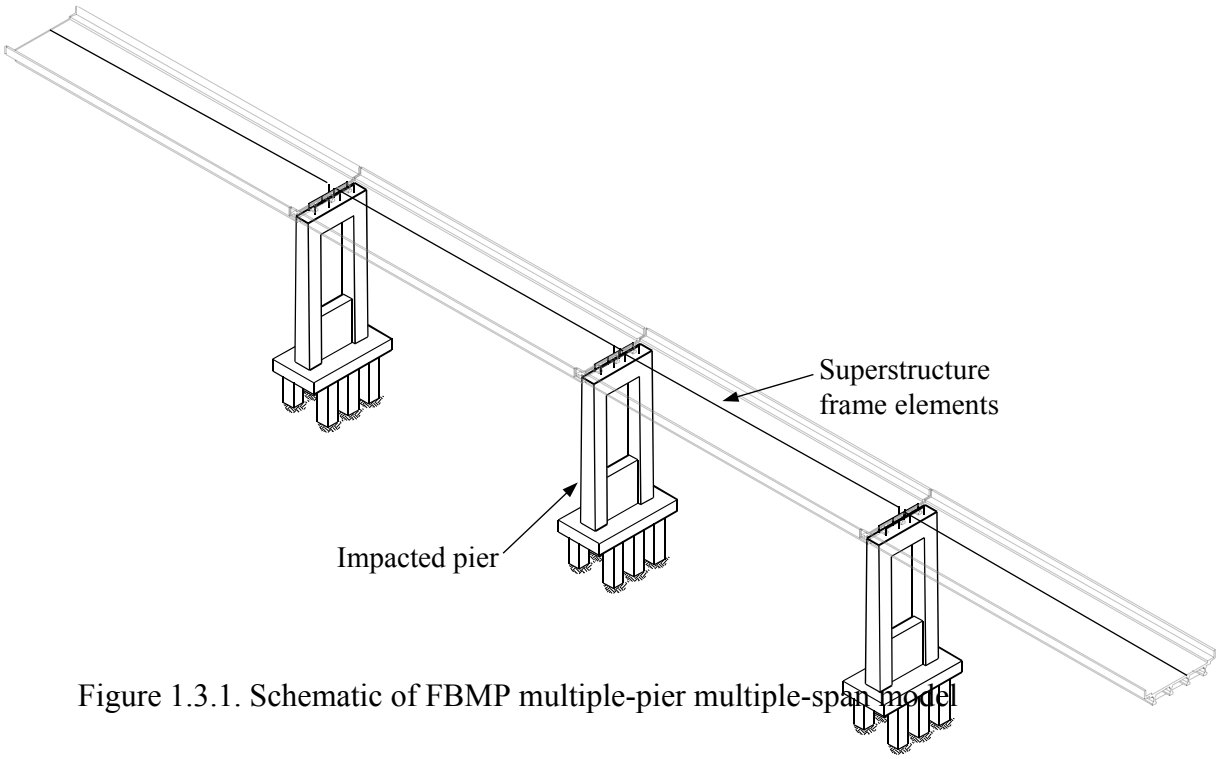

Figure 1.3.1. Schematic of FBMP multiple-pier multiple-span model

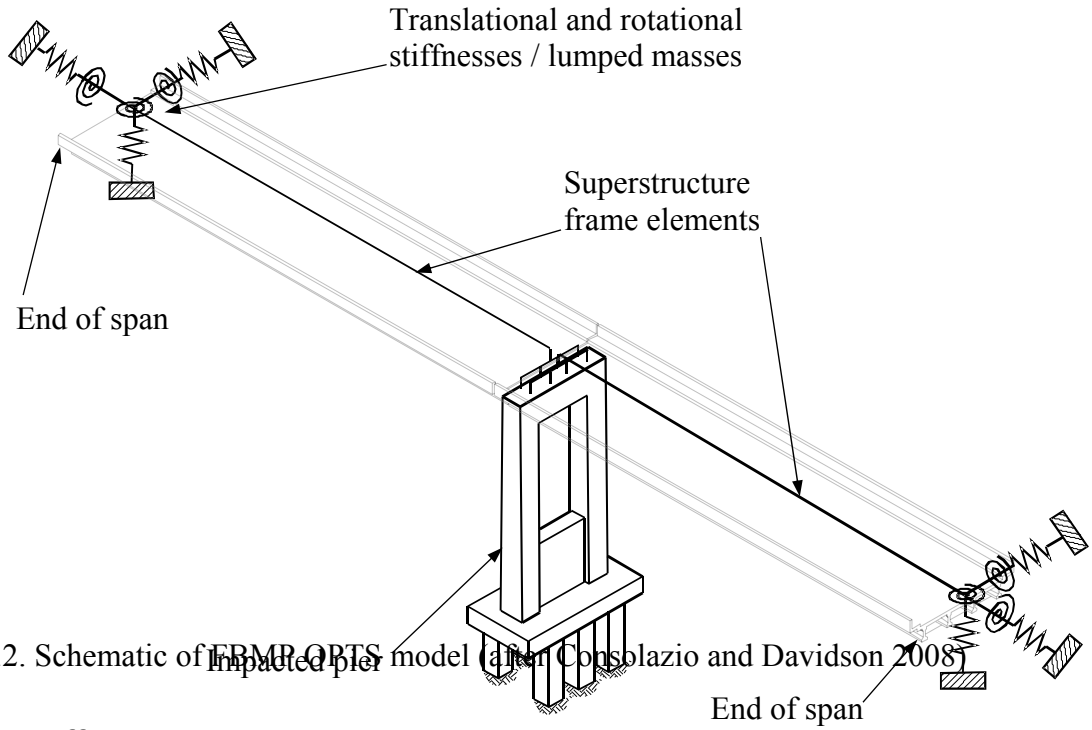

Figure 1.3.2. Schematic of FBMP QPTS model (after Consolazio and Davidson 2008)

1.3.2 Numerically-Efficient Nonlinear Dynamic Vessel-Collision Analysis

Several numerical studies have been carried out to characterize force-deformation relationships for commonly piloted waterway vessels (e.g., Yuan et al., 2008; Consolazio et al., 2009). Vessel characterizations made in the numerical studies greatly facilitate the modeling of barges as single-degree-of-freedom (SDF) systems, where impact-load characteristics can account for vessel size, structural configuration, relative orientation, and the shape (i.e., the geometry) of the impacted surface (e.g., pile cap, pier column). This approach was selected for adoption and use in the analytical framework being implemented in FBMP, which significantly added to the efficiency of dynamic barge-bridge collision analysis. Specifically, coupled vessel impact analysis (CVIA), developed previously (Consolazio and Cowan, 2005), has been implemented for designer-friendly use. In CVIA, a shared contact force, P_B, is used to computationally link a SDF vessel model—with stiffness, mass, and initial velocity—to a multiple-degree-of-freedom (MDF) bridge model (Fig. 1.3.3).

Upon impact, a time-varying impact force is computed, and the MDF bridge model is displaced in response. In turn, internal forces are developed throughout the bridge model. A significant advantage of employing CVIA is that the algorithm does not require *a priori* knowledge of the barge impact load-history. Also, the CVIA technique was previously validated using data from selected full-scale experimental impact tests on bridge structures (Consolazio and Davidson, 2008).

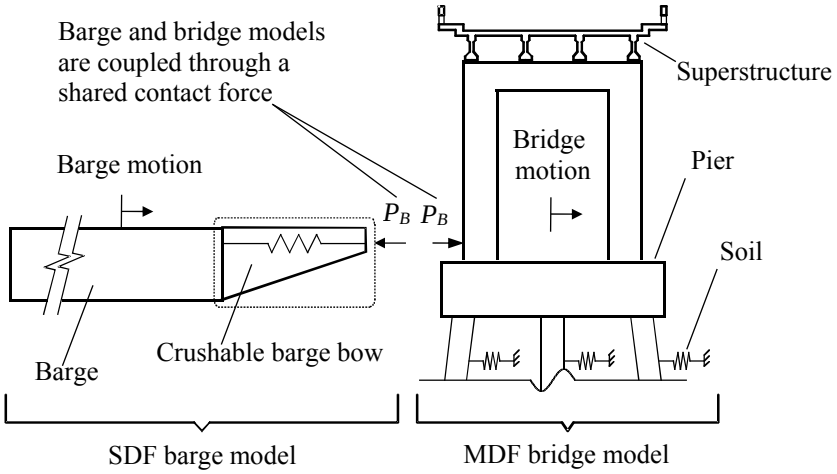

Figure 1.3.3. Coupling between barge and bridge in CVIA (Consolazio and Cowan, 2005)

1.4 Validation-Specific Objectives

Subsequent to completion of the CVIA and OPTS coding efforts (introduced above in Sec. 1.3), the project objectives were shifted toward determining the quality of the CVIA-OPTS implementation in FBMP from both the computer programming (i.e., correctness of coding) and engineering (i.e., utility in design and analysis) perspectives. As detailed in Sec. 2.4 and Sec. 2.5 of this report, validation-specific objectives pertaining to correctness of computer programming were met in part by carrying out verification of the new Graphical User Interface (GUI) features with respect to both saving text input to FBMP model files, and also, displaying the FBMP analysis results. With respect to correctness of coding in the analysis engine, portions of Chapter 4 are dedicated to verification of CVIA module in the analysis engine (e.g., that bridge model results generated through use of loading generated by the CVIA module are inline with those results predicted by equivalent, prescribed loadings).

Validation of the CVIA implementation in FBMP, from an engineering standpoint, is documented in remaining portions of Chapter 4. Therein, comparisons are made between numerical predictions of bridge response to corresponding full-scale experimental barge-bridge collision data. In Chapter 5, a demonstration bridge case is selected and used to verify that the OPTS implementation in the FBMP analysis engine leads to analysis results that are in line with those obtained from multiple-pier, multiple-span (i.e., full-bridge) analysis.

1.5 Assessment-Specific Objectives

As a final study objective, using the verified and validated CVIA-OPTS framework in FBMP, the potential ramifications associated with use of the CVIA-OPTS formulation in bridge design and analysis were investigated. More specifically, in Chapter 6, a cost-benefit analysis is carried out for a selected in-service bridge to demonstrate potential cost differences in sized

structural and foundation members, as identified by comparing results from static and dynamic vessel collision analyses. As discussed in Chapter 7, the effects of various impact conditions and geotechnical considerations on impacted bridge pier response are explored. Also, in Chapter 7, time-of-computation comparisons are made between the full-bridge models and OPTS models employed in the current study.

1.6 Scope of Work Pertaining to Implementation of CVIA and OPTS

Importantly, the work detailed in this report is not intended for interpretation as academic research, but rather the software packages are intended for use as practical, easy-to-use, black-and-white design and analysis tools. Further, these tools were based on scientific interpretation and comprehensive knowledge of recent research findings. To meet industry standards, rigorous testing, thorough verification, and thorough documentation of the software development were carried out. The major tasks involved in the development and implementation of design tools into FBMP are delineated below.

In consideration of recently completed experimental testing and analytical work (Consolazio et al., 2008, Consolazio et al., 2010), the new FBMP features were based on:

- Experimentally-validated nonlinear dynamic analysis (i.e., CVIA, as originally proposed in Consolazio and Cowan, 2005) with use of representative load-deformation curves (e.g., Consolazio et al., 2010) for the barge behavior, in compression against a reinforced concrete pier structure, which can be used in conjunction with either a single pier or a multiple-pier bridge model.
- Numerically-based system response that can be captured by a simplified bridge modeling approach (i.e., OPTS modeling). In particular, this simplified model captures the major characteristics of full-bridge behavior, but only requires the presence of a pier of interest and the spans adjacent to said pier. Further, the CVIA technique can be used in conjunction with, or independent of, the OPTS modeling.
- Dynamic system behavior, for which the response of the soil influences the behavior of the structure and the response of the structure influences the behavior of the soil, i.e., existing FBMP modeling capabilities for nonlinear soil-structure interaction.

Significant portions of the GUI functionality were modularized for CVIA by developing dynamic link libraries (DLLs) written in FORTRAN. In addition, several new features were added to the FBMP GUI to increase its robustness in bridge applications. Importantly, the OPTS modeling technique was incorporated so that only a single pier definition is required for analysis, as opposed to an entire bridge.

The CVIA module and OPTS model type, as developed for the FBMP GUI, have been shown to be fully compatible with other FBMP analysis modules. Particularly, compatibility was

maintained for the dynamic relaxation analysis module, where in this context, static equilibrium of the system (for a given model) is first computed, and subsequently the CVIA module is used to simulate contact-impact loading on the initialized (deformed) system as part of a dynamic analysis. Significant updates were made in the analysis engine to ensure compatibility. A listing of programming tasks required for implementation of the CVIA module and OPTS model type into the FBMP GUI have been presented in Sec. 1.6.1 and Sec. 1.6.2. Similarly, a listing of programming tasks completed as part of the CVIA and OPTS feature implementation in the FBMP analysis engine have been subsequently provided in Sec. 1.6.3.

1.6.1 Tasks for the Development of GUI Data Input Features for Automated Model Generation

1. The CVIA module of FBMP is a critical component of dynamic (time-history, or transient) vessel-impact analysis on bridge structures, where analysis is carried out (in part) based on the characteristics of a moving waterway vessel. Using vessel mass, initial velocity, the load-deformation characteristics of the vessel bow, and the transient pier response, the loading (pier excitation) can be calculated as part of the simulation and applied to the structure at each point in time. Per Consolazio et al. (2010), vessel bows exhibit behavior that can be characterized as elastic-perfectly plastic, where quantitative force-deformation relationships governing bow crushing behavior can be formed based on user-supplied vessel characteristics and the geometry of the impacted surface. Alternatively, vessel force-deformation relationships that are entirely user-defined can be specified if desired. Therefore, tasks associated with implementing CVIA into the FBMP GUI included the creation of:

a. A vessel-impact data input dialog, where users can specify vessel characteristics such as weight, speed, type, and impact width; for the calculation of crush depth at impact, a separate DLL was written to generate a crush depth and corresponding force due to the plastic deformation.

b. A vessel-impact directional input dialog, where users specify the direction at which a given barge impacts a bridge pier of interest; this new dialog was incorporated into the functionality of the Load Page of FBMP.

c. A vessel-impact load function dialog, where users can either specify loading curve(s) in a Load Function Editing Table, or choose a type of loading among built-in force-deformation curves.

2. The OPTS model of FBMP allows engineers to analyze the structural response of a bridge pier where the influence of other portions of the bridge are retained. OPTS models consist of a single pier with a connecting span on each side of the pier. Further, OPTS models contain springs and lumped masses at the two retained span ends so as to incorporate the influence of excluded portions of the overall bridge structure. Consequently, OPTS models can very efficiently capture the response of bridge models for applications such as vessel collision loading, where the bridge

models may contain multiple piers and spans. The application of OPTS was aimed to facilitate rapid bridge model creation, and simultaneously, to reduce simulation times. Used in conjunction with appropriately determined span spring stiffnesses and masses, OPTS models employ a single pier and two spans to produce pier-response output of similar accuracy with respect to that obtained from analyzing a true multiple-pier, multiple-span bridge model. Thus, the simplified bridge modeling approach enables users to perform numerous simulations of vessel collision conditions within a fraction of the computational (and post-processing) time that would be required for impact simulations on a full-bridge model. Users can conduct CVIA in combination with (or independent of) the OPTS model. The corresponding tasks associated with implementing the OPTS feature in FBMP included:

a. A spring application directly on spans extents of OPTS models, where users apply springs to desired nodal locations on the bridge spans; a higher degree of accuracy in the computation of spring stiffness can be obtained from static analysis of a full-bridge model.

b. A mass application directly on span extents of OPTS models, where users apply span masses to desired nodal locations on the bridge spans; a simple calculation for determining nodal span mass values is given in Consolazio and Davidson (2008).

c. A three-dimensional (3D) Bridge View that displays nodal locations, applied loads, springs and masses. Complimentary to the 3D Bridge View display is a Span Offset dialog, where retained span geometry and orientation can be specified.

1.6.2 Tasks for the Development of GUI Input and Output Displays

1. GUI implementation was an iterative process in which testing and validation of new GUI functionality required numerous cycles of fixes and updates. The main thrust of the tasks listed below is the validation of the new GUI graphical features through thorough, repeated checks to meet industry standards. In addition, a streamlined, easy-to-input process was incorporated into the overall layouts of the new GUI features, which stemmed from several cycles of optimization based on feedback from design engineers. Major tasks relevant to the GUI updates for the CVIA module and OPTS model included:

a. GUI graphics of a 3D view were developed using OPEN GL for visualization of an impact load drawn on a pier, with correct load orientation. A selected load case of either the pier or OPTS model can be displayed in color graphics of both the 3D Bridge View and 3D Results View pages of GUI.

b. Input data of the CVIA module and OPTS model, which users input into new GUI dialogs, were validated against the numerical data of the text input file generated by the FBMP GUI. It was also confirmed that the text input file was successfully read (processed) by the FBMP analysis engine.

c. Output analysis data written in binary format by the FBMP analysis engine can be displayed in 3D Results View for the OPTS model. Also, it was confirmed that numeric output data were written in the text file generated by the FBMP analysis engine.

1.6.3 Tasks for the Development of Engine Subroutines for CVIA and OPTS

1. Incorporated read-in of relevant barge impact input parameters for analysis, including: barge velocity; barge mass; barge global orientation; barge crush depth; and impacted surface width.

2. Updated the Dynamic Relaxation Option to be available for both the OPTS and full-bridge models. This feature enables users to simulate staged loading prior to dynamic time-history analysis such that the system is in static equilibrium with an arbitrary set of static loads, prior to being subjected to dynamic loads (e.g., impact loading). Either OPTS or a full-bridge model can be analyzed for static equilibrium. The CVIA module can then be employed for dynamic analysis of the system. For greatest accuracy, use of the OPTS modeling with CVIA should be combined with dynamic relaxation, wherein the effects of quasi-static loads (e.g., gravity loads) are properly introduced into the dynamic analysis. Accordingly, tasks pertaining to enhancement of the analysis engine included the following:

a. A dynamic relaxation subroutine capable of processing full-bridge and OPTS models, which is required as a prerequisite for dynamic analysis. At the discretion of the user, FBMP automatically conducts a pre-dynamic (i.e., static) analysis. During the static pre-analysis, only quasi-static loads are included in the model. This pre-dynamic analysis produces and saves a global displacement array upon completion. The displacement array is then read-in to initialize the dynamic analysis, given that the restart option is selected for use in the dynamic analysis input file.

b. Use of the dynamic relaxation subroutine requires, as a prerequisite for dynamic analysis, that users obtain the global stiffness array upon completion of the static analysis. The stiffness array is then read-in to initialize the dynamic analysis, given that the restart option is selected for use in the dynamic analysis input file.

c. A subroutine to initialize a system, where if indicated in a dynamic analysis input file, prompts the reading of global stiffness and displacement arrays. These two quantities are then used to properly initialize all quasi-static loads into bridge models such that no artificial system excitation occurs due to sudden application of said (quasi-static) loads.

3. Developed a CVIA module, which governs the input for defining vessel collision scenarios and determines the barge impact force through time.

4. Updated existing analysis engine subroutines that employ user-defined empirical vessel force-deformation loading and unloading curves in determining barge impact force through time.

5. Created analysis engine subroutines to determine superstructure spring stiffness for use in an OPTS model. This option can be used in a two-step analysis procedure; first a full-bridge model static analysis is conducted in order to determine spring stiffnesses, which are then used as model input parameters for subsequent OPTS analyses. Two subroutines were added to the analysis engine:

a. A subroutine that contains a description of the span springs, which governs application of discrete spring stiffnesses to span nodes.

b. A subroutine that contains a description of the span masses, which governs application of discrete inertial mass to span nodes.

6. Implemented the OPTS modeling subroutine as part of the main program of FBMP. For users of the OPTS model, the span spring and mass modules are available (where span-end springs and masses are used to account for extraneous portions of bridges in OPTS models).

7. Created subroutines to print maximum design forces to output in both binary (for graphical display) and text formats.

1.6.4 Tasks for the Development of a User's Guide

So as to facilitate straightforward ease-of-use in forming OPTS models and conducting CVIA analyses, a User's Guide was developed, with three major documentation tasks given below. A Condensed User's Guide is provided in Appendix A, and an Extended User's Guide is provided in Appendix B.

1. Given a full-bridge FBMP model, step-by-step documentation for use of GUI features that facilitate OPTS model formation.

2. Step-by-step documentation for supplying CVIA input for a given vessel collision scenario.

3. Step-by-step documentation for viewing and processing analysis results, including rapid identification of maximum bridge response quantities.

1.6.5 Tasks for the Development of an OPTS Licensing Scheme

Development of a licensing scheme specific to use of the OPTS model in FBMP was necessary for future commercial releases. License scheme formation tasks included:

1. Listing of a new model type, indicating use of a One-Pier Two-Span model, in the Problem Type page within the Global Data dialog of the FBMP GUI.

2. Consideration given as to whether any changes were required for an in-house code generator program to incorporate new license types in generation of new (OPTS model type) security key codes.

3. Ensuring that compatibility issues with popular, actively supported operating systems did not arise due to the addition of any license-related coding changes for the OPTS model type.

1.7 Scope of Work Pertaining to Engineering Validation of CVIA and OPTS Implementations

Included among the implementation-specific tasks described in Sec. 1.6 were validation of the CVIA and OPTS features with respect to GUI and engine coding (i.e., computer programming). For example, as discussed in Chapter 2 of this report, the GUI was verified to properly save formatted text to FBMP model input files. However, as an additional, critical layer of CVIA and OPTS feature validation, the quality of the new features were determined from an engineering standpoint. More specifically, the utility of the CVIA module was investigated with respect to bridge-response prediction capabilities (relative to physical measurements). Also, the utility of the OPTS modeling technique was investigated with respect to pier-of-interest response prediction capabilities (relative to full-bridge response). Major tasks involved in the engineering validation of the CVIA and OPTS features are detailed below.

1.7.1 Tasks for Engineering Validation of the CVIA Module

Engineering validation of the FBMP CVIA module implementation (through validation against full-scale experimental data) was achieved by completing the following three tasks:

1. A test case was selected from among the old St. George Island Causeway full-scale barge impact experiments, carried out in northwest Florida in 2004 (Consolazio et al., 2006). Pertinent physical measurements taken during the selected test case were established as benchmarks for determining the quality of the CVIA (numerically generated) analysis results.

2. An FBMP model was created, matching the structural and geotechnical conditions specific to the selected test case. Using the CVIA module, the FBMP geo-structural model was subjected to vessel collision conditions matching those recorded during the full-scale impact experiment.

3. CVIA results generated for the selected test case were compared to the physical measurements, and the prediction capabilities of the CVIA module were characterized.

1.7.2 Tasks for Engineering Validation of OPTS Modeling

Engineering validation of the FBMP OPTS model implementation (through numerical verification) was achieved by completing the following three tasks:

1. An in-service bridge was identified and selected for use in the numerical verification efforts. Structural drawings were obtained for said bridge, and a multiple-pier, multiple-span FBMP model was developed. The model includes significant soil modeling considerations based on site-specific boring logs and geotechnical reports. So as to demonstrate that the OPTS model implementation remains effective within the context of vessel collision, a barge impact scenario was established based on vessel collision design loads given in the structural drawings. The vessel collision scenario was used to supply CVIA input for the full-bridge model, a dynamic analysis was carried out, and analysis results pertaining to the impacted bridge pier were cataloged.
2. An OPTS model containing the impacted bridge pier and two adjacent spans was created from the FBMP full-bridge model. The OPTS model was subjected to the vessel collision scenario formed as part of item 1. above. Results generated as part of the CVIA-OPTS (dynamic) analysis were cataloged.
3. Results obtained from the full-bridge CVIA analysis and CVIA-OPTS analysis were compared, and the prediction capabilities of the OPTS implementation were characterized.

1.8 Scope of Work Pertaining to Engineering Assessment of CVIA and OPTS Implementations

Subsequent to establishing correctness of coding and significant engineering utility for the CVIA-OPTS framework, a parametric study was undertaken to assess implications for use of the new features in bridge design and analysis applications. Tasks associated with parametric assessment of the CVIA-OPTS framework encompassed:

1. Cost-benefit analysis for a selected, in-service bridge case. In this context, a corresponding FBMP model was used to quantify design-relevant (i.e., maximum) demands in structural and foundation members that were predicted to occur due to vessel collision loading in a static analysis regime. A corresponding (energy-equivalent) dynamic vessel collision analysis was also carried out, and the associated maximum dynamic demands were quantified. Noting that the static analysis regime constitutes the default means of sizing bridge structural and foundation members in current design practice, design considerations were subsequently made for the dynamic analysis model (through member re-sizing) so as to bring the maximum dynamic demands inline with those obtained from the static regime. Changes in construction costs associated with the re-sized members in the dynamic analysis model were then compared to the construction costs associated with the members in the static analysis model.

2. For the selected, in-service bridge case, investigation of the effect that various impact geometries (i.e., round versus flat impacted surface geometries) have on impact force generation and impacted bridge pier response.

3. For the selected, in-service bridge case, investigation of the effect that variation in soil-strength parameters have on collision-induced bridge pier demands.

4. For a collection of full-bridge and OPTS models considered in the current study, a comparison of the computational time requirements.

CHAPTER 2
GRAPHICAL USER-INTERFACES (GUI) DEVELOPMENT

2.1 Introduction

Implementation of the GUI dialogs that are necessary to specify input parameters required for conducting CVIA within FBMP has been completed. To this effect, a "Vessel Collision Analysis Data" dialog (Fig. 2.1.1) has been made available to facilitate waterway vessel-bridge collision analysis input. Within this dialog, users of the FBMP software can characterize the following parameters related to the collision scenario of interest:

- Vessel Weight: the weight or tonnage of the impacting vessel.

- Vessel X Velocity: the vessel transit speed in the global x-direction.

- Vessel Y Velocity: the vessel transit speed in the global y-direction.

Further, using the dialog shown in Fig. 2.1.1, users can specify the Vessel Type, where four vessel definitions are available:

- Elastic-Plastic: wherein the vessel crushing behavior is elastic-perfectly plastic. In this vessel definition, only the load at which the vessel bow yields (Yield Load) and the corresponding yield deformation (Crush at Yield) need to be specified.

- Barge / Flat Surface Impact: wherein only the width of the impacted planar (i.e., flat-faced) bridge pier object that is being struck needs to be specified.

- Barge / Round Surface Impact: wherein only the width of the impacted non-planar (i.e., rounded) bridge pier object that is being struck needs to be specified.

- User Defined: wherein arbitrary loading and unloading curves can be defined to characterize the vessel crushing behavior.

Implementation of the controls that accept user input has been completed, where such implementation included labeling, positioning, data display, and data storage. Four unique vessel models have been made available for use in the CVIA analysis. For each of the four vessel types, when conducting CVIA, either vessel loading or vessel unloading behavior is possible for a given time step within the analysis. For the vessel definition types other than "User Defined", the FBMP analysis engine uses built-in empirical relationships to govern the vessel (barge) loading, yielding, and unloading behavior.

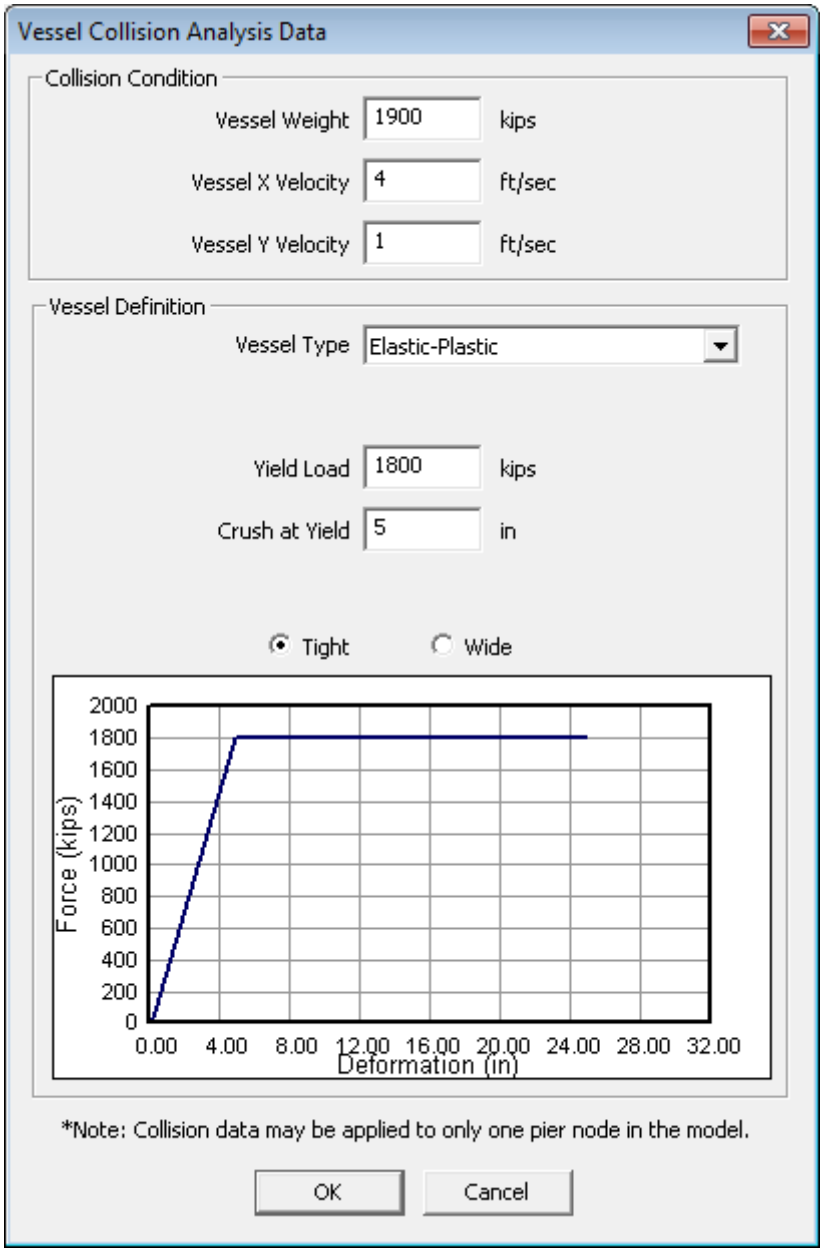

Figure 2.1.1. Vessel collision analysis data dialog

Of particular use for the User Defined vessel definition, however, is the "Load Function Edit Table" dialog (Fig. 2.1.2). Users that have access to specific, detailed design vessel data for ships, barges, or other impacting vessels can make use of this dialog in specifying entirely arbitrary Load Curve and Unloading Curves data. In this context, "Loading Curve" data are used by the analysis engine to determine the vessel force that is imparted during portions of the collision analysis where the vessel and pier are in contact, the vessel deformation level has not yet reached the yield deformation, *and* the vessel is actively continuing to undergo motion toward the impacted surface. At all other times during the collision analysis, the user-defined yield deformation and the unloading curves are taken into consideration to properly determine

the barge impact force during times of vessel unloading, vessel separation (from the impacted surface), and vessel reloading (upon rebound of the impacted structure).

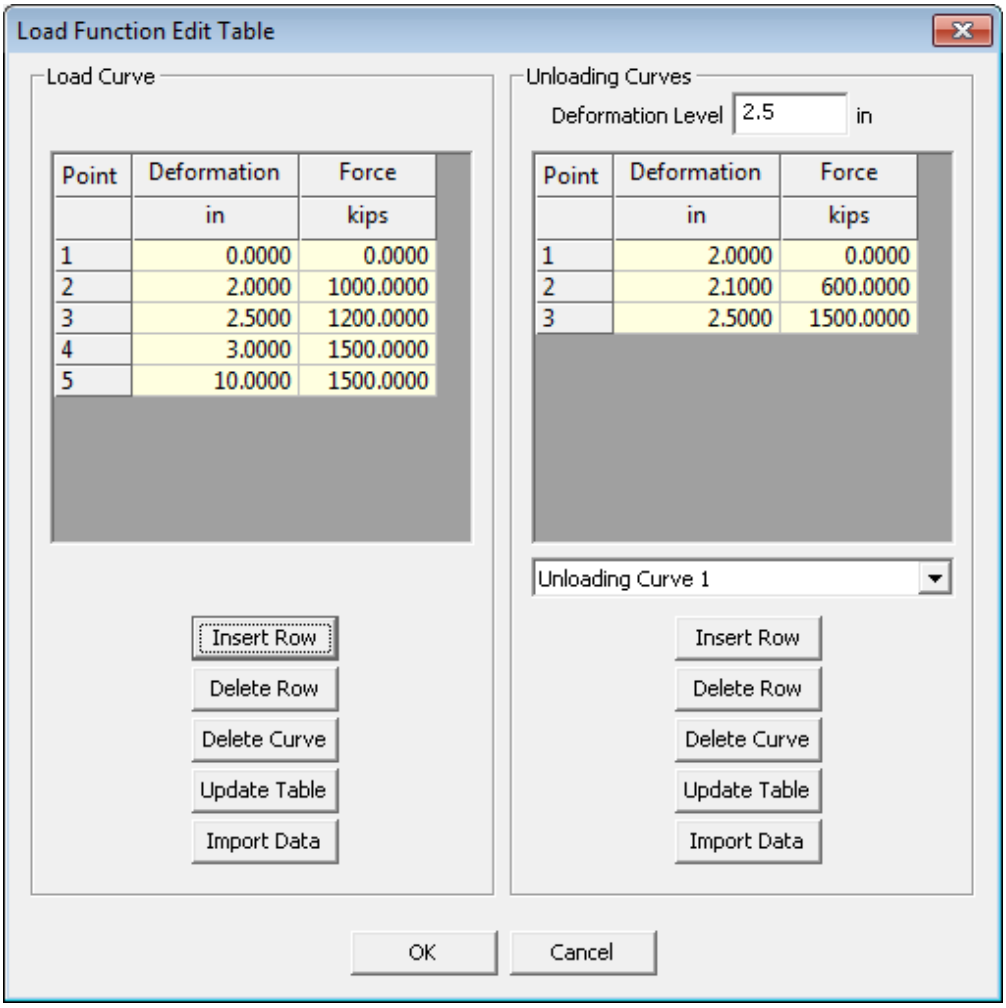

Figure 2.1.2. Load function edit table dialog

Implementation of the utility controls that facilitate dialog navigation in the Load Function Edit Table dialog (Fig 2.1.2) has been completed. These include table manipulation buttons as follows: “Insert Row”, “Delete Row”, “Delete Curve”, “Update Table”, and “Import Data”.

In recognizing the importance of maintaining an intuitive GUI layout in assimilating new features into FBMP, the CVIA feature placement decidedly falls appropriately under the “Load” page within the FBMP “Pier Data” input. Accordingly, as shown in Fig. 2.1.3, CVIA dialogs can be accessed by clicking the “Vessel Col.” (vessel collision) button for any pier-specific nodes that are subjected to a dynamic load. Note that, specific to utilization of the vessel collision loading features, only one node may be selected per FBMP model. This constraint is consistent with the notion that, even in an extreme event scenario, only a single vessel (or vessel group)

will strike a bridge pier within a given collision scenario. The load direction is input on the "Vessel Collision Analysis Data" dialog, via the "Vessel X Velocity" and "Vessel Y Velocity" edit controls.

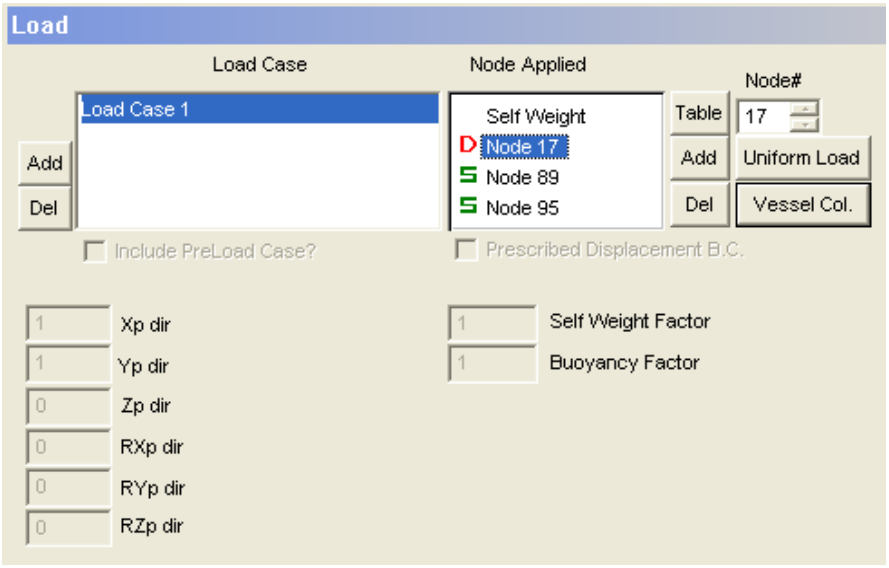

Figure 2.1.3. Load page

The selection of vessel collision as a type of dynamic analysis is made on the "Dynamics" page, as shown in Fig. 2.1.4. Consistent with the other "Time Function" (i.e., dynamic loading) options, only a single selection is permitted. For example, the GUI does not permit users to select both "Vessel Collision" loading and "Applied Load (Load vs. Time)" loading within an individual FBMP model.

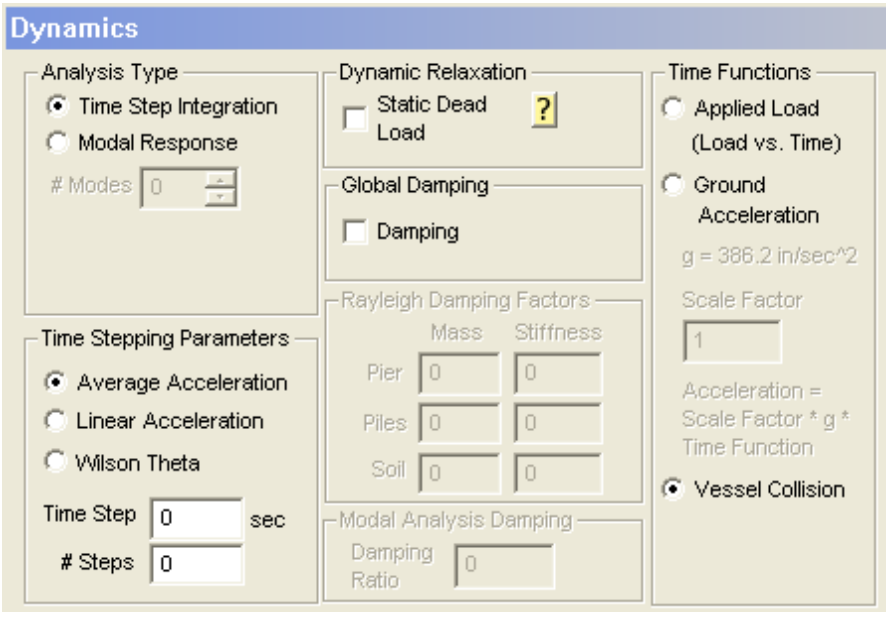

Figure 2.1.4. Dynamics page

2.2 Development of GUI OPTS Model

Development of the GUI dialogs that are necessary to specify input parameters required for conducting OPTS modeling within FBMP has been completed. Specifically, an "OPTS Data" dialogs have been made available for each of the two spans retained in the OPTS model. The Span 1 and Span 2 dialogs are shown in Fig. 2.2.1 and Fig. 2.2.2., respectively. Each dialog enables direct input of OPTS span-offset quantities (i.e., span dimensions), OPTS discrete spring stiffnesses, and OPTS discrete mass input. Note that the spring stiffnesses and discrete masses are located at the respective span ends. Within these dialogs, users of the FBMP software can characterize the following parameters related to the OPTS modeling type:

- Local Spring Coordinates: distances from transfer beam on pier in X, Y and Z directions to each span tip.

- Spring Stiffness: discrete spring stiffnesses for the translational and rotational X, Y, and Z degrees of freedom at the span extents.

- Mass Values: discrete mass values for the translational and rotational X, Y, and Z degrees of freedom at the span extents.

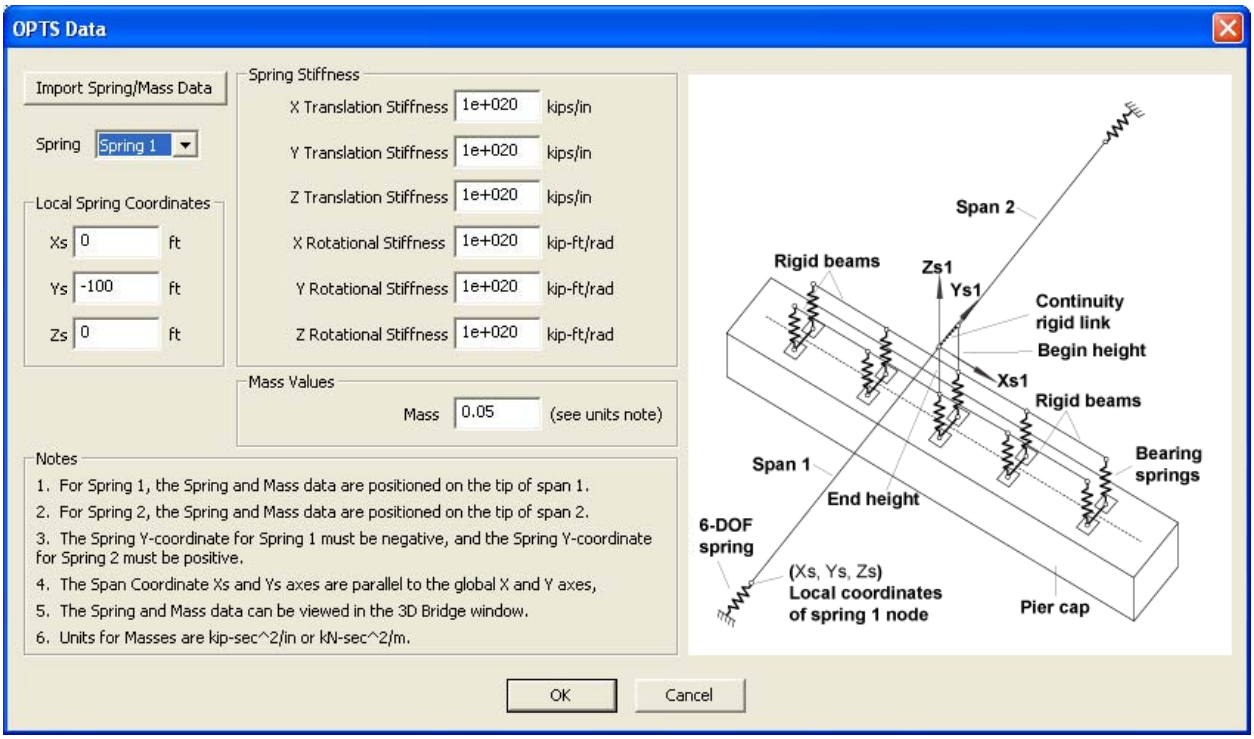

Figure 2.2.1. OPTS data dialog for Span 1 span-end stiffnesses and lumped mass

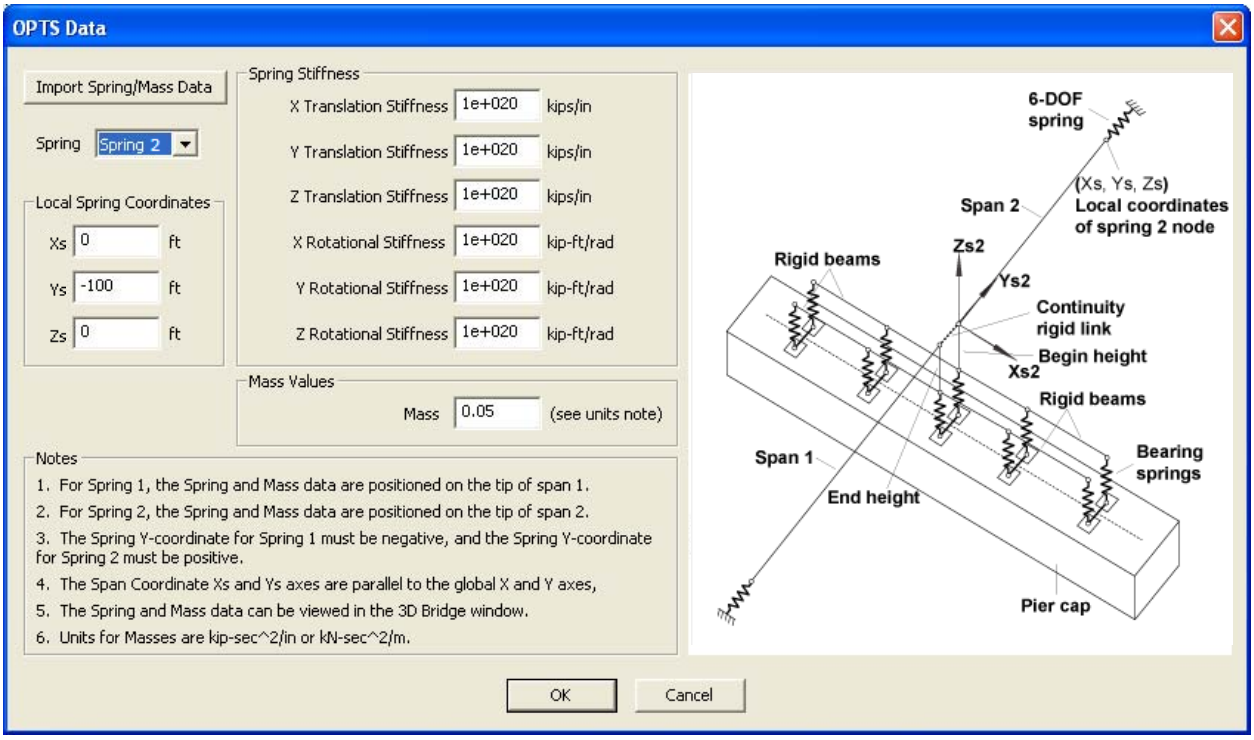

Figure 2.2.2. OPTS data dialog for Span 2 span-end stiffnesses and lumped mass

Implementation of the GUI controls that accept user input has been completed, where such implementation included labeling, positioning, data display, and data storage. The global data structures that store data that is input on the "OPTS Data" dialog have also been put into place, as was coding that permits the exchange of data between the global and local data structures. A schematic of the OPTS model was added to the dialog that is customized based on the selected (active) spring. Lastly, an import feature was added ("Import Spring/Mass Data" button) to facilitate importing spring and mass data from previously conducted analyses of bridge models, geared specifically toward calculating spring and mass data for application to an OPTS model.

The controls to choose the "Calculation of OPTS Springs and Masses" option have been put into place (Fig. 2.2.3) on the Load Table, inside the "Bridge Options" frame. Upon ticking (i.e., selecting) the tick-box for "Calculation of OPTS Springs and Masses", the GUI issues a warning to the user, as illustrated in Fig. 2.2.4. The warning serves to inform users that, by proceeding, all previously-defined loads in the model will be deleted. Such deletion includes any directly applied loads, as well as those loads associated with structural member self-weight and buoyancy. As replacement, only the span-end loads to be used in formation of the OPTS model span-end spring stiffnesses are to be included in any subsequent analyses.

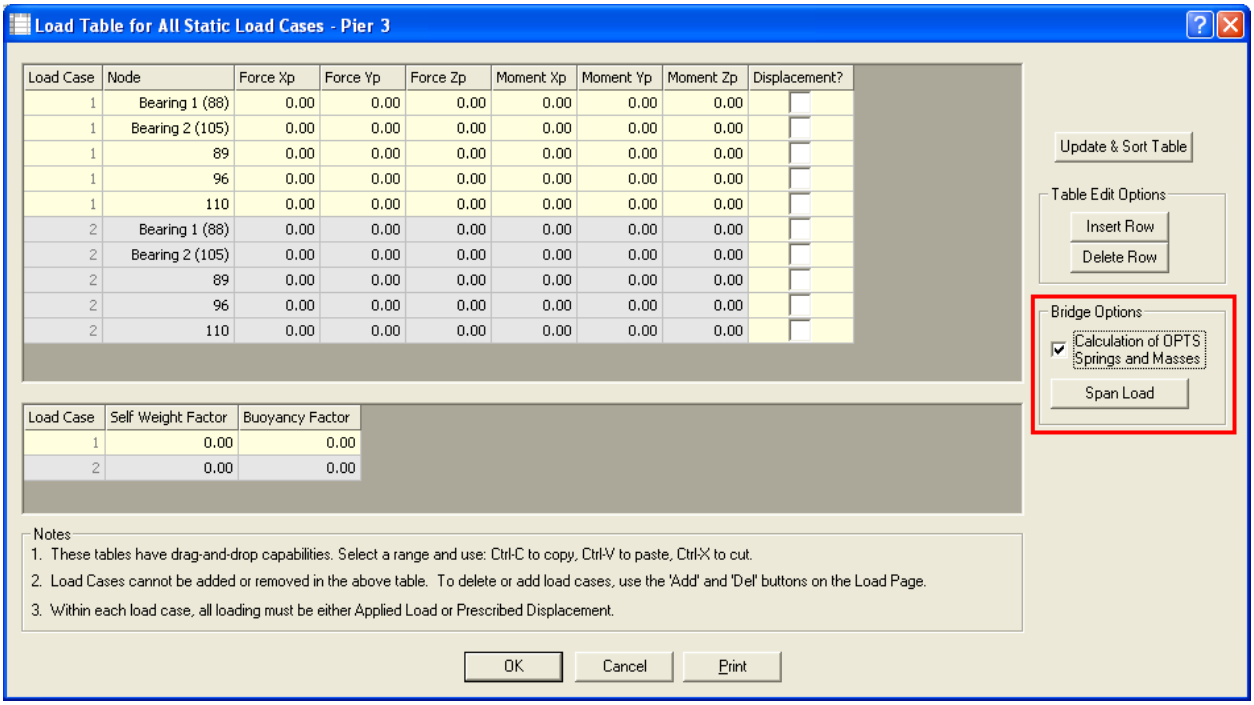

Figure 2.2.3. Load table with bridge options frame

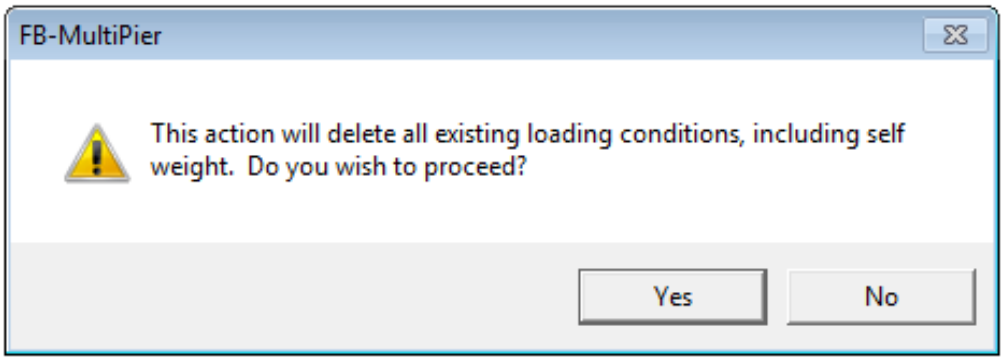

Figure 2.2.4. Warning dialog associated with use of "Calculation of OPTS Springs and Masses" option

The "Loading for OPTS Spring Formation" dialog has been created (Fig. 2.2.5) for OPTS spring formation. This dialog is launched via the "Span Load" button in the "Bridge Options" frame (Fig. 2.2.3). Within the "Loading for OPTS Spring Formation" dialog, users of the FBMP software can characterize the following parameters:

- Pier of Interest for OPTS Modeling: the pier from the existing bridge model for which the span-end Spring Formation procedure is to be undertaken.

- OPTS Model Left Span Loading: loading on the left span tip in the X, Y, Z, RX, RY and RZ directions. This loading will be used to generate a spring on the tip node of the left span (relative to the selected "Pier for OPTS").

- OPTS Model Right Span Loading: loading on the right span tip in the X, Y, Z, RX, RY and RZ directions. This loading will be used to generate a spring on the tip node of the right span (relative to the selected "Pier for OPTS").

Implementation of controls that accept user input has been completed, including labeling, positioning, data display, and data storage. The global data structures that store data which are input on the "Loading for OPTS Spring Formation" dialog have also been put into place, as was the exchange of data between the global and local data structures.

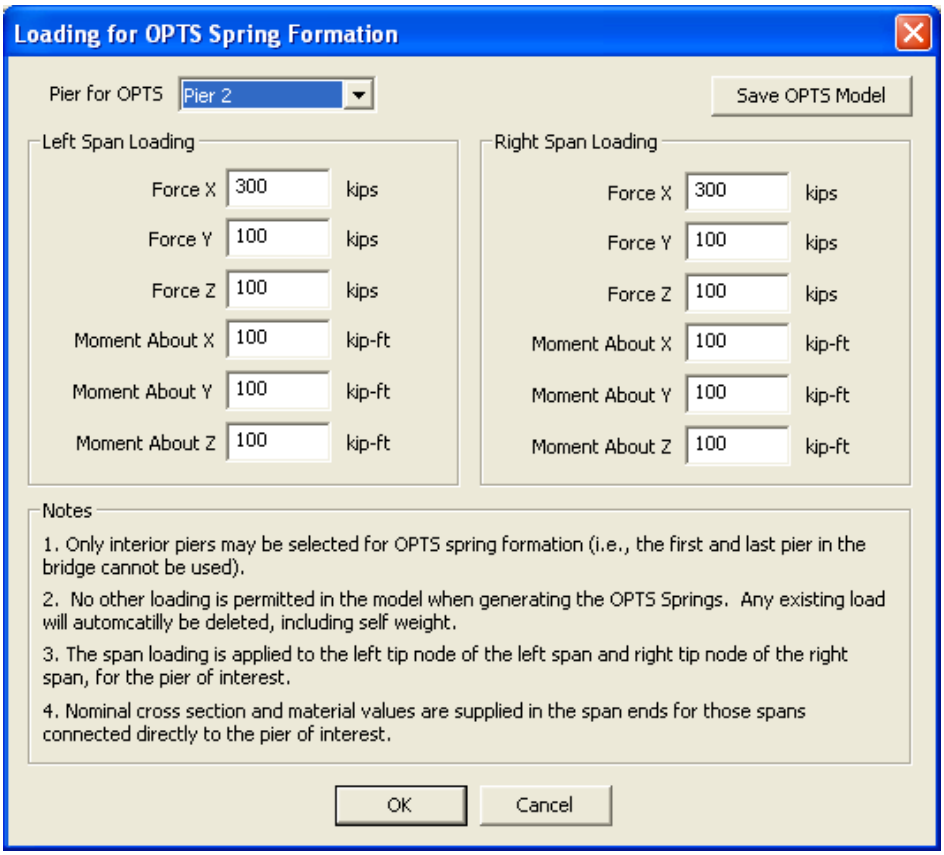

Figure 2.2.5. Loading for OPTS spring formation dialog

2.3 Creation of GUI Graphics

Coding that enables window-view rendering of the OPTS model in 2-dimensional and 3-dimensional form has been completed. The "Bridge Plan View" window, as shown in Fig. 2.3.1, displays the model in plan view. The routines to draw the model in this window have also been fully developed.

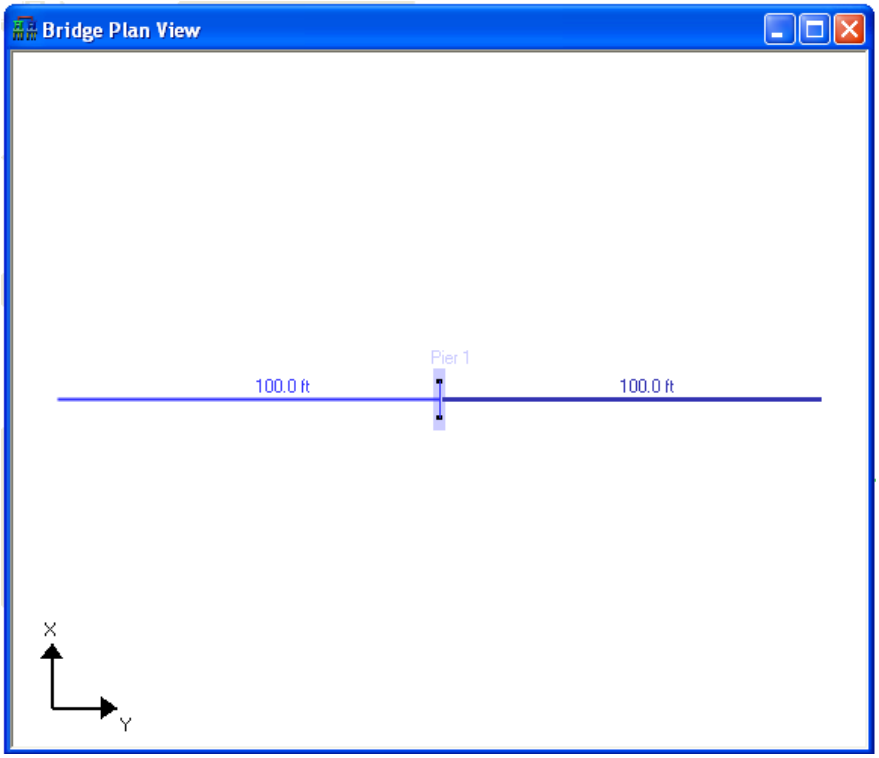

Figure 2.3.1. Bridge plan view

The "3D Bridge View" window, as shown in Figs.2.3.2 and 2.3.3, displays the model in 3D view. The routines to draw the model in this window have been fully developed.

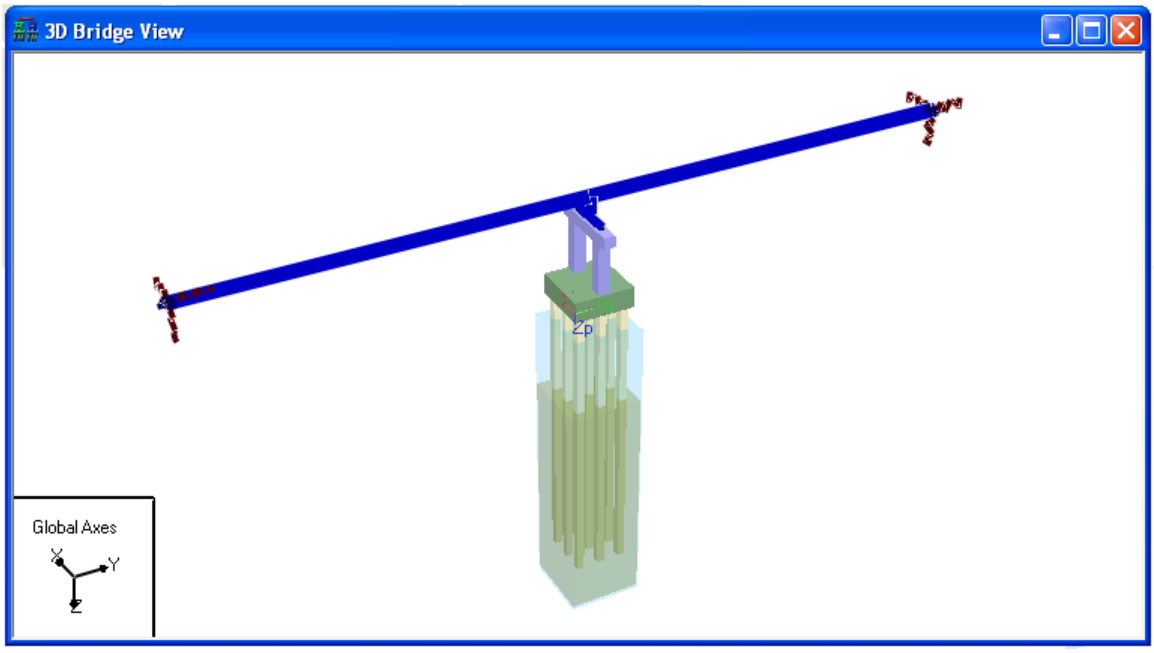

Figure 2.3.2. 3D bridge view (thick view)

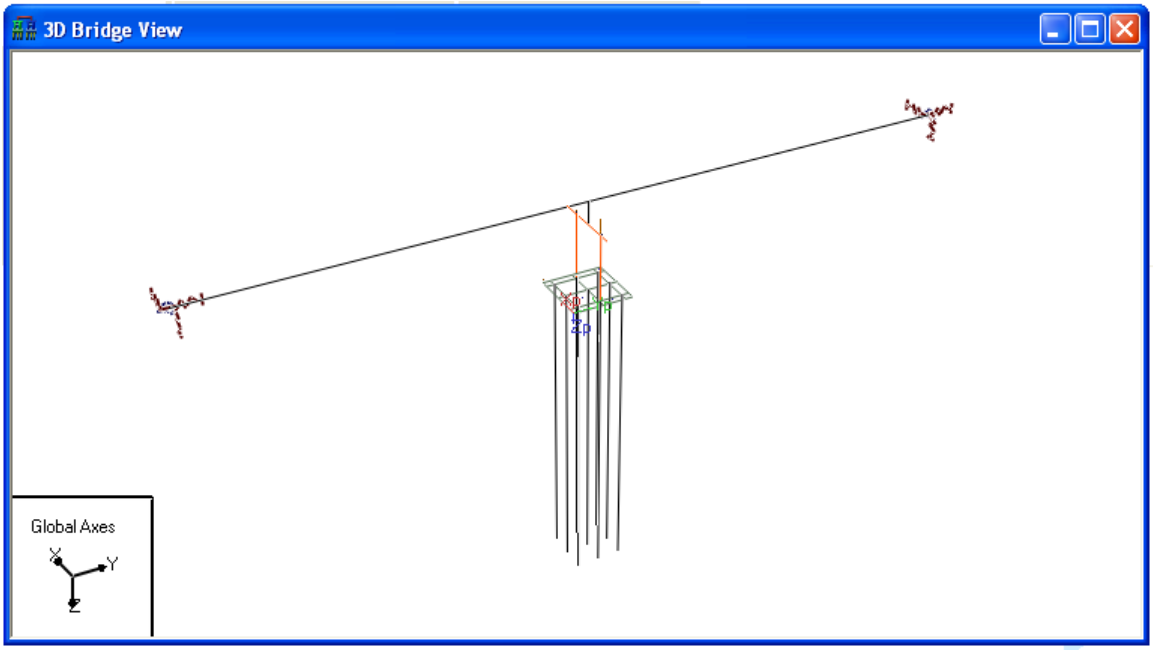

Figure 2.3.3. 3D bridge view (thin element view)

The "3D Results" window, as shown in Fig. 2.3.4, displays the displaced model in 3D view. This includes animated and non-animated view. The routines to draw the model in this window have been fully developed.

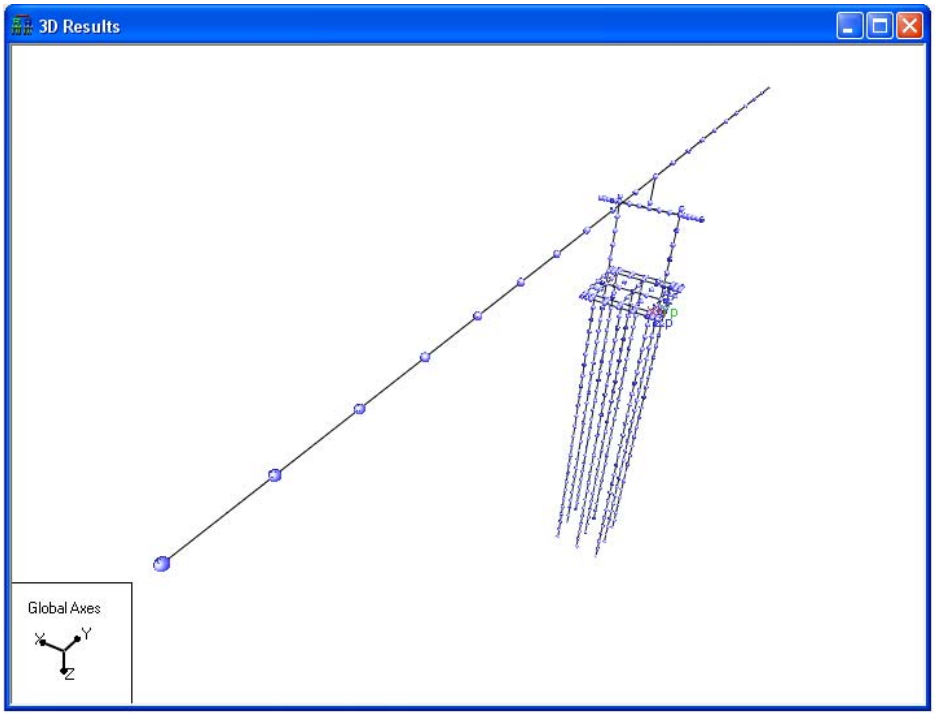

Figure 2.3.4. 3D results window

The software compiler used to build the file containing the GUI features has been verified to be compliant with the currently supported, widely-used operating systems, including Windows 7 and Windows 8. Testing of this GUI's compatibility specific to the newest operating systems, as well as the CVIA and OPTS features usability on the newest operating systems, has been completed.

2.4 Validation of CVIA and OPTS GUI User Input

Validation of CVIA and OPTS GUI user input has been completed. This encompassed the following validation tasks: (a) CVIA and OPTS data input in the aforementioned GUI dialogs is accurately saved to the input file with correct data formatting; (b) CVIA and OPTS data are correctly parsed (read) by the GUI during the reading of the input file; (c) CVIA and OPTS data are correctly loaded into the appropriate dialogs after the input file reading is complete; (d) CVIA and OPTS data are inspected prior to the analysis execution; this is to ensure that all required data are properly input (i.e., required data are not missing), and that the inputted data conforms. For example, certain input parameters must be non-zero in magnitude. Error checking has been completed as well, which ensured that input data meet numerous validity requirements prior to permitting an analysis to be carried out.

2.5 Validation of Analysis Output Displayed in the GUI

Validation of analysis output displayed in the GUI has been completed, where items considered included: (a) Vessel collision time step data displayed on the "Dynamic Animation" dialog; (b) Nodal displacements and rotations for a vessel collision analysis on the "3D Display Control" dialog; (c) Nodal displacements and rotations for an OPTS model on the "3D Display Control" dialog; (d) Pile forces and displacements for a vessel collision analysis on the "Plot Display Control" dialog; (e) Pile forces and displacements for an OPTS model on the "Plot Display Control" dialog; (f) Pier forces for a vessel collision analysis on the "Plot Display Control" dialog; and (g) Pier forces for an OPTS model on the "Plot Display Control" dialog.

2.5.1 Dynamic Animation Dialog

Specific to validation of the vessel collision time step data displayed on the "Dynamic Animation" dialog (Fig. 2.5.1), the number of time steps (i.e., the "Max" value displayed on this dialog) and the time step duration (i.e., the "Time" value displayed on this dialog) has been verified to correspond with ASCII-based text output given in the engine-generated .out file. Also, the set of values displayed in the "Dynamic Animation" dialog has been verified to match analysis engine-generated binary files (.PIL and .NCV files), which hold the corresponding data. This means of verification ensured that the values displayed in the "Dynamic Animation" dialog match those values used by the program module performing the analysis (i.e., the analysis engine). In addition, this verification ensured consistency between the various forms of analysis engine output (i.e., ASCII and binary). In this way, proper FBMP functionality (with respect to GUI processing of dynamic analysis results) was assured not only for vessel collision analyses, but also for general dynamic analyses.

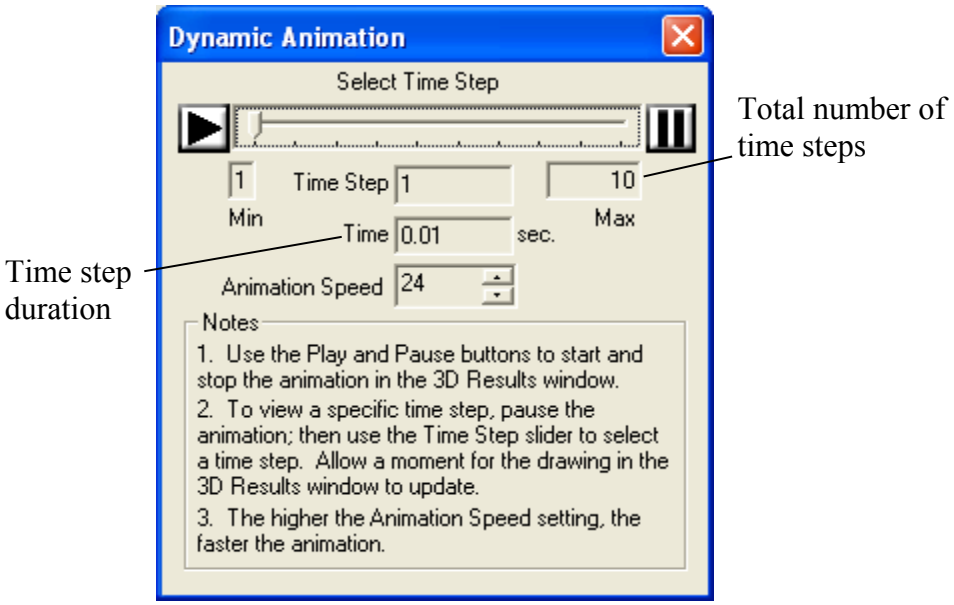

Fig. 2.5.1. Dynamic animation dialog

2.5.2 Nodal Displacements and Rotations for Models Utilizing CVIA

For validation of the nodal displacements and rotations generated as part of a vessel collision analysis on the 3D Display Control dialog: the displacements and rotations displayed on this dialog for the selected node were compared to the text output file (.out file). For example, in Figure 2.5.2, the impact load for a vessel collision analysis is applied at node 17 in the single pier model.

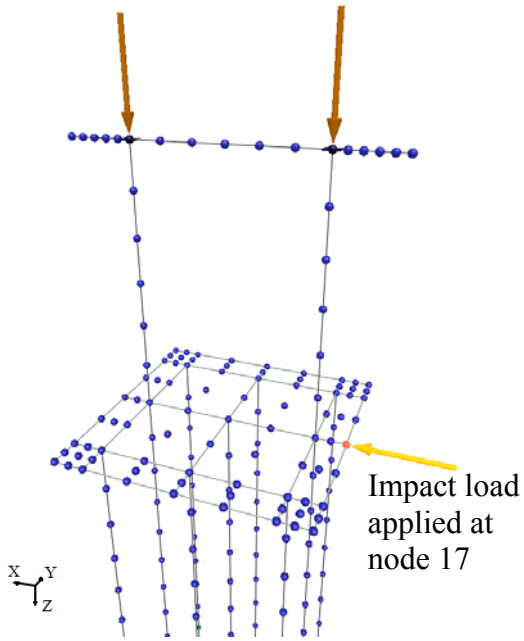

Figure 2.5.2. Structural configuration and loading

For the model shown in Fig. 2.5.2, when time step 1 is displayed on the "Dynamic Animation" dialog (recall Fig. 2.5.1) (or, alternatively, selected in the "Time Step" spinner control in the toolbar), the displacement and rotation data at the impact location (node 17) at time step 1 displays on the "3D Display Control" dialog (Fig. 2.5.3). Specifically, this data displays in the "Translation (Global)" and "Rotation About (Global)" text boxes. This includes the "X", "Y" and "Z" text boxes (Fig. 2.5.3). These displayed values are validated against the analysis-generated text output file (Fig. 2.5.4). For example, both the "3D Display Control" dialog and the text output file display an displacement X value of 0.0105 inches for node 17 in time step 1.

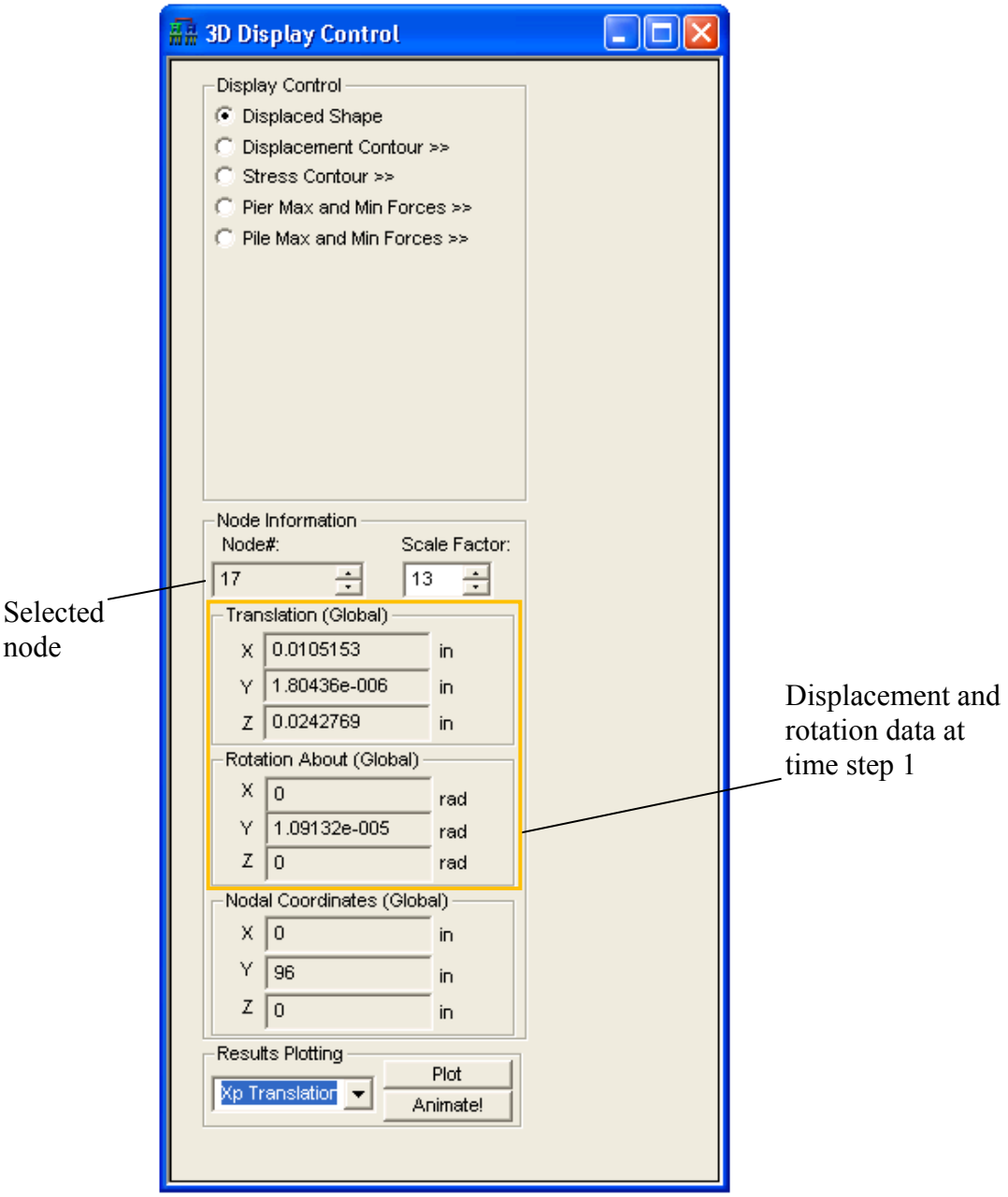

Figure 2.5.3. 3D Display Control dialog data for Node 17

-> TIME STEP # = 1

Pile Cap Displacements (Excluding Pile Heads)

NODE	X	Y	Z	Rx	Ry	Rz
	in	in	in	rad	rad	rad
10	0.9572E-02	0.1661E-03	0.2290E-01	-.1619E-04	0.9315E-05	0.6570E-05
11	0.9094E-02	0.2342E-03	0.2266E-01	-.1562E-04	0.7567E-05	0.1621E-05
12	0.9018E-02	0.2439E-03	0.2209E-01	-.1299E-04	0.1445E-05	-.3032E-06
13	0.8946E-02	0.1472E-03	0.2204E-01	-.1399E-04	-.5242E-05	-.9890E-06
14	0.8887E-02	0.1129E-03	0.2210E-01	-.1285E-04	-.4618E-05	-.1301E-05
15	0.9753E-02	-.1607E-04	0.2328E-01	-.1400E-04	0.7468E-05	0.3168E-05
16	0.8866E-02	0.2785E-04	0.2245E-01	-.1307E-04	-.2937E-05	-.7955E-06
17	0.1052E-01	0.1804E-05	0.2428E-01	0.2121E-07	0.1091E-04	-.1816E-09
18	0.8843E-02	0.1803E-05	0.2330E-01	0.2121E-07	-.4241E-05	0.1723E-09
19	0.9753E-02	0.1966E-04	0.2328E-01	0.1404E-04	0.7467E-05	-.3168E-05
20	0.8866E-02	-.2426E-04	0.2245E-01	0.1311E-04	-.2937E-05	0.7957E-06
21	0.9572E-02	-.1625E-03	0.2289E-01	0.1623E-04	0.9314E-05	-.6570E-05
22	0.9094E-02	-.2306E-03	0.2266E-01	0.1566E-04	0.7566E-05	-.1622E-05
23	0.9018E-02	-.2403E-03	0.2209E-01	0.1303E-04	0.1445E-05	0.3032E-06
24	0.8946E-02	-.1436E-03	0.2204E-01	0.1403E-04	-.5241E-05	0.9892E-06
25	0.8887E-02	-.1093E-03	0.2210E-01	0.1289E-04	-.4618E-05	0.1301E-05
26	0.8843E-02	-.2330E-03	0.2370E-01	-.1351E-04	0.1130E-04	0.0000E+00
27	0.8973E-02	-.2866E-04	0.2321E-01	-.1183E-04	0.9569E-05	0.0000E+00
28	0.8966E-02	-.1175E-04	0.2289E-01	-.1150E-04	0.1536E-05	0.0000E+00
29	0.8962E-02	-.3147E-04	0.2296E-01	-.1362E-04	-.1214E-05	0.0000E+00
30	0.8831E-02	-.1944E-03	0.2402E-01	-.1455E-04	0.1066E-04	0.0000E+00
31	0.9135E-02	-.3977E-04	0.2339E-01	-.1443E-04	0.9465E-05	0.0000E+00
32	0.8970E-02	-.6061E-04	0.2371E-01	-.1356E-04	0.1090E-04	0.0000E+00
33	0.9037E-02	0.9403E-04	0.2294E-01	-.1261E-04	0.7373E-05	0.0000E+00
34	0.8981E-02	0.3113E-04	0.2307E-01	-.1098E-04	0.5527E-05	0.0000E+00
35	0.8962E-02	0.7439E-04	0.2262E-01	-.1195E-04	-.6563E-06	0.0000E+00
36	0.8946E-02	-.1491E-04	0.2306E-01	-.1305E-04	-.4936E-06	0.0000E+00
37	0.8931E-02	0.3203E-04	0.2266E-01	-.1315E-04	-.3277E-05	0.0000E+00
38	0.8968E-02	-.2715E-04	0.2317E-01	-.1389E-04	-.1679E-05	0.0000E+00
39	0.8893E-02	-.1446E-03	0.2410E-01	-.1434E-04	0.1045E-04	0.0000E+00
40	0.9049E-02	0.5472E-04	0.2373E-01	-.1189E-04	0.1023E-04	0.0000E+00
41	0.8960E-02	0.4069E-04	0.2340E-01	-.1142E-04	0.2151E-05	0.0000E+00
42	0.8939E-02	-.1462E-06	0.2333E-01	-.1378E-04	-.1535E-05	0.0000E+00
43	0.8845E-02	-.1198E-03	0.2489E-01	-.8899E-05	0.1316E-04	0.0000E+00
44	0.9338E-02	0.1850E-04	0.2429E-01	-.9142E-05	0.1095E-04	0.0000E+00
45	0.9246E-02	0.1822E-05	0.2490E-01	-.8772E-05	0.1280E-04	0.0000E+00
46	0.9124E-02	0.4411E-04	0.2347E-01	-.7743E-05	0.8841E-05	0.0000E+00
47	0.9034E-02	0.5325E-04	0.2390E-01	-.6993E-05	0.6512E-05	0.0000E+00
48	0.8958E-02	0.3138E-04	0.2315E-01	-.7780E-05	-.1805E-05	0.0000E+00
49	0.8912E-02	0.1828E-05	0.2416E-01	-.8331E-05	0.1054E-05	0.0000E+00
50	0.8899E-02	0.7749E-05	0.2347E-01	-.8356E-05	-.2249E-05	0.0000E+00
51	0.8932E-02	-.4755E-05	0.2394E-01	-.8445E-05	-.2404E-05	0.0000E+00
52	0.9246E-02	0.1829E-05	0.2505E-01	0.2294E-07	0.1385E-04	0.0000E+00
53	0.9246E-02	0.1821E-05	0.2444E-01	0.2294E-07	0.1215E-04	0.0000E+00
54	0.8912E-02	0.1821E-05	0.2420E-01	0.2294E-07	0.1134E-05	0.0000E+00
55	0.8912E-02	0.1828E-05	0.2415E-01	0.2294E-07	-.3122E-05	0.0000E+00
56	0.8845E-02	0.1235E-03	0.2489E-01	0.8942E-05	0.1316E-04	0.0000E+00
57	0.9338E-02	-.1488E-04	0.2429E-01	0.9184E-05	0.1095E-04	0.0000E+00
58	0.9246E-02	0.1832E-05	0.2490E-01	0.8816E-05	0.1280E-04	0.0000E+00
59	0.9124E-02	-.4050E-04	0.2347E-01	0.7785E-05	0.8840E-05	0.0000E+00
60	0.9034E-02	-.4962E-04	0.2390E-01	0.7036E-05	0.6512E-05	0.0000E+00
61	0.8958E-02	-.2777E-04	0.2314E-01	0.7822E-05	-.1805E-05	0.0000E+00
62	0.8912E-02	0.1825E-05	0.2416E-01	0.8375E-05	0.1054E-05	0.0000E+00
63	0.8899E-02	-.4125E-05	0.2347E-01	0.8397E-05	-.2249E-05	0.0000E+00

Figure 2.5.4. Text output file with displacement and rotation data at node 17

2.5.3 Nodal Displacements and Rotations for OPTS Models

For validation of the nodal displacements generated as part of an analysis where OPTS modeling is employed, again, focus was placed on data presented via the "3D Display Control" dialog. In this way, the validation closely paralleled that used in the vessel collision validation

efforts (discussed in Sec. 2.5.2). Alternatively stated, for instances where OPTS models are employed, data displayed on the "3D Display Control" are found to match ASCII-based and binary output.

2.5.4 Pile Forces for Models Utilizing CVIA

For validation of the pile forces for a vessel collision analysis on the "Plot Display Control" dialog: the member forces (Shear 2, Shear 3, Moment 2, Moment 3, Axial, D/C Ratio), pile displacements (Lateral X, Lateral Y, Rotation About X, Rotation About Y), and soil forces (Soil Axial, Soil Lateral X, Soil Lateral Y, Soil Torsion) displayed on this dialog for the selected pile were compared to the text output file (.out file). For example, in Fig. 2.5.5, pile 4 is selected in the "Pile Selection" window. Pile 4 is the pile located nearest the vessel collision impact load applied to node 17, as described previously. On the "Plot Display Control" dialog, a member force is selected. For this example, "Moment 3" is selected (Fig. 2.5.6). The "Max" and "Min" Moment 3 values display for Pile 4 for the currently selected time step (time step 1) (Fig. 2.5.6), and the Moment 3 plot for pile 4 displays in the "Moment 3" plot window (Fig. 2.5.7). The "Max" and "Min" values are compared to the analysis-generated text output file (Fig. 2.5.8). For example, the "Plot Display Control" dialog, "Moment 3" plot window, and text output file all display a Moment 3 minimum value of -3.48 kip-ft for pile 4 in time step 1.

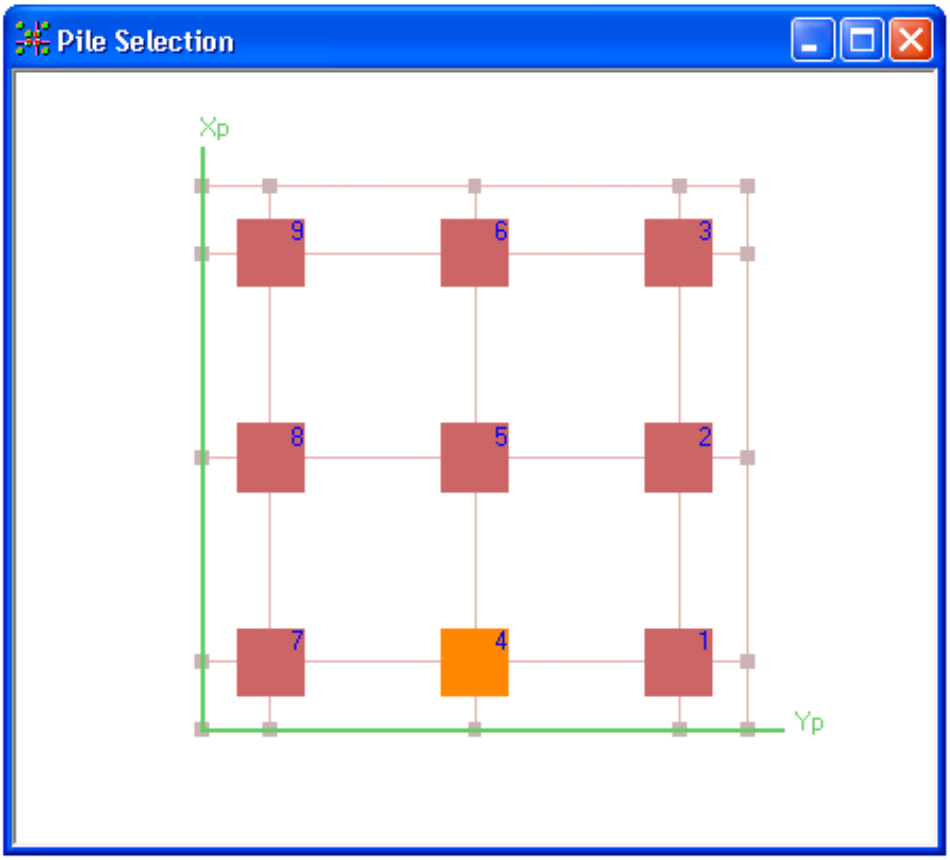

Figure 2.5.5. Pile Selection window with pile 4 selected

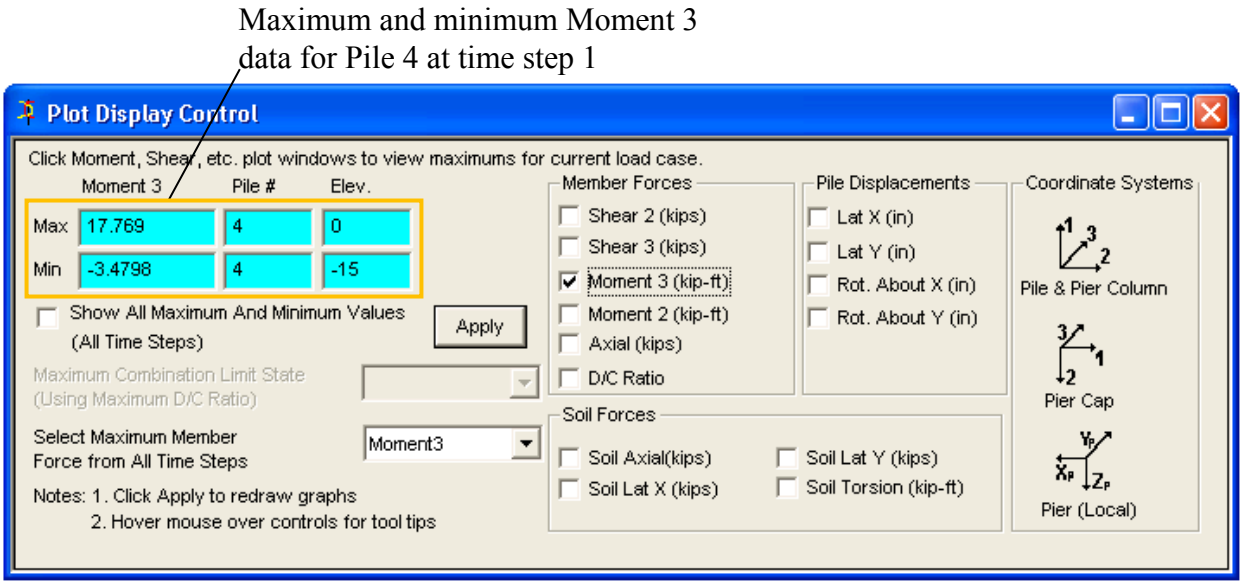

Figure 2.5.6. Plot Display Control dialog with Moment 3 data displayed for Pile 4 at time step 1

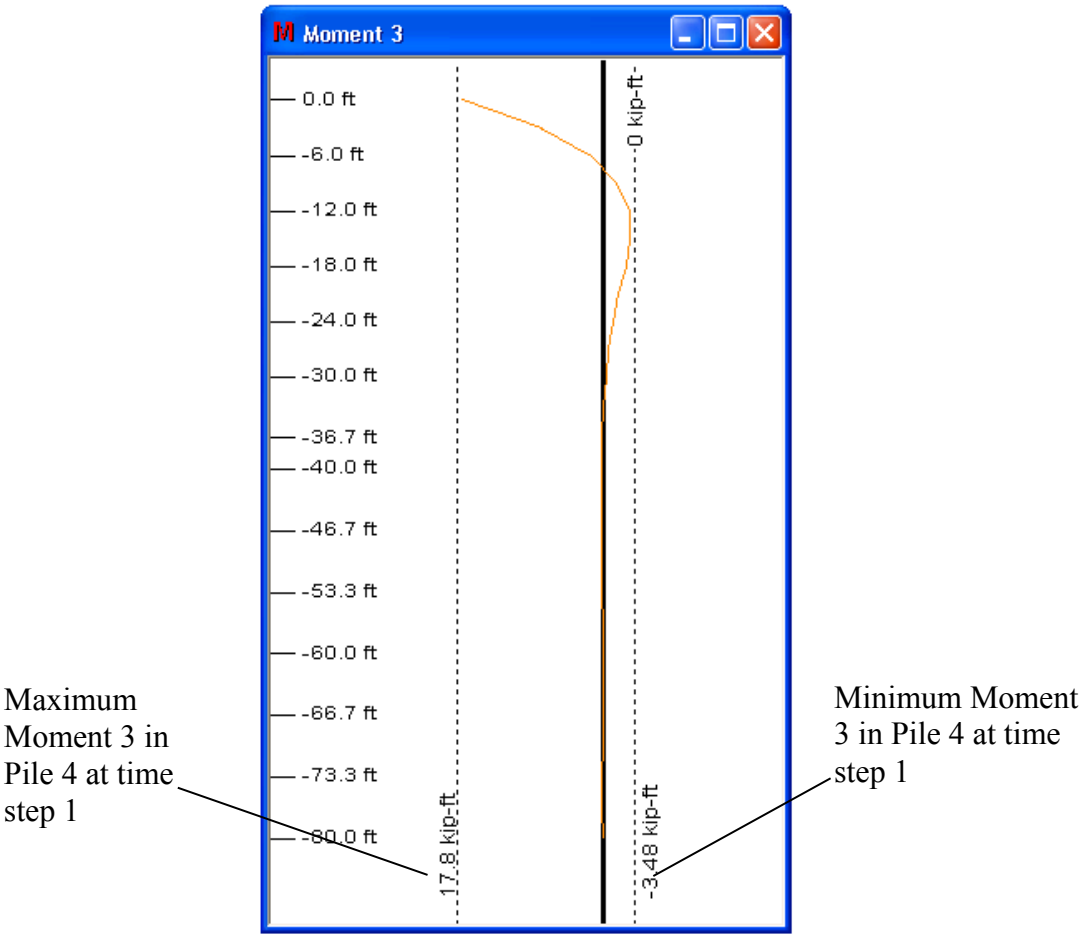

Figure 2.5.7. Moment 3 plot window for Pile 4 at time step 1

-> TIME STEP # = 1

- Pile Number 4 -

ELEM NO.	PROP NO.	NODE NO.	LOAD CASE	FAX kips	F22 kips	F33 kips	M22 kip-ft	M33 kip-ft	TORQUE kip-ft	D/C Ratio
112	1	4	1	-39.38	3.32	0.00	0.00	-17.77	0.00	0.04
	1	186	1	39.53	-3.32	0.00	0.00	7.81	0.00	0.03
113	1	186	1	-36.78	2.12	0.00	0.00	-7.85	0.00	0.03
	1	187	1	38.58	-2.12	0.00	0.00	1.49	0.00	0.02
114	1	187	1	-36.25	1.16	0.00	0.00	-1.54	0.00	0.02
	1	188	1	38.05	-1.16	0.00	0.00	-1.94	0.00	0.02
115	1	188	1	-35.70	0.48	0.00	0.00	1.88	0.00	0.02
	1	189	1	37.00	-0.48	0.00	0.00	-3.33	0.00	0.02
116	1	189	1	-34.57	0.06	0.00	0.00	3.29	0.00	0.02
	1	190	1	35.62	-0.06	0.00	0.00	-3.48	0.00	0.02
117	1	190	1	-33.21	-0.16	0.00	0.00	3.45	0.00	0.02
	1	191	1	34.26	0.16	0.00	0.00	-2.97	0.00	0.02
118	1	191	1	-31.92	-0.24	0.00	0.00	2.95	0.00	0.02
	1	192	1	32.98	0.24	0.00	0.00	-2.22	0.00	0.02
119	1	192	1	-30.70	-0.25	0.00	0.00	2.21	0.00	0.02
	1	193	1	31.75	0.25	0.00	0.00	-1.47	0.00	0.02
120	1	193	1	-29.55	-0.21	0.00	0.00	1.47	0.00	0.02
	1	194	1	30.60	0.21	0.00	0.00	-0.85	0.00	0.02
121	1	194	1	-28.45	-0.16	0.00	0.00	0.85	0.00	0.02
	1	195	1	29.51	0.16	0.00	0.00	-0.38	0.00	0.02
122	1	195	1	-26.97	-0.11	0.00	0.00	0.38	0.00	0.02
	1	196	1	28.14	0.11	0.00	0.00	-0.02	0.00	0.02
123	1	196	1	-25.17	-0.05	0.00	0.00	0.02	0.00	0.02
	1	197	1	26.34	0.05	0.00	0.00	0.16	0.00	0.02
124	1	197	1	-23.39	-0.01	0.00	0.00	-0.16	0.00	0.02
	1	198	1	24.56	0.01	0.00	0.00	0.20	0.00	0.02
125	1	198	1	-21.63	0.01	0.00	0.00	-0.20	0.00	0.01
	1	199	1	22.80	-0.01	0.00	0.00	0.16	0.00	0.01
126	1	199	1	-19.89	0.02	0.00	0.00	-0.16	0.00	0.01
	1	200	1	21.06	-0.02	0.00	0.00	0.10	0.00	0.01
127	1	200	1	-18.16	0.02	0.00	0.00	-0.10	0.00	0.01
	1	201	1	19.32	-0.02	0.00	0.00	0.04	0.00	0.01
128	1	201	1	-16.43	0.01	0.00	0.00	-0.04	0.00	0.01
	1	202	1	17.60	-0.01	0.00	0.00	0.01	0.00	0.01
129	1	202	1	-14.71	0.00	0.00	0.00	-0.01	0.00	0.01
	1	203	1	15.88	0.00	0.00	0.00	-0.01	0.00	0.01
130	1	203	1	-12.99	0.00	0.00	0.00	0.01	0.00	0.01
	1	204	1	14.15	0.00	0.00	0.00	-0.01	0.00	0.01
131	1	204	1	-11.26	0.00	0.00	0.00	0.01	0.00	0.01
	1	205	1	12.43	0.00	0.00	0.00	-0.01	0.00	0.01
132	1	205	1	-9.52	0.00	0.00	0.00	0.01	0.00	0.01
	1	206	1	10.69	0.00	0.00	0.00	0.00	0.00	0.01
133	1	206	1	-7.77	0.00	0.00	0.00	0.00	0.00	0.01
	1	207	1	8.94	0.00	0.00	0.00	0.00	0.00	0.01
134	1	207	1	-6.00	0.00	0.00	0.00	0.00	0.00	0.00
	1	208	1	7.17	0.00	0.00	0.00	0.00	0.00	0.00
135	1	208	1	-4.20	0.00	0.00	0.00	0.00	0.00	0.00
	1	209	1	5.37	0.00	0.00	0.00	0.00	0.00	0.00
136	1	209	1	-2.37	0.00	0.00	0.00	0.00	0.00	0.00
	1	210	1	3.53	0.00	0.00	0.00	0.00	0.00	0.00

Figure 2.5.8. Text output file showing Moment 3 data for Pile 4 at time step 1

2.5.5 Pile Forces for Models Utilizing OPTS Modeling

For validation of the pile forces for an OPTS model, with focus on the "Plot Display Control" dialog: the validation methods employed paralleled those used for the vessel collision validation (discussed in Sec. 2.5.4). Consequently, data displayed on "Plot Display Control" dialog and the "Moment 3" plot window were validated against the ASCII-based (text) output file.

2.5.6 Pier Forces for Models Utilizing CVIA

For validation of the pier forces for a vessel collision analysis on the "Plot Display Control" dialog: the member forces (Shear 2, Shear 3, Moment 2, Moment 3, Axial, D/C Ratio) displayed on this dialog for the selected pier component (column or pier cap) were compared to

the text output file (.out file). For example, in Fig. 2.5.9, column 1 is selected in the "Pier Selection" window. Column 1 is the column located nearest the vessel collision impact as described previously. On the "Plot Display Control" dialog, a member force is selected. For this example, "Moment 3" is selected (Fig. 2.5.10). The "Max" and "Min" Moment 3 values display for column 1 for the currently selected time step (time step 1), and the Moment 3 plot for column 1 displays in the "Moment 3" plot window (Fig. 2.5.11). The "Max" and "Min" value are compared to the analysis-generated text output file (Fig. 2.5.12). For example, the "Plot Display Control" dialog, "Moment 3" plot window, and text output file all display a Moment 3 minimum value of -58.9 kip-ft for column 1 in time step 1.

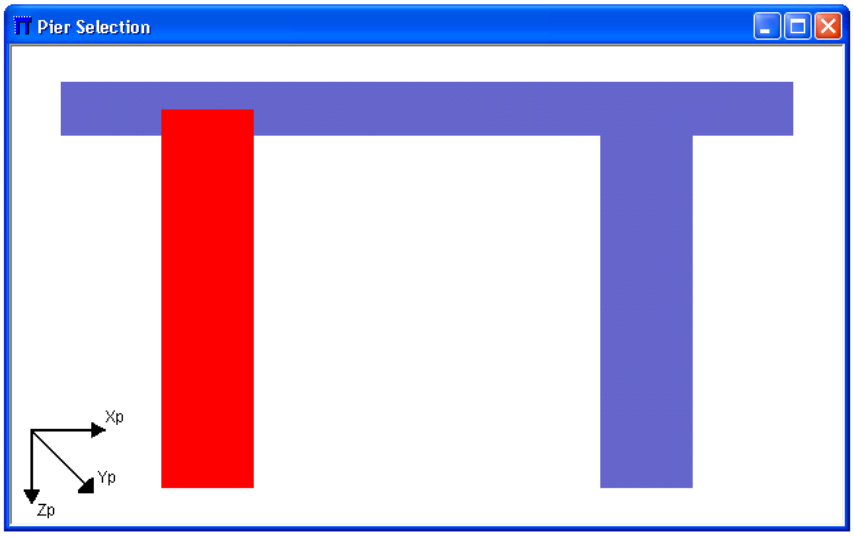

Figure 2.5.9. Pier Selection window with Column 1 selected

Maximum and minimum Moment 3 data for Column 1 at time step 1

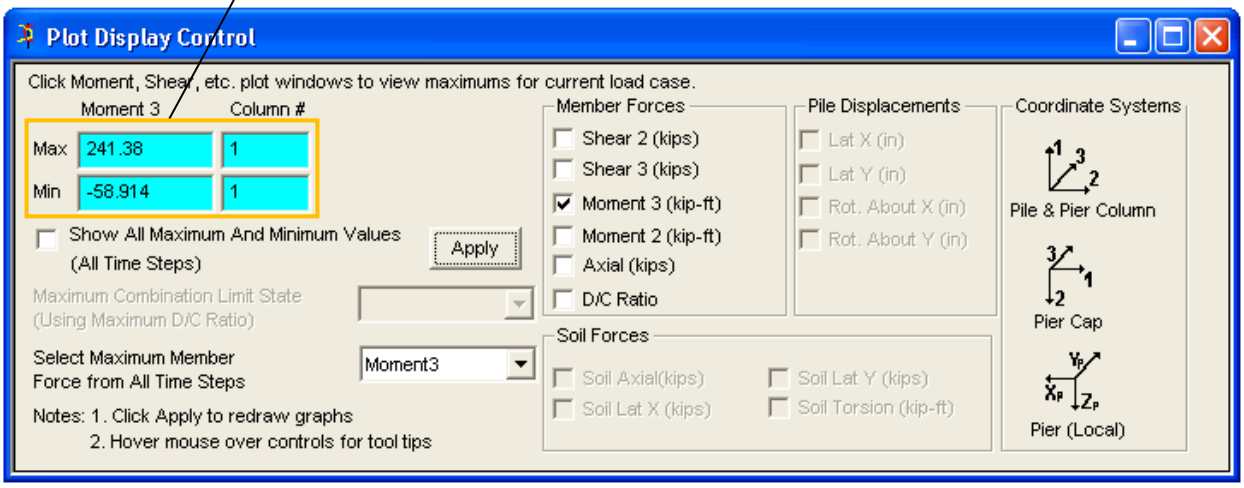

Figure 2.5.10. Plot Display Control dialog with Moment 3 data for Column 1 at time step 1

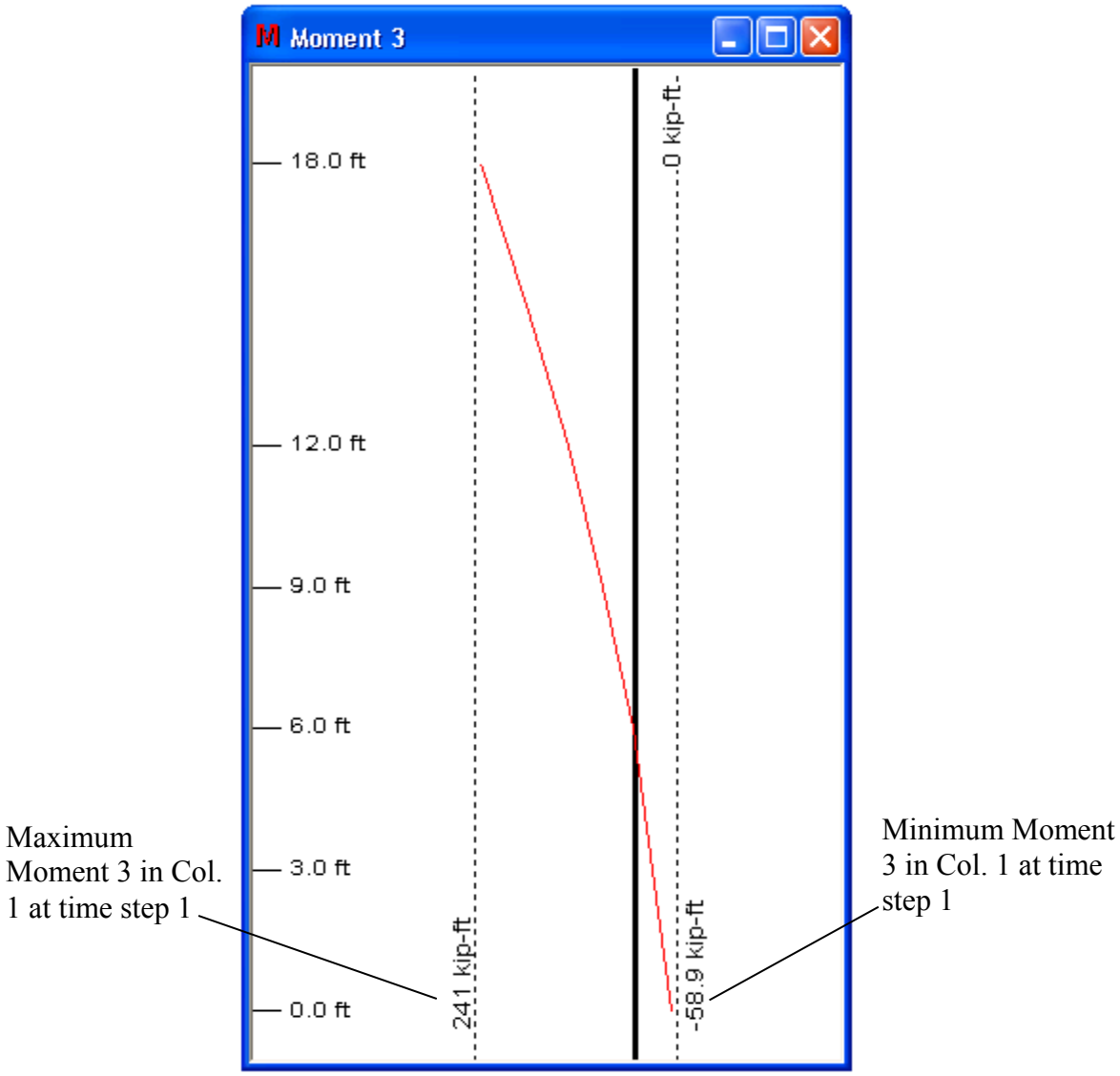

Figure 2.5.11. Moment 3 plot window for Column 1 at time step 1

-> TIME STEP # = 1

- Column Segments For Column Number 1

ELEM	PROP	NODE	LOAD	FAX	F22	F33	M22	M33	TORQUE	D/C
9	2	82	1	221.90	-9.09	0.02	-0.12	-58.91	0.00	0.05
	2	83		-221.57	9.09	-0.02	0.07	31.66	0.00	0.04
10	2	83	1	228.81	-11.99	0.02	-0.07	-31.69	0.00	0.04
	2	84		-224.76	11.99	-0.02	0.02	-4.29	0.00	0.04
11	2	84	1	231.61	-15.12	0.02	-0.02	4.24	0.00	0.04
	2	85		-227.56	15.12	-0.02	-0.04	-49.59	0.00	0.05
12	2	85	1	234.81	-18.43	0.02	0.04	49.58	0.00	0.05
	2	86		-230.76	18.43	-0.02	-0.11	-104.85	0.00	0.06
13	2	86	1	238.42	-21.59	0.03	0.11	104.94	0.00	0.06
	2	87		-234.37	21.59	-0.03	-0.19	-169.64	0.00	0.08
14	2	87	1	242.87	-23.86	0.03	0.19	169.92	0.00	0.08
	2	88		-240.84	23.86	-0.03	-0.29	-241.38	0.00	0.10

Figure 2.5.12. Text output file showing Moment 3 data for Pile 4 at time step 1

2.5.7 Pier Forces for Models Utilizing OPTS Modeling

For validation of the pier forces generated in association with use of an OPTS model, with emphasis on the "Plot Display Control" dialog: the validation methods employed paralleled those used for the vessel collision validation (discussed in Sec. 2.5.6). Alternatively stated, data displayed on the "Plot Display Control" dialog and the "Moment 3" plot window were validated against the ASCII-based text output file.

2.6 Development of OPTS License Scheme

A plan was established to integrate CVIA-OPTS modeling directly within the licensing structure of pre-existing (current) FBMP license options. Accordingly, vessel collision analysis would be available in the following dynamic analysis license types: (a) Single Pier Modeling with Dynamics; (b) Three Pier Modeling with Dynamics; and (c) Full Bridge Modeling with Dynamics. Also, the OPTS modeling option would be available in the following static and dynamic analysis license types: (a) Single Pier Modeling without Dynamics; (b) Single Pier Modeling with Dynamics; (c) Three Pier Modeling with Dynamics; and (d) Full Bridge Modeling with Dynamics.

In this way, the need to carry out modifications to existing in-house license security key coding was precluded, because the CVIA feature was subsumed within existing dynamic licensing. Similarly, the as-planned OPTS licensing structure fell directly within the pre-existing license options. Further, the above-defined licensing scheme precluded the need to conduct any operating system compatibility checks beyond those that were already in place for the pre-existing licensing options.

CHAPTER 3
ANALYSIS ENGINE DEVELOPMENT

3.1 Development of CVIA Input Reading Routines

The CVIA input reading routines have been fully implemented in the analysis engine. After testing of the GUI CVIA implementation was undertaken as part of the development of the GUI CVIA module (see chapter 2.1), parameters necessary to characterize a given collision scenario were identified and finalized. Accordingly, the finalized list of parameters that must be supplied in text input files is given below, where formatting matches that pertaining to FBMP model (text) input files. Note that, although text file input formatting is necessarily documented below, the recommended method for creating models in FBMP is through use of the GUI.

3.1.1 Coupled Vessel Impact Analysis (CVIA) Final Input Parameter List for Text-File Input

With the COUPLED header active, FBMP conducts an impact analysis on the pier structure based upon the characteristics of a moving vessel. Using vessel weight and initial velocity, as well as the load-deformation characteristics of the vessel bow, the impact loading can be quantified at each time step, and applied to the impacted pier. The vessel bow can be characterized using elastic-plastic behavior, or arbitrarily defined bow load-deformation data. To use the COUPLED analysis feature, the external force modification flag (MODEXT) must be set to "1" in the LOADYN header.

COUPLED
D=IDEFN I=IVTYPE W=WB V=VBIX,VBIY

IDEFN	is the vessel definition method [Pre-defined=1, User-defined=2]
IVTYPE	is the vessel type: If definition is Pre-defined (IDEFN=1): IVTYPE=1 indicates the vessel is a barge If definition is User-defined (IDEFN=2) IVTYPE=1 indicates the vessel is defined by an elastic, perfectly-plastic curve IVTYPE=2 indicates the vessel is defined by general load and unloading curves
WB	is the weight of the vessel
VBIX	is the initial velocity of the vessel in the x-direction
VBIY	is the initial velocity of the vessel in the y-direction

- If IDEFN=1 and IVTYPE=1 (Pre-defined vessel, barge)

W=WIDTH S=SURF

WIDTH	is the effective impact zone width on the vessel bow
SURF	is the shape of the impact surface (1=planar surface, 2=non-planar surface)

- If IDEFN=2 and IVTYPE=1 (User-defined vessel, elastic, perfectly-plastic)

A=ABY P=PBY

ABY is the crush depth at yield for the vessel bow
PBY is the yield load for the vessel bow

- If IDEFN=2 and IVTYPE=2 (User-defined, general loading and unloading)

N=NABPB

NABPB is the number of points in bow force-deformation curve [limited to 200 points]

AB(1) PB(1)
AB(2) PB(2)
AB is the abscissa for the user-defined vessel bow load-deformation curve
PB is the ordinate for the user-defined vessel bow load-deformation curve

N=NABPBU X=ABMAXU

NABPBU is the number of points in current unloading curve [limited to 25 points]
ABMAXU is the crush level at which the loading and unloading curves intersect

ABU(1) PBU(1)
ABU(2) PBU(2)

ABU is the abscissa for the current user-defined vessel bow unloading curve
PBU is the ordinate for the user-defined vessel bow unloading curve

To clarify the above input layout, consider the following examples that make use of CVIA:

Example 1. A 1,900 ton (3,800 kip) barge traveling at 3 knots (5.06 ft/s) in the x-direction impacting head-on with a 5 ft wide rectangular pier column.

Necessary Input:
COUPLED
D=1 **I**=1 **W**=3800 **V**=5.06**,**0 **A**=90
W=5 **S**=1

Example 2. Two 1,900 ton (3,800 kip) barges traveling at 4.5 knots (7.60 ft/s) with equal velocity components in the x-direction and y-direction, impacting a 4 ft wide circular pier column.

Necessary Input:
COUPLED
D=1 **I**=1 **W**=7600 **V**=5.37**,**5.37
W=4 **S**=2

Example 3. One empty vessel (280 ton, 560 kip) traveling at 0.5 knots (0.84 ft/s) in the x-direction, impacting a bridge pier. Sufficient data are available to, for the impact scenario, characterize the barge yield deformation as 2 in. and the corresponding impact load at this deformation level is determined to be 1,400 kips.

Necessary Input:
COUPLED
D=2 **I**=1 **W**=7600 **V**=0.84**,**0
A=2 **P**=1400

3.2 Update of CVIA Engine Subroutines

A research-based CVIA subroutine (Consolazio and Cowan, 2005) was previously created in the FBMP analysis engine, and as part of the current study, modifications were made to the subroutine to accommodate the input layout defined above. Furthermore, testing of the input file reading portion of the subroutine (to ensure robustness of the input-reading control logic) has been completed.

In conjunction with the CVIA input reading routines, the empirical equations that govern pre-defined barge bow crushing behavior (i.e., force-deformation behavior) were updated based on research given in Chapter 9 of Consolazio et al. (2010). More specifically, the process schematic given in Fig. 3.2.1 was implemented into the subroutine epabypby.f, which is called by the CVIA routines when barge impact analyses that utilize pre-defined barge bow crush-curves are being conducted.

The process summarized in Fig. 3.2.1 governs pre-defined impacts on both flat and round impact surfaces (e.g., pier columns), where barge bow crushing behavior is approximated by elastic-perfectly plastic force-deformation relationships. For flat-faced (square, rectangular) surfaces of a given width, wp, and a relative deviation angle, θ, between the barge-surface, the plastic barge impact force is given by:

$$P_{BY}(w_P, \theta) = 1400 + \left[130 - \frac{68}{1 + e^{3.8 - 0.31 \cdot \theta}} \right] \cdot w_P \qquad \text{(Eq. 3.2.1)}$$

Importantly, Eq. 3.2.1 was developed to conservatively account for variations in the deviation, given the expected value of the deviation angle (θ). The barge bow deformation (a_{BY}) that corresponds to yielding of the barge (and, simultaneously, a force level of P_{BY}) is set to 2 in, per Consolazio et al. (2010). Summarily, an elastic-perfectly plastic force deformation curve is constructed based on P_{BY} and a_{BY}, where elastic barge crushing behavior is assumed up to a barge bow deformation level of 2 in.

For barge impacts on round surfaces, elastic-perfectly plastic force-deformation curves are formed based on a barge bow yield deformation (a_{BY}) of 2 in. per Consolazio et al. (2010) and a maximum impact force (P_{BY}) that is calculated as:

$$P_{BY}(w_P) = 1400 + 30 \cdot w_P \qquad \text{(Eq. 3.2.2)}$$

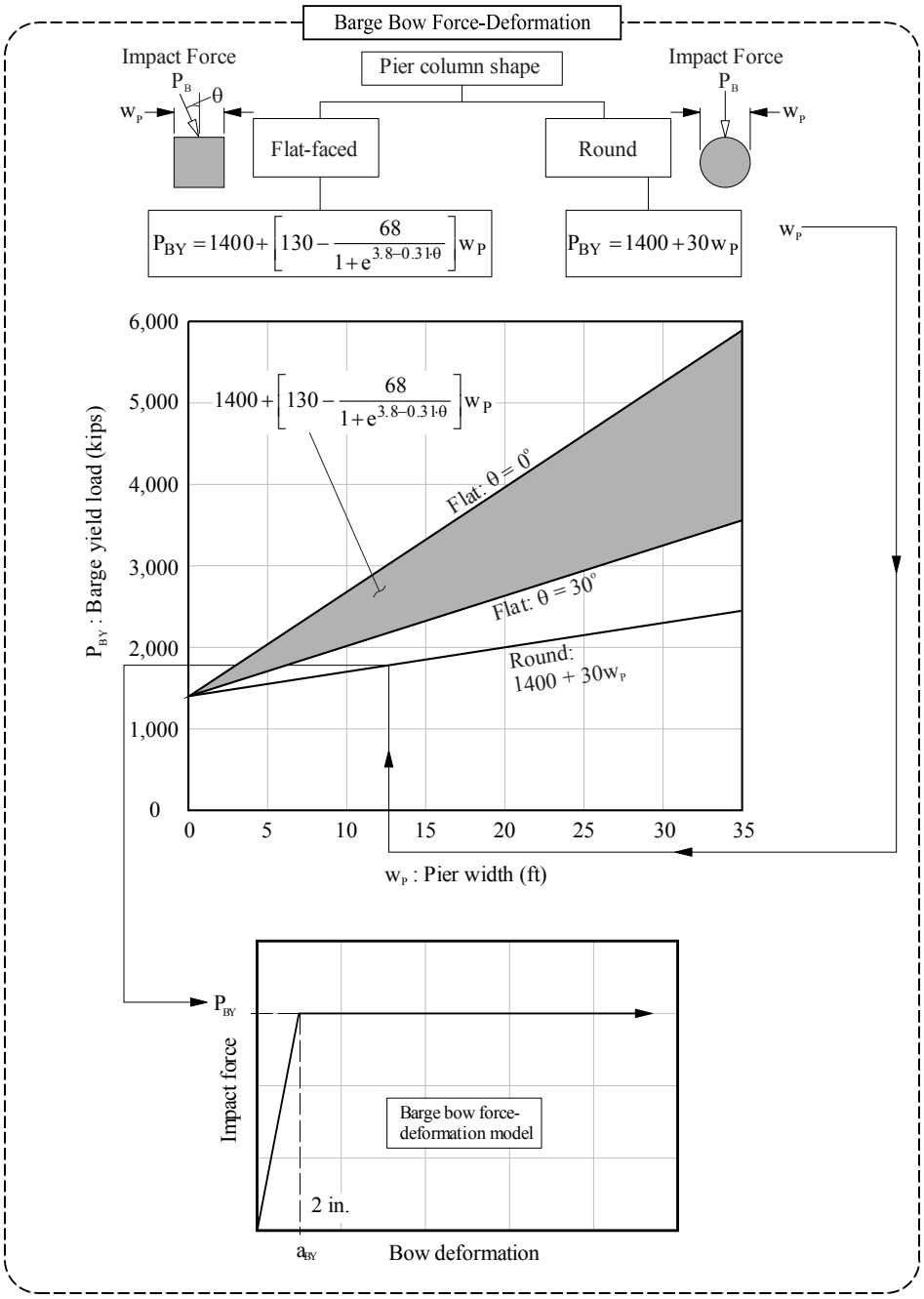

Figure 3.2.1. Schematic of empirical equations used to form pre-defined barge bow force-deformation relationships (Consolazio et al., 2010)

3.3 Implementation of OPTS Modeling Routines

In accordance with the newly developed GUI dialogs that facilitate OPTS modeling, and as part of the development of the GUI OPTS Model (see chapter 2), parallel efforts were made to implement OPTS modeling routines within the FBMP analysis engine, in satisfying the creation of the GUI graphics (see chapter 2.3). Building on control logic that was previously developed within the analysis engine, OPTS modeling consists of manipulation of numerous pier geometry and span geometry subroutines. Accordingly, the finalized list of parameters that must be supplied in FBMP model (text) input files is given below.

3.3.1 One-Pier Two-Span (OPTS) Modeling Final Input Parameter List for Text-File Input

The OPTS header contains input to determine whether or not a one-pier two-span analysis will be conducted. If OPTS analysis is utilized, then the input file must also contain the x-axis, y-axis, and z-axis (all parallel to the respective global axes) offsets from the top node of the vertical link element (see Transfer Beam Properties in the FBMP help manual, Chung 2014a) of the pier. Used in conjunction with appropriately determined span springs and span masses, OPTS analysis employs a single pier and two spans to produce output of similar accuracy with respect to that obtained from analyzing a full multiple-pier model (see Davidson 2007).

OPTS
X=SXPXL Y=SPYL Z=SPZL
X=SXPXR Y=SPYR Z=SPZR

SPXL is the x-axis offset from the top of the vertical links of the pier to the end-node of the left span.
SPYL is the y-axis offset from the top of the vertical links of the pier to the end-node of the left span.
SPZL is the z-axis offset from the top of the vertical links of the pier to the end-node of the left span.
SPXR is the x-axis offset from the top of the vertical links of the pier to the end-node of the right span.
SPYR is the y-axis offset from the top of the vertical links of the pier to the end-node of the right span.
SPZR is the z-axis offset from the top of the vertical links of the pier to the end-node of the right span.

Notes:
5. In the English system, units are feet for span offsets.
6. In the SI system, units are meters for span offsets.

OPTS models are initialized using a control logic flag in the main engine routine. Additionally, span offset variables are initialized, where these offsets are used to dictate span lengths for the left and right spans of the OPTS model. The control logic flag that indicates use of the OPTS feature, as well as the span offsets, is then called by subroutines to properly initialize intermediate superstructure elements such that only those elements above the single

pier are supplied with non-zero properties. Further, while input are needed to define the left and right spans of the OPTS model, appropriate shifts in the pier numbering are included so that only the pier that resides between the left and right spans are defined. In this way, only the single, central pier, the overlying intermediate superstructure elements (the left and right spans) will be defined when the OPTS modeling feature is activated.

3.4 Update of Dynamic Relaxation Analysis Feature

Dynamic relaxation has been available as an FBMP feature since 2009 (Chung 2014a), and allows for permanent loading (e.g., dead loads) to be incorporated into dynamic (time-history) analyses in such a way that the introduction of the permanent loads into the dynamic system do not artificially excite the system mass. The FBMP GUI includes the Dynamic Relaxation Option in conjunction with the batch processing (i.e., direct use of the analysis engine) feature. As a result, multiple models can be analyzed in a single batch process through direct calls to the analysis engine for simulating system equilibrium under quasi-static loads prior to dynamic excitation. Shown in Fig. 3.4.1 is a schematic depiction of the use of dynamic relaxation in conjunction with CVIA, where the schematic itself was developed as part of an effort to document several pre-existing (and relevant to vessel collision loading) analytical features in Consolazio et al. (2010).

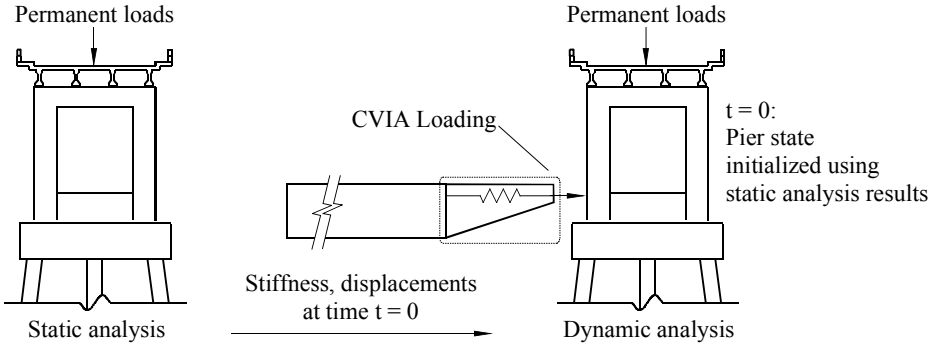

Figure 3.4.1. Incorporation of permanent loads into dynamic analysis

As part of the current project, the dynamic relaxation analysis feature was examined, and updated so as to allow for the initialization of a wider array of dynamic (time-history) analysis bridge models (Chung 2014a). More specifically, the dynamic relaxation feature was enhanced such that pier, bridge, and OPTS models that contain discrete springs or discrete masses attached to any pier elements (as opposed to just span elements) can also utilize dynamic relaxation. This enhancement is important to bridge modeling because it enables users of FBMP to account for both the stiffness and mass of those bridge portions not included in a multiple-pier, multiple-span model by placing springs and lumped masses at the tops of the outermost (modeled) piers. The effectiveness of the dynamic relaxation process is illustrated for the bridge model shown Fig. 3.4.2, where the left-most and right-most piers (as oriented) contain springs and discrete masses at the pier cap centers. The bridge model is subjected only to permanent (dead) loads and subjected to two analyses: a static analysis, and a time-history analysis. As indicated by the Pier

1 pier cap beam vertical displacement comparison (Fig. 3.4.3), the permanent loads are incorporated into the dynamic analysis without artificially exciting the dynamic bridge model.

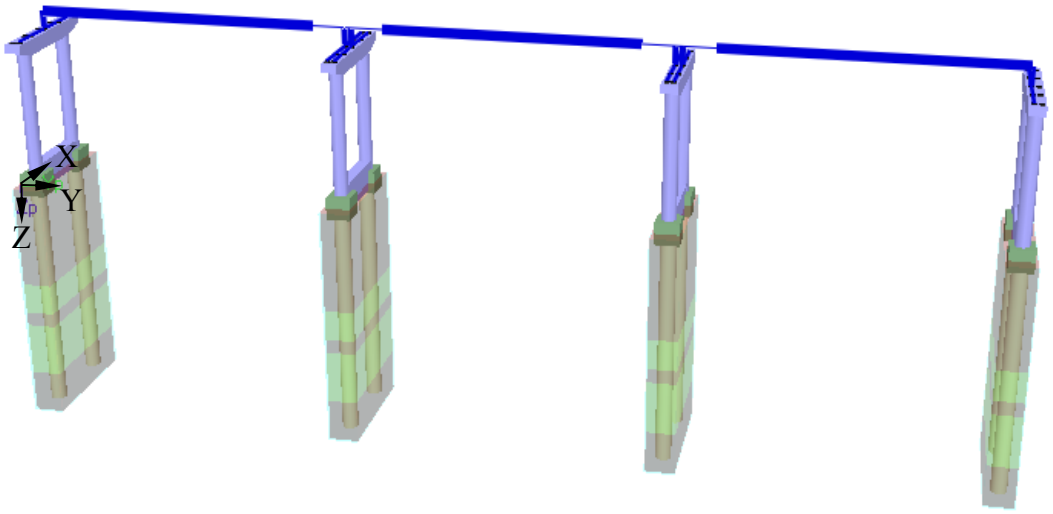

Figure 3.4.2. Bridge model used for dynamic relaxation demonstration

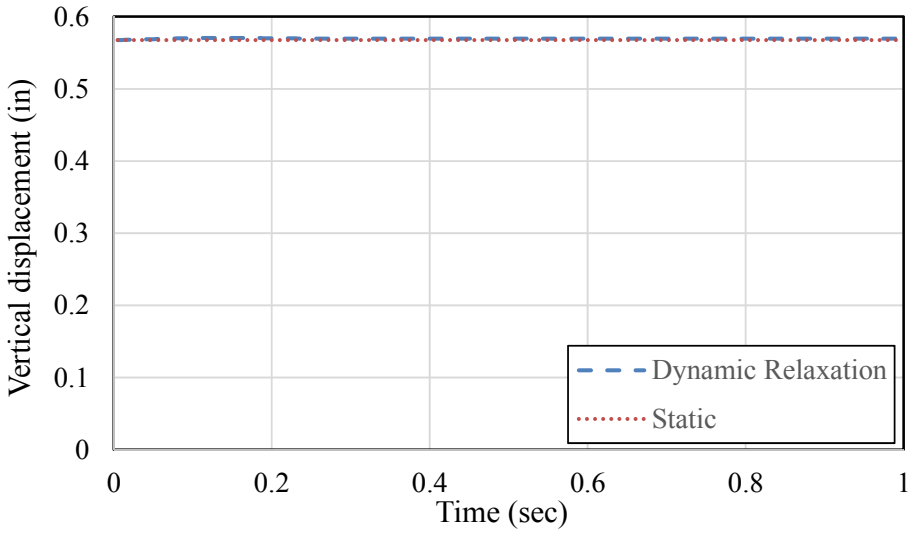

Figure 3.4.3. Comparison of vertical displacements at the pier cap beam of Pier 1 from dynamic relaxation and static analysis

3.5 Development of Superstructure Stiffness and Mass

Engine enhancements are made in relation to the stiffness and mass of superstructure entities within FBMP, as a means of facilitating OPTS model development:

1. **Span springs**. The SPANSPRING header contains input that allows users to specify additional displacement-based stiffness at span nodes. The input indicates which span(s) and node(s) to which the spring(s) will be applied. Accordingly, engineers can supply discrete spring stiffnesses to any span node degree-of-freedom (DOF) by supplying the following input:

   SPANSPRING
   NODE K=KTX,KTY,KTZ,KRX,KRY,KRZ S=SPAN (one line per nodal spring set)
   …
   :

NODE	is the span node number to which the springs will be applied
KTX	is stiffness added to the x-axis translational DOF
KTY	is stiffness added to the y-axis translational DOF
KTZ	is stiffness added to the z-axis translational DOF
KRX	is stiffness added to the x-axis rotational DOF
KRY	is stiffness added to the y-axis rotational DOF
KRZ	is stiffness added to the z-axis rotational DOF
NODE	is the span to which the springs will be applied

   Notes:
   1.) In English system, units are kip/in for translational DOF and kip-ft/rad for rotational DOF.
   2.) In SI system, units are kN/m for translational DOF and kN-m/rad for rotational DOF.

2. **Span masses**. Engineers can supply point masses to any span node by supplying the following input:

   The SPANMASS header contains input that allows users to add concentrated masses to span nodes. The input indicates the spans and nodes to which the masses will be applied.

   SPANMASS
   NODE M=MTX,MTY,MTZ,MRX,MRY,MRZ S=SPAN (one line per nodal mass set)
   …
   :

NODE	is the span node number to which the masses will be applied
MTX	is mass added to the x-axis translational DOF
MTY	is mass added to the y-axis translational DOF
MTZ	is mass added to the z-axis translational DOF

MRX is mass added to the x-axis rotational DOF
MRY is mass added to the y-axis rotational DOF
MRZ is mass added to the z-axis rotational DOF
NODE is the span to which the masses will be applied

Notes:
1.) In English system, units are kip-sec^2/in for translational DOF and kip-sec^2/rad for rotational DOF.
2.) In SI system, units are kN-sec^2/m for translational DOF and kN-sec^2/rad for rotational DOF.
3.) Previous versions of FBMP only permitted the inclusion of discrete masses within models subjected to dynamic analyses. Modifications were made to the engine to permit use of—and account for—the vertical gravity loads associated with discrete masses in static analyses. This enhancement was critical to the proper functioning of dynamic relaxation, where the total mass and stiffness in the sustained load (i.e., static) model must exactly match the total mass and stiffness of the dynamic model.

3.6 Update of Subroutines of User-Defined Loading

User-defined loading condition for use in the CVIA was implemented to facilitate scenarios where bridge engineers possess knowledge of specific loading and unloading curves, which collectively correspond to a given design vessel. The subroutine barge.f within the analysis engine was examined to ensure that the control logic is consistent with the algorithm documented in pages 67-73 of the FDOT Structures Research Report 2008/5117 (Consolazio et al., 2008).

3.7 Development of Engine Output Routines

The engine output routines are divided into two portions: (1) Output pertaining to CVIA; and (2) Output pertaining to OPTS results. Regarding the output specific to CVIA, and building upon the user-defined vessel collision loading routine introduced in Sec. 3.6, a scenario was introduced, which is described immediately below along with GUI dialogs,, input mechanisms, and the associated output. Such a scenario could be of use to engineers when vessel-specific data are available to characterize impact load-deformation behavior. The user-defined vessel collision loading components include all of load-deformation, yield deformation, unloading, and reloading of the impacting vessel portion. Input related to user-defined loading within the FBMP CVIA module was implemented in the GUI, and associated input file processing functionality was also implemented in the engine.

As shown in Fig. 3.7.1, user-defined vessel characterization can be carried out by selecting “User Defined” from the “Vessel Type” pull-down list within the “Vessel Collision Analysis Data” dialog. Additionally, the vessel-impacting portion of the deformation, which corresponds to yielding (i.e., inelastic deformation), is specified in the “Crush at Yield” input box. The vessel custom-defined loading and unloading curves are accessed by selecting “Edit

Force-Deformation Data," after which a "Load Function Edit Table" appears (Fig. 3.7.2). Here, abscissa values of deformation and ordinate values of force are input for the loading curve (the leftmost table of input). Paired values of deformation and load are also specified for any unloading curves (the rightmost table of input). For each unloading curve, the "Deformation Level" input box is populated to indicate the deformation level at which the unloading curves intersect the loading curve. For unloading which occurs between two unloading curve "Deformation Level" inputs, interpolation is used to calculate the vessel unloading curve.

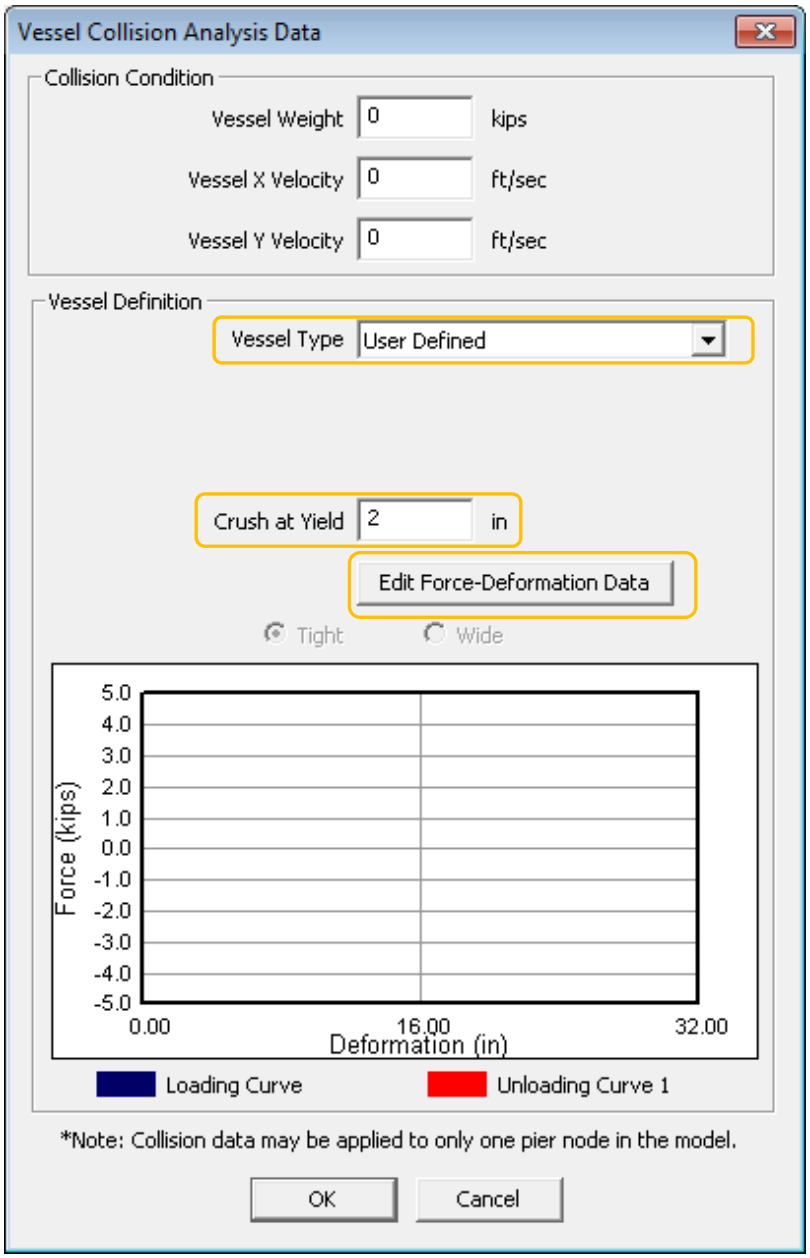

Figure 3.7.1. Vessel Collision Analysis Data dialog for inputting user-defined vessel collision force-deformation curves

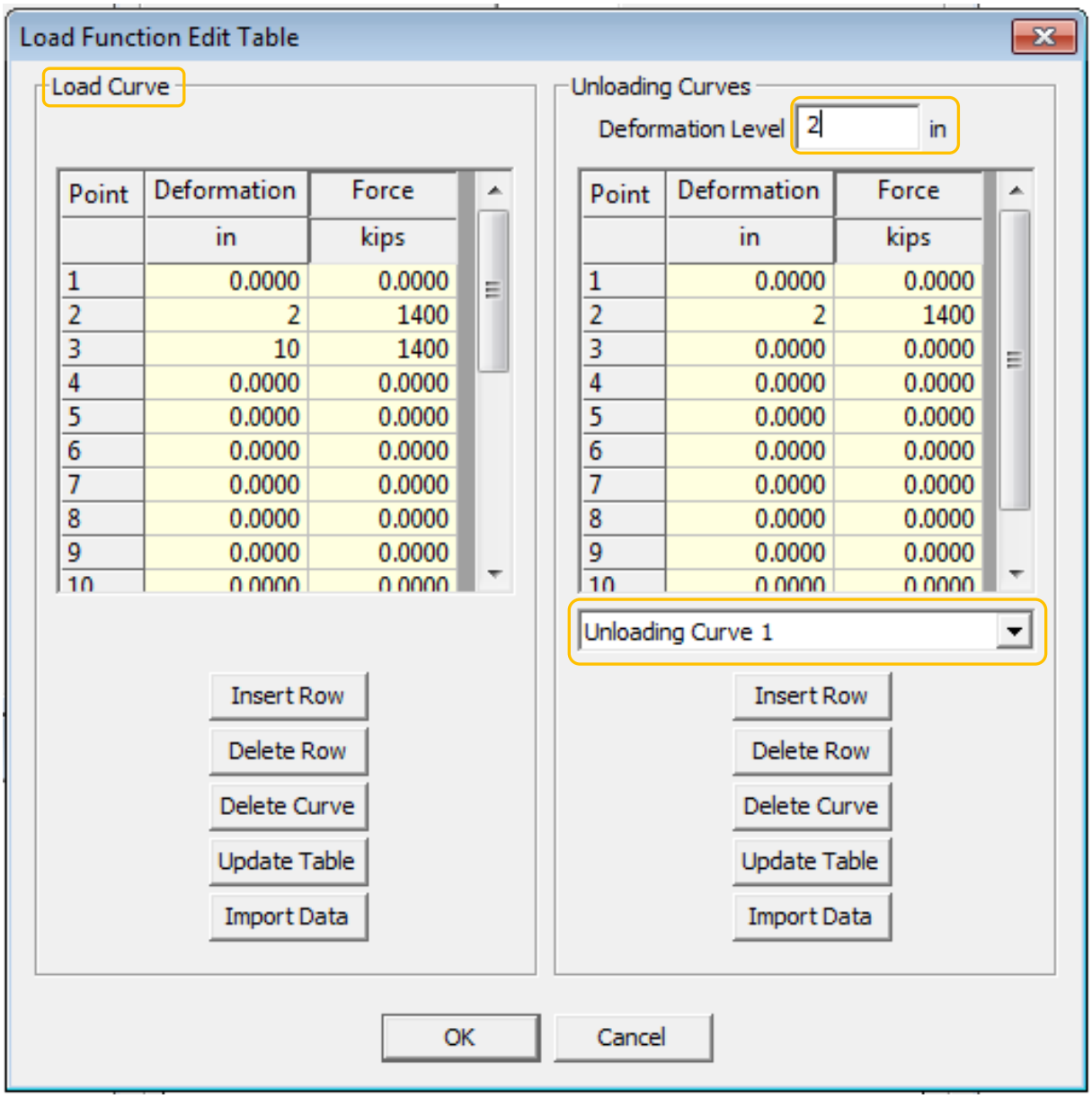

Figure 3.7.2. Load Function Edit Table for defining custom loading and unloading curves of vessel force-deformation

The CVIA portion of the output subroutines have been fully implemented. As illustration of the output generation, consider the OPTS model shown in Fig. 3.7.3. When this model is subjected to vessel collision loading, as characterized in Fig. 3.7.4, the analysis engine creates an ASCII output file (with extension .VES) containing the pertinent vessel collision quantities. Namely, the user-input values of impacting vessel weight, and initial velocity components are provided at the top of the file (Fig. 3.7.5). Additionally, for each time step, the vessel force and corresponding level of vessel bow crush depth are printed. Importantly, the structural response quantities for the impacted pier of the OPTS model are reported in the usual way in the ASCII .out file (as discussed below).

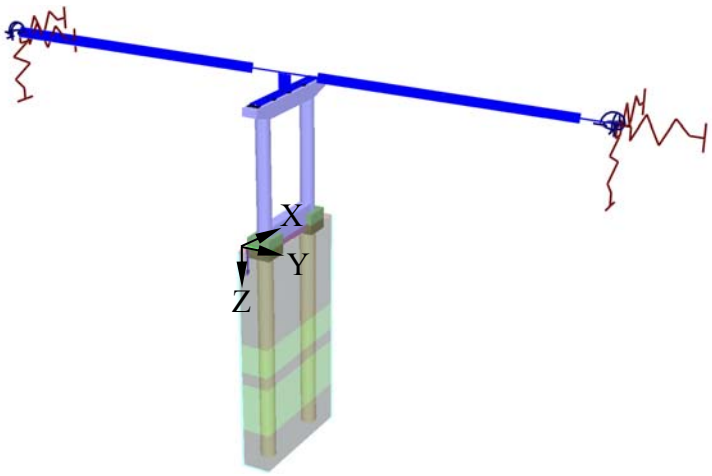

Figure 3.7.3. CVIA-OPTS model used to demonstrate generation of CVIA output

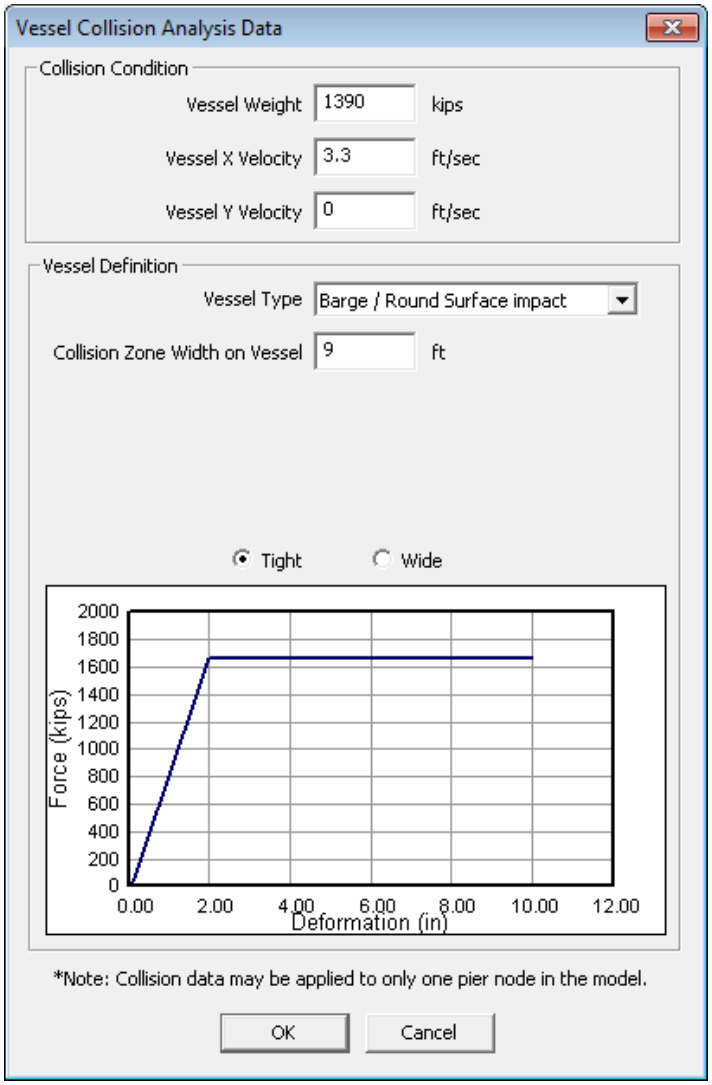

Figure 3.7.4. Vessel collision conditions

```
* * * * * * * * * * * * * * * * * * * * * * * * * * * * * * * * * * * * * * *
*            COUPLED VESSEL IMPACT ANALYSIS RESULTS                         *
* * * * * * * * * * * * * * * * * * * * * * * * * * * * * * * * * * * * * * *

*********************************************************************
*                 IMPACTING VESSEL CHARACTERISTICS                  *
*********************************************************************

Vessel Weight =  1390.0000 kips
X-Velocity    =     3.3000 ft/sec
Y-Velocity    =     0.0000 ft/sec

*********************************************************************
*                      IMPACT FORCE-HISTORY       |                  *
*********************************************************************

          TIME    IMPACT FORCE     CRUSH DEPTH
           sec            kips              in
 0.5000000E-02  0.1650581E+03  0.1976824E+00
 0.1000000E-01  0.3229341E+03  0.3867554E+00
 0.1500000E-01  0.4724652E+03  0.5658440E+00
 0.2000000E-01  0.6112220E+03  0.7319867E+00
 0.2500000E-01  0.7370789E+03  0.8827238E+00
 0.3000000E-01  0.8484153E+03  0.1016059E+01
 0.3500000E-01  0.9439500E+03  0.1130470E+01
 0.4000000E-01  0.1022881E+04  0.1224996E+01
 0.4500000E-01  0.1084865E+04  0.1299226E+01
 0.5000000E-01  0.1130012E+04  0.1353292E+01
 0.5500000E-01  0.1158804E+04  0.1387771E+01
 0.6000000E-01  0.1172030E+04  0.1403609E+01
 0.6500000E-01  0.1170657E+04  0.1401996E+01
 0.7000000E-01  0.1155937E+04  0.1384369E+01
 0.7500000E-01  0.1129337E+04  0.1352513E+01
 0.8000000E-01  0.1092554E+04  0.1308462E+01
 0.8500000E-01  0.1047341E+04  0.1254314E+01
 0.9000000E-01  0.9955302E+03  0.1192266E+01
 0.9500000E-01  0.9389437E+03  0.1124498E+01
 0.1000000E+00  0.8793245E+03  0.1053097E+01
```

Figure 3.7.5. Corresponding .VES file output for first twenty time-steps

Control logic added to FBMP, which enables use of the OPTS modeling technique, builds upon previously developed control schemes. Regarding OPTS-specific output, results pertaining to the pier and soil portions of OPTS models utilize pre-existing pier and soil output printing options (see Chung 2014a for details). However, results pertaining to the span portions of OPTS models required that additional control logic be incorporated into the FBMP analysis engine. Accordingly, subroutines to handle printing of span element forces and span node displacements, specific to OPTS model results, have been put into place. The output formatting was crafted so that it is consistent with span output for multiple-pier, multiple-span bridge models.

As demonstration, consider the OPTS model shown in Fig. 3.7.6. This model consists of one “default” FBMP pier and two spans, where “default” properties were used to populate span, soil, and self-weight loading conditions. Stiff springs (with translational stiffnesses of 1E+20 kips/in and rotational stiffnesses of 1E+20 kip-ft/rad) were placed at the extents of the OPTS model for simplicity in the numerical verification. Note that users of the OPTS features in FBMP

can specify individual degree-of-freedom stiffness values of their choosing at the two span extents of OPTS models by making use of GUI features discussed in detail in Appendix B. The pier portion of the OPTS model is shown in Fig. 3.7.7, where applied loading consists of self-weight, such as those placed at the two bearing locations.

Shown in Fig. 3.7.8 are the first 40 lines of analysis log output displayed in the GUI, during analysis. A header with log-consistent formatting is printed to indicate that the OPTS feature is being utilized. Correspondingly, as part of the "FORMATION OF SYSTEM EQUATIONS," the full span 1 and span 2 stiffness matrices are formed, with inclusion of any span-end spring stiffnesses that are defined. Also, inclusion of discrete masses placed at the span extents are reported in the analysis log. Shown below in Fig. 3.7.9 are the prints of span node (global) displacements and span element (local) internal forces (Fig. 3.7.10).

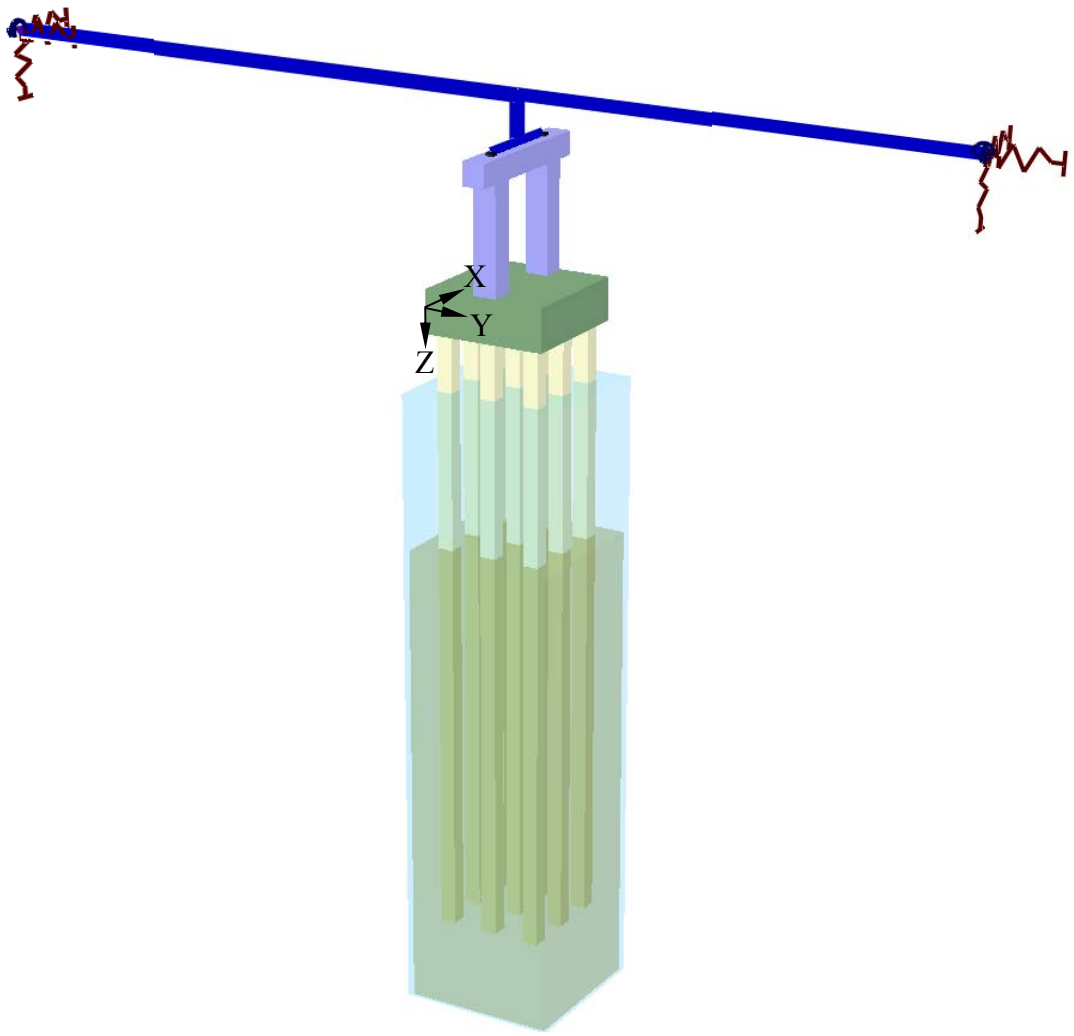

Figure 3.7.6. OPTS structural configuration

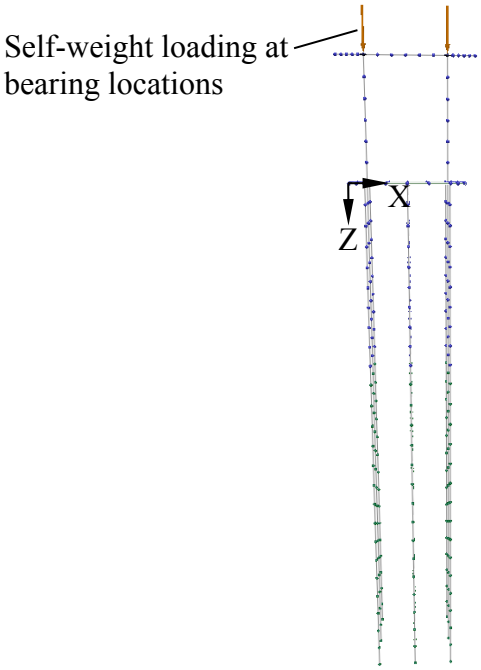

Figure 3.7.7. Loading applied to pier (superstructure not shown)

```
*****************************************************
*          READING INPUT FILE CONTENTS              *
*****************************************************


*****************************************************
*    UTILIZING ONE-PIER TWO SPAN (OPTS) MODEL       *
*****************************************************

*****************************************************
*            PERFORMING STATIC ANALYSIS             *
*****************************************************

*****************************************************
*  DETERMINING MATERIAL PROPERTIES FOR PIER  1      *
*****************************************************


-----------------------------------------------------
FORMATION OF SYSTEM EQUATIONS

FORMATION OF BRIDGE SPAN  1 STIFFNESS MATRIX

FORMATION OF BRIDGE SPAN  2 STIFFNESS MATRIX

DISCRETE MASS ADDED TO SPAN

FORMATION OF SYSTEM STIFFNESS MATRIX FOR PIER    1
GENERATION OF INTERACTION DIAGRAMS FOR PIER      1

-----------------------------------------------------
SOLUTION OF SYSTEM EQUATIONS

LOAD CASE =    1

LOAD CASE =    1  ITERATION =  1
MAXIMUM OUT-OF-BALANCE FORCES PER PIER:
PIER =  1  NODE =  99  FORCE  =  31.189
PIER =  1  NODE =  94  MOMENT =    52.2
```

Figure 3.7.8. First 40 lines of analysis log output displayed in GUI

```
*****************************************************************
*          ANALYSIS RESULTS FOR BRIDGE SPAN ELEMENTS            *
*****************************************************************

Load Case =    1
_____________________________________________________________________
Bridge Span Node Displacements

Span No. =   1

NODE             X             Y             Z            Rx            Ry            Rz
                in            in            in           rad           rad           rad
   1    0.0000E+00    0.0000E+00    0.0000E+00    0.0000E+00    0.0000E+00    0.0000E+00
   2    0.2330E-28    0.2546E-29    0.9113E-17    0.4557E-16   -0.4319E-27   -0.1165E-26
   3    0.2135E-11    0.1389E-14    0.7301E-01    0.1087E-02   -0.1697E-13   -0.3432E-13
   4    0.7932E-11    0.2777E-14    0.2330E+00    0.1477E-02   -0.3393E-13   -0.6101E-13
   5    0.1647E-10    0.4166E-14    0.4066E+00    0.1342E-02   -0.5090E-13   -0.8008E-13
   6    0.2685E-10    0.5554E-14    0.5410E+00    0.8524E-03   -0.6786E-13   -0.9152E-13
   7    0.3813E-10    0.6943E-14    0.6038E+00    0.1777E-03   -0.8483E-13   -0.9534E-13
   8    0.4942E-10    0.8332E-14    0.5830E+00   -0.5112E-03   -0.1018E-12   -0.9152E-13
   9    0.5979E-10    0.9720E-14    0.4873E+00   -0.1044E-02   -0.1188E-12   -0.8008E-13
  10    0.6834E-10    0.1111E-13    0.3456E+00   -0.1250E-02   -0.1357E-12   -0.6102E-13
  11    0.7413E-10    0.1250E-13    0.2072E+00   -0.9588E-03   -0.1527E-12   -0.3432E-13
  12    0.7627E-10    0.1389E-13    0.1422E+00    0.2493E-15   -0.1697E-12   -0.4807E-17
  13    0.6210E-10   -0.4116E-14    0.1424E+00    0.2512E-15   -0.2267E-12   -0.4813E-17
  14    0.0000E+00    0.0000E+00    0.0000E+00    0.0000E+00    0.0000E+00    0.0000E+00
  15    0.0000E+00    0.0000E+00    0.0000E+00    0.0000E+00    0.0000E+00    0.0000E+00
  16   -0.9069E-05   -0.3737E-14    0.1425E+00    0.2517E-15    0.1922E-07   -0.5429E-17
  17    0.9070E-05   -0.4424E-14    0.1425E+00    0.2517E-15   -0.1922E-07   -0.3923E-17

Span No. =   2

NODE             X             Y             Z            Rx            Ry            Rz
                in            in            in           rad           rad           rad
   1    0.6210E-10   -0.4116E-14    0.1423E+00    0.2512E-15   -0.2267E-12   -0.4814E-17
   2    0.7627E-10    0.1389E-13    0.1422E+00    0.2493E-15   -0.1697E-12   -0.4807E-17
   3    0.7413E-10    0.1250E-13    0.2072E+00    0.9588E-03   -0.1527E-12    0.3432E-13
   4    0.6834E-10    0.1111E-13    0.3456E+00    0.1250E-02   -0.1357E-12    0.6101E-13
   5    0.5980E-10    0.9720E-14    0.4873E+00    0.1044E-02   -0.1188E-12    0.8008E-13
   6    0.4942E-10    0.8332E-14    0.5830E+00    0.5112E-03   -0.1018E-12    0.9152E-13
   7    0.3814E-10    0.6943E-14    0.6038E+00   -0.1777E-03   -0.8483E-13    0.9534E-13
   8    0.2685E-10    0.5554E-14    0.5410E+00   -0.8524E-03   -0.6786E-13    0.9152E-13
   9    0.1647E-10    0.4166E-14    0.4066E+00   -0.1342E-02   -0.5090E-13    0.8008E-13
  10    0.7932E-11    0.2777E-14    0.2330E+00   -0.1477E-02   -0.3393E-13    0.6102E-13
  11    0.2136E-11    0.1389E-14    0.7301E-01   -0.1087E-02   -0.1697E-13    0.3432E-13
  12    0.2331E-28    0.2546E-29    0.9113E-17   -0.4557E-16   -0.4319E-27    0.1165E-26
  13    0.0000E+00    0.0000E+00    0.0000E+00    0.0000E+00    0.0000E+00    0.0000E+00
  14   -0.9069E-05   -0.3737E-14    0.1424E+00    0.2517E-15    0.1921E-07   -0.5429E-17
  15    0.9070E-05   -0.4424E-14    0.1424E+00    0.2517E-15   -0.1922E-07   -0.3923E-17
  16    0.0000E+00    0.0000E+00    0.0000E+00    0.0000E+00    0.0000E+00    0.0000E+00
  17    0.0000E+00    0.0000E+00    0.0000E+00    0.0000E+00    0.0000E+00    0.0000E+00
```

Figure 3.7.9. Text output of span node (global) displacements

Analytical force results for bridge span elements

Span No. = 1

ELEM NO.	NODE NO.	LOAD	FAX kips	F22 kips	F33 kips	M22 kip-in	M33 kip-in	TORQUE kip-in
12	12	1	-0.477E+01	0.233E-08	-0.255E-09	0.218E-07	0.686E-06	-0.706E-10
	13		0.477E+01	-0.233E-08	0.255E-09	-0.345E-08	-0.518E-06	
2	2	1	-0.255E-09	-0.265E+03	-0.233E-08	0.140E-05	-0.547E+05	-0.518E-06
	3		0.255E-09	0.213E+03	0.233E-08	-0.112E-05	0.260E+05	
3	3	1	-0.255E-09	-0.213E+03	-0.233E-08	0.112E-05	-0.260E+05	-0.518E-06
	4		0.255E-09	0.161E+03	0.233E-08	-0.839E-06	0.365E+04	
4	4	1	-0.255E-09	-0.161E+03	-0.233E-08	0.839E-06	-0.365E+04	-0.518E-06
	5		0.255E-09	0.109E+03	0.233E-08	-0.559E-06	-0.125E+05	
5	5	1	-0.255E-09	-0.109E+03	-0.233E-08	0.559E-06	0.125E+05	-0.518E-06
	6		0.255E-09	0.564E+02	0.233E-08	-0.280E-06	-0.224E+05	
6	6	1	-0.255E-09	-0.564E+02	-0.233E-08	0.280E-06	0.224E+05	-0.518E-06
	7		0.255E-09	0.434E+01	0.233E-08	-0.176E-10	-0.260E+05	
7	7	1	-0.255E-09	-0.434E+01	-0.233E-08	0.176E-10	0.260E+05	-0.518E-06
	8		0.255E-09	-0.477E+02	0.233E-08	0.280E-06	-0.234E+05	
8	8	1	-0.255E-09	0.477E+02	-0.233E-08	-0.280E-06	0.234E+05	-0.518E-06
	9		0.255E-09	-0.998E+02	0.233E-08	0.559E-06	-0.146E+05	
9	9	1	-0.255E-09	0.998E+02	-0.233E-08	-0.559E-06	0.146E+05	-0.518E-06
	10		0.255E-09	-0.152E+03	0.233E-08	0.839E-06	0.520E+03	
10	10	1	-0.255E-09	0.152E+03	-0.233E-08	-0.839E-06	-0.520E+03	-0.518E-06
	11		0.255E-09	-0.204E+03	0.233E-08	0.112E-05	0.219E+05	
11	11	1	-0.255E-09	0.204E+03	-0.233E-08	-0.112E-05	-0.219E+05	-0.518E-06
	12		0.255E-09	-0.256E+03	0.233E-08	0.140E-05	0.495E+05	

Span No. = 2

ELEM NO.	NODE NO.	LOAD	FAX kips	F22 kips	F33 kips	M22 kip-in	M33 kip-in	TORQUE kip-in
1	1	1	-0.392E+01	0.233E-08	-0.254E-09	0.218E-07	0.686E-06	-0.712E-10
	2		0.392E+01	-0.233E-08	0.254E-09	-0.346E-08	-0.518E-06	
2	2	1	0.255E-09	-0.256E+03	0.233E-08	-0.140E-05	-0.495E+05	0.518E-06
	3		-0.255E-09	0.204E+03	-0.233E-08	0.112E-05	0.219E+05	
3	3	1	0.255E-09	-0.204E+03	0.233E-08	-0.112E-05	-0.219E+05	0.518E-06
	4		-0.255E-09	0.152E+03	-0.233E-08	0.839E-06	0.520E+03	
4	4	1	0.255E-09	-0.152E+03	0.233E-08	-0.839E-06	-0.520E+03	0.518E-06
	5		-0.255E-09	0.998E+02	-0.233E-08	0.559E-06	-0.146E+05	
5	5	1	0.255E-09	-0.998E+02	0.233E-08	-0.559E-06	0.146E+05	0.518E-06
	6		-0.255E-09	0.477E+02	-0.233E-08	0.280E-06	-0.234E+05	
6	6	1	0.255E-09	-0.477E+02	0.233E-08	-0.280E-06	0.234E+05	0.518E-06
	7		-0.255E-09	-0.434E+01	-0.233E-08	0.176E-10	-0.260E+05	
7	7	1	0.255E-09	0.434E+01	0.233E-08	-0.176E-10	0.260E+05	0.518E-06
	8		-0.255E-09	-0.564E+02	-0.233E-08	-0.280E-06	-0.224E+05	
8	8	1	0.255E-09	0.564E+02	0.233E-08	0.280E-06	0.224E+05	0.518E-06
	9		-0.255E-09	-0.109E+03	-0.233E-08	-0.559E-06	-0.125E+05	
9	9	1	0.255E-09	0.109E+03	0.233E-08	0.559E-06	0.125E+05	0.518E-06
	10		-0.255E-09	-0.161E+03	-0.233E-08	-0.839E-06	0.365E+04	
10	10	1	0.255E-09	0.161E+03	0.233E-08	0.839E-06	-0.365E+04	0.518E-06
	11		-0.255E-09	-0.213E+03	-0.233E-08	-0.112E-05	0.260E+05	
11	11	1	0.255E-09	0.213E+03	0.233E-08	0.112E-05	-0.260E+05	0.518E-06
	12		-0.255E-09	-0.265E+03	-0.233E-08	-0.140E-05	0.547E+05	

Figure 3.7.10. Text output of span element (local) internal forces

CHAPTER 4
VALIDATION OF FB-MULTIPIER VESSEL-PIER COLLISION ANALYSIS MODULES

4.1 Introduction

A necessary facet of any endeavor consisting predominately of software development tasks is found in validation of all updated and newly implemented features. Of relevance to the current study, two major software enhancements (i.e., features) were incorporated into the FB-MultiPier (FBMP) software program (Chung 2014a). One of the two newly-developed features is a module that facilitates nonlinear coupled vessel-bridge impact analysis, referred to as CVIA. The other newly developed FBMP feature, which can be used in both static and dynamic analyses either independent of CVIA or in conjunction with CVIA, is a simplified representation of bridge, i.e., the One-Pier Two-Span (OPTS) model. Validation of both of these new features is presented in the next two chapters.

In Chapter 2, documentation was given pertaining to validation of the GUI coding, and specific to the CVIA module. Furthermore, validation of numerous support features in FBMP (relative to the CVIA and OPTS implementations) was documented in Chapter 3 (e.g., dynamic relaxation). In the current chapter (Chapter 4), validation efforts concerned exclusively with the CVIA module, as implemented in FBMP, are detailed. Validation efforts specific to the OPTS modeling technique, as well as combined CVIA-OPTS utilization, are documented in Chapter 5.

4.2 Overview

Two separate measures of validation were taken to ensure both the accuracy of the programming itself and robustness of input-to-output transitions (from the GUI to the engine prior to analysis and from the engine to the GUI subsequent to analysis) for the CVIA implementation in FBMP. First, programming specific to the CVIA module in the FBMP analysis engine was assessed. More specifically, in Sec. 4.3, numerical verification of the CVIA is demonstrated by: (1) Subjecting a multiple-pier, multiple-span FBMP model to vessel collision loading via CVIA; (2) Cataloging the impact force-history that is generated as part of the CVIA; (3) Subjecting an identical multiple-pier, multiple-span model to a directly-applied force-history matching that generated during the CVIA; and 4) Comparing the numerical predictions of impacted bridge pier response between the CVIA and directly-applied force-history analyses. In this way, the numerical predictions of pier responses to vessel impact have been validated.

In Sec. 4.4 and Sec. 4.5, the predictive power and robustness of the CVIA module are examined. This second validation component consisted of drawing from data collected during a series of previously conducted full-scale barge impact experiments (Consolazio et al., 2006). A multiple-pier model was created in FBMP using structural and geotechnical input parameters, which collectively match an extensive set of field measurements (taken as part of the full-scale experiments). In comparison with measured data (from the previously conducted full-scale experiments) and in consideration of analytical solution procedures per a selected, individual

barge impact test, several layouts of the GUI CVIA module were formed. Subsequently, these layouts were tested for design applications by conducting corresponding vessel collision analyses. The numerical predictions of bridge pier response, obtained using the FBMP CVIA features, have been shown to compare favorably with the respective physical-test records.

4.3 Numerical Verification of the CVIA Module

Consider the three-pier bridge model shown in Fig. 4.3.1. Because the numerical verification being undertaken involves the use of identical bridge models (i.e., identical structural and soil input) between the CVIA and directly-applied force-history analyses, three default FBMP piers, default soil layering, and two default spans are used in building up the multiple-pier configuration. Non-collision loads included in the three-pier model consist of self-weight and buoyancy. Regarding vessel collision loading, the central pier is selected as the impacted pier (Fig. 4.3.2), and the first column node above the central-pier pile cap is selected as the impact node. The vessel collision scenario is summarized as shown in the "Vessel Collision Analysis Data" GUI dialog (Fig. 4.3.3). Namely, impact on the 3-ft flat pier column is considered in conjunction with a 1,900 kip vessel, traveling at an initial speed of 2 ft/s in the global X-direction.

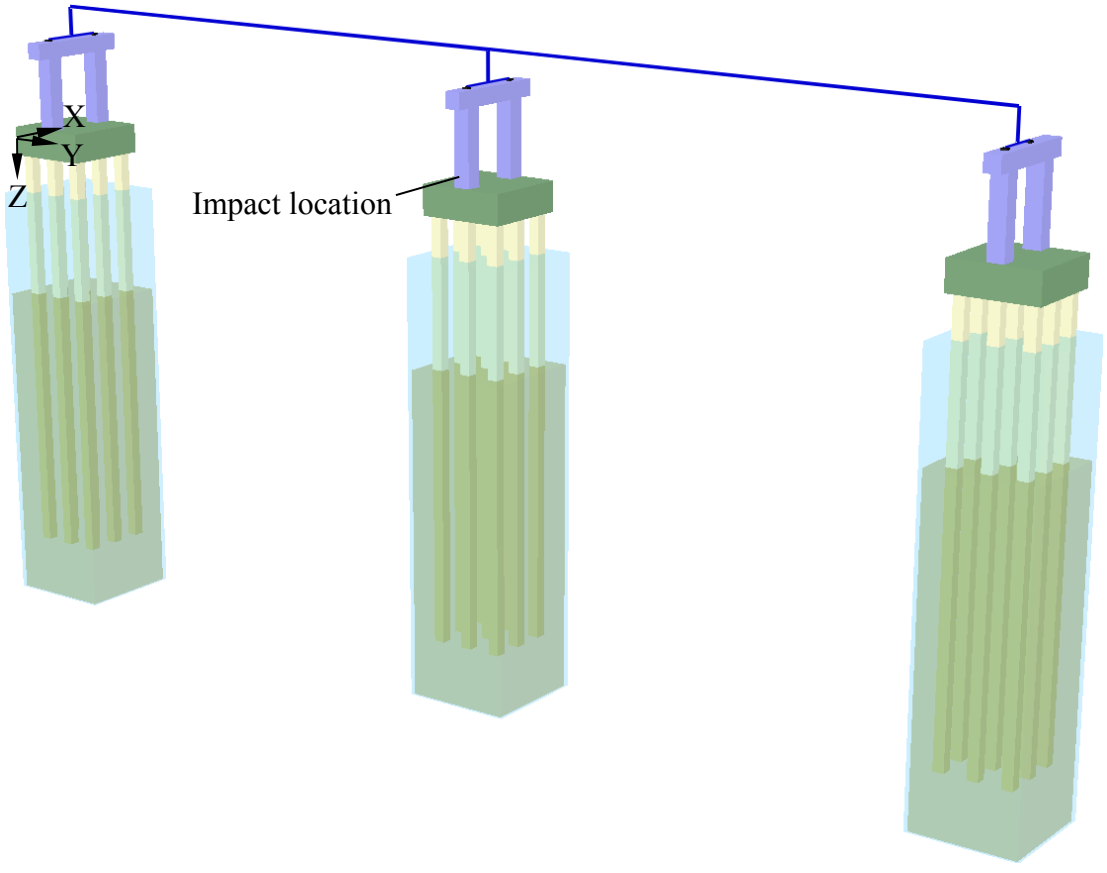

Figure 4.3.1. Three-pier structural configuration

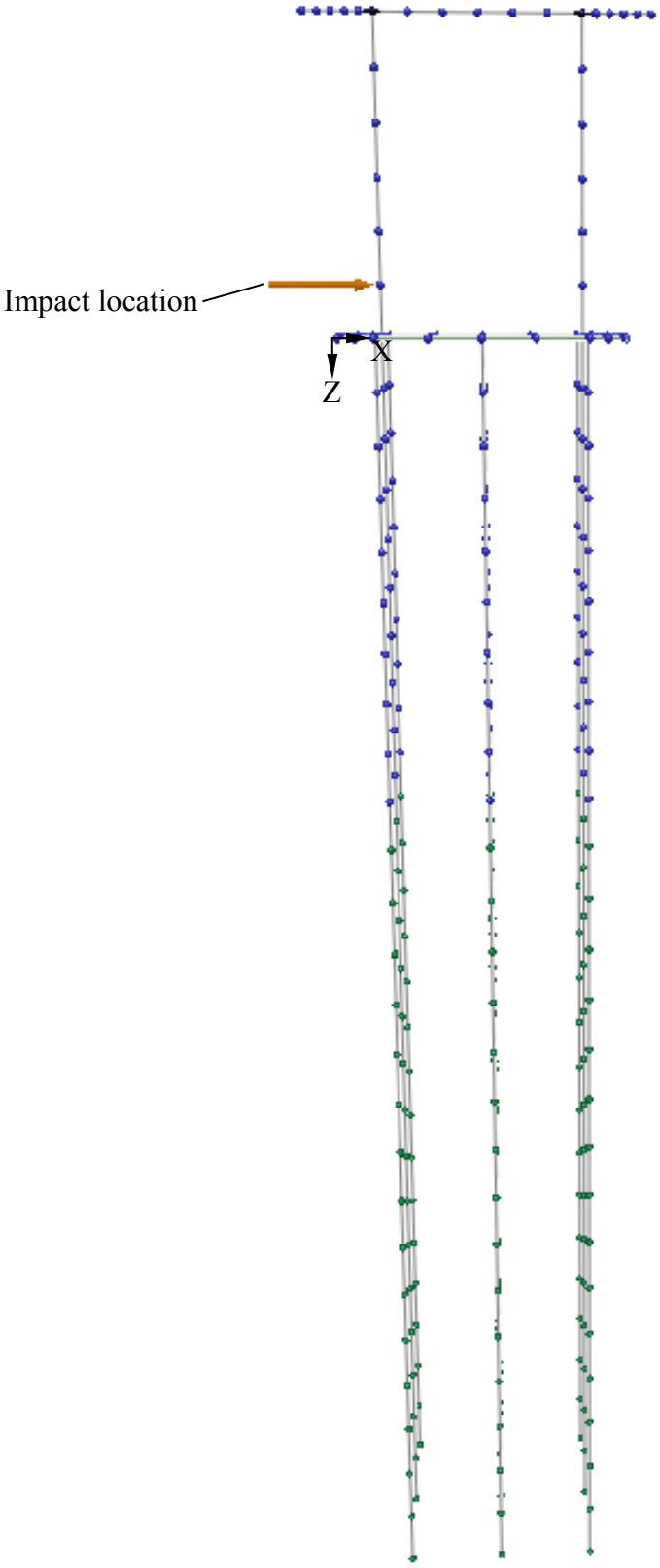

Figure 4.3.2. Impact location on pier column of central pier

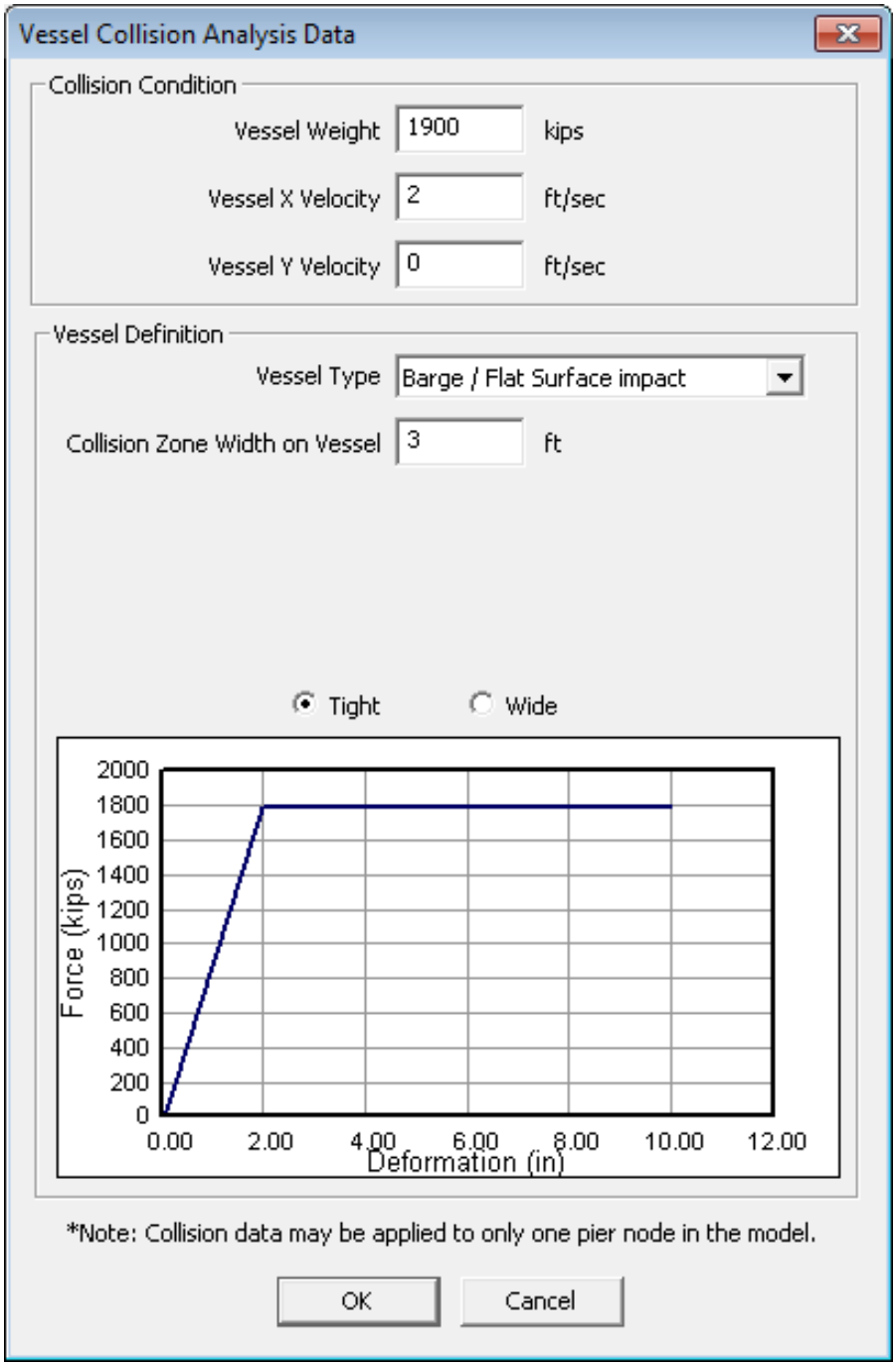

Figure 4.3.3. Vessel collision conditions

Shown in Fig. 4.3.4 is a plot of the vessel collision impact force history generated as part of the CVIA, where the resultant plot data are extracted from the .VES ASCII output file over the first 100 time-steps. Intrinsic to use of the CVIA module, bridge response is calculated simultaneous to automatic calculation of the impact force history (by the FBMP analysis engine). In fulfillment of numerical verification of the CVIA module, an additional impact force-history analysis is carried out where the force-history (Fig. 4.3.4) is applied (as a global X-direction force-history) to the same three-pier model (recall Fig. 4.3.1). In this way, it is expected that the

structural response between the CVIA results and the applied force-history results should be approximately identical (minor differences due to round-off in the applied load function are expected). Comparative plots of the global X-direction impact-point displacement-histories are shown for the CVIA and directly-applied force-history analyses in Fig. 4.3.5. As expected, the impacted bridge responses are nearly identical between the two analyses, where such high level of agreement numerically verifies the accuracy of programming for the FBMP CVIA module.

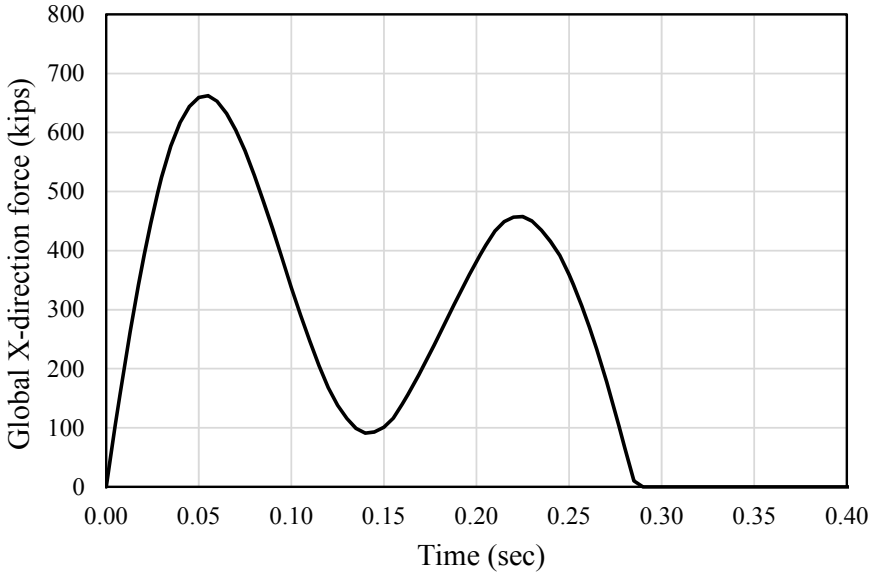

Figure 4.3.4. Vessel collision (X-direction) force-history generated simultaneous to bridge response as part of the CVIA

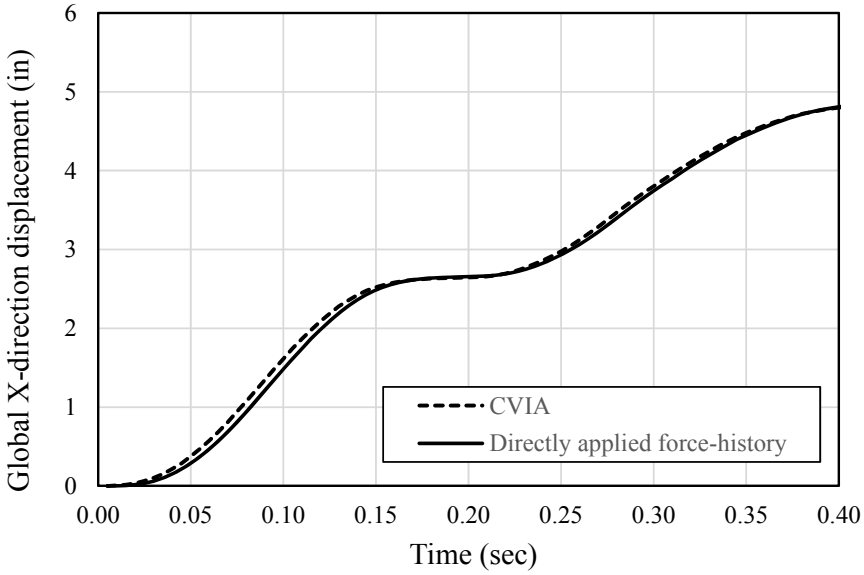

Figure 4.3.5. Global X-direction displacement-history comparison between the CVIA and directly-applied force-history analyses

4.4 Validation of CVIA Module Using Full-Scale Vessel Collision Data

Having numerically verified the functionality of CVIA, focus was shifted on the validation of numerical prediction of system response where CVIA-driven predictions of impacted bridge response are compared to full-scale physical response measurements. More specifically, physical measurements of bridge lateral displacement were drawn upon, where such measurements were recorded during the 2004 UF-FDOT old St. George Island Causeway barge impact experiments in northwestern Florida. The 2004 full-scale physical testing involved instrumenting a 150 ft long by 50 wide construction deck barge and multiple piers of the old St. George Island Causeway, and then ramming the barge into selected bridge piers over a range of impact speeds, barge payloads, and for three distinct structural configurations. Details of the old St. George Island Causeway bridge structural configuration, test setups, and physically measured structural response data (e.g., impact forces, bridge pier motions) are provided in Consolazio et al. (2006). Details specific to the site-specific soil conditions, static, and dynamic soil responses, as well as results from numerous laboratory tests of soil properties, are given in McVay et al. (2005a).

4.4.1 Selection of Validation Case

Among the three structural configurations involved in the 2004 UF-FDOT barge impact experiments, the second test series involved direct, head-on barge impacts on an intermediate pier (Pier 3-S) within a partial bridge structure (Fig. 4.4.1). In contrast, the two additional test series involved impacts on single piers in isolation. As a means of ensuring that the CVIA module can predict impacted pier responses for multiple-pier, multiple-span structures, the partial bridge configuration was selected for inclusion in the validation efforts of the current study. During the 2004 partial-bridge impact tests, four separate collisions were investigated. Of these four collisions, the fourth test (referred to as B3T4) contained the most severe impact conditions, and generated the most extreme bridge response relative to the other three partial-bridge tests (Consolazio et al., 2006). Therefore, test B3T4 was selected as the validation case in the current study.

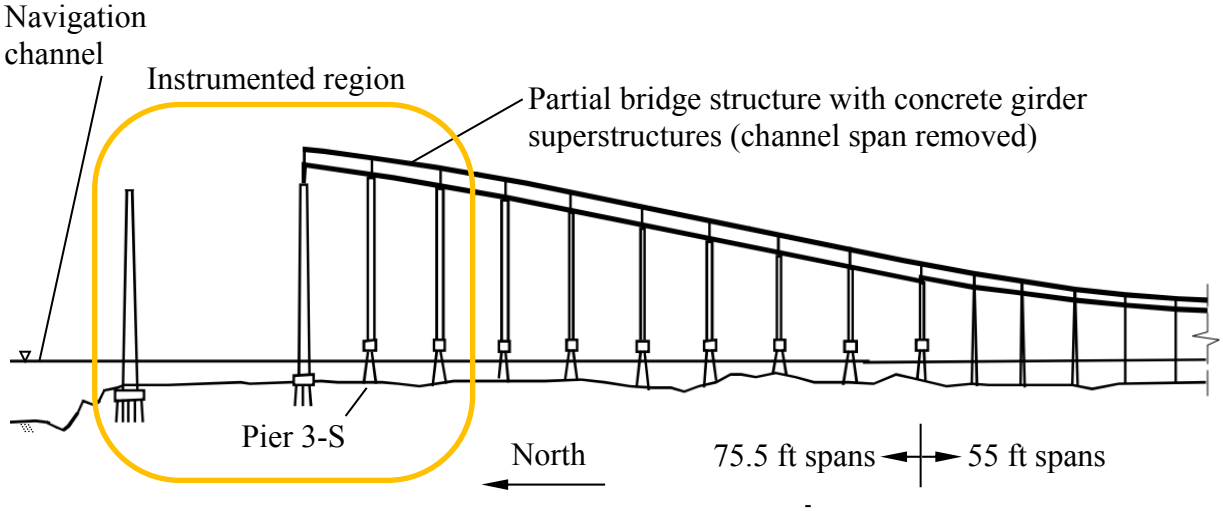

Figure 4.4.1. Structural configuration at old St. George Island Causeway Bridge during the partial bridge test series (after Consolazio et al., 2008)

4.4.2 B3T4 Test Conditions and Results

Shown in Fig. 4.4.2 is a schematic of the B3T4 impact test conditions at Pier 3-S (superstructure not shown), with denotation of the pertinent experimental instrumentation. During test B3T4, the 344 ton construction deck barge impacted the pier at an initial head-on velocity of 1.53 knots. Load was imparted to the western (left) pier column approximately 7.5 ft above the mean sea level (MSL) waterline via a relatively rigid impact block and intermediate (between load block and pier column) biaxial load cells. Impact load transferred through the biaxial load cells was cataloged as part of the experimental measurements.

Simultaneous to measurement of the B3T4 impact load, pier motions were measured using displacement transducers and accelerometers. Specific to the test setup, a stationary platform fitted with displacement transducers, where pier attachment points are indicated in Fig. 4.5, were used to measure the pier displacements at the (approximate) elevation of impact. As redundancy, accelerometers oriented parallel to the (head-on) impact direction were also monitored during the testing; subsequent to the experiments, acceleration records were twice-integrated and then compared to the displacement transducer readings. The record of impact force and corresponding impact-elevation pier displacement-history are shown in Fig. 4.4.3 and Fig. 4.4.4, respectively. Highly detailed treatments of the instrumentation installation and calibration, impact forces, and impact response quantities are given in Consolazio et al. (2006) and McVay et al. (2005a).

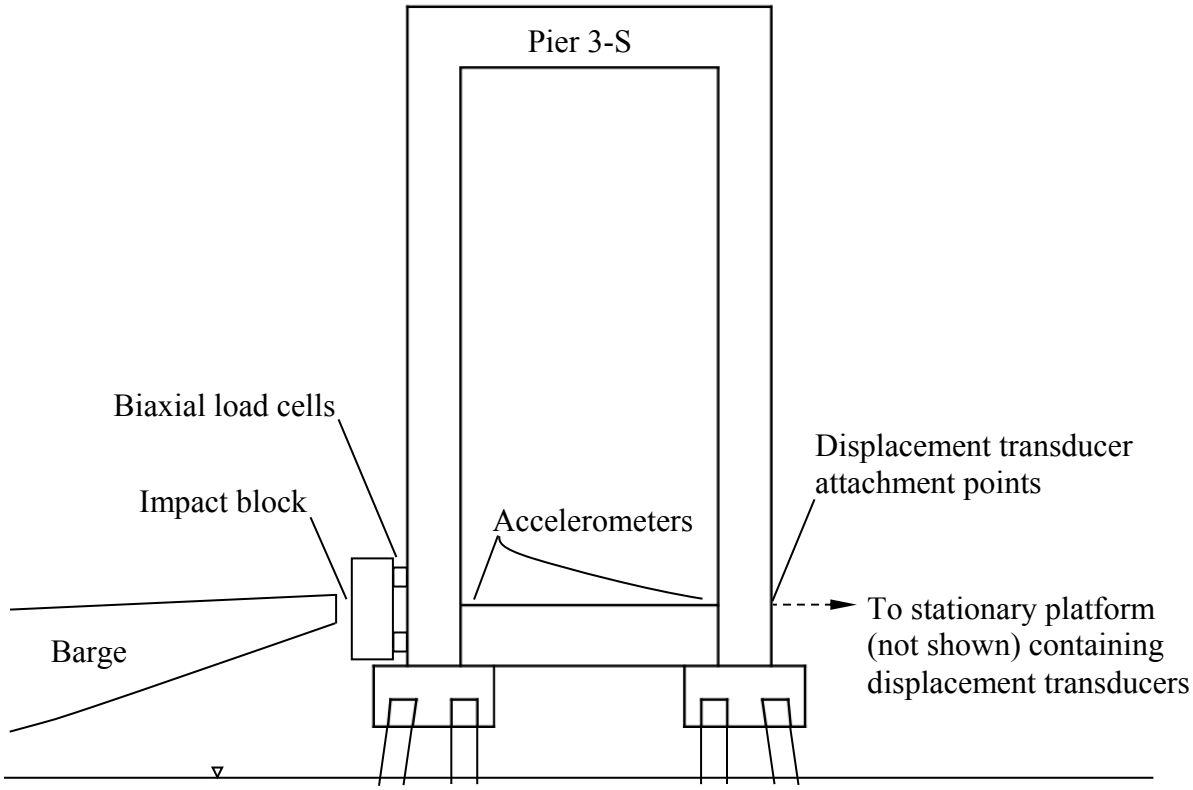

Figure 4.4.2. Schematic of test B3T4 at Pier 3-S (superstructure not shown)

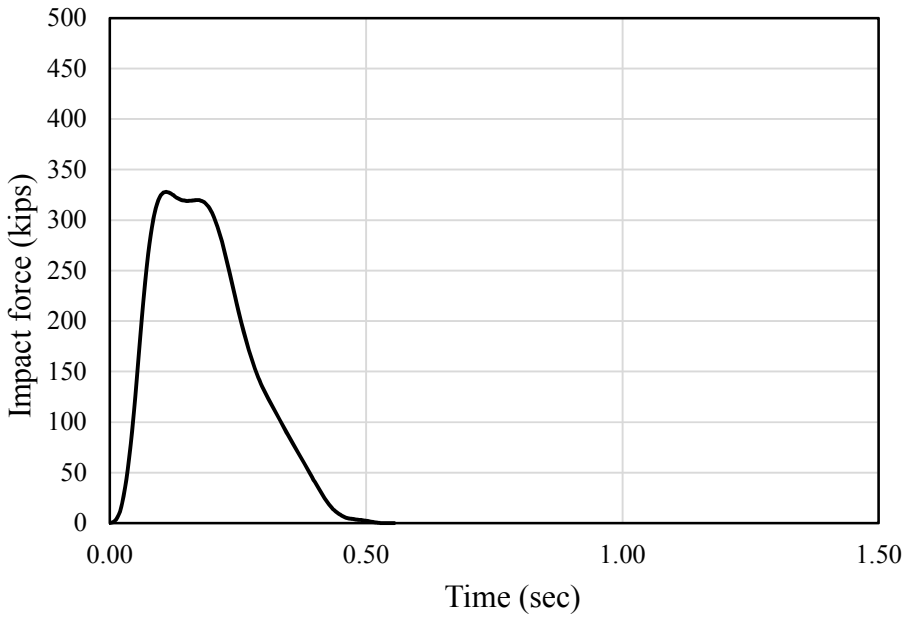

Figure 4.4.3. Impact force-history measured during test B3T4 (Consolazio et al., 2006)

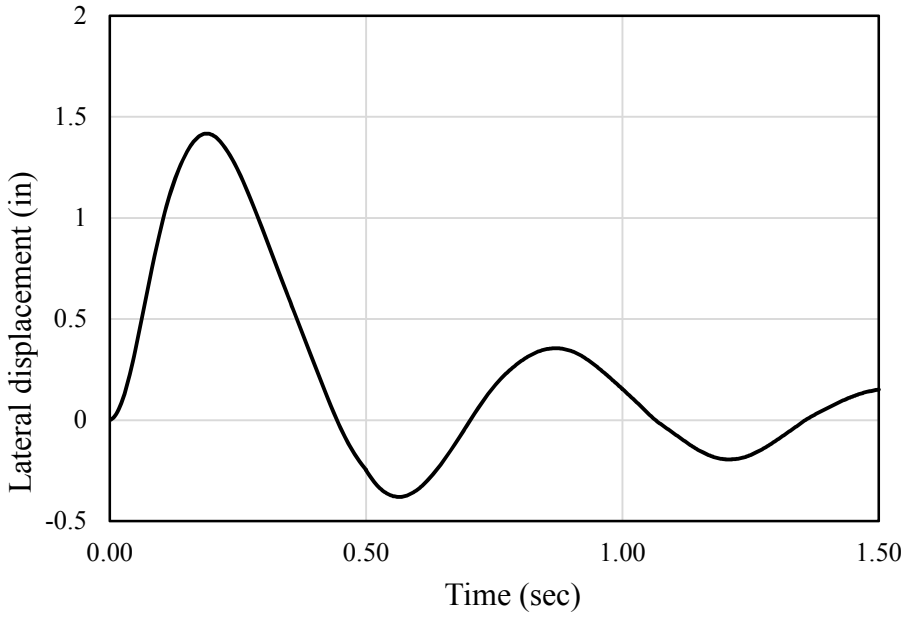

Figure 4.4.4. Lateral displacement-history measured at the impact elevation during test B3T4 (Consolazio et al., 2006)

4.4.3 FB-MultiPier Model of Partial-Bridge Structure

Taking the full-scale barge impact experiment B3T4 test results (and in particular, Fig. 4.4.4) as benchmarks of impacted bridge pier response, the FBMP CVIA module was validated through the generation of numerical results for a corresponding vessel collision scenario. An overview schematic of the validation-case FBMP model for the old St. George Island Causeway

partial-bridge configuration is shown in Fig. 4.4.5. In forming an FBMP model of the old St. George Island Causeway partial-bridge structure, structural and geotechnical details given in McVay et al. (2005a), Consolazio et al. (2006), and Consolazio et al. (2008) are repeatedly drawn upon. More specifically, the bridge geometry, structural material parameters, estimates of soil layering, and soil input parameters are matched to those delineated in the aforementioned technical reports. Further, consistent with Consolazio and Davidson (2008), the four northernmost piers of the partial-bridge structure (and three accompanying spans) are explicitly modeled in FBMP (Fig. 4.4.6). All spans and piers of the partial-bridge structure that are not explicitly modeled are accounted for by supplying springs at the top of southernmost (rightmost) pier cap extents. The pier cap beam of the northernmost (left) pier in the model is unrestrained given that the built-up plate girder channel span was removed prior to testing.

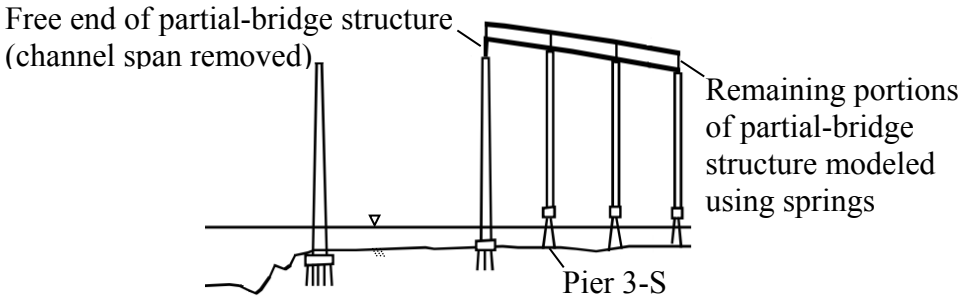

Figure 4.4.5. Overview schematic of test structures (Consolazio et al., 2008)

As shown in Fig. 4.4.6, each of the four piers contain two reinforced concrete pier columns and partial-height shear struts at the pier column bases, where the Pier 2-S pier columns, pier cap beam, and shear strut are relatively more substantial. Spanning between each pier are 75.5 ft concrete girder superstructures, which slope downward from north to south (left to right) and contain simple span-end bearing conditions. As additionally depicted in Fig. 4.4.7, the northernmost pier (Pier 2-S) is founded on a thick mudline footing and three rows of nine steel h-piles. In contrast, each pier column of Pier 3-S, Pier 4-S, and Pier 5-S overlies a relatively thin waterline footing, which in turn, is supported by four battered prestressed concrete piles. Exhaustive structural configuration dimensions, member cross-section layouts, and structural material properties are given in Consolazio et al. (2006).

As delineated in Consolazio et al. (2006) and McVay et al. (2005a), soil conditions across the modeled piers of the partial-bridge structure are such that the top of soil elevation lies approximately 8 ft below MSL (Fig. 4.4.7). Consistent with Consolazio and Davidson (2008), the soil strata beneath the four piers are divided into five layers, four of which are sandy layers and the second of which is a clay layer. Soil strength parameters for each layer are given in Consolazio et al. (2006). Due to the exhaustive physical data collection associated with the 2003 barge impact experiments, rate dependent soil resistance in the form of discrete damping is known for the B3T4 test, and is incorporated into the FBMP model (Fig. 4.4.8). Damping values and discrete damper placement is matched to that of Consolazio et al. (2006). Additional in-situ test datasets, as well as static and dynamic soil properties are given in McVay et al. (2005a).

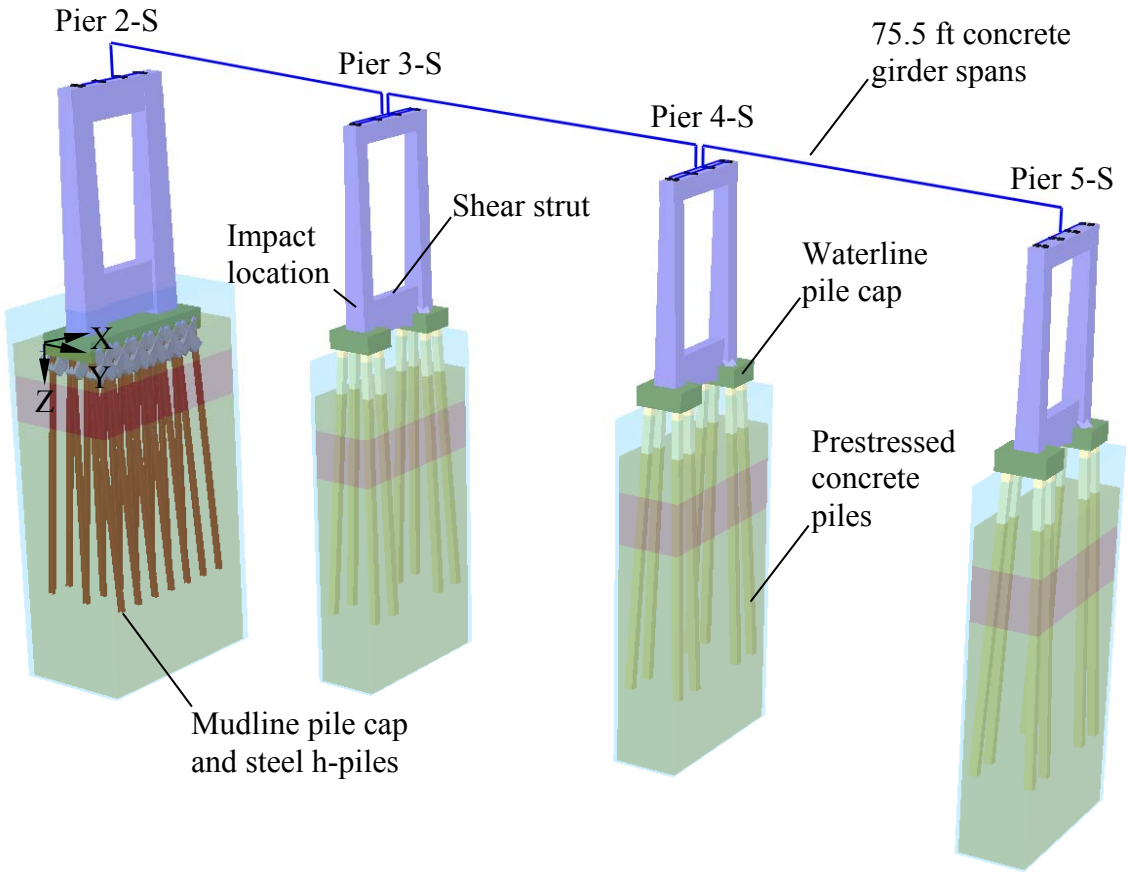

Figure 4.4.6. Old St. George Island Causeway bridge partial-bridge FBMP structural model

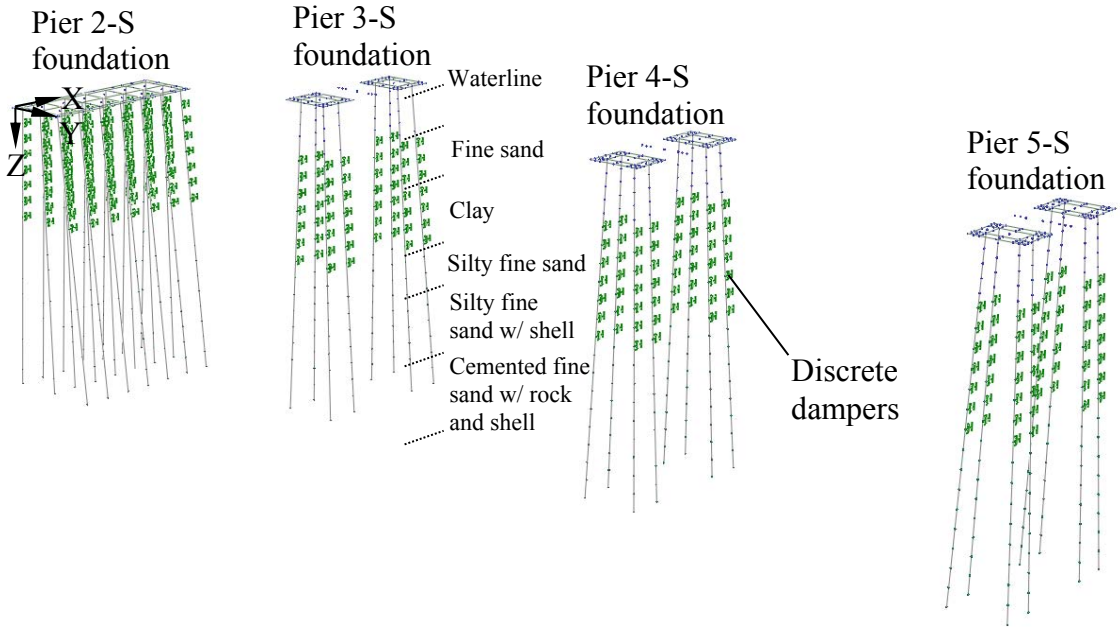

Figure 4.4.7. Foundation models for partial-bridge structure

4.4.4 Vessel Collision Scenario

The vessel collision scenario used in the CVIA module validation matches those test conditions delineated for test B3T4 in Consolazio et al. (2006). Shown in Fig. 4.4.9 is the FBMP model of the impacted Pier 3-S (superstructure not shown), where the impact location is specified on the west (left) pier column near the top of the shear strut. Model input specific to the vessel collision scenario is given in Fig. 4.4.10, which includes specification of vessel impact weight (688 kips) and head-on (i.e., global X-direction) initial impact velocity (2.58 ft/s). In addition to vessel collision loading, self-weight, buoyancy, and soil resistance forces are also accounted for in the FBMP model.

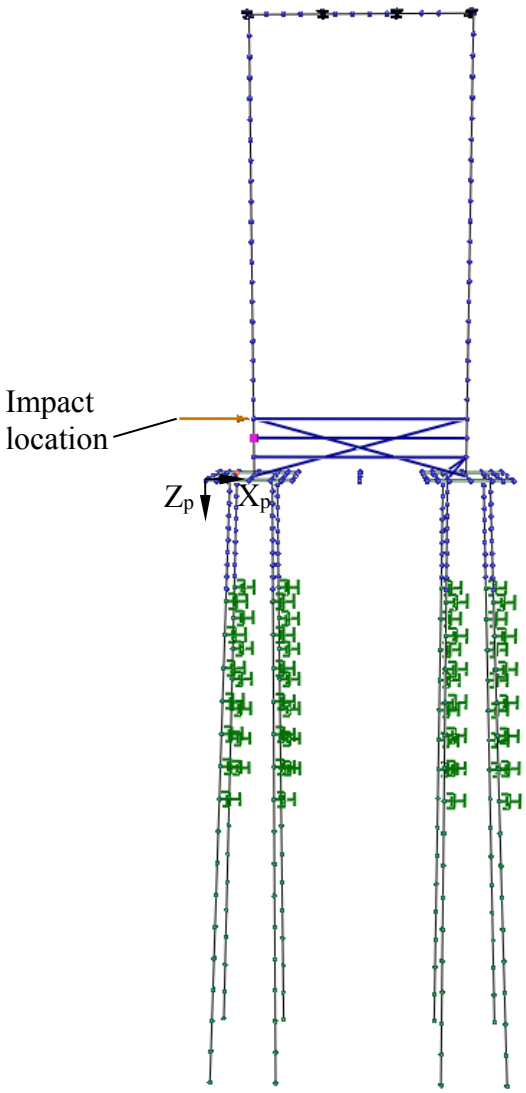

Figure 4.4.8. Pier 3-S finite element model (superstructure not shown)

A user-defined force-deformation relationship is supplied for the vessel bow (Fig. 4.4.9, bottom). This component of the CVIA module was introduced within the context of functionality

and implementation in Sec. 3.6 and Sec. 3.7. Utilization of the User-Defined vessel characterization option is recommended for applications where a known, physical vessel is going to be involved in the impact scenario of interest, and when highly detailed data are available to characterize contact-impact behavior for that same vessel. For the current validation process, the vessel bow load-deformation is derived from previously conducted research (Consolazio and Davidson, 2008), where impact-specific measurements such as mappings of bow deformation and barge bow impact force (Consolazio et al., 2006) were relied upon in characterizing the construction deck barge bow behavior.

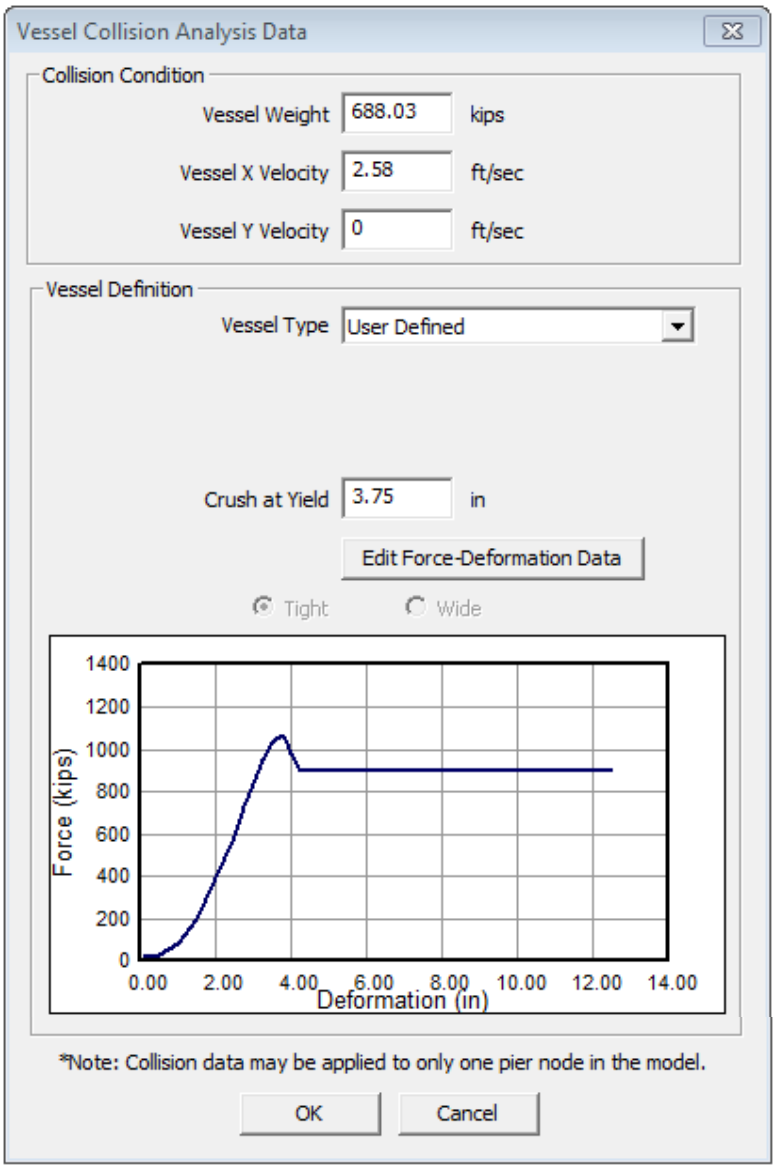

Figure 4.4.9. Vessel collision conditions for the validation case

The constitutive (load-deformation) relationship shown in Fig. 4.4.9 was formulated to be specific to the construction deck barge and, further, specific to the test B3T4 conditions. The

impact conditions for test B3T4 were such that the directly engaged (contacted) barge bow portion occurred in a previously undamaged zone (Consolazio et al., 2006). Therefore, the user-defined vessel bow load-deformation relationship used to approximately characterize the test B3T4 construction deck barge bow behavior in the current study (Fig. 4.4.9) does not include a softened region for low values of deformation (relative to that of Consolazio and Davidson, 2008). In addition, because the barge bow was concluded to behave elastically during test B3T4 (Consolazio et al., 2006), the barge bow deformation level that signifies the onset of inelastic behavior (i.e., the "Crush at Yield") is input at a relatively large level of bow deformation (3.75 in.). For the validation case analysis considered in the current study, the barge bow deformation level corresponding to yielding was not reached.

4.4.5 Comparison of Experimental Measurements and CVIA Results

As validation of the CVIA module, numerical results obtained from use of CVIA in FBMP have been shown to compare favorably with the previously identified B3T4 physical-record benchmark (i.e., impacted bridge pier response). A comparative plot of the numerically generated (through CVIA) and physically measured (during B3T4) impact-point displacement-histories is presented in Fig. 4.5.3. Overall, the two response records show good agreement, particularly during the (approximately) 0.5 sec load duration. At approximately 0.2 sec, the maximum displacement occurs for both the numerical predictions and the physical record of response. With respect to maximum displacement magnitudes, the CVIA results (1.62 in.) indicate reasonable agreement to that of the physical record (1.44 in.). Oscillatory responses for times beyond 0.5 sec indicate that the FBMP bridge-pier-soil model intrinsically possesses (independent of use of the CVIA module) a shorter free-vibration period than that of the physically tested partial-bridge structure. This difference can potentially be remedied through incorporation of more advanced soil modeling techniques, and can be explored as part of future research efforts.

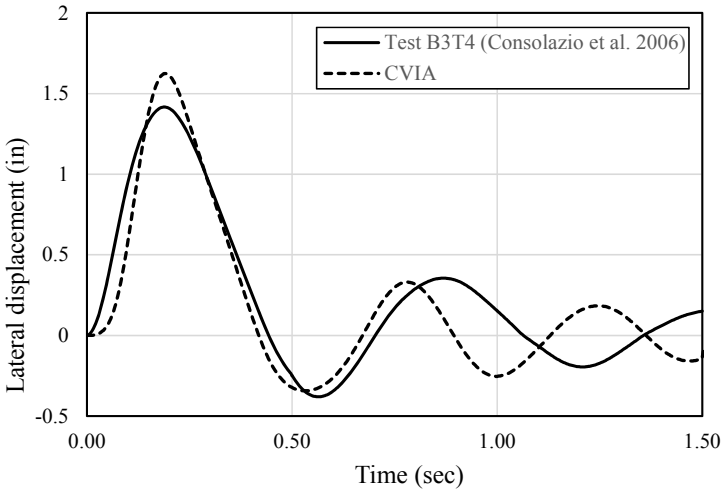

Figure 4.4.10. Lateral displacement comparison between physical test B3T4 and CVIA

4.5 Demonstration of CVIA Module Robustness

As an extension of the CVIA module validation efforts, the robustness of the CVIA feature implementation in FBMP has been demonstrated. Specifically, the vessel-specific, impact-specific load-deformation curve (Fig. 4.4.9, bottom) used in making comparisons to full-scale measurements of impacted bridge pier response (i.e., validation of the CVIA module) is replaced with a more generalized elastic, perfectly-plastic load-deformation curve (Fig. 4.5.1). The generalized curve is representative of the library of built-in load-deformation curves available for use as part of the CVIA module (recall Sec. 3.2). Using the replacement (i.e., generalized) barge bow load-deformation curve, an additional vessel collision analysis (using CVIA) is carried out in conjunction with re-use of the old St. George Island Causeway partial-bridge FBMP model, as well as re-use of the impact weight and initial velocity recorded during the B3T4 test (Fig. 4.5.2).

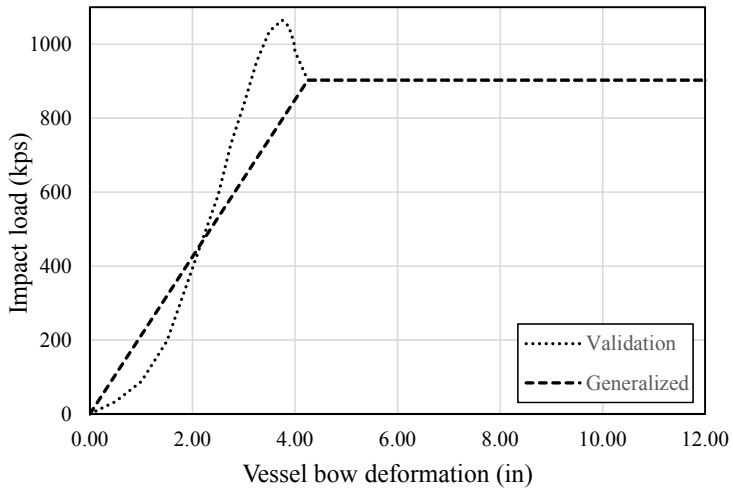

Figure 4.5.1. Replacement of vessel-specific, impact-specific load-deformation curve with generalized load-deformation curve

Numerical predictions of bridge pier (Pier 3-S) lateral displacement at the B3T4 impact location, obtained from use of the vessel collision conditions and generalized load-deformation curve given in Fig. 4.5.2, are plotted in Fig. 4.5.3. As a contextual facilitation, results from the CVIA validation case analysis and the physical record of B3T4 pier motions (Consolazio et al., 2006) are also plotted in Fig. 4.5.3. Importantly, as demonstration of the robustness of the CVIA module implemented in FBMP, the through-time record of Pier 3-S response predictions obtained from utilization of the generalized load-deformation relationship do not differ substantially from those of either the validation case (Fig. 4.4.9) or the 2004 full-scale experimental results. Specifically, the maximum lateral displacement associated with the generalized load-deformation curve (1.5 in.) falls between that of the validation case results and the physical B3T4 test results. Given that such good agreement is maintained among the impacted bridge pier responses, despite the employment of a generalized vessel characterization, it is concluded that, for the bridge-pier-soil configuration considered (Fig. 4.4.6), that the CVIA module implemented in FBMP is capable of robustly generating response predictions that show good agreement with full-scale experimental results.

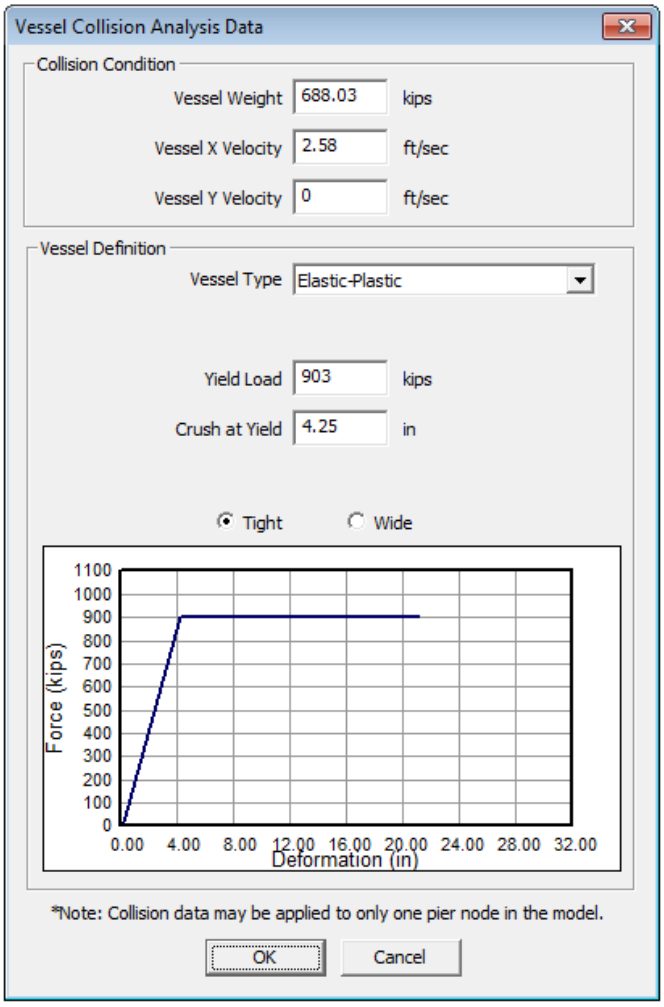

Figure 4.5.2. Vessel collision conditions with use of the generalized load-deformation curve

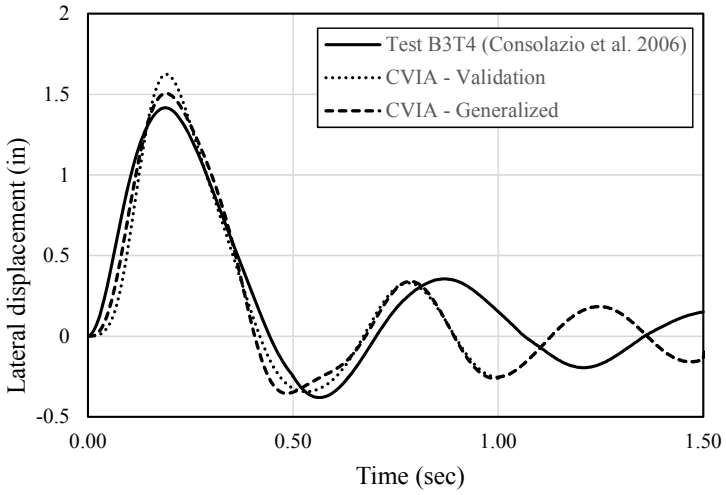

Figure 4.5.3. Lateral displacement comparison between physical test B3T4 and CVIA results

CHAPTER 5
ENGINEERING VERIFICATION OF CVIA-OPTS IN FB-MULTIPIER

5.1 Introduction

As a natural extension of the validation efforts dedicated to the CVIA module in the previous chapter (Chapter 4), the focus of Chapter 5 is directed toward validation of the OPTS implementation in FBMP. In particular, the combined CVIA-OPTS implementation has been numerically verified by comparing a range of results obtained from dynamic vessel collision analysis (CVIA) for a true multiple-pier, multiple-span model (i.e., full-bridge model) to those obtained using a corresponding CVIA-OPTS model.

By demonstrating strong agreement between numerical predictions of impact loading and response for full-bridge and respective OPTS models, the validation efforts of Chapter 5 support the assertion that the OPTS modeling implementation is of good quality with respect to correctness of coding. Additionally, the full-bridge and OPTS model results presented in Chapter 5 have been subjected to critical analysis from an engineering perspective, and thereby, the predictive capabilities of the OPTS modeling technique (relative to multiple-pier, multiple-span bridge models) have been judged to be sound. Simultaneously, in association with the engineering-based critical analysis, the bridge case considered herein serves as a start-to-finish example for successful modeling and use of an OPTS model in nonlinear dynamic vessel collision analysis.

5.2 Bridge Case

An inventory, totaling seventeen bridge pier finite element models (in FBMP) for bridges located throughout Florida, USA was developed as part of a previous study (Consolazio et al., 2008). As part of the current study, a single bridge case was identified (in part) based on modeling efforts and techniques used for bridge piers from the previously developed bridge model inventory. However, because the current study entailed the use of a single bridge case in carrying out numerical verification of the CVIA-OPTS implementation in FBMP, additional considerations have been made for any instances where both extensive (physical) site measurements and analytical study results are available for a given bridge site.

In partial satisfaction of the aforementioned bridge-case-selection criteria, the State Road 20 (SR-20) at Blountstown Bridge was modeled in full-bridge and OPTS configurations. Critically though, extensive geotechnical data are also available for the SR-20 bridge site as a result of previously conducted full-scale testing of the bridge foundation members (McVay et al., 2003). Further, structural drawings, foundation installation tables, and a record of boring logs are available. Therefore, the SR-20 at Blountstown Bridge was selected as the bride case for carrying out the CVIA-OPTS numerical verification tasks as part of the current study. Accordingly, FBMP models of the full-bridge (i.e., multiple-pier, multiple-span) and OPTS configurations were developed, as discussed in detail below. As demonstration of the capabilities of the FBMP analytical framework for barge-bridge collision analysis, a vessel collision scenario has been established based on site-specific waterway traffic; both the full-bridge and OPTS models have

been subjected to identical barge impact loading using CVIA; and finally, the analytical results have been compared.

5.2.1 SR-20 at Blountstown Bridge

The 1.6 mile long SR-20 at Blountstown Bridge was constructed in 1998 to span the Apalachicola River in northwestern Florida (Fig. 5.2.1). Constructed alongside the historical SR-20 Trammel Bridge (the northernmost, or top roadway in Fig. 5.2.1), the relatively newer bridge (the southernmost, or bottom roadway in Fig. 5.2.1) carries all eastbound traffic along a series of (generally) simply supported 150 ft prestressed girder spans up to the main channel spans. Within the immediate vicinity of the Apalachicola River, and its 150 ft wide navigation channel, the three spans associated with main channel span unit each exceed 200 ft, and are carried along four haunched steel plate girders (Fig. 5.2.2).

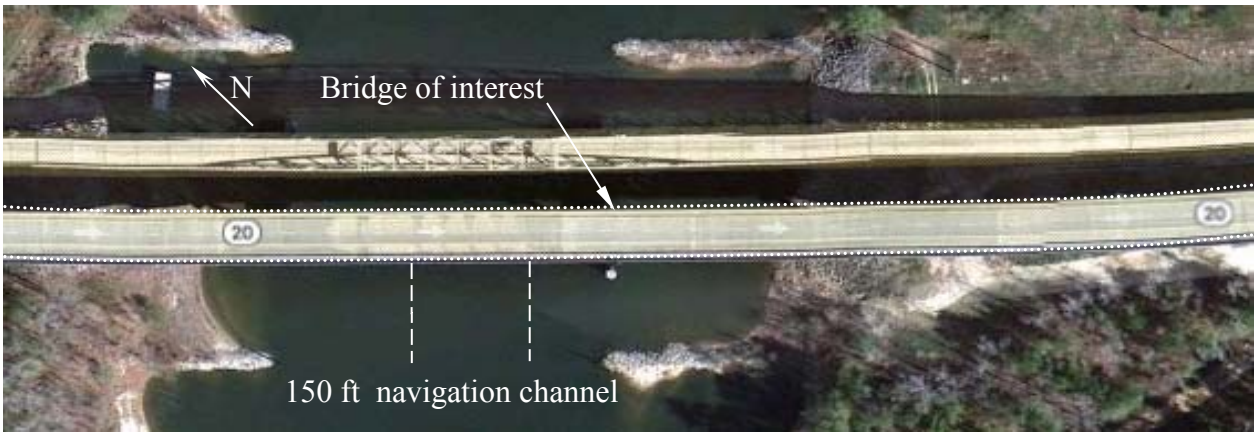

Figure 5.2.1. SR-20 at Blountstown site (image source: Google Maps)

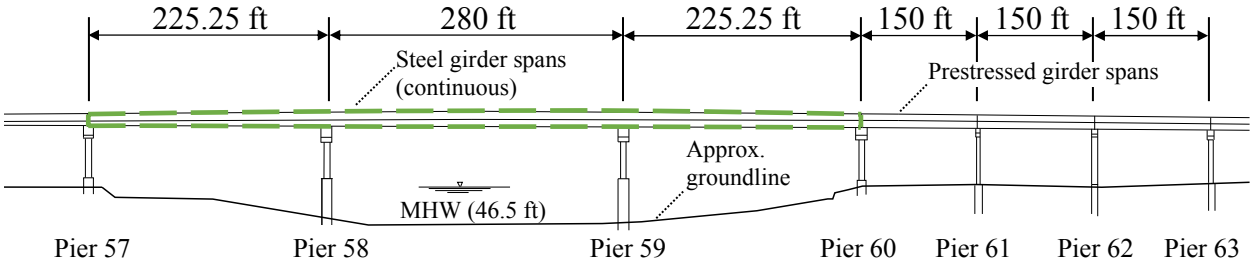

Figure 5.2.2. Elevation schematic of SR-20 at Blountstown Pier 57 through Pier 63

Of primary interest in the current study was the eastern channel pier, Pier 59, for which a corresponding OPTS model was formed (as discussed in Sec. 5.2.3). Based on structural drawings, boring logs, and previously established bridge modeling techniques (e.g., Consolazio et al., 2008), a multiple-pier, multiple-span (full-bridge) model of the SR-20 bridge was created in FBMP (Fig. 5.2.3). Bridge member material properties, obtained from the structural drawings, are listed in Table 5.2.1. The full-bridge model includes all piers supporting the continuous steel

girder spans (Piers 57 through 60), as well as three piers (Piers 61 through 63) and spans extending eastward from the channel span. As a result, and within the context of vessel collision loading applied to Pier 59 (discussed in Sec. 5.2.6), the full-bridge model includes a sufficient number of spans and piers to ensure that collision-induced load propagation throughout the bridge model will have dissipated to nominal levels before reaching the bridge model extents. All piers shown in Fig. 5.2.3 contain two drilled shafts and overlying, collinear pier columns. For the four piers that support the continuous steel girder spans (Piers 57 through 60), the drilled shafts and pier columns are integrated through reinforced concrete shear walls. As also indicated in Fig. 5.2.3, the diameters of drilled shafts decrease (from 9 ft to 6 ft) for increasing positions away from the main channel span.

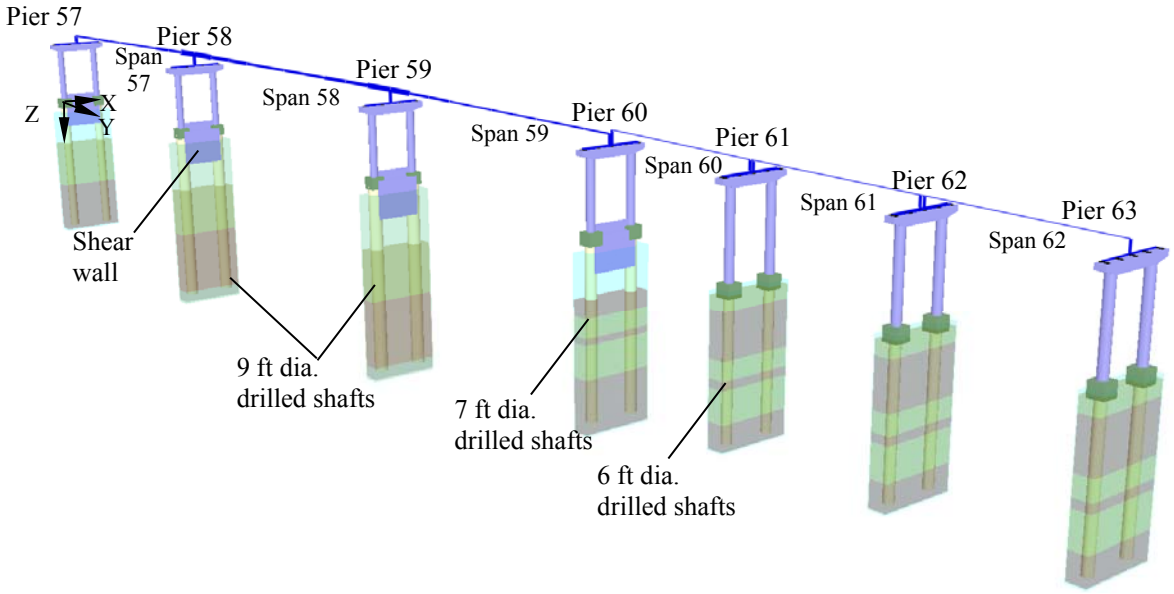

Table 5.2.1. Mechanical properties of SR-20 at Blountstown bridge structural members

Structural component	Parameter	Value	Unit
Superstructure deck concrete	Compressive strength	4.5	ksi
Superstructure deck concrete	Elastic modulus	3,370	ksi
Superstructure deck concrete	Poisson's ratio	0.2	--
Superstructure deck concrete	Unit weight	150	pcf
Mild steel reinforcement	Elastic modulus	29,000	ksi
Mild steel reinforcement	Poisson's ratio	0.3	--
Mild steel reinforcement	Unit weight	490	pcf
Mild steel reinforcement	Yield stress	60	ksi
Steel plate girders	Elastic modulus	29,000	ksi
Steel plate girders	Poisson's ratio	0.3	--
Steel plate girders	Unit weight	490	pcf
Pier concrete	Compressive strength	5.5	ksi
Pier concrete	Elastic modulus	4,200	ksi
Pier concrete	Poisson's ratio	0.2	--
Pier concrete	Unit weight	150	pcf
Drilled shaft concrete	Compressive strength	4.1	ksi
Drilled shaft concrete	Elastic modulus	3,270	ksi
Drilled shaft concrete	Poisson's ratio	0.2	--
Drilled shaft concrete	Unit weight	150	pcf

5.2.2 Pier 59 Structural Configuration

As stated above, the eastern channel pier, Pier 59, was selected as the impacted pier for the CVIA-OPTS numerical validation efforts. The structural configuration for Pier 59 is shown in Fig. 5.2.4. The reinforced concrete channel pier structure consists of two round (5.5 ft diameter, 37.1 ft tall) pier columns spaced 30 ft apart. Two 9 ft diameter drilled shafts tie-in directly beneath the pier columns, and the axially collinear pier columns and drilled shafts are further integrated by a 30.5 ft tall shear wall (which includes a relatively thin, top-placed 5 ft tall architectural shear strut). The shear wall vertical extents are intended to align approximately at the above-grade mid-height of the pier.

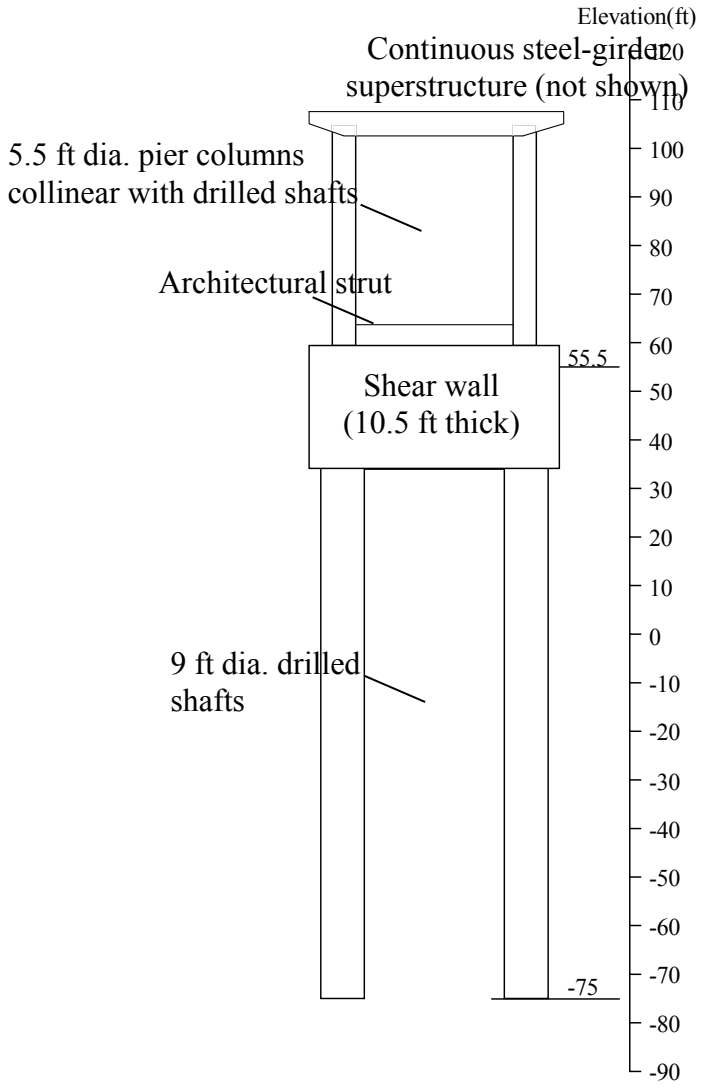

Figure 5.2.4. Pier 59 structural configuration (superstructure not shown)

The Pier 59 shear wall contains 10.5 ft wide semi-circular ends that encompass the pier columns and drilled shafts well below and well above the 46.5 ft mean-high water (MHW)

elevation for the Apalachicola River. In accordance with current vessel-bridge collision design practice (FDOT 2014), the Apalachicola River is assumed to be staged at the MHW elevation for purposes of CVIA-OPTS numerical verification. Consequently, the channel pier was configured so that it contains rounded impact surfaces, within the context of head-on impact scenarios. The FBMP model of Pier 59 (superstructure not shown) is shown in Fig. 5.2.5, where the impact location is indicated (the vessel collision scenario associated with Pier 59 is discussed in detail Sec. 5.2.6).

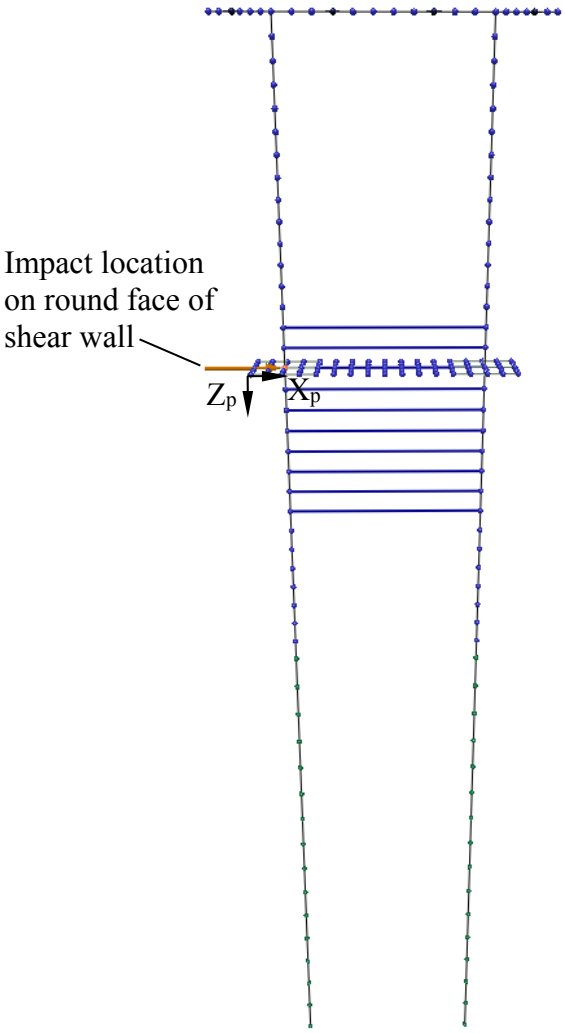

Figure 5.2.5. Pier 59 finite element model (superstructure not shown)

5.2.3 Pier 59 OPTS Model

The Pier 59 OPTS model, developed based on structural drawings and site-specific geotechnical data (discussed in Sec. 5.2.4 and Sec. 5.2.5), is shown in Fig 5.2.6. Adjacent to the channel pier, the 280-ft channel and 225.25-ft flanking superstructure spans (Spans 58 and 59) consist of four, continuous steel plate girders and a reinforced concrete slab. Load transfer devices at the substructure-superstructure interface are evenly spaced under the four steel plate

girders along the Pier 59 pier cap beam centerline. Each load transfer device consists of a 3 in thick steel bearing bevel plate that overlies an elastomeric bearing pad. Four end-threaded, cast-in-place anchor bolts pass through each bearing bevel plate and into the pier cap beam. The threaded tops of the anchor bolts are capped with nuts, which provide resistance against bearing uplift.

The condensed stiffness, and in turn, the series of springs placed at the left and right ends of the OPTS model were formulated, conceptually, in accordance with Consolazio and Davidson (2008). Namely, the set of springs placed at the left end of the OPTS model (Table 5.2.2) were formed using flexibility matrix formulation and inversion, by iteratively operating on an isolated sub-model of Span 57 and its associated piers. The iterative procedure for characterizing OPTS model span-end stiffnesses is given in Appendix A. An analogous procedure was employed in forming the right-end span springs, using an isolated model of Spans 60 through 62 and the associated piers. The mass of the right half of Span 57 was used to determine the lumped mass on the left end of the OPTS model, and the mass of the left half of Span 60 was used to determine the lumped mass value at the right end of the OPTS model.

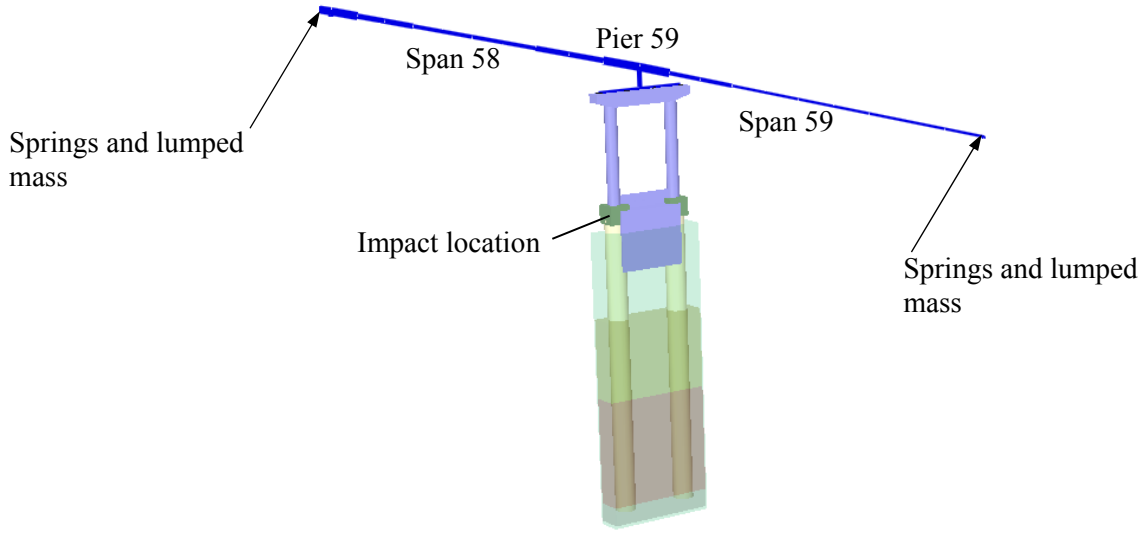

Table 5.2.2. Span-end spring stiffnesses

Span	X-Translation (kip/in)	Y-Translation (kip/in)	Z-Translation (kip/in)	X-Rotation (kip-ft/rad)	Y-Rotation (kip-ft/rad)	Z-Rotation (kip-ft/rad)
58	93	71	7,620	6.8E+06	1.2E+07	5.0E+06
59	145	37	4,030	8.1E+04	3.6E+06	2.3E+05

5.2.4 Considerations for Modeling of Pier 59 Drilled-Shaft Soil Resistance

Soil modeling constitutes a necessary consideration in forming a representative bridge finite element model, where soil resistance can play a significant role in the impacted bridge response (Consolazio et al., 2006, McVay et al., 2005a). The means by which soil modeling are formed for use in FBMP for the selected bridge case has been documented as part of the current study efforts, with emphasis on the modeling of Pier 59 (analogous soil modeling approaches are employed at other pier locations). Those considerations given to modeling of Pier 59 non-tip soil

properties (e.g., axial skin resistance) are discussed immediately below, whereas tip layer considerations are discussed in Sec. 5.2.5.

Per the bridge structural drawings, the axial design capacity for the 9-ft-diameter drilled shafts at Pier 59, with designed tip elevations of -75 ft, is listed as 2,000 tons (4,000 kips). So as to maintain consistency with the bridge design laid out in the structural drawings (and, correspondingly, the physical bridge structure), a deterministic soil modeling approach was elected, where the set of borings local to Pier 59 was investigated to identify an individual boring with an approximately equal axial capacity. Current design practice in Florida dictates that, for drilled shaft axial capacity, failure of the member is taken as the axial load corresponding to a vertical tip displacement of $1/30^{th}$ of the shaft diameter (FDOT 2014). Given the 2,000-ton axial capacity listed in the structural drawings and the FDOT drilled shaft failure criterion, FB-Deep models (FB-Deep 2014) of the four borings local to Pier 59 were created (Fig. 5.2.7) to quantify boring-specific axial capacities in association with the 9-ft-diameter drilled shafts. Among these four borings, axial shaft capacities were found to range from 2,169 tons (for boring 59-4) up to 2,694 tons (for boring 59-1). The estimate of axial capacity associated with boring 59-4 fell nearest to the 2,000 ton axial capacity (within 8%), and therefore, it was used in forming estimates of soil layering (Fig. 5.2.8) and soil-strength parameters at Pier 59. Note that, in maintaining consistency with current design practice, one half of the long-term (i.e., 100 year) scour depth was discounted from the top of the boring 59-4 soil strata, as reflected in Fig. 5.2.8. As a result, the top soil layer elevation is located at an elevation of 6 ft, based on the scour depth listed in the structural drawings.

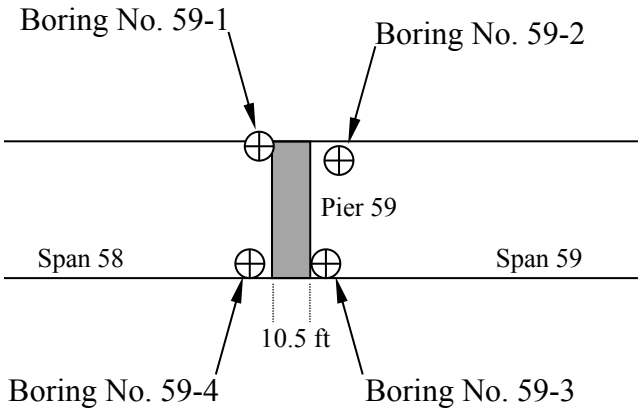

Figure 5.2.7. Plan-view schematic of boring placement near Pier 59

The soil model formulation of FBMP involves the definition of constitutively nonlinear soil resistance springs (axial, lateral, torsional), distributed along the nodes of all embedded

foundation elements. In building up the soil resistance springs, standard penetration test (SPT) blow counts (for sand layers), and undrained shear strength, C_u, (for clay layers) were taken directly from boring 59-4, as listed in Table 5.2.3. Empirical correlations given in the FB-Deep Help Manual (Chung 2014b) and the FBMP Help Manual (Chung 2014a) were then employed in estimating soil strength parameters for all non-tip soil layers in the FBMP model.

In addition to containing sand and clay layering, the soil profile for boring 59-4 also includes layers of limestone. The modeling of distributed nonlinear soil springs for drilled shafts embedded in limestone requires the estimation of several additional soil-strength parameters specific to the limestone found at the bridge site (Table 5.2.4). For example, unconfined compressive strength (q_u); mass modulus (E_m); the ratio of mass to intact modulus (E_m/E_i); and split tensile strength (q_t) are all required. Further, the drilled shaft concrete slump and 28-day elastic modulus are required as part of the limestone layer description in FBMP. Drawing directly from boring 59-4 and the structural drawings, layer-based averages of unconfined compressive strength (q_u), split tensile strength (q_t), concrete slump, and drilled shaft elastic modulus (3,270 ksi) were obtained. Extensive field testing and core sampling datasets, recorded as part of McVay et al. (2003), were additionally used to relate quantities such as core sample recovery (%) to the ratio of mass modulus and intact modulus (E_m/E_i); unconfined compressive strength (q_u) to intact modulus (E_i); and to estimate borehole surface conditions. All other layer-based soil strength parameters listed in Table 5.2.4 were estimated based on empirical relationships given in the FB-Deep Help Manual (Chung 2014b) and the FBMP Help Manual (Chung 2014a).

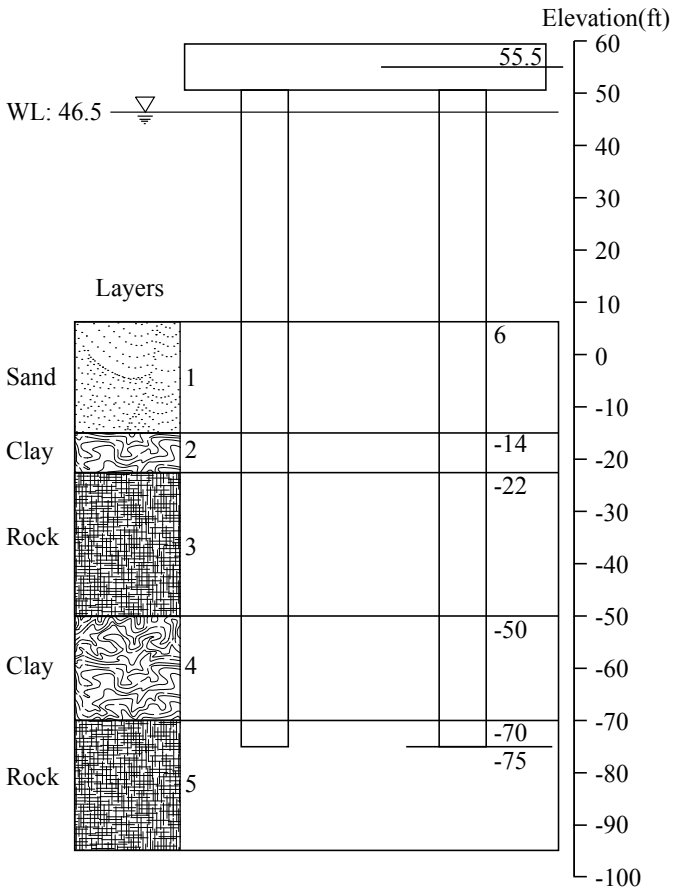

Figure 5.2.8. Soil layering for Boring 59-4

Table 5.2.3. Boring 59-4 sand and clay properties at Pier 59

Layer	Soil Type	SPT	Top Elev. (ft)	ɣ (pcf)	φ (°)	k (pci)	C_u (psf)	ε_{50}	G (ksi)	τ_u (psf)
1	Sand	3-30	6	90-130	29-36	20-100	NA	NA	0.23-1.67	20-1,212
2	Clay	NA	-14	140	NA	1,000	3,150	0.004	5	3,150
4	Clay	NA	-50	140	NA	2,000	12,250	0.004	6.77	12,250

Table 5.2.4. Boring 59-4 rock (limestone) properties at Pier 59

Layer	Top Elev. (ft)	Recovery (%)	q_u (psf)	q_t (psf)	Slump (in)	ɣ (pcf)	φ (°)	G (ksi)	ν	τ_u (psf)	E_m (ksi)	E_m/E_i	Surface
3	-22	33	63,760	6,376	8	130	37	8.95	0.22	8,092	21.9	0.1	Rough
5	-70	69	29,000	2,900	8	130	37	29.7	0.22	6,838	24.9	0.62	Rough

5.2.5 Considerations for Modeling of Drilled-Shaft End Bearing Resistance

Consistent with the layer depth estimates for boring 59-4 (Fig. 5.2.8) and previously conducted field testing (McVay et al., 2003), the 9 ft diameter drilled shafts of Pier 59 are embedded nearly 70 ft into soil and rock before terminating within a limestone layer at the shaft tips. For the specific case of vessel collision analysis of the Pier 59 foundation configuration, and

for the specific use of boring 59-4 in modeling non-tip soil (and limestone) resistance, the tip resistance does not play a significant role in the impacted bridge pier response. However, in general, point-bearing resistance at the tips of drilled-shaft foundations may contribute significantly to overall foundation response (Chung et al., 2012). Therefore, the process of forming estimates of tip resistance for the limestone tip layer at Pier 59 of the SR-20 bridge site is presented below, which serves as a guide for calculation of load-displacement characteristics for cases where soil-shaft interaction strongly influences overall bridge pier response.

The overall process was initiated by cataloging all available rock coring data from borings within reasonable proximity to the foundation members of interest (i.e., the drilled shafts of Pier 59). In this instance, coring data were extracted from boring logs taken at Pier 58, Pier 59, and Pier 60 from the SR 20 bridge site (Table 5.2.5). Specifically, spatially point-specific (i.e., individual) values of unconfined compressive strength (q_u), core recovery (%), and rock quality designation (RQD) were all directly determined in this way. Then, the intact moduli (E_i) were estimated, where due to the extensive geotechnical investigation conducted at the SR-20 bridge by McVay et al. (2003), a site-specific relation is employed:

$$E_i = 584.35 \cdot q_u \qquad \text{(Eqn. 5.2.1)}$$

Based on coring data given in McVay et al. (2003), the coefficient of variation (CV_{Ei}) associated with use of the correlation given in Eqn. 5.2.1 was found to be 0.6. Such coefficient of variation values are used below in adjusting deterministic stiffness values to account for dispersion-related uncertainties found among the correlations.

Ratios of mass modulus to intact modulus (E_m/E_i) were then estimated based on correlations with recovery (%) and/or RQD values (see for McVay et al., 2003 for an instance of using recovery percentages; and see O'Neill 1996 for an instance of using RQD values). For the bridge case in the current study, the methodology specific to the SR-20 site for correlating between core recovery percentage and E_m/E_i values was employed (McVay et al., 2003), where the modular ratios are listed in Table 5.2.5. Due to a lack of available data, the associated coefficient of variation ($CV_{Em/Ei}$) for utilizing the core recovery percentage to E_m/E_i value correlation given in McVay et al. (2003) was assumed to be 0.25.

Table 5.2.5. Rock coring data from Piers 58 through 60

Boring	Elev. (ft)	q_u (tsf)	Core Recovery	RQD	E_m/E_i	E_i (ksi)	E_m (ksi)
P59-1	-27.5	1	0.65	0.37	0.56	8.116	4.565
P59-1	-56	4.85	0.4	0.23	0.12	39.362	4.592
P59-1	-61.5	5.9	1	0.5	1.00	47.884	47.884
P59-3	-30	4.2	0.85	0.67	0.85	34.087	28.974
P59-3	-60.5	9.95	1	0.8	1.00	80.754	80.754
P59-4	-28	3.15	0.5	0.45	0.15	25.565	3.835
P59-4	-47	60.65	0.27	0.13	0.07	492.234	36.097
P59-4	-61	9.8	1	0.77	1.00	79.537	79.537
P59-4	-69	14.3	1	0.85	1.00	116.058	116.058
P58-1	-53	5.7	0.65	0.3	0.56	46.261	26.022
P58-1	-69	7.05	0.65	0.23	0.56	57.218	32.185

P58-2	-32.5	2	0.63	0.47	0.51	16.232	8.238
P58-2	-64	5.6	0.83	0.72	0.83	45.449	37.723
P58-2	-68	12.35	0.83	0.72	0.83	100.232	83.193
P58-3	-26	3.1	0.75	0.68	0.75	25.160	18.870
P58-4	-44	37.05	0.37	0.25	0.11	300.697	32.074
P59-4	-61.5	0.2	1	0.82	1.00	1.623	1.623
P60-1	-39	16.95	0.35	0.08	0.10	137.566	13.757
P60-1	-51	60.4	0.37	0.07	0.11	490.205	52.289
P60-1	-55	6.25	1	0.83	1.00	50.725	50.725
P60-1	-57	8.7	1	0.83	1.00	70.609	70.609
P60-1	-65	9	0.92	0.57	0.92	73.044	67.200
P60-3	-63	6.2	0.93	0.82	0.93	50.319	46.797
P60-3	-69	4.1	1	0.82	1.00	33.275	33.275

Individual estimates of mass modulus (E_m), also listed in Table 5.2.5, were calculated by taking the product of the intact modulus (E_i) and the corresponding modular ratio (E_m/E_i). Outlier values of mass modulus (E_m) obtained in this way were excluded from Table 5.2.5, where in this context, an outlier was defined as a mass modulus (E_m) value falling more than three standard deviations outside of the dataset mean. Having formed individual estimates of mass modulus (E_m) and cataloging values of unconfined compressive strength (q_u), finite element analysis (FEA) was employed to quantify deterministic, macroscopic (i.e., foundation member level) tip stiffnesses (K_{det}).

In the current study, the methodology set forth in Chung et al. (2012) was utilized in the associated FEA. Namely, using the general purpose FEA software ADINA (2014), an axisymmetric finite element model of the 9-ft diameter drilled-shaft was formed (Fig. 5.2.9), loaded axially, and the tip deflection was calculated. Detailed examples that aid in selection of various model components (e.g., element formulation, material model selection, active degrees of freedom, boundary conditions) are given in Chung et al. (2012). Material properties for elements representing the drilled shaft were supplied in accordance with quantities listed in Table 5.2.1, and the embedded length of the drilled shaft elements within the surrounding medium of elements representing the rock was selected to be consistent with the tip layering for boring 59-4.

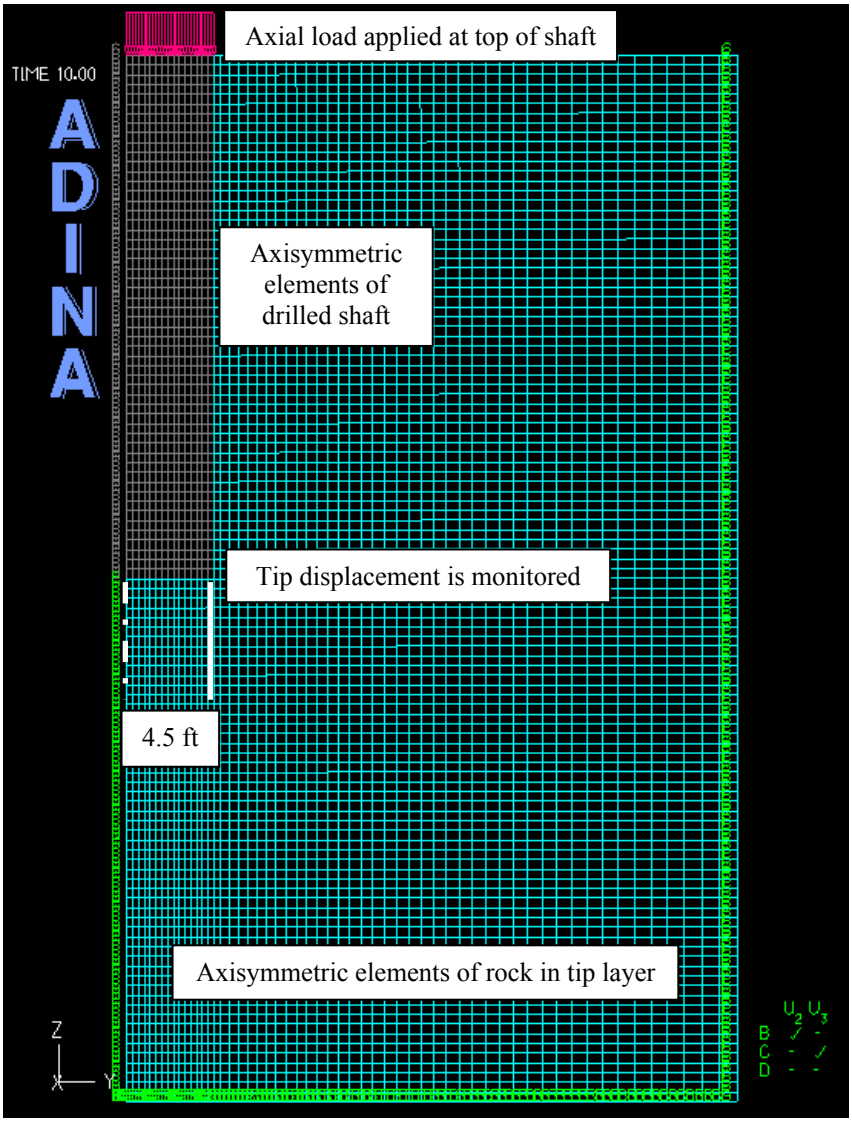

Figure 5.2.9. Estimating a deterministic tip stiffness (K_{det}) of drilled shafts (of Pier 59) with a 27-ft embedment

As a means of bounding the deterministic estimates of drilled shaft tip stiffness (K_{det}) for Pier 59, two simulations were carried out using the axisymmetric model. In the first simulation, material properties (E_m, q_u) for elements representing the rock were homogenously taken as the average of all individual estimates local to Pier 59 (Table 5.2.5). In the second simulation, the average of all estimates of input material properties (E_m, q_u) listed in Table 5.2.5, for those elements representing the homogenous rock, were taken from across the wider spatial domain (i.e., from across coring data for Piers 58 through 60). In this way, estimates of deterministic tip stiffness (K_{det}) were made both for the relatively local (to Pier 59) rock coring data, as well as for rock coring data that are more representative of the wider soil conditions at the bridge site.

The deterministic tip stiffness (K_{det}) obtained from the ADINA simulations was estimated to be 3,727 kip/in (for coring data local to Pier 59) and 3,394 kip/in (across Piers 58 through 60).

Importantly, in order to account for the dispersion present among the correlations used in estimating the mass modulus (E_m) values, the deterministic tip stiffness values (K_{det}) was adjusted. Accordingly, a coefficient of variation ($CV_{constituent}$) was first determined as 0.65 by taking the square root sum of squares (SRSS) for the constituent coefficients (i.e., CV_{Ei} and $CV_{Em/Ei}$).

As a next step, coefficients of variation (CV_{Em}) for the mass modulus (E_m) values were determined, separately, to be 0.9 for the local Pier 59 data listed in Table 5.2.5 and 0.74 for the Piers 58 through 60 data listed in Table 5.2.5. Then, an effective coefficient of variation (CV_{eff}), which accounts for both the dispersion of the E_m values themselves as well as the dispersion associated with use of constituent correlations in arriving at the E_m value estimates, was calculated (separately) for the local Pier 59 data and for the Piers 58 through 60 data through SRSS:

$$CV_{eff} = [CV_{Em}^2 + CV_{constituent}^2]^{0.5} \quad \text{(Eqn. 5.2.2)}$$

Using Eqn. 5.2.2, the effective coefficient of variation (CV_{eff}) for the local (to Pier 59) mass modulus (E_m) values was determined to be 1.11. The respective CV_{eff} for all E_m values listed in Table 5.2.5 (i.e., encompassing coring data from Pier 58 through 60) is 0.98. Finally, each CV_{eff} value was paired with the corresponding value of K_{det} to form an effective stiffness (K_{eff}):

$$K_{eff} = K_{det} / (1 + CV_{eff}^2) \quad \text{(Eqn. 5.2.3)}$$

For the bridge case of interest in the current study, and in particular for Pier 59, Eqn. 5.2.3 yielded effective stiffness (K_{eff}) estimates of 1,670 kip/in (local to Pier 59) and 1,731 kip/in (across Piers 58 through 60), as plotted in Fig. 5.2.10. As aforementioned, for the SR-20 bridge case, which contains relatively long embedment depths for the sizable drilled shafts, the range of tip stiffnesses do not correspond to significant changes in structural member demand. Given the insensitivity, the lower bound stiffness value was used in the SR-20 full-bridge and OPTS models.

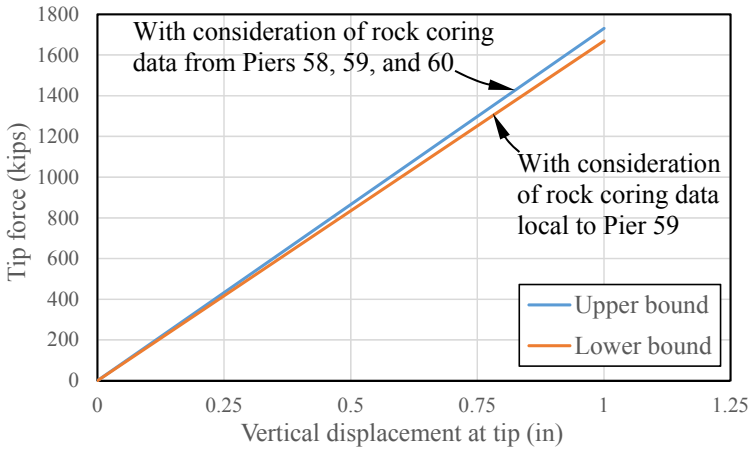

Figure 5.2.10. Bounded estimates of Pier 59 drilled shaft tip stiffness

5.2.6 Barge-Bridge Collision Scenario

For an impacting barge (or barge flotilla), the corresponding weight, in-transit velocity, and transit direction play significant roles in the impact forces generated. Therefore, prior to performing nonlinear dynamic vessel collision analysis (CVIA), it is important to ascertain a reasonable estimate of the vessel collision characteristics. As a first step, the initial impact velocity is estimated by making use of waterway-specific (i.e., Apalachicola River) traffic characteristics.

In a previous study, Liu and Wang (2001) tabulated annually averaged waterway vessel traffic characteristics for all navigable waterways in Florida. As part of the tabulation efforts, the types of vessels traversing each of the Florida waterways were divided, by draft, into vessel groups and expressed in one-year intervals. An excerpt of the data is listed in Table 5.2.6 for waterway vessel traffic of the Apalachicola River. The data listed in Table 5.2.6 include flotilla weight (W, MN); hydrodynamic mass coefficient (C_H); transit velocity (V, m/s); and transit angle (°) in the vicinity of the SR-20 at Blountstown Bridge.

Table 5.2.6. Waterway vessel traffic data for the Apalachicola River (Liu and Wang, 2001)

Vessel group	C_H	W (kips)	Draft (ft)	V (knots)	Transit angle (°)
1	1.05	5,460	2.0	6.5	90
2	1.05	11,960	5.2	5.5	90
3	1.05	16,640	8.2	5.5	90
4	1.05	17,980	9.8	5.5	90

From Table 5.2.6, the vessel transit velocities range from 5.5 knots to 6.5 knots, and all transit angles are found to be 90°. Given the waterway-specific velocities, an initial head-on impact velocity of 5.9 knots (10 ft/s) was selected for use in the current study.

As the next step in formulating an impact scenario for use in the SR-20 at Blountstown Bridge case, the static vessel collision design load (2,550 kips) was taken directly from the structural drawings. Given the static vessel collision design load (P_B), the empirical load determination equations given in the American Association of State Highway Transportation Officials (AASHTO) *Guide Specifications and Commentary for Vessel Collision Design of Highway Bridges* (AASHTO 1991, AASHTO 2009), which encompasses design for waterway vessel collision, were used to back-calculate a kinetic energy associated with the impact scenario. In particular, the static vessel collision load, P_B in kips, is related to a vessel bow crush depth, a_B in ft:

$$P_B = \begin{cases} 4112 a_B R_B & \text{if } a_B < 0.34 \\ (1349 + 110 a_B) R_B & \text{if } a_B \geq 0.34 \end{cases} \qquad \text{(Eqn. 5.2.4)}$$

where R_B is a vessel width correction factor (taken as unity for this scenario), and further, it was assumed that the vessel bow crush depth (a_B) exceeds 0.34 ft. Then, the initial kinetic energy available to the impacting vessel (*KE*) was back-calculated from:

$$a_B = \left[\left(1 + \frac{KE}{5672} \right)^{1/2} - 1 \right] \frac{10.2}{R_B} \qquad \text{(Eqn. 5.2.5)}$$

Lastly, given the initial kinetic energy, *KE* in kip-ft, and the estimate of initial velocity (*V*), taken as 10 ft/s, the impacting vessel weight was back-calculated using:

$$KE = \frac{C_H W V^2}{29.2} \qquad \text{(Eqn. 5.2.6)}$$

where the hydrodynamic mass coefficient (C_H) was taken as 1.05 and *W* is the impacting vessel weight (tonnes).

By following the back-calculation procedure described above, the following barge characteristics were selected for the impact scenario considered in the current study: a barge flotilla weighing 11,430 kips; a hydrodynamic mass coefficient (C_H) of 1.05; traveling at 10 ft/s perpendicular to the bridge span; and possessing an associated kinetic energy (*KE*) of 18,648 kip-ft. Regarding impact location, the vessel collision load was applied at the same location as that specified in the structural drawings (55.5 ft). Therefore, the impact location falls upon the 10.5 wide rounded shear wall surface, at 9 ft above the MHW elevation of 46.5 ft. As part of the CVIA vessel characterization in FBMP, impact upon the shear wall surface corresponds to a barge bow yield force (P_{BY}) of 1,750 kips (recall Fig. 3.2.1) in forming the barge bow force-deformation relationship (with a yield crush depth of 2 in). Note that, by following the approach given above, energy equivalence was maintained between the static vessel collision design load and the dynamic vessel collision (CVIA) scenario.

5.2.7 Dynamic Analysis Considerations

A consistent mass approach is employed when conducting dynamic analyses in FBMP (Chung 2014a), and therefore, inertial effects were intrinsically accounted for in the current study by supplying unit weight values for all structural members in the FBMP dynamic analysis models. Permanent (i.e., quasi-static) loads such as self-weight were incorporated into the dynamic analyses through use of the dynamic relaxation feature (see Sec. 3.4). Lastly, Rayleigh damping (i.e., mass and stiffness proportional damping) was included in the dynamic analyses such that the first five natural modes of vibration in each model are damped at a level of approximately 5% (relative to critical damping levels). The formation of Rayleigh damping coefficients is illustrated in a step-by-step manner in Appendix A, where the methodology is

consistent with experimental findings (Paultre et al., 1992) and previously conducted analytical studies of vessel-bridge collision (e.g., Davidson et al., 2010).

5.3 Comparison of Full-Bridge and OPTS Barge-Bridge Collision Analysis Results

Full-bridge versus OPTS summary data for CVIA analyses of the SR-20 at Blountstown eastern channel pier are presented in Figs. 5.3.1 through 5.3.7. The structural configuration (excepting the superstructure) of the impacted pier is also shown in the response plots to spatially contextualize the bridge pier response quantities, where excellent agreement is consistently observed across the set of plots.

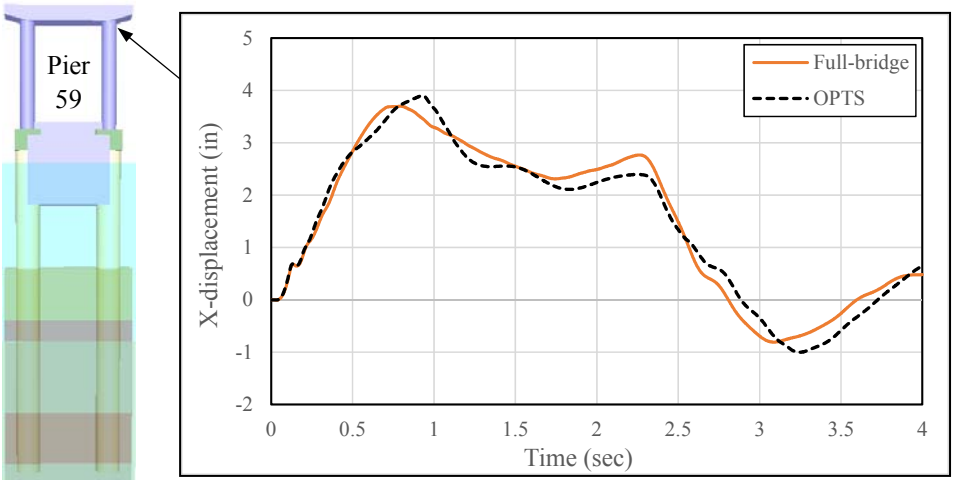

Figure 5.3.1. Time-histories of X-displacement at the top of the impacted column

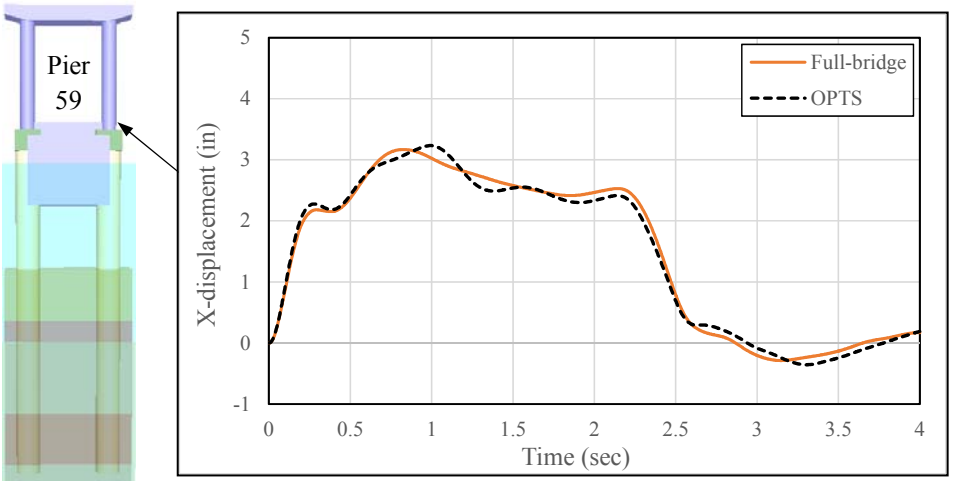

Figure 5.3.2. Time-histories of X-displacement at the base of the impacted column

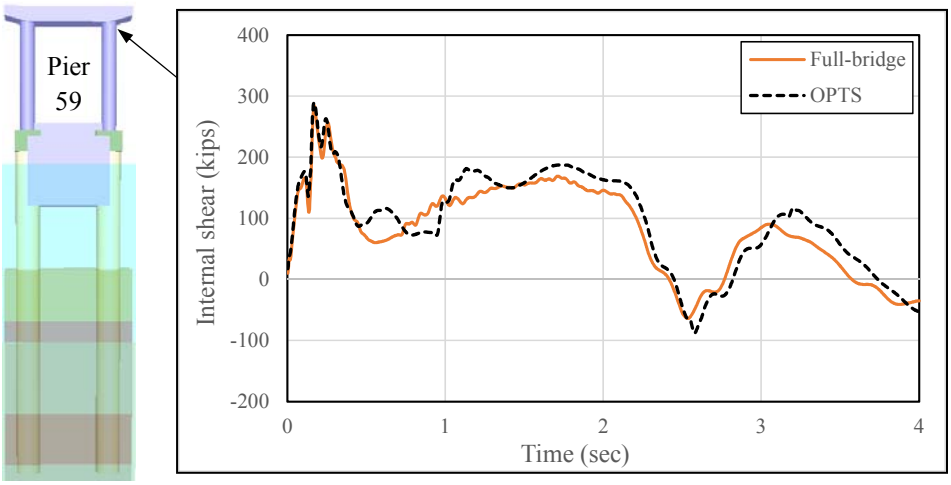

Figure 5.3.3. Time-histories of internal shear at the top of the impacted column

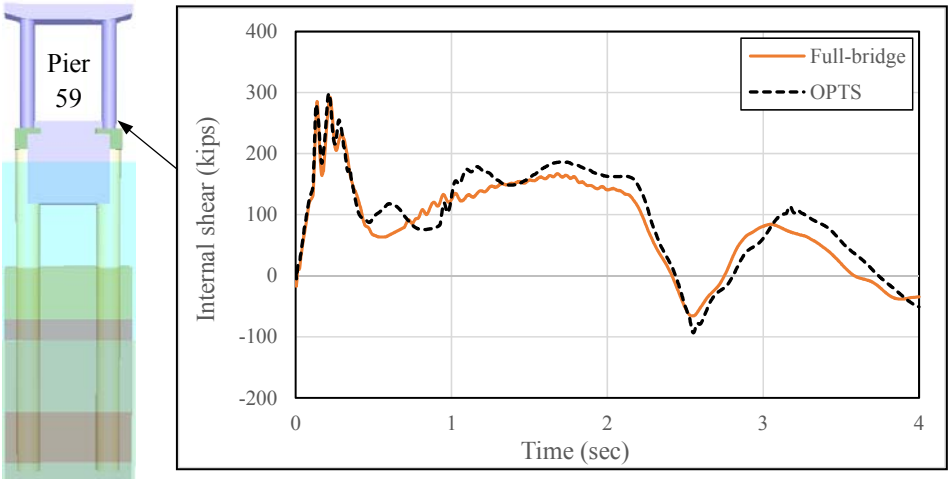

Figure 5.3.4. Time-histories of internal shear at the base of the impacted column

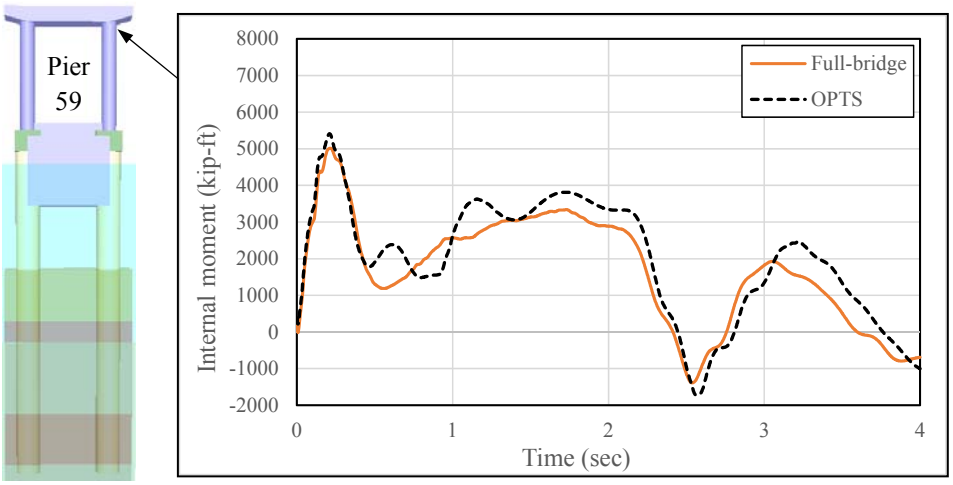

Figure 5.3.5. Time-histories of internal moment at the top of the impacted column

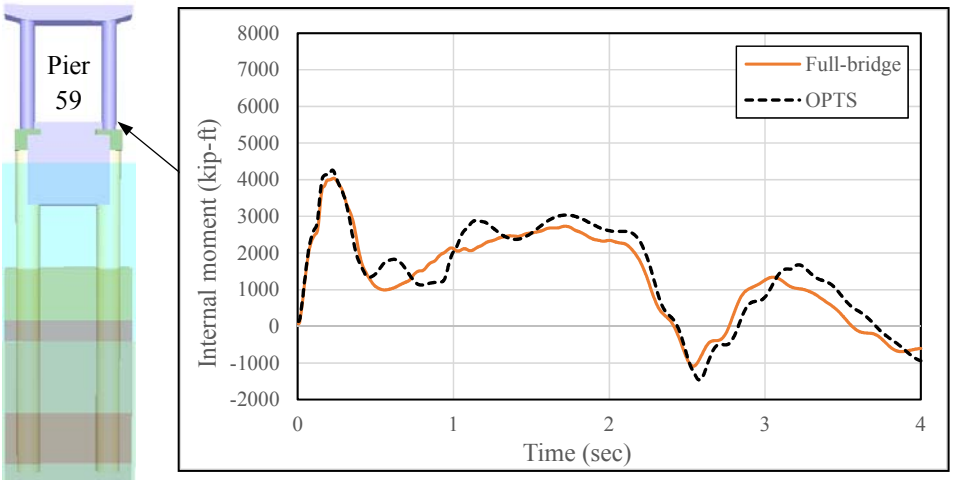

Figure 5.3.6. Time-histories of internal moment at the base of the impacted column

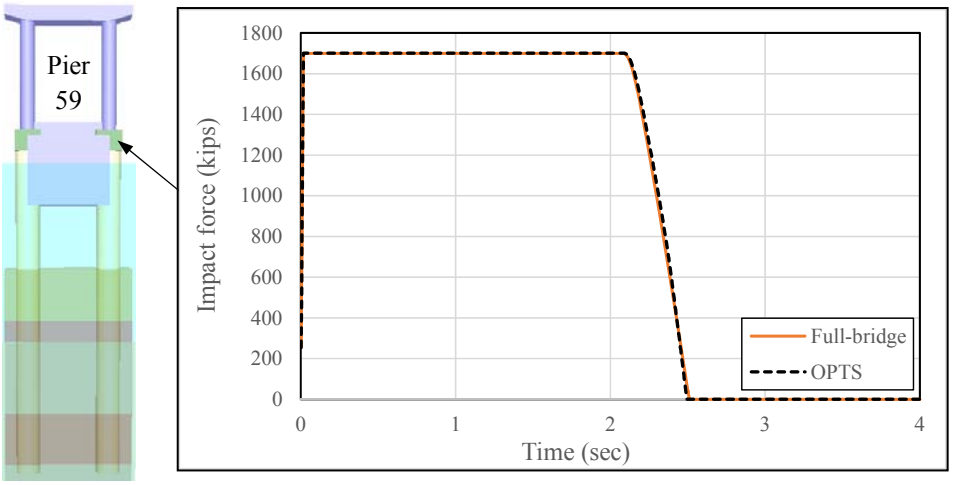

Figure 5.3.7. Time-histories of impact force

Of particular relevance to design practice are the through-time maximums of structural demand relative to corresponding member capacity. Plotted in Fig. 5.3.8 are the full-bridge and OPTS model CVIA predictions of (relative) maximum pier column and drilled shaft demand in the form of biaxial demand-capacity ratios (D/C). Across both comparisons, the member-specific maximum D/C values differ by less than 2%.

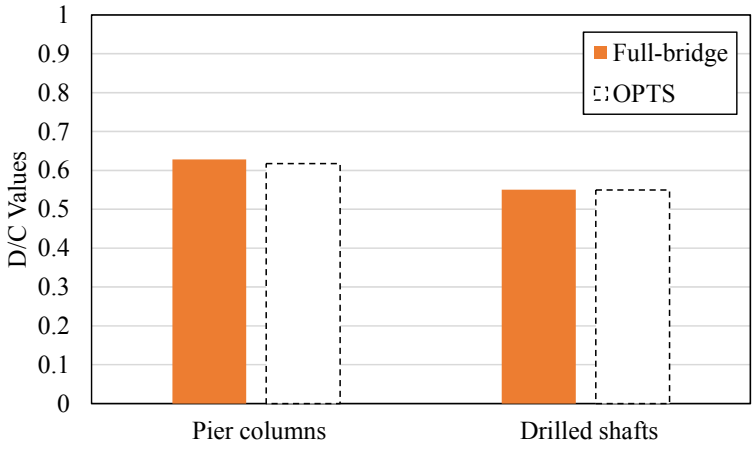

Figure 5.3.8. Maximum D/C values through time

5.4 Observations

Based on the nonlinear dynamic vessel collision analyses associated with the SR-20 full-bridge and OPTS models, the following observations were made:

- In general, OPTS analyses were found to predict maximum internal forces that range from nominally different to moderately conservative in comparison to corresponding values computed from full-bridge analyses (Consolazio et al., 2008). For the SR-20 bridge case examined as part of the current study, the corresponding full-bridge and OPTS analysis results were found to be nominally different. Further, an extensive set of favorably comparative (full-bridge versus OPTS) cases can be found in Consolazio et al. (2008). Given that consistently good agreement between full-bridge and OPTS analyses was obtained for the selected bridge case in the current study, as well as for a wide range of bridge and pier types as part of previous studies, it is concluded that the OPTS modeling technique can be used as a suitably accurate replacement for full-bridge models in conducting vessel collision analysis. Based on this conclusion, the remaining analyses conducted for this study utilize only OPTS models.

- Figs. 5.3.1 through 5.3.7 above indicate that the computed pier response was strongly influenced by the inertia of the superstructure. This is evidenced by noting the relative lag in the pier column top displacements (Fig. 5.3.1) relative to those of the impact point (Fig. 5.3.2) over the first 1 sec. of impact. The relative lag in displacement near the top of the pier, gives rise to transient spikes in internal demands, which manifest throughout the pier over the first 1 sec. of analysis (Figs. 5.3.3 through 5.3.6). This finding is consistent with previously conducted analytical studies (e.g., Davidson et al., 2010). The ramifications associated with adoption of a dynamic approach in assessing collision-induced structural demands are further explored in Chapter 6.

- Capturing the collision-specific phenomena necessitates use of dynamic analysis, and the efficiency of the CVIA-OPTS framework has been highlighted in this context. Namely, all analyses described above were conducted on an ordinary desktop computer. However, the time required to conduct the 4-second transient (CVIA) analysis of the full-bridge model totaled 96 min. In contrast, the CVIA-OPTS analysis, as implemented in FBMP (Chung 2014a), required only 5 min. to run to completion.

CHAPTER 6
COST-BENEFIT ANALYSIS

6.1 Introduction

The AASHTO specifications pertaining to vessel collision design of highway bridges (AASHTO 1991, AASHTO 2009) have served the practice of bridge engineering very well, and continue to do so. Namely, since 1991, all bridges spanning navigable U.S. waterways have been designed using the AASHTO vessel-collision specifications. The AASHTO organization encourages research, and when available and feasible, the use of more accurate analysis and design methods, as indicated in Chapter 4 ("Structural Analysis and Evaluation") of the AASHTO LRFD Bridge Design Specifications (AASHTO 2012). Further, the AASHTO LRFD Code is founded upon reliability concepts (i.e., load factors and resistance factors that promote uniform reliability levels against failures of bridge systems). Consistent with the spirit of the AASHTO LRFD Code (AASHTO 2012), the dynamic analysis and bridge modeling techniques developed in FBMP as part of the current study were intended to provide a practical means of making accurate bridge response predictions for vessel collision loading applications. Widespread, sustained use of these newly developed FBMP tools may increase uniform levels of reliability in performance prediction of bridge systems.

The numerically verified bridge modeling (OPTS) and validated analysis (CVIA) features of FBMP introduced in previous chapters are easy-to-use and efficient for the design purpose of conducting nonlinear dynamic barge-bridge collision analyses in practice. Further, dynamic analysis of vessel-bridge collisions is now viable given commonly available computational resources, and can potentially become a routine method of analysis for vessel collision loading in the near future. When considering deployment of reliable design and analysis procedures, potential changes in associated construction and retrofit costs (relative to those associated with existing design and analysis practice) are of particular interest.

A cost-benefit analysis has been performed by characterizing construction cost differences associated with bridge member sizing to resist barge-collision loading. In particular, two realistic design scenarios were considered: (1) Bridge member design (sizing) based on use of barge impact analysis techniques that are consistent with current practice (i.e., static analysis techniques); and (2) Member design based on use of the newly developed (dynamic) vessel collision analysis tools of FBMP. In both scenarios, the FBMP OPTS model of Pier 59 from the SR-20 bridge (see Sec. 5.2) were utilized in conjunction with a realistic barge impact scenario (which was formulated in Sec. 5.2.6). Levels of bridge pier structural demand (relative to constitutively nonlinear cross-section capacity), as well as profiles of internal demand for drilled shaft and pier column members were first quantified under the static analysis regime, through application of an energy-equivalent static impact load. Further, the numerical predictions of static demand were established as benchmarks in making member sizing (i.e., design) decisions.

Subsequently, an energy-equivalent dynamic vessel collision analysis (CVIA) was carried out for the same OPTS model (i.e., Pier 59 of the SR-20 bridge) in FBMP. Maximum

member demand-capacity values as well as profiles of internal member demand were again cataloged, and comparisons were made to the static analysis results. Then, the pier structural members and foundation members of the OPTS model were iteratively modified and subjected to the same barge impact scenario (through utilization of the CVIA module) until numerical predictions of structural member and foundation member demands obtained from the dynamic analysis results converged to the previously established benchmark values of static demands. Upon observing matching design-level (i.e., maximum) member demands between the benchmark static analysis results (which correspond to the original SR-20 bridge configuration) and the dynamic analysis results (which, after several iterations, correspond to the modified SR-20 bridge configuration), the changes in construction costs were quantified between the two bridge pier configurations.

6.1.1 Parity Considerations between Static and Dynamic Barge Impact Scenarios

For the models utilized in comparing static and dynamic analysis results, maintaining fidelity between the structural and soil models was trivial. Alternatively stated, the original Pier 59 OPTS model soil-structural configuration was used for both the static analysis and for the first dynamic analysis (i.e., prior to iterative member resizing). However, for all analyses conducted, care was taken to ensure that parity existed between the impact loading attributed to the Pier 59 static and dynamic OPTS models. Namely, parity was ensured among the static and dynamic vessel collision loading through energy-equivalence, as discussed below.

Shown in Fig. 6.2.1a is a schematic of a physical (head-on) barge impact scenario. At the onset of the collision event, the initial barge velocity propels it forward such that the barge bow makes contact with the impacted pier surface. The collision load that arises over the next several seconds is sensitive to many aspects of the overall, physical scenario. One aspect of the collision event that plays a significant role in dictating the impact loading is the kinetic energy initially attributed to the barge. This kinetic energy is a function (in part) of the barge, any cargo contained therein, and the barge velocity. If the barge is to be brought to a halt by the impacted structure, then the entirety of the initial kinetic energy must be absorbed through inelastic deformation of the barge bow and/or transferred into the bridge-pier-soil system. Until the initial kinetic energy is entirely dissipated, loads are generated along the barge-pier interface, and are sensitive to the relative orientation of the barge and pier, as well as the impacted surface geometry (Consolazio et al., 2008, Yuan et al., 2008). During the collision event, the contact-impact load varies in accordance with the interplay of the barge motion, pier motion, and the relative effective stiffnesses at the barge-pier interface. In current design practice, the initial kinetic energy of the impacting vessel is predominant in empirically determining an “energy-equivalent” static impact load (Fig. 6.2.1b). As previously detailed in Sec. 5.2.6, for a current AASHTO methodology (AASHTO 2012), design-barge weight and initial velocity were used to calculate an initial kinetic energy. In turn, the kinetic energy was empirically correlated with a barge bow crush depth, which was then used to determine a representative, static barge impact load.

In the current study, the static vessel-collision design load has been provided (in the original structural drawings which was obtained from the FDOT Structures Design Office) as 2,550 kips for Pier 59 of the SR-20 bridge. As noted in Sec. 5.2.6, the kinetic energy associated with the static load (18,648 kip-ft) was maintained for the dynamic (CVIA) barge impact scenario considered in the current chapter (Chapter 6). Specifically, the impact velocity was estimated as 10 ft/s, based on waterway-specific vessel traffic characteristics for the Apalachicola River and the impacting design-vessel weight was taken as 11,430 kips. In addition, the same impact location was maintained among the Pier 59 OPTS models used in the static and dynamic analyses.

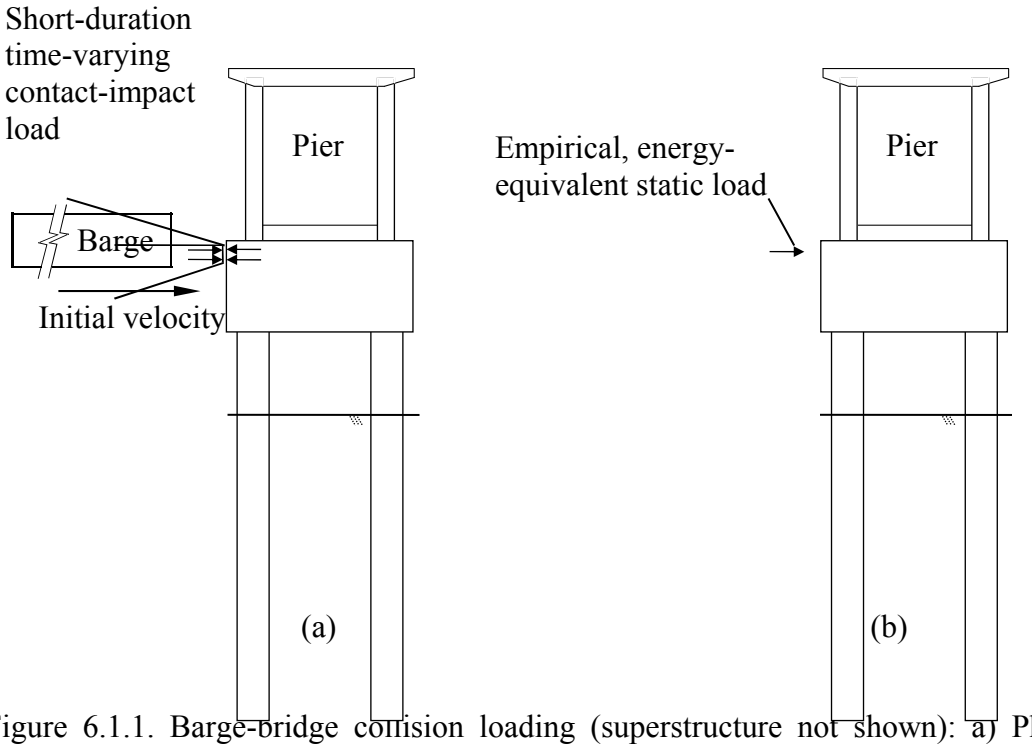

Figure 6.1.1. Barge-bridge collision loading (superstructure not shown): a) Physical schematic; b) Static approximation

6.2 Benchmarks of Impacted Bridge Pier Structural Demand

Given that current design practice for vessel collision design of highway bridges in the U.S. typically entails the use of static bridge analysis, the numerical predictions of demand obtained from subjecting the Pier 59 OPTS model to self-weight, buoyancy, and a 2,550 kip impact load were identified as the benchmarks of demand for all analyses used in characterizing construction cost differences. As shown in Fig. 6.2.1, the static impact load is located on the southern (left) portion of the Pier 59 rounded-edge shear wall, at an elevation of 55.5 ft. Also shown in Fig. 6.2.1 are statically induced structural demands, as obtained from the FBMP analysis results. Included among the results displayed in Fig. 6.2.1. are the maximum values of biaxial demand versus capacity (i.e., D/C values) for the two 5.5-ft diameter reinforced concrete pier columns as well as for the two 9-ft diameter drilled shafts. Note that the drilled shaft tip elevations are located at an elevation of -75 ft.

From the static analysis results pertaining to pier column response, both the maximum moment (which marginally exceeds 5,000 kip-ft, as shown in the top plot in Fig. 6.2.1) and the maximum D/C value (0.66) occur at the top of the northernmost (rightmost) pier column. In contrast, the maximum structural response within the foundation members occurs at the top of the drilled shafts, and specifically, at the top of the southernmost (leftmost) drilled shaft. At this shaft-top location, the maximum internal moment exceeds 22,000 kip-ft and the maximum D/C value reaches 0.77. Relative to the stiffness of the pier columns and drilled shafts, the shear wall is relatively rigid, and so, no significant structural demands (relative to capacity) are generated within the shear wall region.

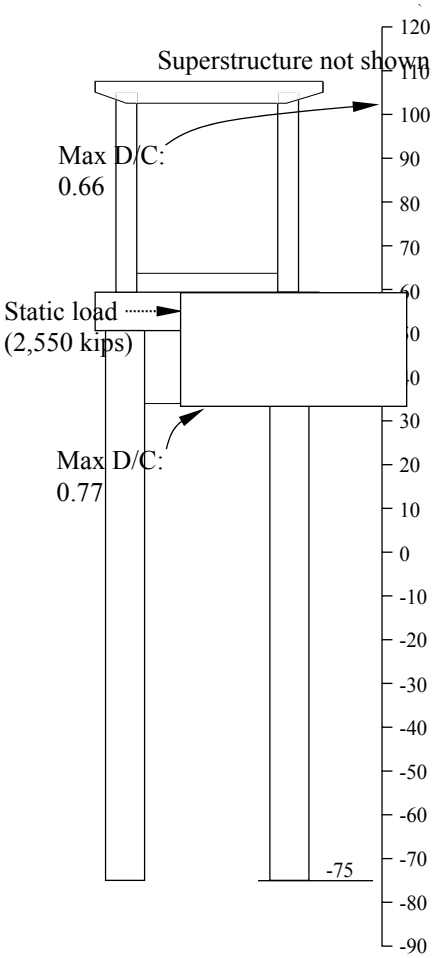

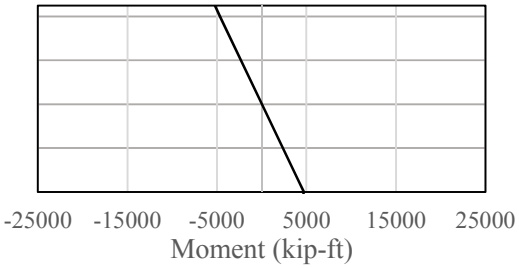

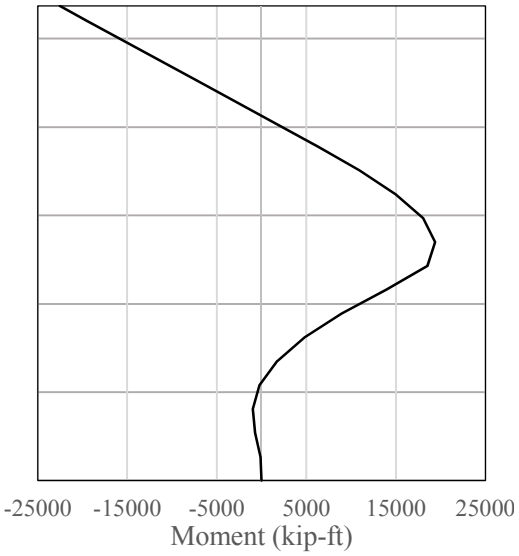

Figure 6.2.1. Pier 59 structural demand predictions from static analysis

For the static analysis, only displacement-based resistance was included in determining the deformed state of the impacted structure. Two load paths are available to transfer the static impact load into the bridge-pier-soil model: upward through the pier columns and into the superstructure; and downward through the drilled shafts into the soil. The presence of the integrated, sizable drilled shafts (embedded over a length of nearly 70 ft into soil and rock) coincides with a downward load path which is of greater displacement-based stiffness than that of the "upward" load path. As a result, 495 kips of shear (parallel to the impact load) are (in total) generated in the pier top elastomeric bearing pads, and the remaining 2,055 kips of shear from the impact load are absorbed through the Pier 59 foundation. Accordingly, the structural demand generated in the foundation members is substantially greater than that generated above the impact location (i.e., throughout the pier columns).

6.3 Static versus Dynamic Demand Predictions

Presented in Fig. 6.3.1 are comparative demand plots and member-specific D/C values obtained from FBMP through use of the Pier 59 OPTS model in the static (2,550 kip) vessel collision analysis (as discussed above in Sec. 6.2) and in a dynamic vessel collision analysis. For the dynamic vessel collision analysis, the CVIA module in FBMP was utilized, where the energy-equivalent barge impact conditions were supplied as input (i.e., a 11,430 kip design-vessel traveling at 10 ft/s). Further, the head-on impact location of 55.5 ft (as indicated in Fig. 6.3.1) is consistent with that of the static analysis, and corresponds to barge bow contact with a 10.5 ft diameter, rounded shear wall surface.

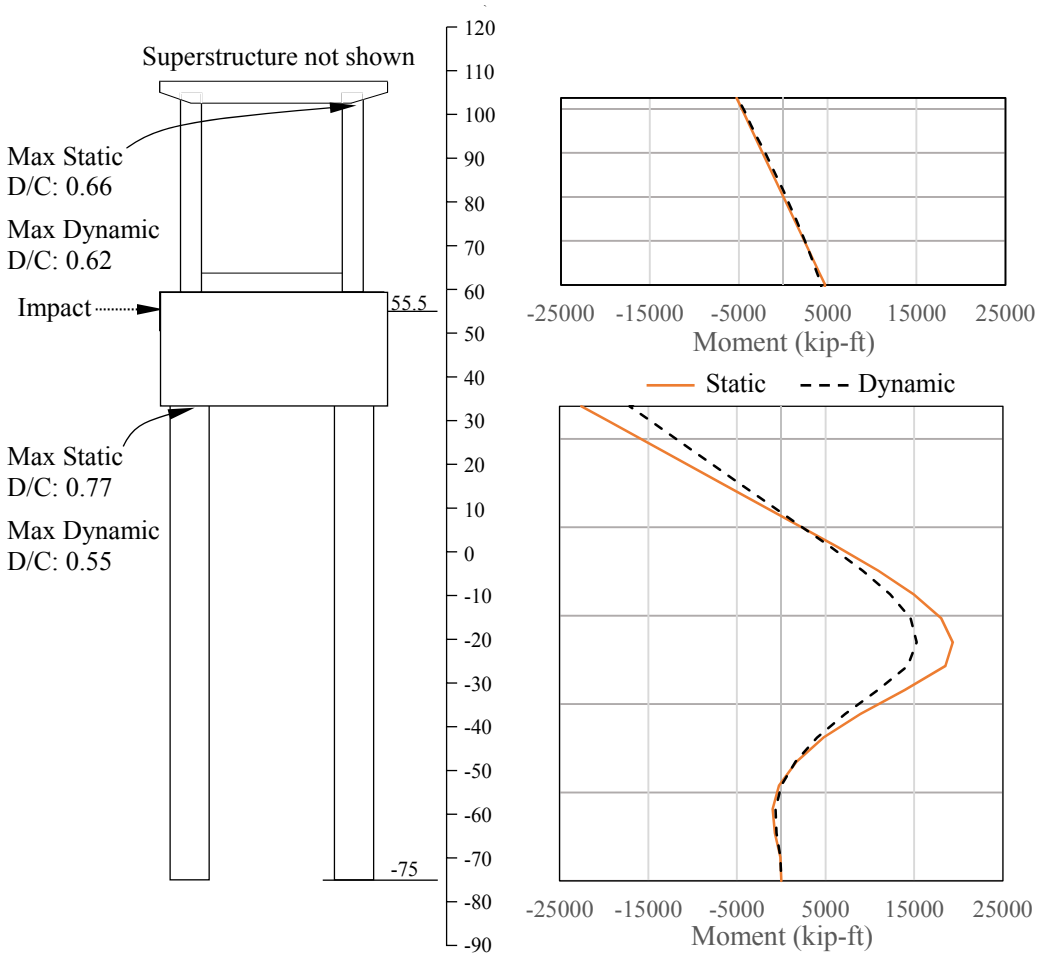

Figure 6.3.1. Pier 59 demand comparison between static and dynamic (CVIA) analyses

As discussed in Sec. 3.2, an important component of the FBMP CVIA feature is that, for barge impact loading, the relative barge-pier interface was taken into account in forming the scenario-specific barge bow force-deformation relationship. Because barge bow force deformation relationships are approximately elastic, perfectly-plastic in shape (Consolazio et al., 2008), the impacting vessel yield force that was used in forming a given force-deformation relationship simultaneously dictated the maximum possible impact load. Further, barge impacts on round surfaces have been found to generate smaller maximum impact loads relative to impacts on flat surfaces of equivalent width (Consolazio et al., 2008, Yuan et al., 2008). As a result, the maximum possible impact force (i.e., bow yield force) associated with dynamic (CVIA) analysis, and use of the Pier 59 OPTS model, is 1,750 kips (recall Fig. 3.2.1). In a relative sense, the maximum dynamic impact force is 69% as large as the corresponding (energy-equivalent) static impact force. Consequently, for the Pier 59 configuration, structural demands generated as part of the dynamic (CVIA) analysis are altogether less than those from the static analysis results.

For the dynamic (CVIA) analysis, both displacement-based resistance and acceleration-based (inertial) resistance were taken into account. Considering that the steel-girder

superstructure of the two spans overlying Pier 59 constitute a mass that is approximately twice as large as the total mass of Pier 59, significant inertial resistance is stored in the superstructure. Consequently, significantly more impact load was absorbed as internal shear through the aforementioned "upward" load path (i.e., through the pier columns) in the dynamic analysis, as compared to that of the static analysis. Namely, the through-time maximum (total) shear force in the pier-top elastomeric bearing pads reached 1,114 kips during a time in which the impact load was 1,750 kips. This phenomenon has been observed to occur over a variety of bridge pier configurations (Davidson et al., 2010), and is referred to as dynamic amplification.

While, for the barge impact scenario considered, dynamic amplification contributed to increased demands in the pier columns, it simultaneously reduced the remaining portion of impact load that can be absorbed through the Pier 59 foundation (i.e., the "downward" load path). Therefore, the maximum D/C value generated in the pier columns remained similar between the static (0.66) and dynamic (0.62) analyses, despite the substantially lower maximum impact load available in the dynamic analysis (1,750 kips versus 2,550 kips). Furthermore, proportionally more of the total (1,750 kips) impact load was absorbed through the "upward" load path in the dynamic analysis, and so, a sizable reduction occurred for the maximum D/C value in the drilled shafts (0.55), relative to the corresponding static analysis D/C value (0.77).

6.4 Revised Drilled Shaft Design Based on Maximum Dynamic Demands

Using the member-specific maximum D/C values from the static barge impact analysis as benchmark values, the Pier 59 OPTS model was iteratively modified and subjected to energy-equivalent dynamic barge impact analysis (through CVIA) until the member-specific maximum D/C values predicted using the dynamic (CVIA) analysis matched the (static) benchmark values. During this process, the drilled shafts were first taken into consideration, where the two shaft diameters, shaft tip elevations, and longitudinal reinforcement were iteratively modified. Also, for each iteration, the rounded-edged shear wall was modified to maintain a 1.5 ft larger diameter than that of the drilled shafts. As a parity consideration, and prior to each dynamic analysis iteration, it was ensured that the shaft axial capacity (as defined in FDOT 2014) was maintained equal to or greater than the Pier 59, 2,000 ton drilled shaft design capacity listed in the SR-20 bridge structural drawings.

The iterative foundation member resizing and dynamic (CVIA) analyses led to convergence for the following foundation member specifications: two 7.5 ft diameter drilled shafts with 33 #18 Gr. 60 deformed steel reinforcement bars and tip elevations of -78 ft (Fig. 6.4.1). Alternatively stated, a dynamic (CVIA) analysis using the Pier 59 OPTS model, with the 7.5 ft diameter drilled shafts, gives numerical predictions of maximum D/C values of 0.78 in the southernmost (leftmost) drilled shaft. This D/C value, 0.78, is nominally different from the benchmark D/C value (0.77). Note that the revised longitudinal reinforcement layout for the drilled shafts was configured in accordance with development length, bar spacing, and reinforcement ratio requirements set forth in the AASHTO LRFD Code (AASHTO 2012).

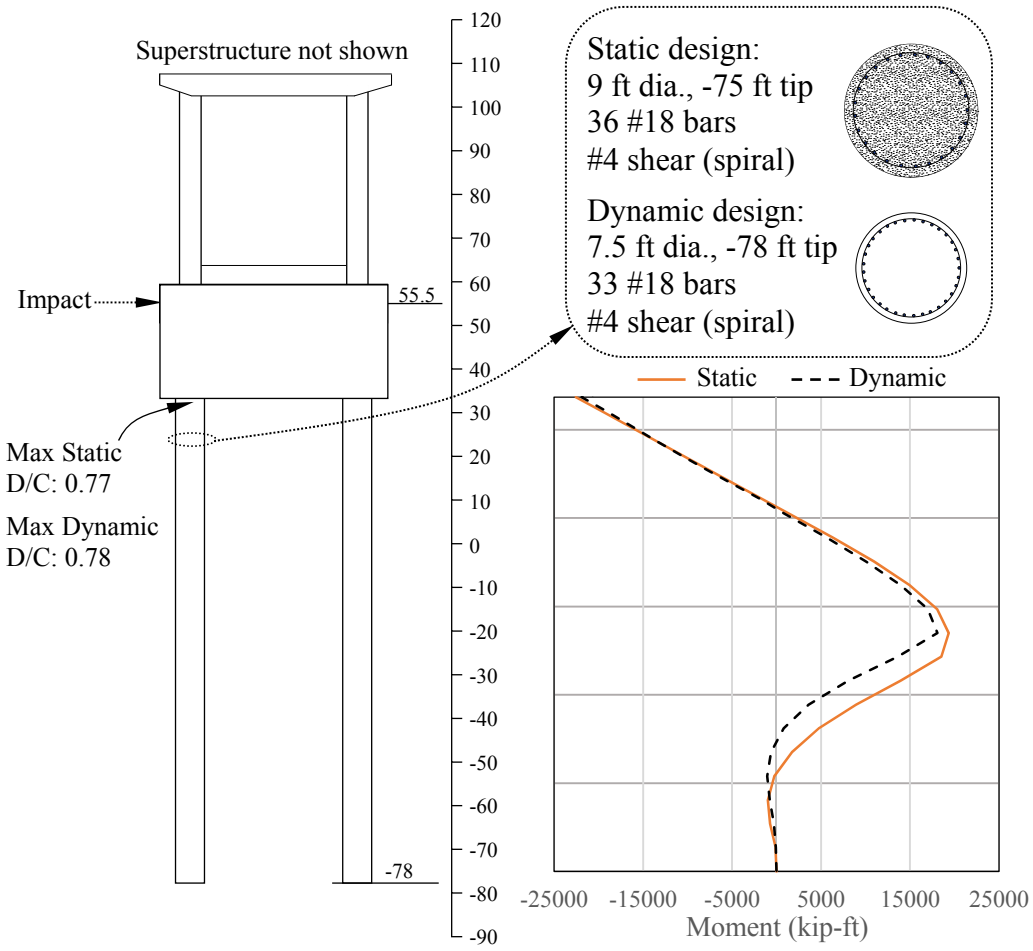

Figure 6.4.1. Pier 59 drilled shaft demand comparison for static and dynamic (CVIA) member sizing

6.5 Revised Pier Column Design Based on Maximum Dynamic Demands

When the reduced, modified drilled shaft sections are employed in the dynamic (CVIA) vessel collision analysis, the demands in the pier columns increase substantially. Therefore, member resizing for the pier columns in the Pier 59 OPTS model (based on dynamic, CVIA, analysis results) was required. For this bridge case and barge impact scenario, convergence to the benchmark (static) maximum D/C values was achieved in the pier columns by increasing the volume of longitudinal reinforcement. Specifically, when the Gr. 60 deformed steel reinforcement in the pier columns was increased from 25 #11 bars to 26 #14 bars, the corresponding dynamic (CVIA) analysis prediction of maximum D/C values reached values of 0.66. For all reinforcement layout changes, the requirements given in AASHTO (2012) are satisfied.

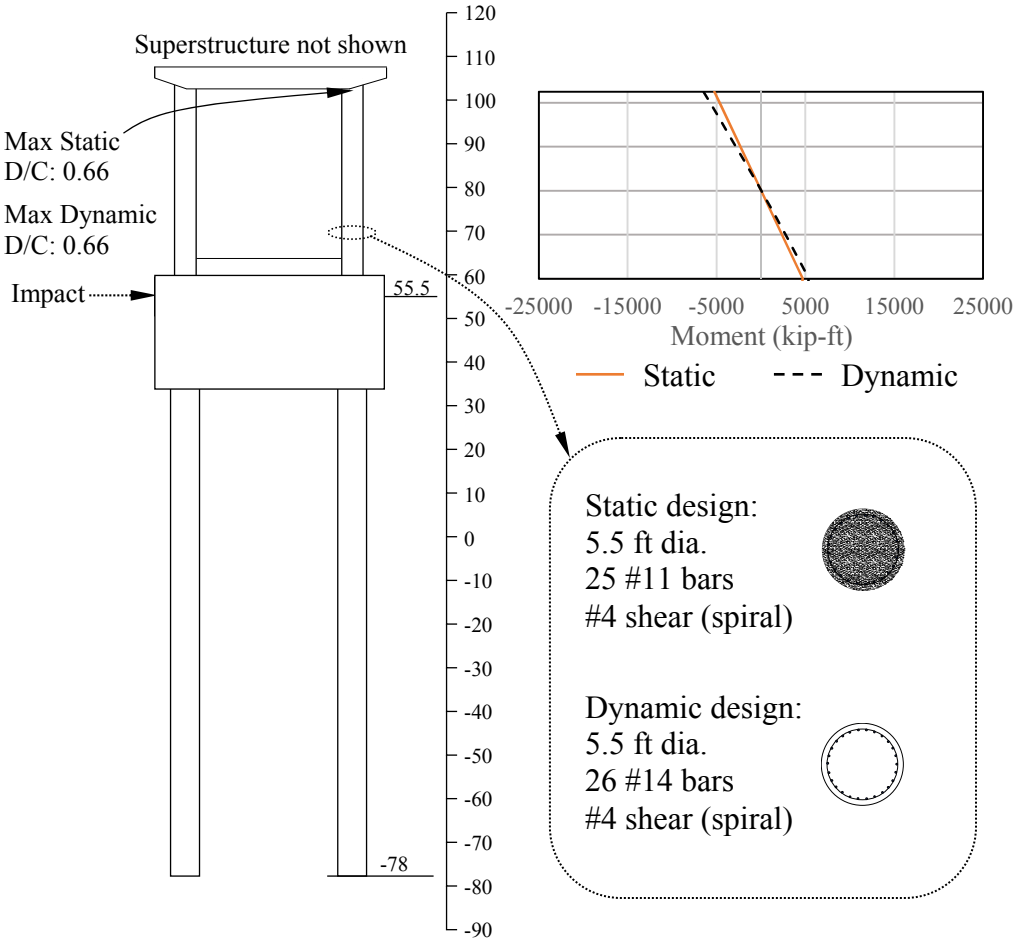

Figure 6.5.1. Pier 59 pier column demand comparison for static and dynamic (CVIA) member sizing

6.6 Cost Comparison between Static-Based and Dynamic-Based Designs

Two major factors contributed to differences found among the static and dynamic analysis results presented above. First, the maximum impact load associated with the static analysis (2,550 kips) was nearly 50% greater than the maximum dynamic impact load (1,750 kips). The sizable difference in maximum impact load magnitudes resulted in altogether reduced demand predictions when making use of the dynamic (CVIA) analysis. Ultimately, smaller foundation members were found to satisfy benchmark demand levels (in association with dynamic analysis) because of the difference in (static versus dynamic) maximum impact loads. Further, for the case considered, the phenomenon of dynamic amplification tended to shift proportionally more load through the pier columns into the superstructure (i.e., away from the Pier 59 foundation), which permitted further reductions in the foundation member sizing. However, precisely because the dynamic amplification phenomenon led to proportionally greater impact load absorption along the "upward" load path, the need arose to increase the amount of longitudinal reinforcement in the pier columns so that benchmark levels of demand were maintained.

Summarily, modifications to Pier 59 (by accounting for dynamic vessel collision phenomena and maintaining benchmark, or static, demand levels) consisted of: 1.5 ft reductions in the drilled shaft diameters; 3 ft increases in the drilled shaft tip elevations; 1.5 ft reduction in the shear wall thickness; and increased longitudinal reinforcement in the pier columns. From a construction cost standpoint, these modifications cumulatively lead to a total cost savings of approximately $160,000 for Pier 59 of the SR-20 bridge (Table 6.6.1). Demonstration of the potential for such significant cost savings on a per-pier basis supports the need for a wider, design-oriented investigation aimed at elucidating the ramifications associated with use of the newly developed dynamic vessel collision analysis features in FBMP.

Table 6.6.1. Construction cost difference for Pier 59

Cost item	Length (ft)	Width (ft)	Depth (ft)	$/ Cy	$ / ft	# bars	Quantity	Cost ($) [a]
9 ft dia. drilled shafts (static)	-130.5				1,900		2	-495,900
7.5 ft dia. drilled shafts (dynamic)	133.5				1,300		2	347,100
Reduction in shear wall thickness	-39	1.5	24.5	600			1	-31,850
Rebar in columns (static)	-60				4.78	25	2	-14,340
Rebar in columns (dynamic)	60				7.65	33	2	30,294
							Total	-164,696

[a] - Unit costs obtained from the 2014 FDOT Structures Design Guidelines Chapter 9 BDR Cost Estimating (FDOT 2014)

CHAPTER 7
PARAMETRIC STUDY

7.1 Introduction

As an extension of the construction cost analyses conducted in Chapter 6, the focus of the current chapter (Chapter 7) is placed on exploring additional aspects of the newly developed vessel collision analysis (CVIA) and bridge modeling (OPTS) techniques through parametric investigation. Namely, to facilitate advances in the understanding of SR-20 bridge impact response quantities (e.g., impact force generation, impacted bridge pier response), three aspects of the CVIA-OPTS analytical tools are explored: (1) Impacted surface shape; (2) Variation of the site-specific (i.e., local to the SR-20 bridge) soil parameters; and (3) Required wall-clock time to complete full-bridge versus OPTS vessel collision analyses using ordinary computing devices.

7.2 Benchmarks of Impacted Bridge Pier Structural Demand

The as-designed structural configuration for Pier 59 of the SR-20 bridge (i.e., the configuration detailed in the structural drawings) is shown in Fig. 7.2.1. Also shown are the member-specific maximum D/C values and concurrent profiles of pier column and drilled shaft internal moment. For all analyses conducted as part of the parametric study, the structural demands shown in Fig. 7.2.1 were employed as benchmark values as a means of contextualizing the numerous parametric study results.

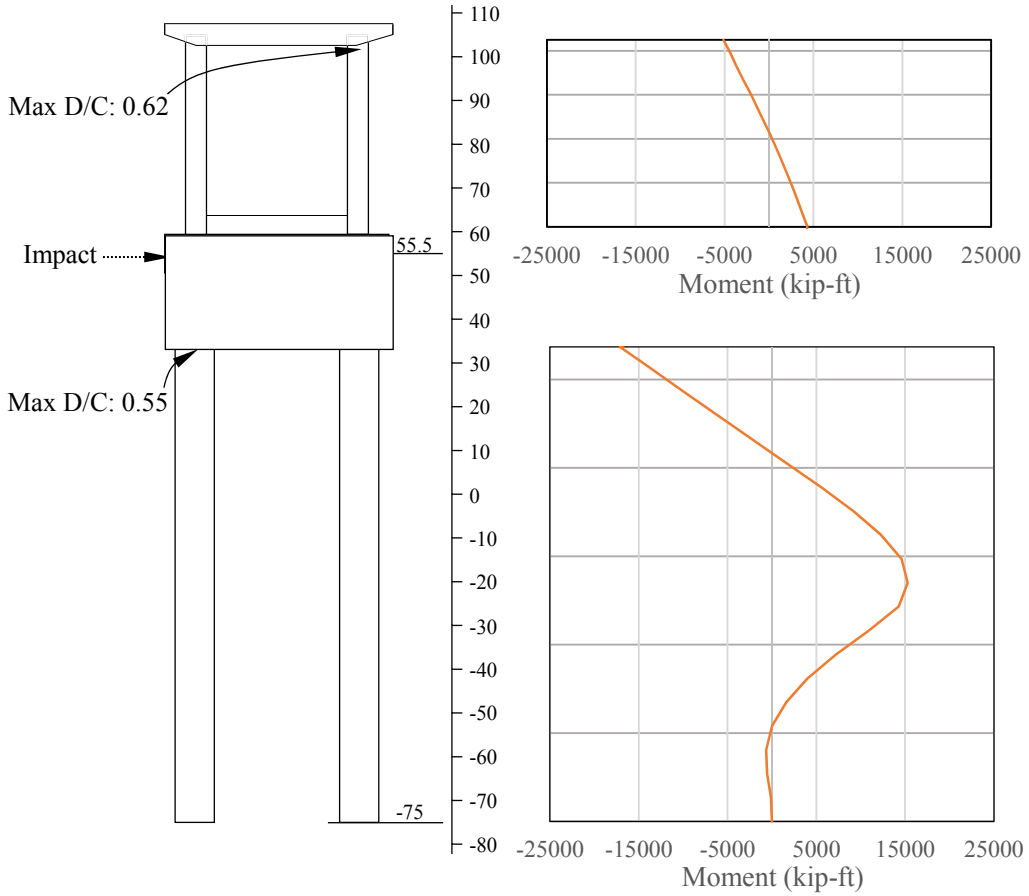

Figure 7.2.1. Pier 59 structural demand predictions from dynamic (CVIA) analysis

7.3 Effect of Impact Surface Geometry

Previous studies of barge bow crushing behavior (e.g., Consolazio et al., 2008, Consolazio et al., 2010, Yuan et al., 2008) have consistently found that, for a given impact scenario, the geometry of the impacted surface plays a significant role in dictating the maximum impact force. As explicit demonstration of how the newly developed CVIA framework in FBMP (Chung 2014a) can elucidate the consequences of impact surface shape-dependent phenomena, two additional CVIA cases were analyzed and compared. The Pier 59 OPTS model (developed in Chapter 5) and the physical barge flotilla parameters (also determined in Chapter 5) were again employed, where the centrally located rounded-edge shear wall of the OPTS model (Fig. 7.3.1) was modified to a rectangular shear wall (Fig. 7.3.2). Other than differences in the impacted surface geometry, all other aspects of the vessel collision scenario were matched between the two cases (Fig. 7.3.3). Alternatively stated, all model parameters were held equal between the two analyses, excepting the shape of the impacted surface. Analysis results obtained using the CVIA feature in FBMP were then compared for the impact scenario on the Pier 59 OPTS model containing the rounded impact surface geometry, and for the impact scenario on the Pier 59 OPTS model containing the flat impact surface geometry.

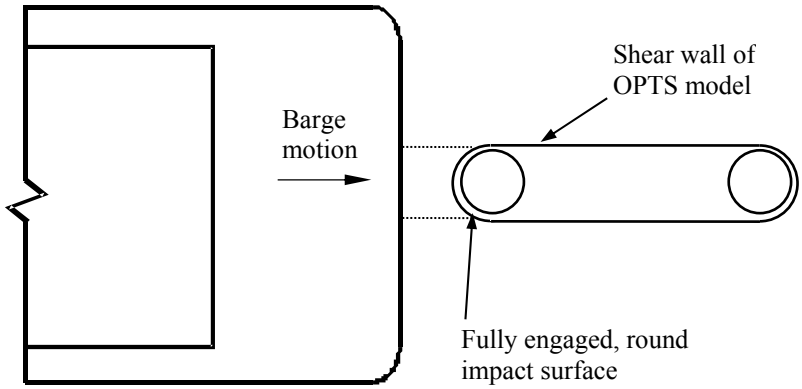

Figure 7.3.1. Schematic for impact scenario on the round shear wall in the OPTS model

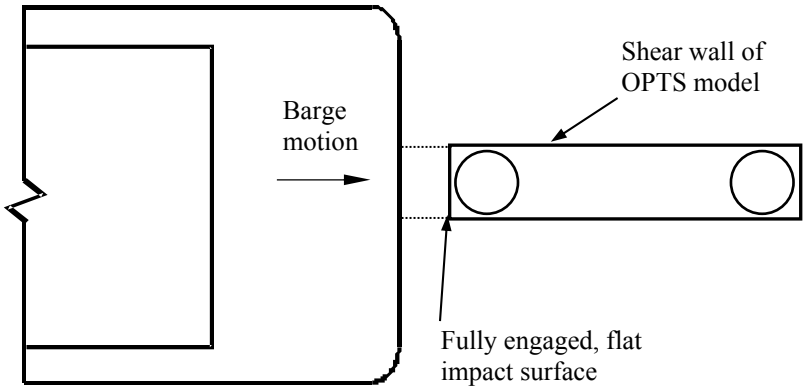

Figure 7.3.2. Schematic for impact scenario on the flat shear

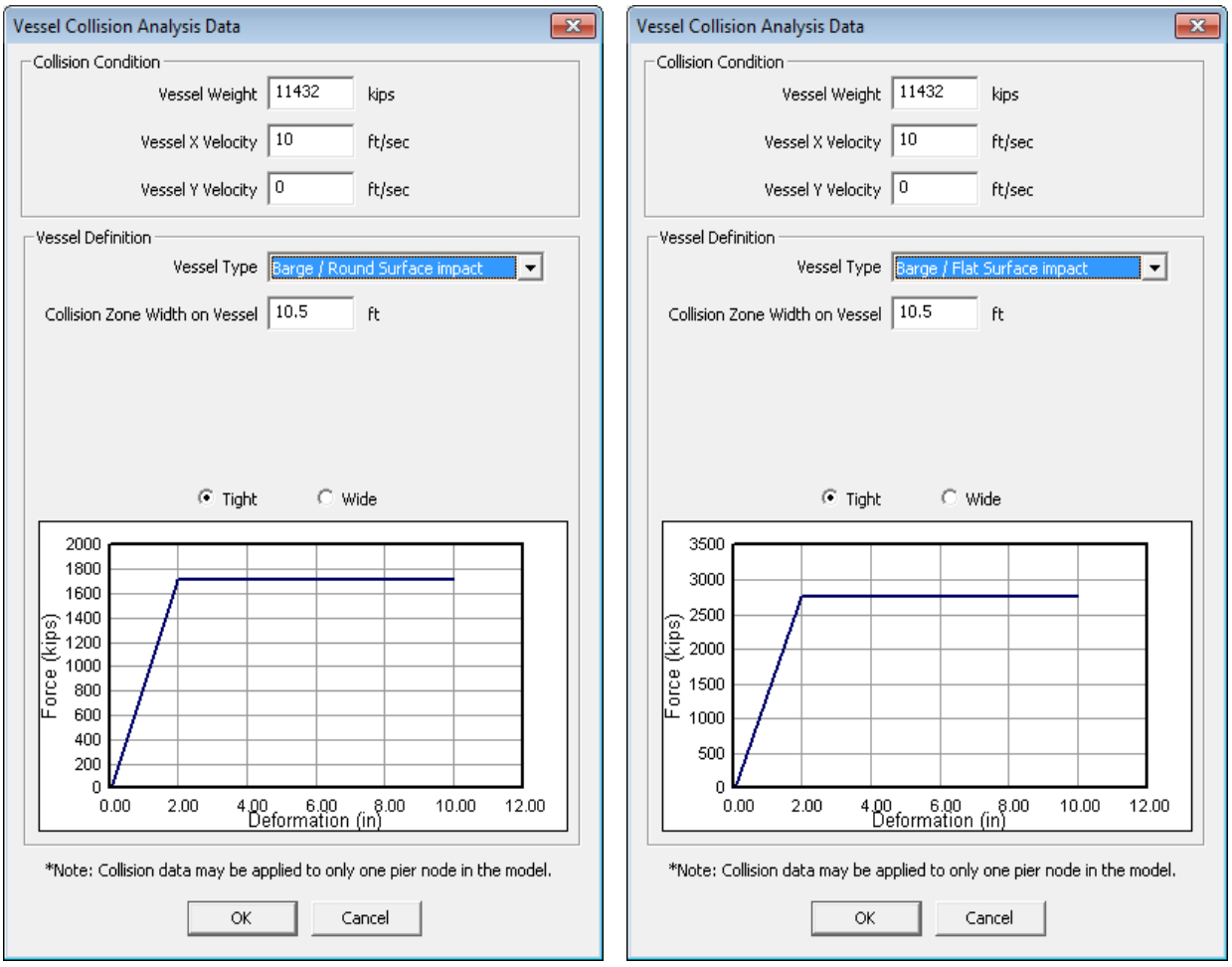

(a) (b)

Figure 7.3.3. Vessel collision scenarios: a) Round; b) Flat

The impact force-histories for the round and flat impact scenarios (Fig. 7.3.3) are shown in Fig. 7.3.4. The structural configuration (excepting the superstructure) of the impacted pier is again shown in the figures to spatially contextualize the bridge pier response quantities. Clearly, the flat impact surface leads to substantially larger impact forces for a head-on strike. Correspondingly, time-histories of displacement (Fig. 7.3.5 and Fig. 7.3.6), shear force (Fig. 7.3.7 and Fig. 7.3.8), and moment (Fig. 7.3.9 and Fig. 7.3.10) for locations throughout the pier indicate that the bridge response corresponds to approximately 80% greater structural demands in the flat-impact case.

Pertinent to the design of bridges for vessel collision loading, the maximum dynamic demands relative to the nonlinear cross-section capacities (in the form of biaxial D/C values) are comparatively plotted in Fig. 7.3.11. Viewed in this manner, the bridge response for the flat-surface impact scenario remains approximately 80% more severe than the corresponding round-surface impact scenario. Collectively, the results suggest that a simple means of mitigating collision-induced bridge structural damage is to design or retrofit bridges to ensure that rounded surfaces are constructed or installed for those regions of members that are susceptible to impact.

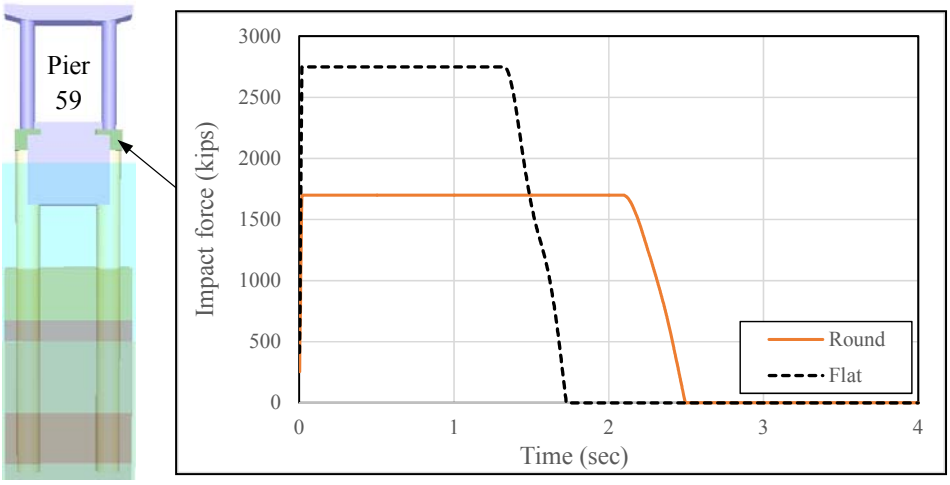

Figure 7.3.4. Time-histories of impact force

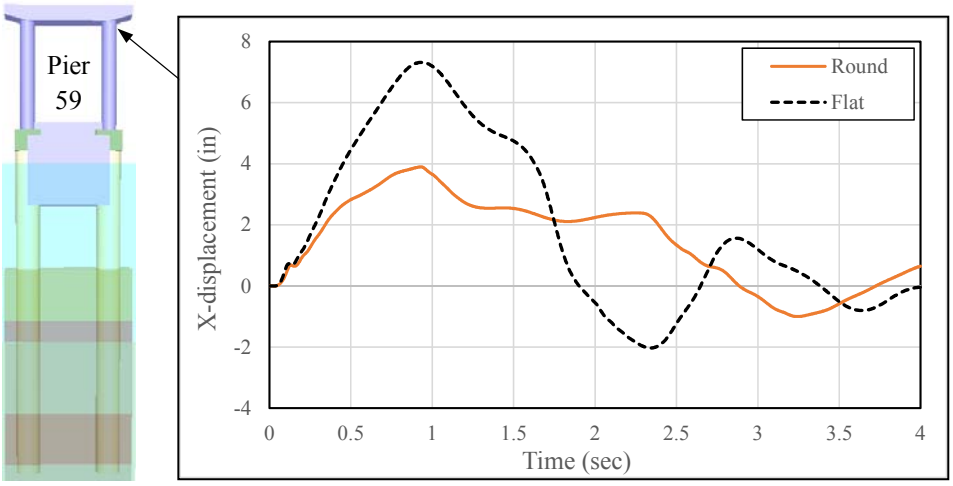

Figure 7.3.5. Time-histories of X-displacement at the top of the impacted column

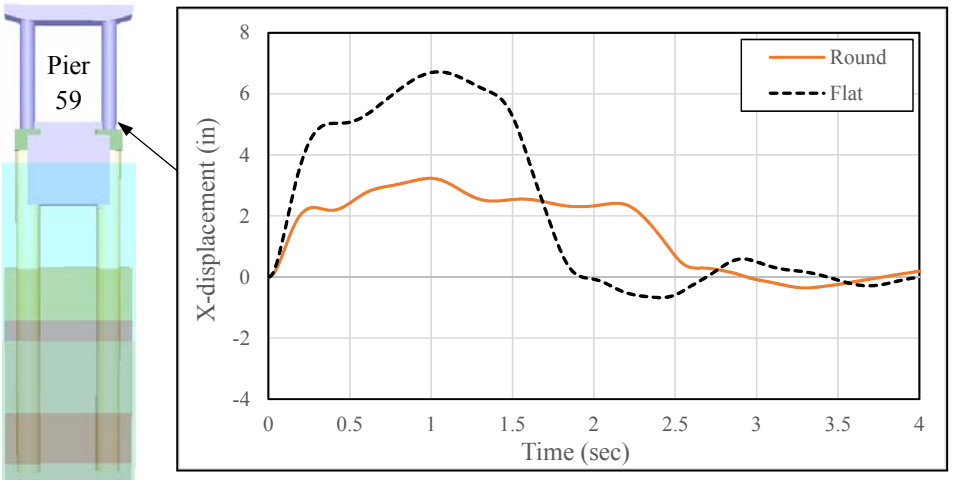

Figure 7.3.6. Time-histories of X-displacement at the base of the impacted column

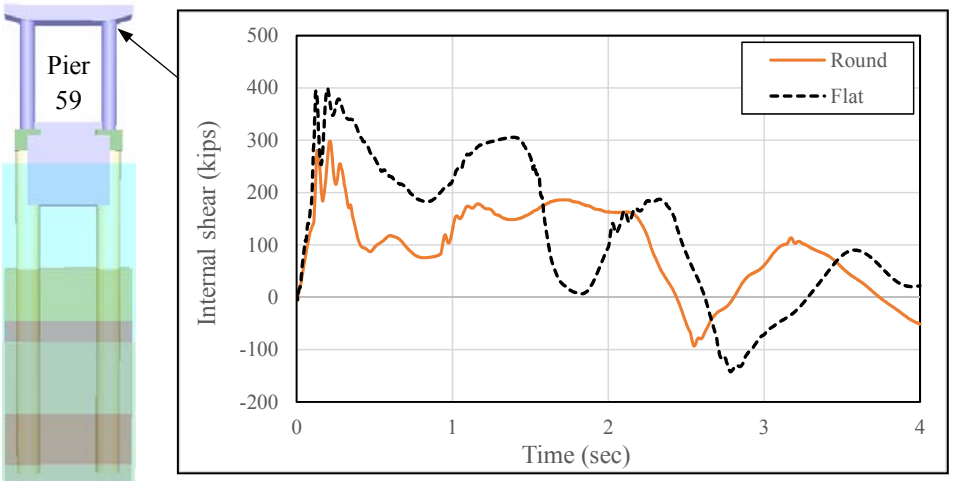

Figure 7.3.7. Time-histories of internal shear at the top of the impacted column

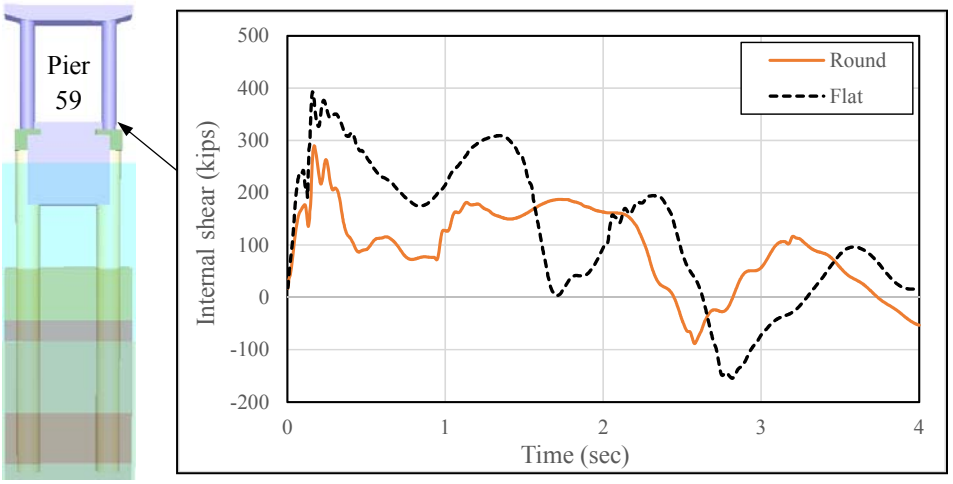

Figure 7.3.8. Time-histories of internal shear at the base of the impacted column

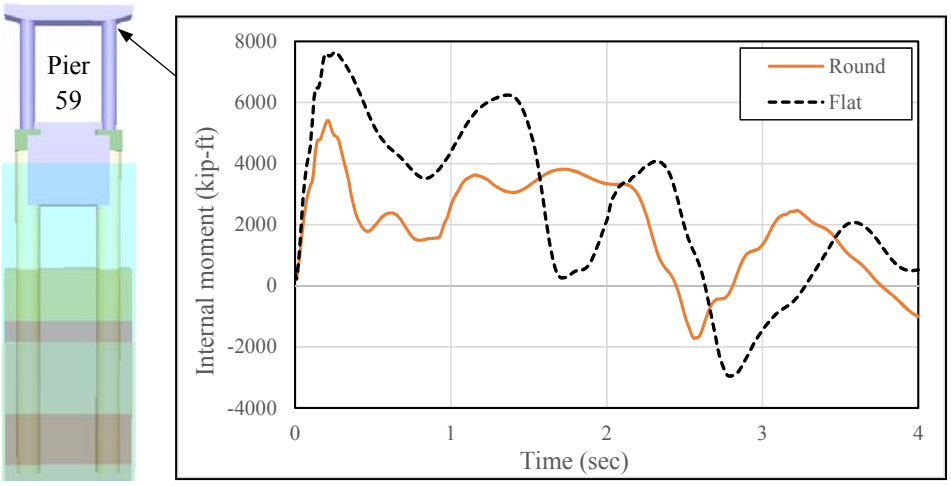

Figure 7.3.9. Time-histories of internal moment at the top of the impacted column

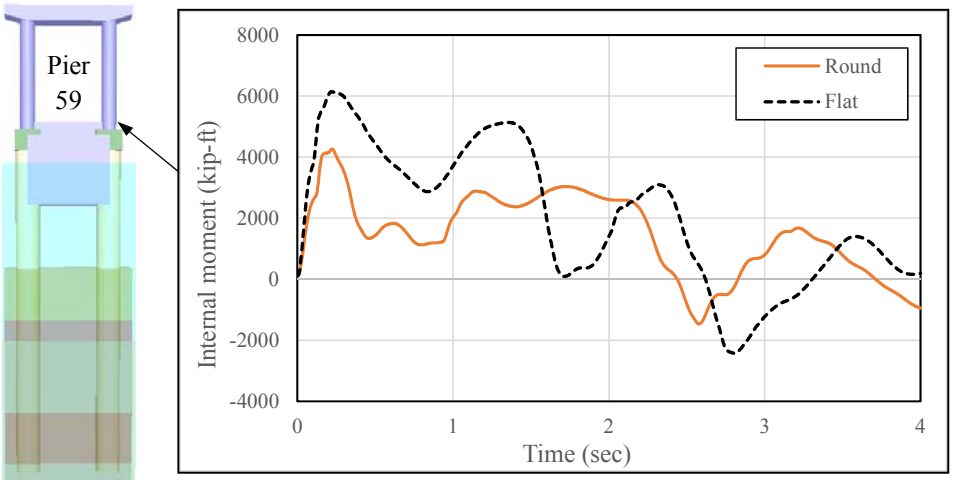

Figure 7.3.10. Time-histories of internal moment at the base of the impacted column

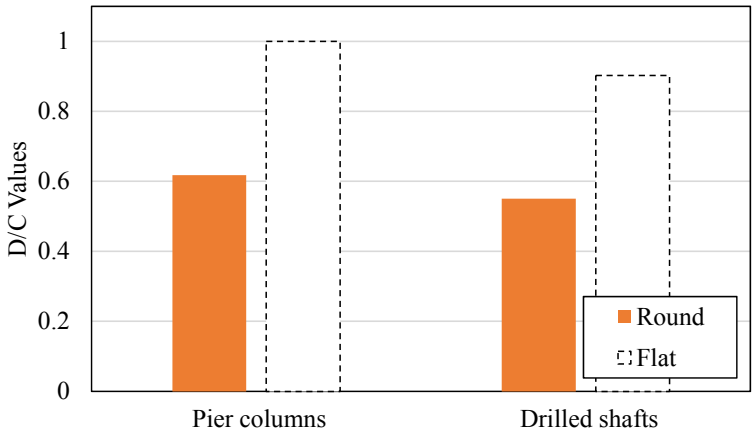

Figure 7.3.11. Maximum D/C values through time

7.4 Effect of Soil Modeling on Impacted Pier Response

The soil conditions in place beneath an impacted bridge pier can, in turn, strongly influence the impacted pier response (Consolazio et al., 2006, McVay et al., 2009b). In particular, for those piers with massive, embedded foundation members, static and dynamic components of soil resistance can provide various, substantial forms of displacement-based (stiffness, gapping), velocity-based (damping), and acceleration-based (radiation damping) load and motion dissipation. The dynamic response of bridge piers, including consideration of soil resistance and response, has been assessed for numerous bridge cases (i.e., pier structural layouts) via FBMP, as part of previously conducted analytical studies (e.g., Consolazio et al., 2008, Davidson et al., 2010). However, for all bridge cases considered, deterministic, displacement-based treatments were given in modeling the soil resistances. Davidson et al. (2013) employed probabilistic simulation techniques to carry out hundreds of thousands of vessel collision simulations (CVIA) in FBMP, where both bridge structural configurations and soil conditions were included among the random variables, to investigate collision-induced bridge pier failure rates. However, all through-depth soil input parameters supplied to models utilized in Davidson et al. (2013) assumed statistical independence throughout the soil-spatial domain. While it is well established that soil typically possesses high levels of variability across a bridge site, and even within the plan area of a single bridge pier foundation, recently completed UF-FDOT research supports that correlated spatial variability exists throughout Florida soil and rock materials. Further, it has been demonstrated (McVay et al., 2009a) that such variability is significant (i.e., can meaningfully affect numerical predictions of bridge response to loading) at scales relevant to pier foundation members.

Based on software tools developed by BSI (2014b) and McVay et al. (2012), Fig. 7.4.1, as well as findings from the long-standing area of geostatistics (Isaaks 1989), a cursory soil variability investigation was undertaken in the current study. More specifically, two aspects of soil variability were incorporated into vessel collision analyses of the SR-20 bridge Pier 59 OPTS model: (1) SR-20 bridge soil-variability with inclusion of spatial correlations in the vertical direction; and (2) Bounded response of the Pier 59 OPTS model when subjected to the vessel collision scenario formulated previously in Sec. 5.2.6. In this context, “bounded response”

denotes the selection of the 5th percentile and 95th percentile soil profile realizations (based on shaft axial capacity), and the use of the associated soil input parameters to conduct two bounding vessel collision (CVIA) analyses. Based on the results of these probabilistic, bounded analyses, insights were made concerning the sensitivity of the SR-20 Pier 59 structural configuration to the underlying soil conditions, within the context of vessel collision analysis.

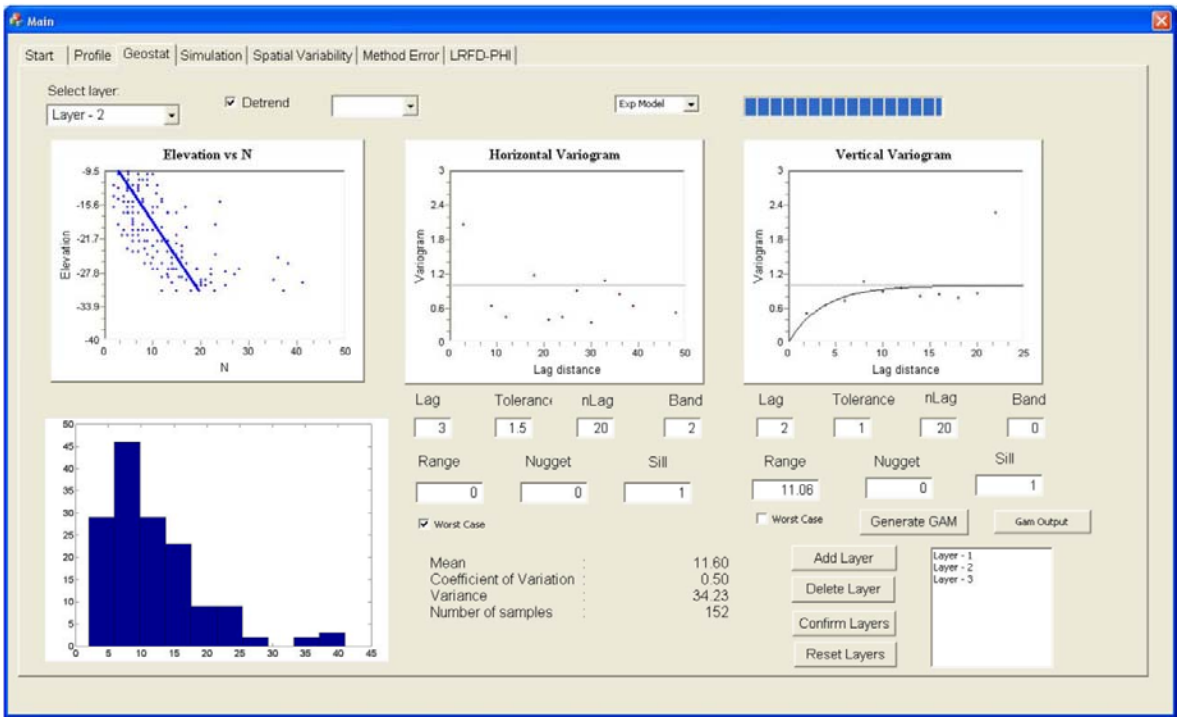

Figure 7.4.1. Soil-spatial modeling software (McVay et al. 2012)

7.4.1 Soil-Spatial Modeling

In formulating the soil-spatial dataset used in the current study, 1,000 realizations of soil-rock profiles within the vicinity of Pier 59 (i.e., conditional realizations) were generated using the soil-spatial modeling software (Fig. 7.4.1) developed as part of McVay et al. (2012). Further, previously cataloged soil and rock data specific to the SR-20 bridge site were drawn upon in generating the 1,000 soil-rock profiles by making use of the FDOT Geotechnical Database (Fig. 7.4.2).

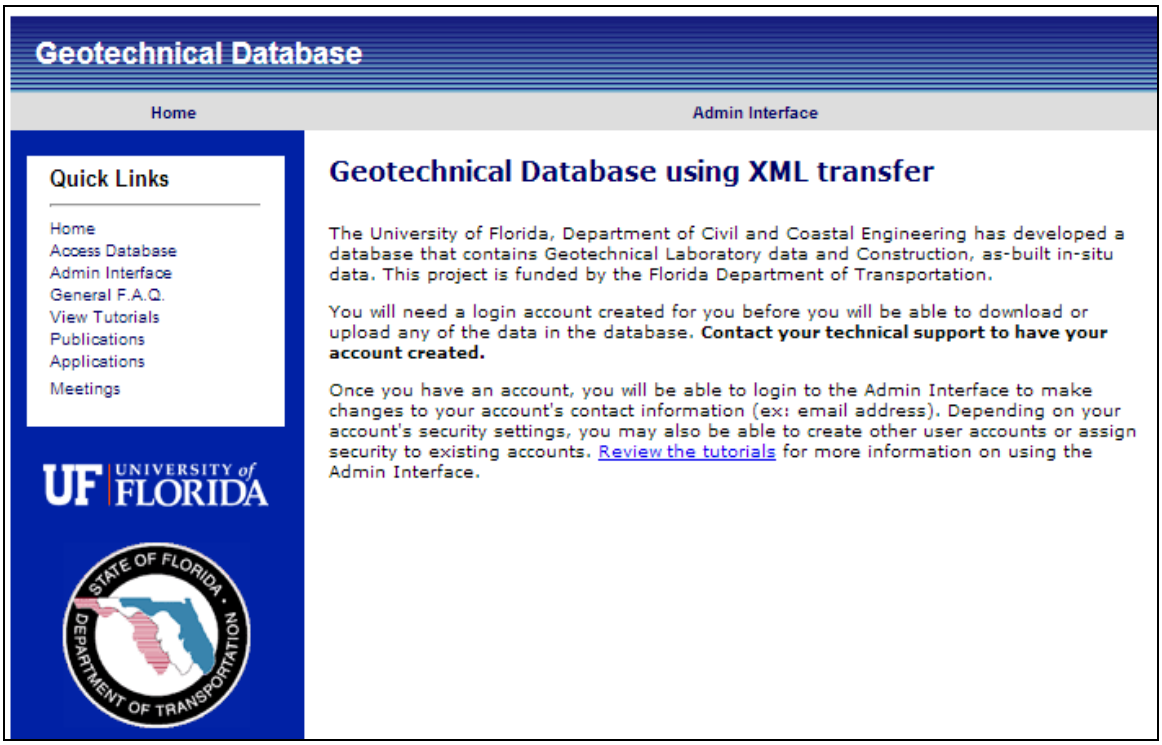

Figure 7.4.2. FDOT Geotechnical Database (fdot.ce.ufl.edu)

While physically, in-situ soil can vary vertically (and horizontally) from soil particle to soil particle (i.e., over very small distances), the input format for FBMP is based on averaged soil properties across soil layers (or, relatively large vertical distances). To facilitate compatibility between the soil-spatial realizations (point-to-point variability) and the FBMP soil input format (layer-based), for each realization, the generated soil-rock profile was divided into two representative pseudo-layers (Fig. 7.4.3). Here, the top pseudo-layer is comprised of 14 sandy soil layers. These sandy layers extend from the top of soil at an elevation of 6 ft, vertically downward to an elevation of -28.89 ft. All elevations below -28.89 ft are associated with the bottom pseudo-layer, which in turn, is made up of 18 rock layers (and 1 underlying tip layer). Note that, as a result of the pseudo-layer approach, a total of 33 FBMP input layers were specified for each realization, where no additional layers were permitted (due to constraints on the density of the drilled shaft nodes) for the Pier 59 FBMP OPTS model.

For each of the one thousand SR-20 Pier 59 soil-rock profiles (realizations), through-depth values of spatially correlated (in the vertical direction), conditional (upon proximity to Pier 59) SPT blow counts were provided for the 14 constituent sandy layers. Likewise, rock strength properties (unconfined compressive strength, q_u; split tensile strength, q_t; core recovery percentage, and RQD) were provided for each of the 19 rock layers. Then, empirical relationships (including site-specific correlations, see Davidson 2010 for details) were used to build up the soil resistance input for an FBMP model, where there was a one-to-one pairing between realizations and FBMP OPTS models of Pier 59 from the SR-20 bridge.

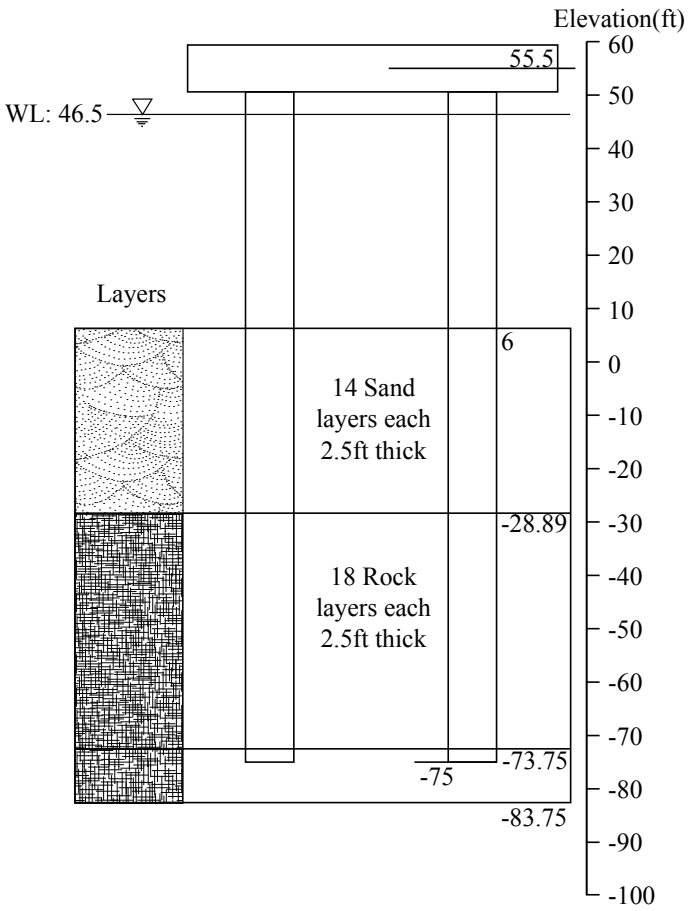

Figure 7.4.3. Soil layering for soil-spatial boring profiles

7.4.2 Predicted versus Measured Drilled Shaft Capacity

As validation of the soil-spatial dataset, as transformed into FBMP model input, shaft axial capacities that were numerically predicted for the 1,000 FBMP models were compared to previously conducted full-scale experimental test data. Specifically, McVay et al. (2003) carried out field testing of a 9 ft diameter drilled shaft installed to a depth of -78 ft, within the immediate vicinity of Pier 59 from the SR-20 bridge. The experimental results cataloged by McVay et al. (2003) are assumed to be suitably comparable to responses predicted for the two 9 ft diameter drilled shafts of Pier 59. Included among the previously conducted physical testing were measurements of skin friction along the embedded test-shaft depth. Shown in Table 7.4.1 are the measurements of test shaft skin friction from (approximately) elevation -23 ft to -60 ft. In total, based on the experimental results, the skin friction associated with the test shaft was estimated to be approximately 14,134 kips.

Table 7.4.1. Physical measurements of test shaft skin friction at Pier 59 (McVay et al., 2003)

Top Elev. (ft)	Bottom Elev. (ft)	Unit skin friction (ksf)	Area (ft^2)	Skin friction (kips)
-23 (approx.)	-33.1	4.66 (approx.)	285.6	1,331 (approx.)
-33.1	-40	10.3	195.1	2,009

-40	-46	8.06	169.6	1,367
-46	-52.9	9.08	195.1	1,771
-52.9	-60	8.38	200.7	1,682
-60	-69.3	22.72	263.0	5,974
			Total	14,134

In addition to the physical measurements of test-shaft skin friction, taken as part of McVay et al. (2003), an Osterberg cell load test was also performed to measure test-shaft tip load-settlement behavior. Per the previously conducted Osterberg cell load testing, and accounting for the cross-sectional area of the 9 ft diameter test shaft, the estimated load-settlement curve is displayed in Fig. 7.4.4. Furthermore, a logarithmic regression of the non-zero load values is shown in Fig. 7.4.4, where the coefficient of determination (R^2) indicates a strong fit. For 9 ft diameter drilled shafts constructed in Florida, the axial load corresponding to a tip vertical displacement of 3.6 in. is defined as the failure load (FDOT 2014). By extrapolating the logarithmic regression curve shown in Fig. 7.4.4 to a tip vertical displacement of 3.6 in., the tip failure load was estimated as 21,040 kips. The sum of the estimated test-shaft skin resistance (14,134 kips) and tip resistance were then summed to form an estimate of the total shaft capacity (35,174 kips).

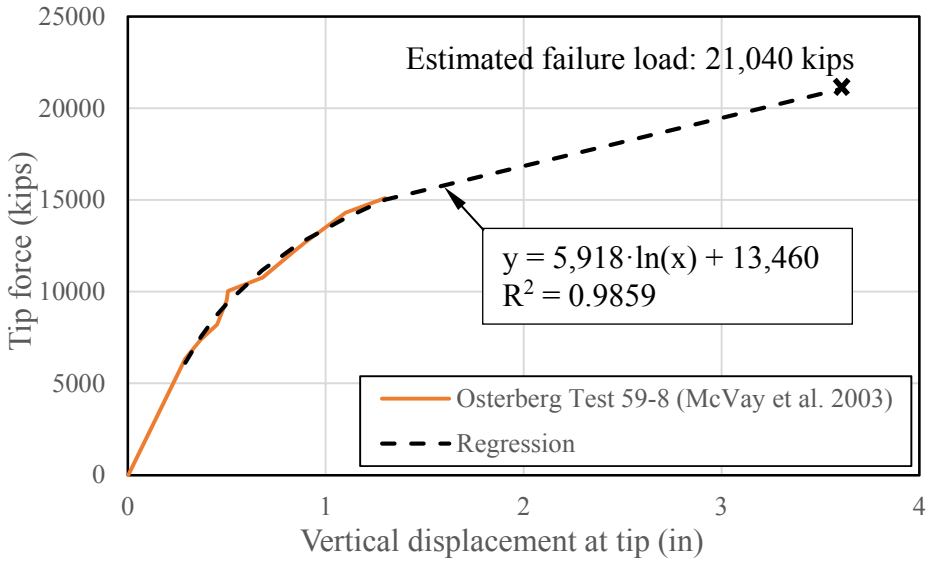

Figure 7.4.4. Test shaft tip force versus vertical displacement

Shown in Fig. 7.4.5 are the histogram and empirical cumulative frequency curve of shaft total capacities (i.e., summed skin and tip capacities) for the 1,000 FBMP models containing the 9 ft drilled shafts of Pier 59 from the SR-20 bridge. Also denoted on Fig. 7.4.5 are the 5th percentile and 95th percentile (numerical) predictions of 9 ft diameter drilled shaft axial capacity at Pier 59. Importantly, the lower (i.e., 5th percentile) and upper (95th percentile) predictions of drilled shaft axial capacity bound the estimate of the test shaft capacity, based on the full-scale test shaft load test measurements conducted by McVay et al. (2003). Given that the lower and upper bound probabilistic predictions of capacity bound the physical measurement, the dataset was accepted as representative of the physical site soil conditions for the purposes of the cursory

soil-spatial variability investigation. Accordingly, the two soil-rock profiles (i.e., numerically generated realizations) that contain drilled shaft capacities, which most closely match the empirical 5th percentile and 95th percentile drilled shaft capacity values, were selected for use in conducting dynamic vessel collision analyses (CVIA) using the Pier 59 OPTS model.

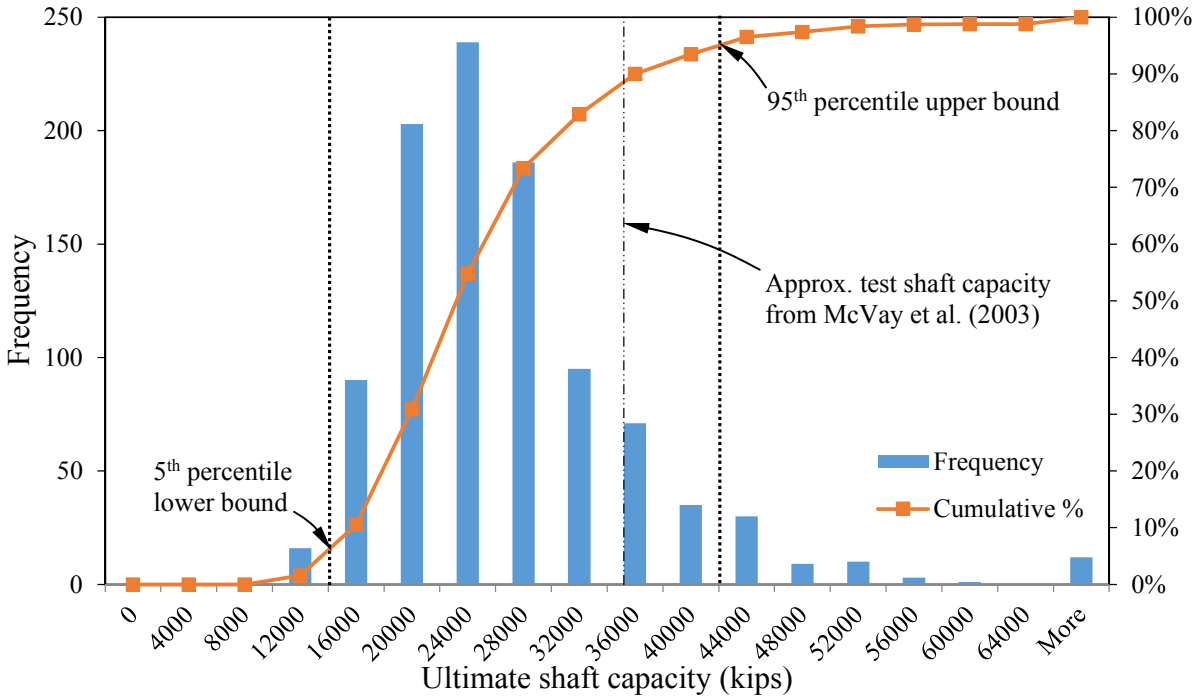

Figure 7.4.5. Histogram of predictions for ultimate shaft capacity

7.4.3 CVIA-OPTS Analysis of Pier 59 Using Soil Parameters from the 5th Percentile Boring

Shown in Fig. 7.4.6 is the soil layer profile associated with the 5th percentile soil-rock profile data. As aforementioned, the soil layering (a collection of 14 sandy sub-layers atop 19 rock sub-layers) is identical across each of the 1,000-realization soil-spatial dataset. Consistent with the 5th percentile soil layering, soil strength parameter values relating to the sandy sub-layers (and supplied to the Pier 59 OPTS model) are listed in Table 7.4.2. Similarly, rock strength parameters for the bottom 19 sub-layers are listed in Table 7.4.3. The 5th percentile profile data were used in conjunction with the Pier 59 OPTS model structural configuration and design-level vessel collision scenario (see Chapter 5) to carry out a dynamic vessel collision analysis (CVIA) in FBMP.

Shown in Fig. 7.4.7 are comparative plots and denotations of maximum D/C values for CVIA-OPTS analysis using the 5th percentile soil-rock profile and the deterministic soil formulation (developed in Chapter 5). While maximum demands in the foundation members remain reasonably comparable (falling within 20% of one another), the pier column demands associated with the 5th percentile soil-rock profile exceed those of the deterministic case by 40%.

The pier column demands associated with the 5th percentile case increase substantially due to the relatively weak (and relatively less stiff) soil conditions.

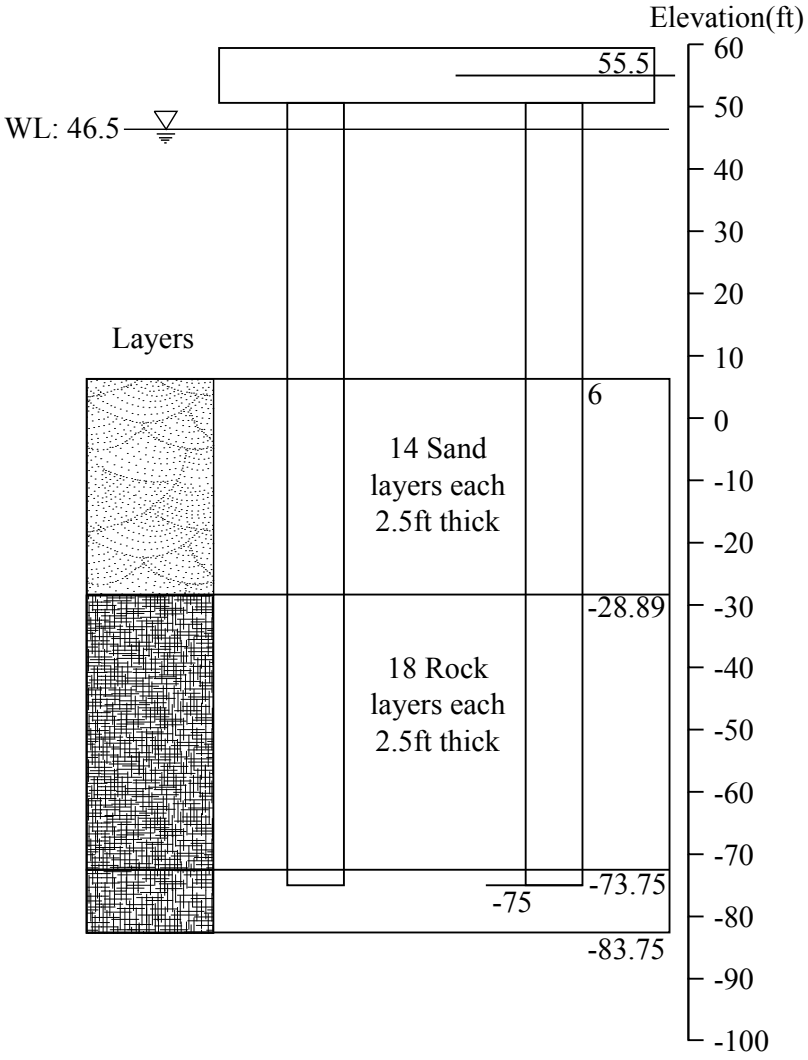

Figure 7.4.6. Soil layering for the 5th percentile boring

Table 7.4.2. 5th percentile sand layer properties

Layer	Soil Type	SPT	Top Elev. (ft)	ɣ (pcf)	φ (°)	k (pci)	G (ksi)	τ_u (psf)
1	Sand	25	6	115	35.77	19.77	0.64	462.63

2	Sand	23	3.52	115	38.42	38.93	1	578.61
3	Sand	15	1.02	110	35.69	19.41	0.63	671.75
4	Sand	13	-1.47	110	33.92	12.14	0.44	756.81
5	Sand	17	-3.96	110	35.69	19.44	0.63	834.41
6	Sand	14	-6.45	110	34.23	13.38	0.47	905.08
7	Sand	12	-8.95	110	33.64	10.98	0.4	969.25
8	Sand	19	-11.44	110	35.45	18.43	0.61	1,027.26
9	Sand	15	-13.93	110	34.14	13.02	0.46	1,079.42
10	Sand	29	-16.42	115	37.72	29.71	0.87	1,135.36
11	Sand	29	-18.92	115	37.88	31.88	0.9	1,185.19
12	Sand	29	-21.41	115	37.62	28.44	0.86	1,229.16
13	Sand	29	-23.9	115	37.51	27.02	0.84	1,267.48
14	Sand	29	-26.39	115	37.23	25.76	0.8	1,300.35

Table 7.4.3. 5th percentile rock layer properties

Layer	Soil Type	Top Elev. (ft)	γ (pcf)	φ (°)	G (ksi)	τ_u (psf)	q_u (psf)	E_m (ksi)	E_m/E_i	Surface	q_t (psf)	γ_c (pcf)	Slump (in)
15	Rock	-28.89	130	34	32.32	958.7	19,516	2.22	0.03	Rough	3,240	150	8
16	Rock	-31.38	130	34	32.52	2,360	19,636	3.11	0.04	Rough	4,248	150	8
17	Rock	-33.87	130	34	33.53	1,293	20,244	1.03	0.01	Rough	4,048	150	8
18	Rock	-36.36	130	34	33.34	1,014	20,128	3.19	0.04	Rough	3,264	150	8
19	Rock	-38.86	130	34	32.87	2,532	19,848	0.93	0.01	Rough	5,844	150	8
20	Rock	-41.35	130	34	97.79	8,195	59,040	29.55	0.12	Rough	9,070	150	8
21	Rock	-43.84	130	34	120.5	15,078	72,748	31.69	0.11	Rough	21,004	150	8
22	Rock	-46.34	130	34	150.2	15,710	90,660	37.03	0.1	Rough	22,100	150	8
23	Rock	-48.83	130	34	89.94	10,658	54,304	52.45	0.24	Rough	13,524	150	8
24	Rock	-51.32	130	34	12.14	2,180	7,332	4.03	0.14	Rough	4,844	150	8
25	Rock	-53.81	130	34	26.41	2,690	15,944	5.95	0.09	Rough	3,188	150	8
26	Rock	-56.31	130	34	42.02	6,258	25,368	13.11	0.13	Rough	10,012	150	8
27	Rock	-58.8	130	34	43.42	4,842	26,216	9.5	0.09	Rough	6,452	150	8
28	Rock	-61.29	130	34	130.8	10,980	78,992	27.78	0.09	Rough	16,560	150	8
29	Rock	-63.78	130	34	118.3	11,089	71,400	110.4	0.38	Rough	12,424	150	8
30	Rock	-66.28	130	34	143	18,611	86,308	145	0.41	Rough	26,540	150	8
31	Rock	-68.77	130	34	162.3	24,410	97,984	47.18	0.12	Rough	41,252	150	8
32	Rock	-71.26	130	34	164.4	14,661	99,264	293.3	0.73	Rough	14,452	150	8
33	Rock	-73.75	130	34	29.75	7,432	38,764	9.31	0.13	Rough	9,861	150	8

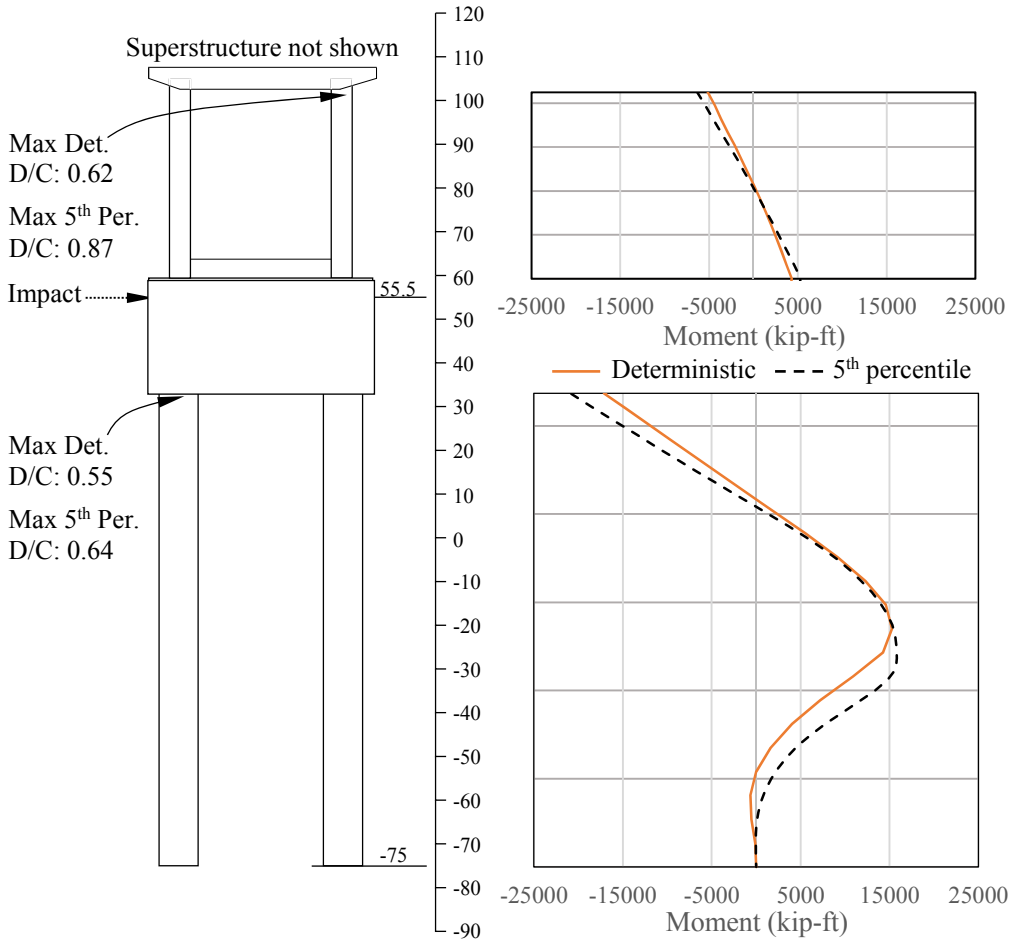

Figure 7.4.7. Pier 59 structural demand comparison for deterministic and 5th percentile soil modeling

7.4.4 CVIA-OPTS Analysis of Pier 59 Using Soil Parameters from the 95th Percentile Boring

The 95th percentile soil-rock profile layering is shown in Fig. 7.4.8 (which is identical to that of the 5th percentile profile). Sandy layer and rock strength parameters corresponding to the 95th percentile layering (Fig. 7.4.8) are listed in Table 7.4.4 and Table 7.4.5, respectively. The CVIA-OPTS results for the 95th percentile case are comparatively presented with the deterministic case (developed in Chapter 5) in Fig. 7.4.9. Due to the presence of relatively strong (and relatively more stiff) soil conditions in the 95th percentile case, the max D/C value in the drilled shafts exceeds that of both the 5th percentile and deterministic cases. Additionally, the pier column demands in the 95th percentile case are reduced relative to the 5th percentile case results, as relatively more load is (proportionally) directed downward into the Pier 59 soil.

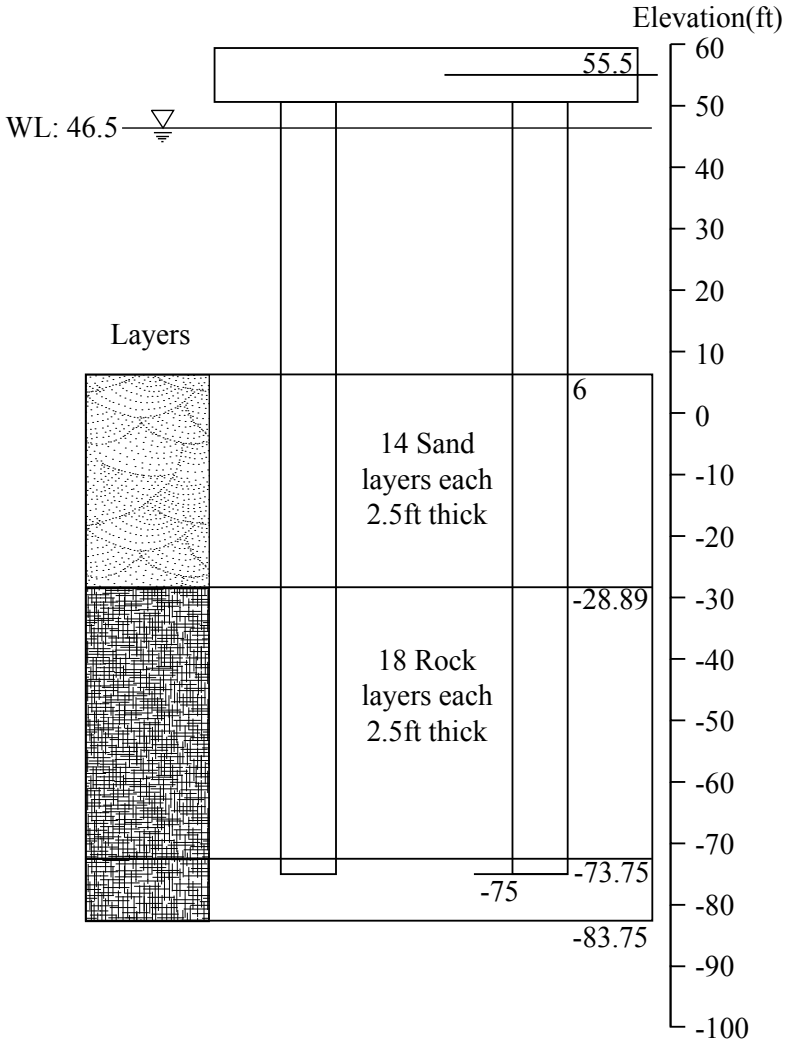

Figure 7.4.8. Soil layering for the 95th percentile boring

Table 7.4.4. 95th percentile boring sand layer properties

Layer	Soil Type	SPT	Top Elev (ft)	ɣ (pcf)	φ (°)	k (pci)	G (ksi)	τ_u (psf)
1	Sand	13	6	110	34.52	14.61	0.5	572.35
2	Sand	20	3.52	110	36.16	21.36	0.68	661.38
3	Sand	22	1.02	115	37.62	28.44	0.86	754.14
4	Sand	16	-1.47	110	34.81	15.81	0.53	827.77
5	Sand	23	-3.96	115	36.83	24.15	0.76	905.28
6	Sand	30	-6.45	120	38.66	42.04	1.05	985.78
7	Sand	23	-8.95	115	36.4	22.37	0.71	1,048.97
8	Sand	30	-11.44	115	37.95	32.77	0.92	1,105.75
9	Sand	29	-13.93	115	37.82	31	0.89	1,156.38
10	Sand	28	-16.42	115	37.52	27.11	0.84	1,201.12
11	Sand	29	-18.92	115	37.5	26.87	0.83	1,240.19
12	Sand	29	-21.41	115	37.42	26.57	0.82	1,273.78
13	Sand	28	-23.9	115	37.24	25.81	0.8	1,302.07
14	Sand	28	-26.39	115	36.9	24.4	0.77	1,325.22

Table 7.4.5. 95th percentile boring rock layer properties

Layer	Soil Type	Top Elev. (ft)	ɣ (pcf)	φ (°)	G (ksi)	τ_u (psf)	q_u (psf)	E_m (ksi)	E_m/E_i	Surface	q_t (psf)	γ_c (pcf)	Slump (in)
15	Rock	-28.89	130	34	32.32	958.7	19,516	2.22	0.03	Rough	3,240	150	8
16	Rock	-31.38	130	34	32.52	2,360	19,636	3.11	0.04	Rough	4,248	150	8
17	Rock	-33.87	130	34	33.53	1,293	20,244	1.03	0.01	Rough	4,048	150	8
18	Rock	-36.36	130	34	33.34	1,014	20,128	3.19	0.04	Rough	3,264	150	8
19	Rock	-38.86	130	34	32.87	2,532	19,848	0.93	0.01	Rough	5,844	150	8
20	Rock	-41.35	130	34	97.79	8,195	59,040	29.55	0.12	Rough	9,070	150	8
21	Rock	-43.84	130	34	120.5	15,078	72,748	31.69	0.11	Rough	21,004	150	8
22	Rock	-46.34	130	34	150.2	15,710	90,660	37.03	0.1	Rough	22,100	150	8
23	Rock	-48.83	130	34	89.94	10,658	54,304	52.45	0.24	Rough	13,524	150	8
24	Rock	-51.32	130	34	12.14	2,180	7,332	4.03	0.14	Rough	4,844	150	8
25	Rock	-53.81	130	34	26.41	2,690	15,944	5.95	0.09	Rough	3,188	150	8
26	Rock	-56.31	130	34	42.02	6,258	25,368	13.11	0.13	Rough	10,012	150	8
27	Rock	-58.8	130	34	43.42	4,842	26,216	9.5	0.09	Rough	6,452	150	8
28	Rock	-61.29	130	34	130.8	10,980	78,992	27.78	0.09	Rough	16,560	150	8
29	Rock	-63.78	130	34	118.3	11,089	71,400	110.4	0.38	Rough	12,424	150	8
30	Rock	-66.28	130	34	143	18,611	86,308	145	0.41	Rough	26,540	150	8
31	Rock	-68.77	130	34	162.3	24,410	97,984	47.18	0.12	Rough	41,252	150	8
32	Rock	-71.26	130	34	164.4	14,661	99,264	293.3	0.73	Rough	14,452	150	8
33	Rock	-73.75	130	34	29.75	7,432	38,764	9.31	0.13	Rough	9,861	150	8

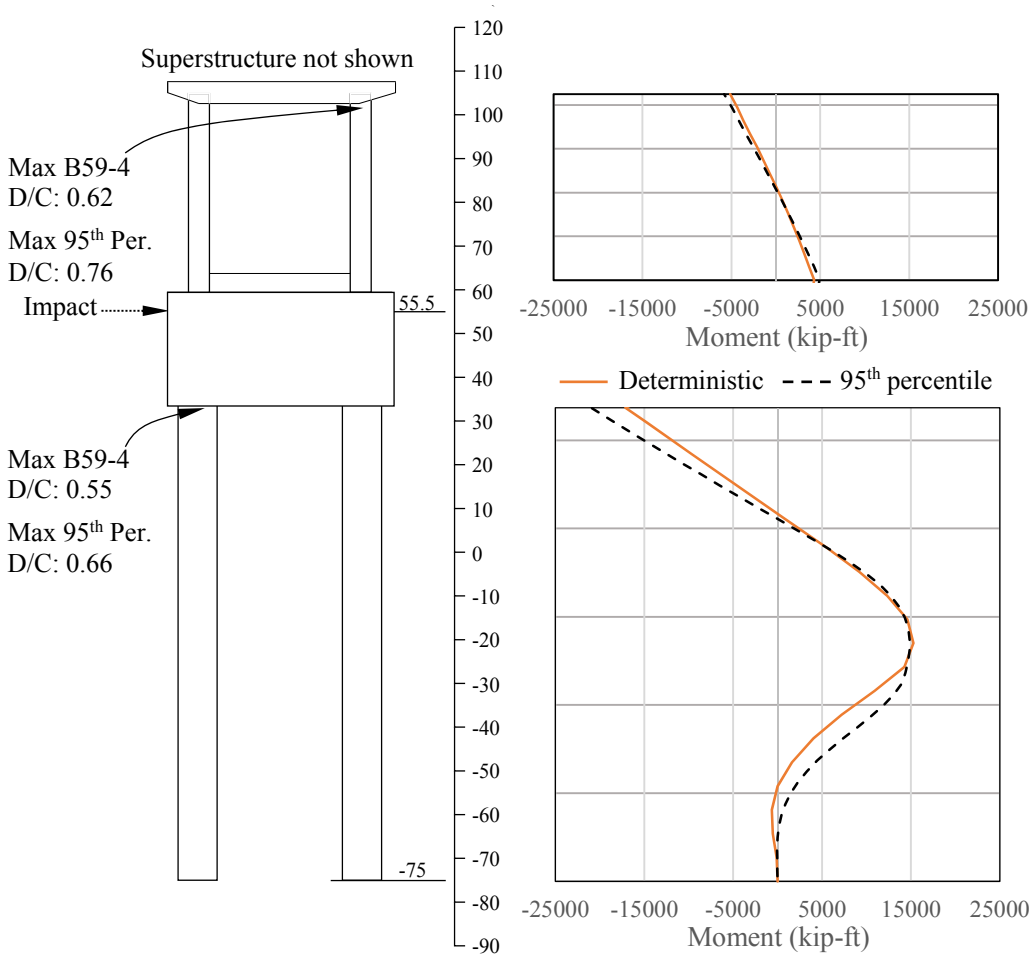

Figure 7.4.9. Pier 59 structural demand comparison for deterministic and 95th percentile soil modeling

7.4.5 Soil-Spatial Modeling Summary

Variations in soil resistance parameters were cursorily investigated for Pier 59 of the SR-20 bridge within the context of how variations in said resistance affect numerical predictions of collision-induced structural demand. The soil modeling approach employed incorporated soil-spatial variability into the through-depth values for the model-input soil strength parameters through vertical correlation and conditional probability. Based on estimates of drilled shaft axial capacity (obtained from full-scale testing of a comparable foundation member located within the immediate vicinity of Pier 59), the soil data were shown to be reasonably representative of the physical site conditions. Using lower and upper bounds of soil data profiles, vessel collision analyses (using the CVIA module in FBMP) were carried out, and the results were compared to those obtained for a deterministic treatment of the soil modeling (as detailed in Chapter 5). Comparisons of biaxial D/C values indicated that: (1) The greatest pier column demand was generated for the lower bound case (i.e., the case with the weakest, or least stiff soil); and (2) The greatest foundation demand (by proportion) was drawn into the foundation members for the upper bound case (i.e., the case pertaining to the strongest, or stiffest soil). The collective results demonstrated that, for the dynamic vessel collision analyses conducted using the Pier 59 OPTS model, the soil conditions can result in significantly altered distributions of structural demand for the impact scenario considered. Further investigation should be carried out to assess the effects that soil can have on collision-induced structural demand for other bridge piers and soil conditions.

7.5 Computational Time Comparisons between Full-Bridge and OPTS Analyses

As a final consideration in the parametric investigations of the current study, the computational time demands associated with conducting dynamic vessel collision analyses (CVIA) using full-bridge models (in comparison to those times required when utilizing respective OPTS models) were quantified for several of the bridge cases considered in the current study. All vessel collision analyses were conducted using a Windows 7© desktop PC with specification of 2 GB of RAM and use of an Intel® Core i7™ 3.4 GHz processor.

Shown in Fig. 7.5.1 are the wall-clock times needed to complete 1,600 time steps (or 4 sec. of simulated time) of CVIA analysis using multiple-pier, multiple-span models and corresponding OPTS models. The required wall-clock analysis times associated with the multiple-pier, multiple-span vessel collision simulations ranged from 24 min. for the 4-pier, 3-span old St. George Island Causeway model (discussed in Chapter 4) to 112 min. for the SR-20 7-pier, 6-span bridge model with boring 59-4 (i.e., deterministic) soil modeling (discussed in Chapter 5). In contrast, the OPTS models consistently required 5 min. or less of wall-clock time to complete the 1,600 time steps of nonlinear dynamic vessel collision analysis. As an added convenience, numerically predicted maximums of dynamic demand can be rapidly cataloged into a formatted table by making use of the FBMP Design Tables feature (see Appendix A).

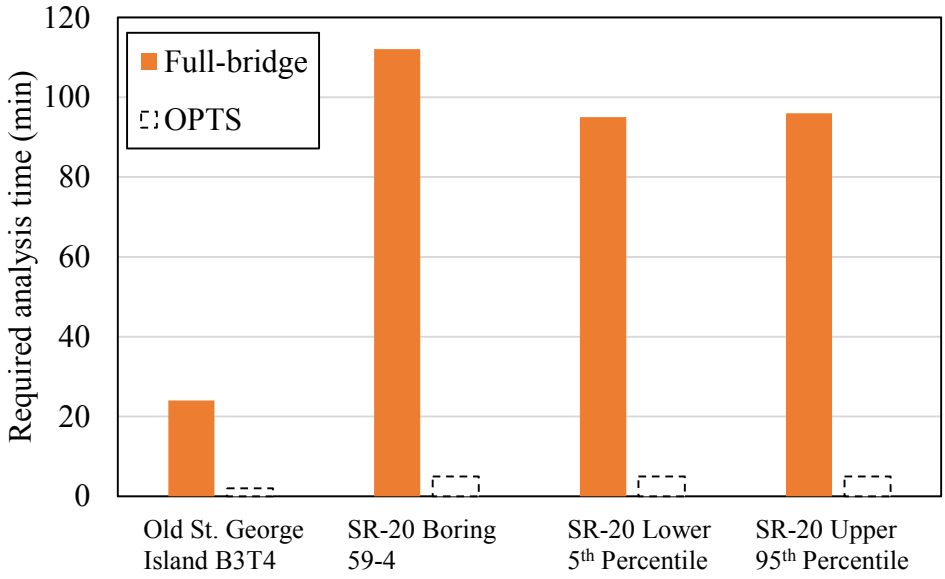

Figure 7.5.1. Required wall-clock time comparison between full-bridge and OPTS dynamic analyses

CHAPTER 8
SUMMARY AND CONCLUSIONS

8.1 Summary of Work Completed

Bridges constructed over navigable waterways are susceptible to collisions from massive waterway vessels such as barges. When vessels impinge upon bridge surfaces, large time-varying (dynamic) lateral forces can be exerted upon impacted bridge substructure components. Because vessel collision forces are generated over relatively short periods of time (over a matter of seconds), significant inertial forces can develop throughout the impacted pier, superstructure, and foundation members. As a result, portions of bridge structures may become (temporarily) restrained by both the stiffness and mass of adjacent members, which can lead to the generation of additional, and severe, structural demands. Thus, aberrant vessels pose significant risks to bridge structures in navigable waterways, and accordingly, the phenomena related to vessel-bridge collisions are typically taken into consideration in bridge design and analysis applications.

Over the past decade, significant advances have been made in the area of vessel-bridge collision. In particular, a group of researchers and engineers at the University of Florida (UF), in collaboration with the Florida Department of Transportation (FDOT), have been cultivating design-oriented vessel bridge collision analysis techniques. Based on these considerable, collective efforts, the current work was undertaken to implement in FB-MultiPier (FBMP): (1) A computationally-efficient vessel collision analysis procedures; and (2) A simplified bridge model for use in computationally-expensive dynamic analysis of full-scale bridge systems. The newly developed FBMP features are referred to as Coupled Vessel Impact Analysis (CVIA) module and One-Pier Two-Span (OPTS) model.

The FBMP CVIA module eliminates the need to prescribe vessel collision loading, while the FBMP OPTS model enables engineers to rapidly obtain analysis results that retain the accuracy associated with a true multiple-pier, multiple-span bridge model. Both the models were implemented as part of the current study such that they could be utilized separately or in conjunction with one another. The commercial-grade FBMP CVIA-OPTS constitutes a powerful, straightforward framework for quickly characterizing nonlinear dynamic bridge response to vessel collision loading.

Validation of the FBMP CVIA model was demonstrated in the current study with respect to correctness of computer programming in the graphical user interfaces (GUI), and separately, the analysis engine. In addition, the FBMP CVIA model was demonstrated to hold predictive capabilities that agreed well with full-scale experimental barge-bridge impact measurements. Likewise, the FBMP OPTS model was verified to be correctly coded in both the GUI and analysis engine. Further, application of the OPTS modeling to analysis of a full bridge subjected to a vessel collision loading condition was verified to be capable of predicting impacted bridge pier response that is in agreement with response predictions obtained from analysis of a full-bridge system.

Potential cost-savings associated with use of a combined CVIA-OPTS analysis in bridge design applications was investigated by carrying out a parametric study for a selected bridge case. Numerous, detailed FBMP models of multiple-pier, multiple-span models and OPTS models were developed for the selected in-service bridge case. Required analysis run-times were cataloged for several of the multiple-pier, multiple-span and (respective) OPTS models. The robustness of accounting for impact surface shape-dependent phenomena (which is included in the CVIA methodology) was demonstrated in impact analyses on equal-width flat and round impact surfaces. Further, a cost-benefit analysis was carried out to demonstrate potential cost differences in sized structural and foundation members, as identified by comparing results from static and dynamic vessel collision analyses. For the purpose of design application, the effects of various impact conditions and geotechnical considerations on impacted bridge pier response were analyzed by making use of the CVIA-OPTS model, previous research findings obtained from several past FDOT-sponsored projects, and the FDOT Geotechnical Database.

8.2 Conclusions

Based on completion of the FBMP CVIA and OPTS implementation, validation, and assessment tasks, the following conclusions are drawn, where topics that warrant further investigation are italicized:

1. In general, FBMP OPTS analyses are found to predict maximum internal forces that range from nominally different to moderately conservative in comparison to corresponding values computed from full bridge analyses. For the in-service bridge case examined as part of the current study, the corresponding full-bridge and OPTS analysis results are found to be nominally different within a margin of error. Further, it is recommended that an extensive set of favorably comparative (full-bridge versus OPTS) cases be performed. In the current study, consistently good agreement between full-bridge and OPTS analyses for the bridge case investigated suggests that the FBMP OPTS model can be used as a suitably accurate replacement for full-bridge models in conducting not only vessel collision analysis but also quasi-static analysis.

2. Plots of structural-demand histories throughout the impacted pier of the selected bridge case in the current study consistently indicate that the computed pier response is strongly influenced by the: (1) Inertia of the superstructure (discussed immediately below), and (2) Soil resistance of the foundation (see item 7. below). Superstructure inertial effects are evident such that pronounced, relative lags occur in the pier column top displacements, relative to the pier column bottom displacements shortly after the onset of impact. The relative displacement lag that occurs near the top of the pier gives rise to transient spikes in internal demands, which manifest throughout the pier over the early (actively loaded) portions of the vessel collision analysis. This observation is consistent with previously conducted analytical and experimental studies.

3. Capturing the collision-specific phenomena necessitates use of dynamic analysis, and the efficiency of the FBMP CVIA-OPTS modeling tool are highlighted in this context. Namely, all analyses conducted for this study were conducted on an ordinary desktop computer. However, the wall-clock time required to conduct 4 second duration CVIA analysis of full-bridge models ranged from 24 min. to 112 min., while the wall-clock times associated with use of the FB-MultiPier CVIA-OPTS features required between 2 min. and 5 min. to run to completion.

4. The FBMP CVIA module enables bridge engineers to easily (through an automated input and output process) account for impact surface geometry. By using the CVIA module in conjunction with the OPTS model, case studies of impacts on flat surfaces and impacts on round surfaces can be analyzed in a matter of minutes. Consequently, vessel collision analysis results can be displayed in the FB-MultiPier GUI, demonstrating that (for instance) impacts on round surfaces versus impacts on flat surfaces lead to increases in both maximum impact load magnitude, and correspondingly, significant changes in structural demand. Such simple, robust bridge modeling and vessel-collision analysis tools prove useful in rapidly identifying ways to design or/and retrofit bridge piers such that the efficiency of structural design may well be increased for those regions of members that are susceptible to impact.

5. For the selected bridge case of the current study, two pivotal design parameters are identified by investigating differences found among the static and dynamic analysis results. First, despite maintaining equivalent kinetic energies between the empirically determined static impact load and the generation of the time-varying impact load, the maximum impact load magnitude associated with the static analysis was nearly 50% greater than that of the dynamic (CVIA) analysis. The sizable difference in maximum impact load magnitudes, which arose in this case because the CVIA module accounts for impact surface geometry, resulted in altogether reduced demand predictions when making use of the dynamic (CVIA) analysis. As a result, for certain cases, foundation members of smaller size may satisfy benchmark demand levels (in association with dynamic analysis) because of the difference in (static versus dynamic) maximum impact loads. Further, dynamic amplification phenomena, present only in the dynamic analysis, acted to shift impact load absorption upward into the pier columns and superstructure. In turn, dynamic amplification permitted further reductions in the foundation member sizing. *However, precisely because the soil-structure interaction and associated dynamic amplification phenomena led to proportionally greater impact load absorption along the upward load path, the need may arise to either increase or decrease the amount of longitudinal reinforcement in the pier columns and the design capacities of pile foundations (for dynamic analysis, relative to static analysis).*

6. Regarding the static versus dynamic cost-benefit analysis, modifications to the impacted pier (Pier 59 of the SR-20 bridge) consist of: 1.5 ft reductions in the drilled shaft diameters; 3 ft increases in the drilled shaft tip elevations; 1.5 ft reduction in the

shear wall thickness; and increased longitudinal reinforcement in the pier columns. From a construction cost standpoint, these modifications cumulatively led to a total cost savings of approximately $160,000 for the impacted pier. *Demonstration of the potential for significant cost savings on a per-pier basis supports the need for a wider, design-oriented investigation aimed at further exploring potential advantages associated with use of the newly developed dynamic vessel collision analysis features in FBMP.*

7. Spatial variations in soil resistance parameters were cursorily investigated for the selected in-service bridge case, and within the context of how variations in said resistance affect numerical predictions of collision-induced structural demand. The soil modeling approach employed incorporated soil-spatial variability by making use of the FDOT Geotechnical Database into the through-depth values for the model-input soil strength parameters through vertical correlation and conditional probability. Soil boring and rock core data of the selected bridge site were collected and uploaded to the FDOT Geotechnical Database. Lower and upper bounds of soil data profiles, which are representative of the bridge site conditions, were used in vessel collision analyses (using the FBMP CVIA module), and the analysis results were compared to those obtained for a typical, deterministic treatment of soil-foundation interaction modeling. For the selected bridge case, comparisons of biaxial D/C values obtained from across the lower bound, upper bound, and deterministic analyses indicated that: (1) The greatest pier column demand was generated in the case with the least stiff soil; and (2) The greatest foundation demand (by proportion) was drawn into the foundation members for the upper bound case (i.e., the case with the stiffest soil). *The collective results demonstrate that, for the dynamic vessel collision analyses conducted on the selected in-service bridge case, the soil conditions can result in significantly altered distributions of structural demand for the impact scenario considered. Further investigation could assess the effects of soil-pile interaction on collision-induced structural demands for representative bridge piers and soil conditions. Subsequently, representative target values of demand-capacity ratios could be determined for use in a reliability-based design of pier columns and pile foundations of bridges subjected to extreme event loading, e.g., AASHTO Extreme Limit States.*

CHAPTER 9
REFERENCES

ADINA Research and Development Inc. (2014). *ADINA Theory and Modeling Guide.* Report 01-7, Watertown, MA.

American Association of State Highway and Transportation Officials (AASHTO). 2012. *AASHTO LRFD Bridge Design Specifications*. 6th Edition, Washington, D.C.

AASHTO. 2009. *Guide Specifications and Commentary for Vessel Collision Design of Highway Bridges, 2nd Edition*. Washington, D.C.

AASHTO. 1991. *Guide Specifications and Commentary for Vessel Collision Design of Highway Bridges, 1st Edition*. Washington, D.C.

Chung, J.H. 2014a. *FB-MultiPier User's Manual*. Bridge Software Institute, University of Florida, Gainesville, FL.

Chung, J.H. 2014b. *FB-Deep User's Manual*. Bridge Software Institute, University of Florida, Gainesville, FL.

Chung, J.H., Ko J., Klammler H., McVay M. C., and Lai P. 2012. "A Numerical and Experimental Study of Bearing Stiffness of Drilled Shafts Socketed in Heterogeneous Rock." *Computers and Structures*, 90-91, 145-152.

Consolazio, G. R., Cook, R. A., and McVay, M. C. 2006. "Barge Impact Testing of the St. George Island Causeway Bridge Phase III: Physical Testing and Data Interpretation." *Structures Research Report No. 2006/26868*, Engineering and Industrial Experiment Station, University of Florida, Gainesville, FL, March.

Consolazio, G. R., and Cowan, D. R. 2005. "Numerically Efficient Dynamic Analysis of Barge Collisions with Bridge Piers." American Society of Civil Engineers (ASCE) *Journal of Structural Engineering*. 131(8), 1256–1266.

Consolazio, G. R., and Davidson, M. T. 2008. "Simplified Dynamic Barge Collision Analysis for Bridge Design." *Transportation Research Record*. *2050*, Transportation Research Board, Washington, D.C., 13–25.

Consolazio, G. R., Davidson, M. T., and Cowan, D. R. 2009. "Barge Bow Force-Deformation Relationships for Barge-Bridge Collision Analysis." *Transportation Research Record. 2131*, Transportation Research Board, Washington, D.C., 3–14.

Consolazio, G. R., Davidson, M. T., and Getter, D. J. 2010. "Vessel Crushing and Structural Collapse Relationships for Bridge Design." *Structures Research Report No. 2010/72908/74039*, Engineering and Industrial Experiment Station, University of Florida, Gainesville, FL, August.

Consolazio, G. R., McVay, M. C., Cowan, D. R., Davidson, M. T., and Getter, D. J. 2008. "Development of Improved Bridge Design Provisions for Barge Impact Loading." *Structures Research Report No. 51117*, Engineering and Industrial Experiment Station, University of Florida, Gainesville, FL, April.

Davidson, M. T. 2007. "Simplified Dynamic Barge Collision Analysis for Bridge Pier Design." Thesis, Dept. of Civil and Coastal Engineering, University of Florida, Gainesville, Fla.

Davidson, M. T., Consolazio, G. R., and Getter, D. 2010. "Dynamic Amplification of Pier Column Internal Forces Due to Barge-Bridge Collision." *Transportation Research Record*. Transportation Research Board, No. 2172, 11-22, Washington, D.C.

Davidson, M. T., Consolazio, G. R., Getter, D., and Shah, F. 2013. "Probability of Collapse Expression for Bridges Subject to Barge Collision." ASCE *Journal of Bridge Engineering*, 18(4), 287–296.

Florida Department of Transportation (FDOT). (2014). *Structures Design Guidelines*, Tallahassee, FL.

Isaaks, E. H. 1989. *An Introduction to Applied Geostatistics*, Oxford University Press.

Liu, C. and Wang, T. 2001. "Statewide Vessel Collision Design for Bridges." ASCE *Journal of Bridge Engineering*, 6(3), 213-219.

McVay, M.C., Ellis, R. D., Kim, M., Villegas, J., Kim, S., Lee, S. 2003. "Static and Dynamic Field Testing of Drilled Shafts: Suggested Guidelines on Their Use for FDOT Structures." *Geotechnical Research Report No. 4910-4504-725-12*. Engineering and Industrial Experimental Station, University of Florida, Gainesville, FL, October.

McVay, M. C., Hoit, M., Hughes, E., Nguyen, T., and Lai, P. 2005b. "Development of a Web Based Design, and Construction Bridge Substructure Database." *84th Annual Meeting, Transportation Research Board*, January 9-13, Washington D.C.

McVay, M.C., Klammler, H., Bloomquist, D., Otero, J., and Faraone, M., 2009a. "Modification of LRFD Resistance Factors Based on Site Variability." *FDOT Geotechnical Research Report No. BD-545, RPWO #76*. Engineering and Industrial Experimental Station, University of Florida, Gainesville, FL, June.

McVay, M.C., Wasman, S. J., Consolazio, G. R., Bullock, P. J., Cowan, D. R., and Bollmann, H. T. (2009b). "Dynamic Soil-Structure Interaction of Bridge Superstructure Subject to Vessel Impact" *ASCE Journal of Bridge Engineering*, Vol. 14, No. 1, pp. 7-16.

McVay, M.C., Klammler, H., Faraone, M., Dase, K., and Jenneisch, C. 2012. "Development of Variable LRFD ϕ Factors for Deep Foundation Design Due to Site Variability." *FDOT Geotechnical Research Report No. BDK75 977-23*. Engineering and Industrial Experimental Station, University of Florida, Gainesville, FL, June.

McVay, M. C., Wasman, S. J., and Bullock, P.J. 2005a. "St. George Geotechnical Investigation of Vessel Pier Impact." *Geotechnical Research Report No. 4910-4554-016-12*. Engineering and Industrial Experiment Station, University of Florida, Gainesville, FL.

Paultre, P., Chaallal, O., and Proulx, J. 1992. "Bridge Dynamics and Dynamics Amplification Factors – A Review of Analytical and Experimental Findings." *Canadian Journal of Civil Engineering*, 19, 260-278.

Yuan, P., Harik, I. E., and Davidson, M. T. 2008. "Multi-Barge Flotilla Impact Forces on Bridges." *Kentucky Transportation Center Research Report No. KTC-05/SPR261-03-1F*, University of Kentucky, Lexington, KY.

APPENDIX A
CONDENSED USER'S GUIDE FOR VESSEL COLLISION ANALYSIS AND DESIGN LOAD TABLES IN FB-MULTIPIER

Presented in the following pages is the body of a condensed User's Guide that contains step-by-step instructions for utilizing the CVIA-OPTS features in FB-MultiPier. In addition, step-by-step instructions are given for an example of efficiently post-processing analysis results through use of the Design Tables feature in FB-MultiPier. An extended edition of the User's Guide is provided below in Appendix B.

Condensed User's Guide for Vessel Collision Analysis and Design Load Tables in FB-MultiPier

Jae H. Chung, Michael Davidson, Clint Monari, Henry Bollmann, Anand Patil

Bridge Software Institute, College of Engineering, University of Florida, Gainesville FL, 32611

Contact: BSI@CE.UFL.EDU (352)392-9537 ext. 1514

1. INTRODUCTION

This document provides users with a step-by-step guide for making use of new features that facilitate designer friendly assessments of structural response for bridge piers that are subject to waterway vessel collision loading. Namely, a simplified bridge modeling procedure (one-pier two-span, or OPTS) and a numerically-efficient dynamic vessel-collision analysis technique (coupled vessel impact analysis, or CVIA) are the focus of this guide. Further, key analysis results are made available in a user-friendly, robust output format by making use of the Design Load Table feature in FBMP. The modeling and analysis techniques identified above, as being implemented in FBMP, give bridge engineers a powerful, rapid means of carrying out nonlinear dynamic vessel collision analyses on bridge structures.

2. COUPLED VESSEL IMPACT ANALYSIS (CVIA) OF BRIDGE MODEL

The bridge shown in Fig. 2.1 constitutes the demonstration case for this user's guide, and is intended to represent a high level approach structure leading up to the main span on a causeway-type bridge. Throughout this user's guide, the configuration shown in Fig. 2.1 is referred to as the "full-bridge model", and the (highlighted) pier of interest is referred to as Pier 2. Further, the impact location (node 12) considered in this guide is shown in Fig. 2.2.

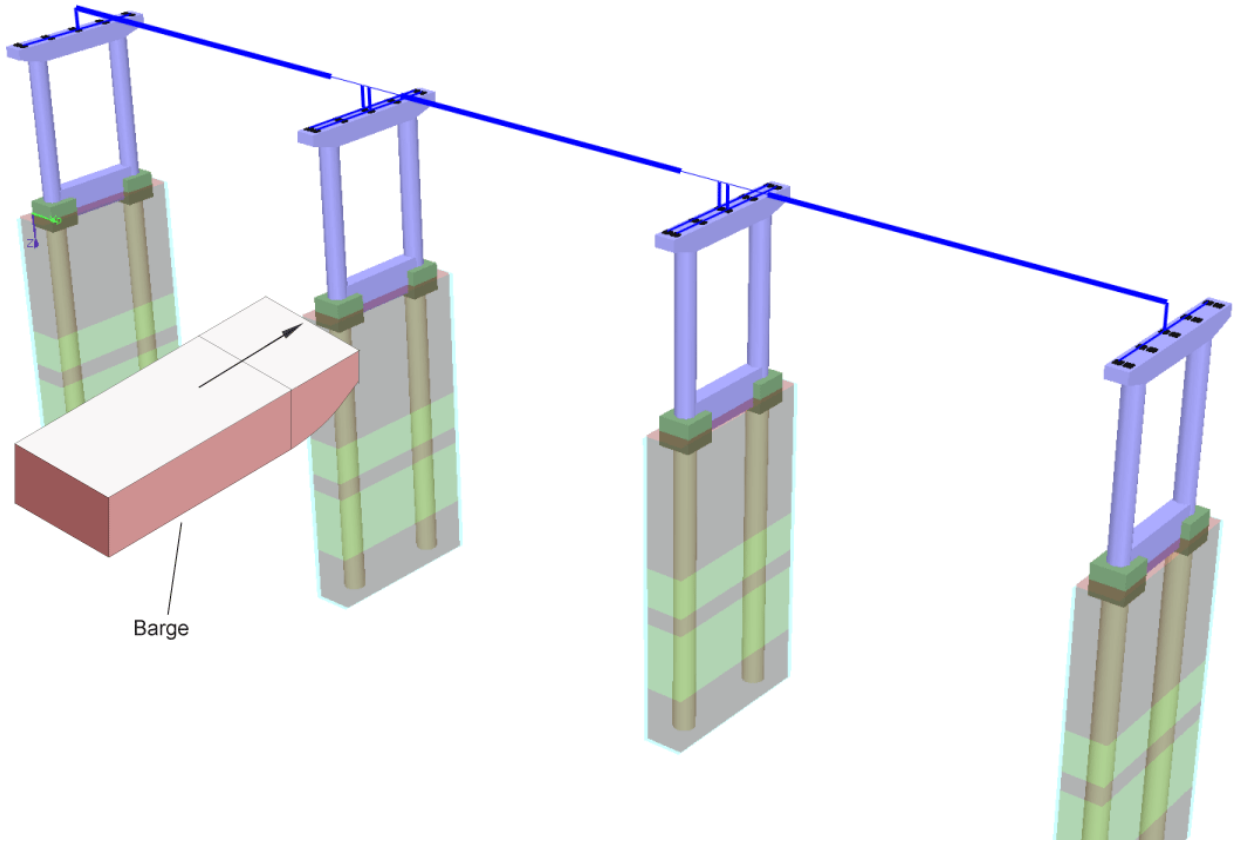

Figure 2.1. Schematic of collision scenario for the four-pier three-span bridge model

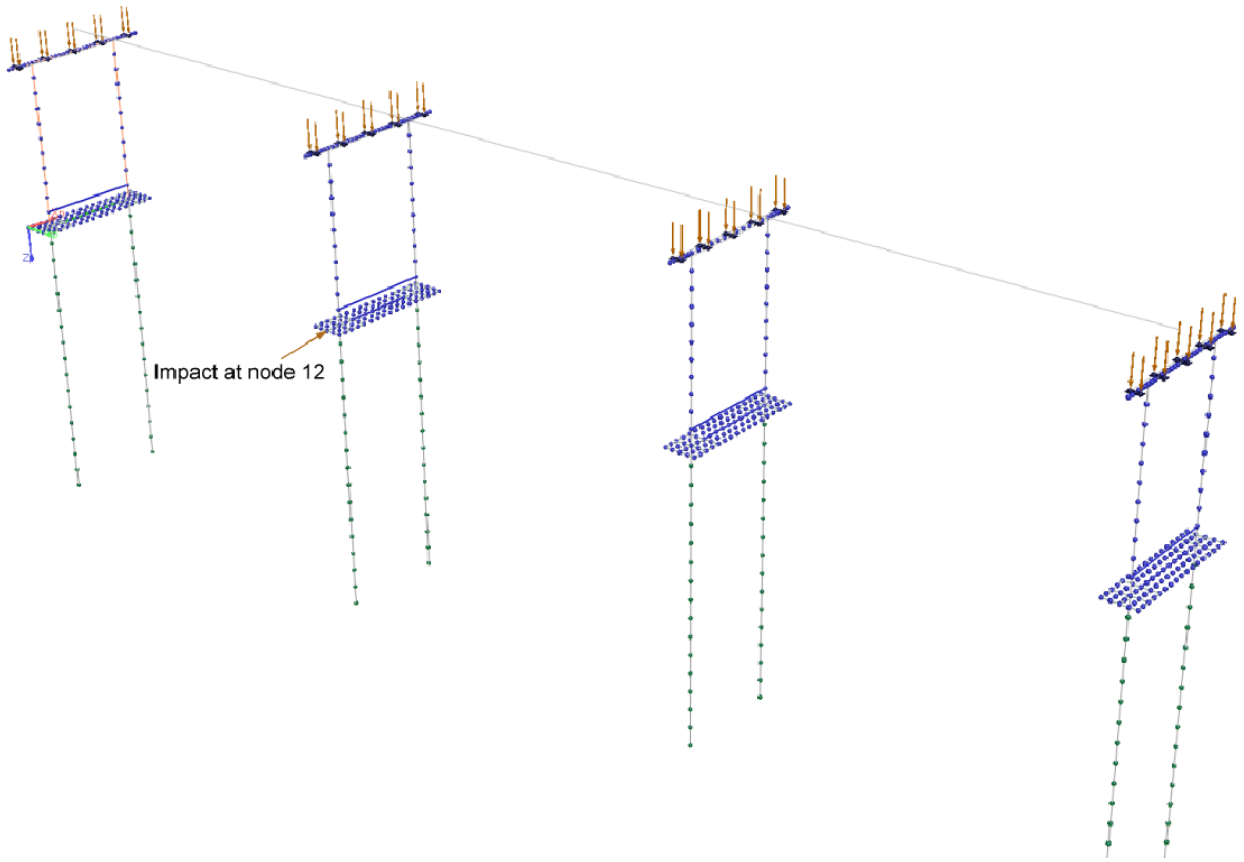

Figure 2.2. Loading of four-pier three-span bridge model

DYNAMIC PARAMETER INPUT

In FBMP, modal analysis is carried out to determine dynamic input such as Rayleigh damping coefficients, which in turn, produce 5% of critical damping over the first five modes of vibration in subsequent time-history analyses. Modal analysis is enabled by selecting the "Dynamic" analysis type in the "Analysis" page (Fig. 2.3). Modal response input is then entered in the "Dynamics" page (Fig. 2.4). The "Modal Response" option should be selected in the "Analysis Type" section, and the "# Modes" should be set to 5 or greater. Additionally, both the "Stop Analysis after Eigenvector Results" and "Calculate Rayleigh Damping Factors" checkboxes should be checked. After completing the modal analysis input on the "Dynamics" page, a modal analysis is carried out by clicking the "Analysis" button on the toolbar (Fig 2.5). The Rayleigh damping coefficients are printed to the output file (Fig 2.6).

Rayleigh damping coefficients are imported from the output file into a time-history analysis from within the "Dynamics" page. Here, analysis type is set to "Time Step Integration" (Fig. 2.7). Additionally, the "Dynamic Relaxation" option is selected by checking the "Static Dead Load" tick-box. For CVIA, the "Vessel Collision" time function type is selected, and the time step information is supplied. For this demonstration case, an analysis duration of 2 sec. (i.e., 400 time steps) is selected.

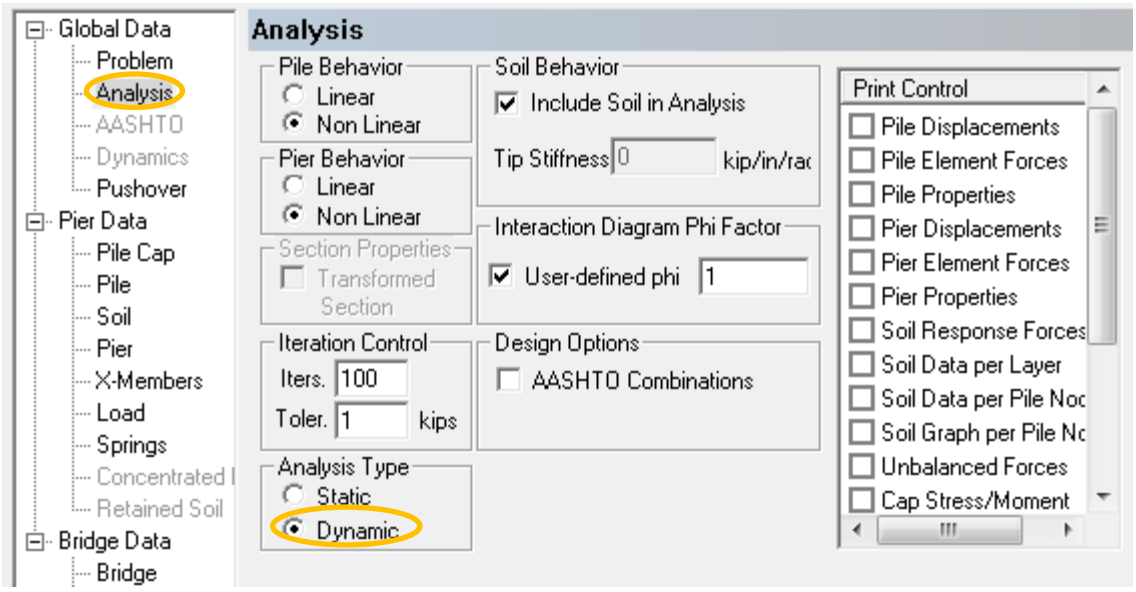

Figure 2.3 Selection of dynamic analysis in the Analysis page

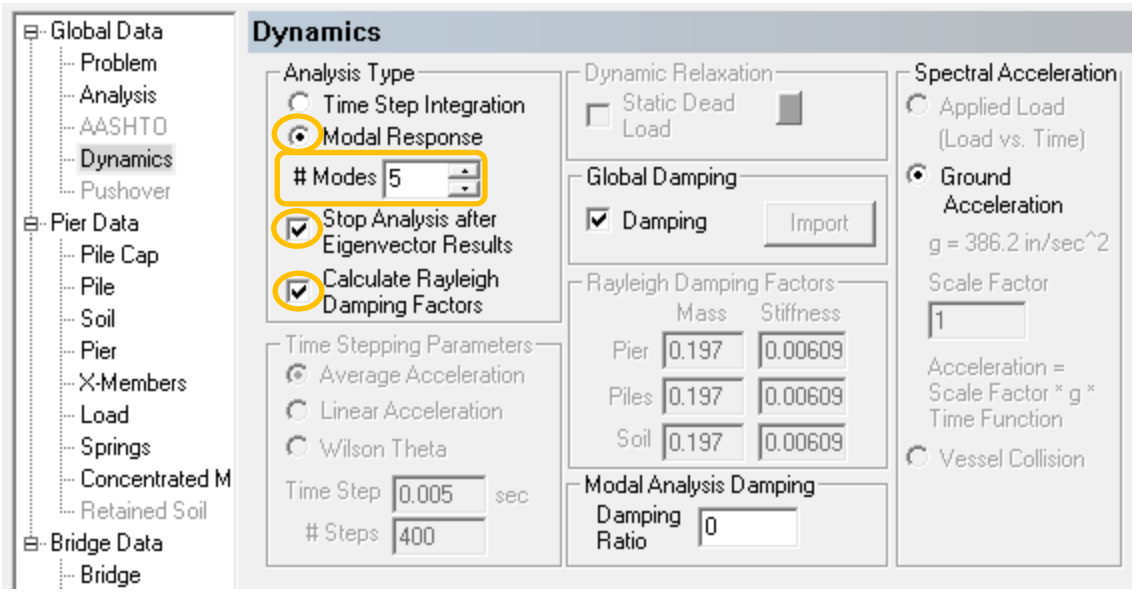

Figure 2.4. Selection of Modal Analysis (to determine Rayleigh damping coefficients)

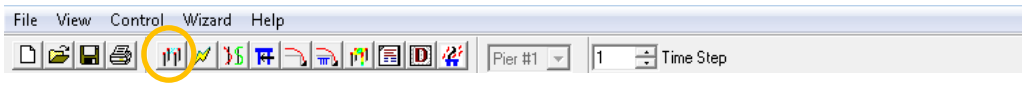

Figure 2.5 Analysis toolbar button

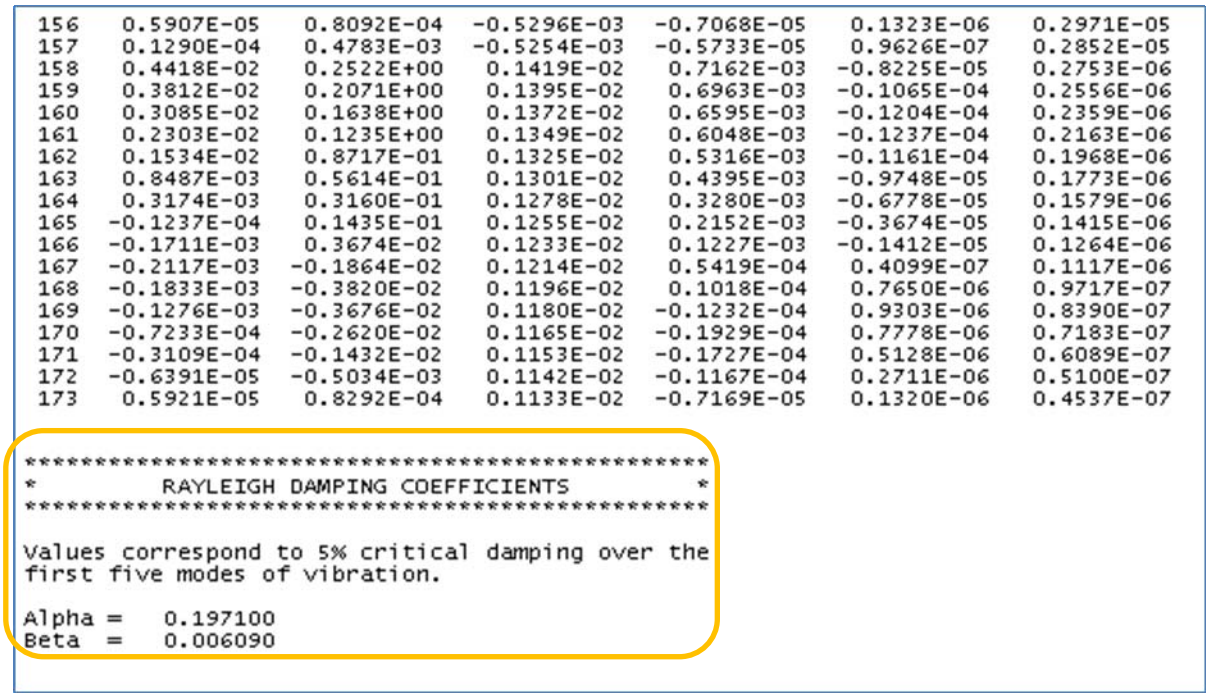

156	0.5907E-05	0.8092E-04	-0.5296E-03	-0.7068E-05	0.1323E-06	0.2971E-05
157	0.1290E-04	0.4783E-03	-0.5254E-03	-0.5733E-05	0.9626E-07	0.2852E-05
158	0.4418E-02	0.2522E+00	0.1419E-02	0.7162E-03	-0.8225E-05	0.2753E-06
159	0.3812E-02	0.2071E+00	0.1395E-02	0.6963E-03	-0.1065E-04	0.2556E-06
160	0.3085E-02	0.1638E+00	0.1372E-02	0.6595E-03	-0.1204E-04	0.2359E-06
161	0.2303E-02	0.1235E+00	0.1349E-02	0.6048E-03	-0.1237E-04	0.2163E-06
162	0.1534E-02	0.8717E-01	0.1325E-02	0.5316E-03	-0.1161E-04	0.1968E-06
163	0.8487E-03	0.5614E-01	0.1301E-02	0.4395E-03	-0.9748E-05	0.1773E-06
164	0.3174E-03	0.3160E-01	0.1278E-02	0.3280E-03	-0.6778E-05	0.1579E-06
165	-0.1237E-04	0.1435E-01	0.1255E-02	0.2152E-03	-0.3674E-05	0.1415E-06
166	-0.1711E-03	0.3674E-02	0.1233E-02	0.1227E-03	-0.1412E-05	0.1264E-06
167	-0.2117E-03	-0.1864E-02	0.1214E-02	0.5419E-04	0.4099E-07	0.1117E-06
168	-0.1833E-03	-0.3820E-02	0.1196E-02	0.1018E-04	0.7650E-06	0.9717E-07
169	-0.1276E-03	-0.3676E-02	0.1180E-02	-0.1232E-04	0.9303E-06	0.8390E-07
170	-0.7233E-04	-0.2620E-02	0.1165E-02	-0.1929E-04	0.7778E-06	0.7183E-07
171	-0.3109E-04	-0.1432E-02	0.1153E-02	-0.1727E-04	0.5128E-06	0.6089E-07
172	-0.6391E-05	-0.5034E-03	0.1142E-02	-0.1167E-04	0.2711E-06	0.5100E-07
173	0.5921E-05	0.8292E-04	0.1133E-02	-0.7169E-05	0.1320E-06	0.4537E-07

```
*************************************************
*         RAYLEIGH DAMPING COEFFICIENTS         *
*************************************************

Values correspond to 5% critical damping over the
first five modes of vibration.

Alpha =    0.197100
Beta  =    0.006090
```

Figure 2.6 Rayleigh damping coefficients in output file

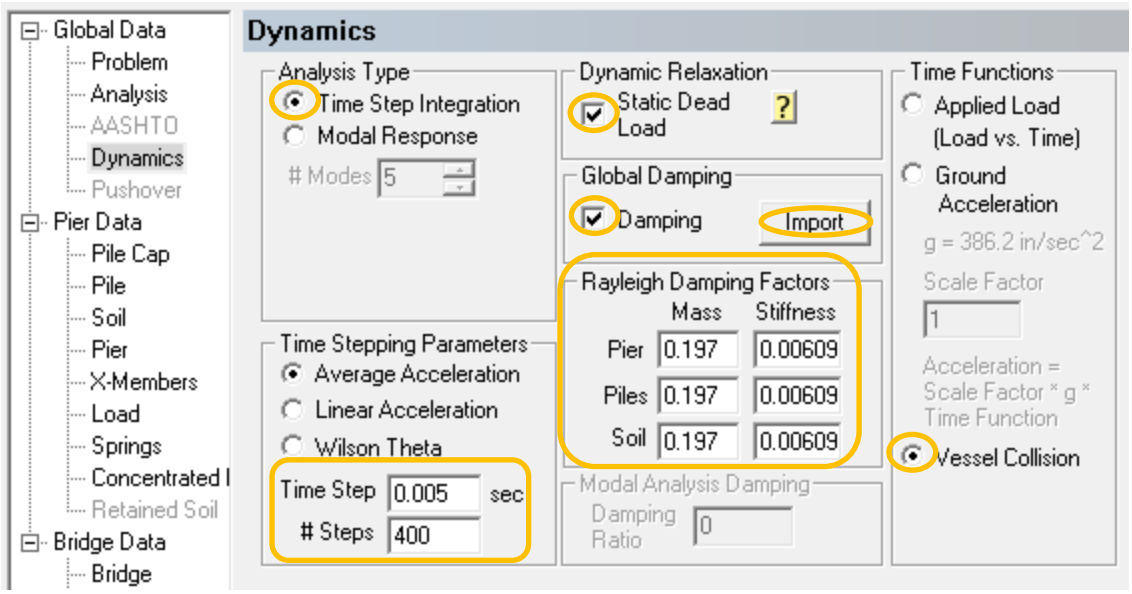

Figure 2.7 Selection of dynamic analysis in the Dynamics page

INPUT FOR VESSEL COLLISION LOADING

The impact location is defined by applying a dynamic load at a selected node (node 12) on the "Load" page in the "Node Applied" list box (Fig. 2.8). Vessel data are input by clicking the "Vessel Col." button in the "Load" page (Fig. 2.8). Then, in the "Vessel Collision Analysis Data" dialog (Fig. 2.9), the impacting vessel weight, initial x-velocity, and initial y-velocity (if non-zero) can be input directly. For the demonstration case, a vessel weight of 1,390 kips and a head-on (i.e., x-velocity) of 3.3 ft/sec are entered. In addition, the vessel type is selected from the pull-down menu. For demonstration, impact is taken between a barge and a 9 ft diameter round surface. After completing the input on the "Vessel Collision Analysis Data" dialog, CVIA-OPTS is carried out by submitting the model for analysis via the "Analysis" toolbar button (Fig. 2.5). Results are given in Chapter 4.

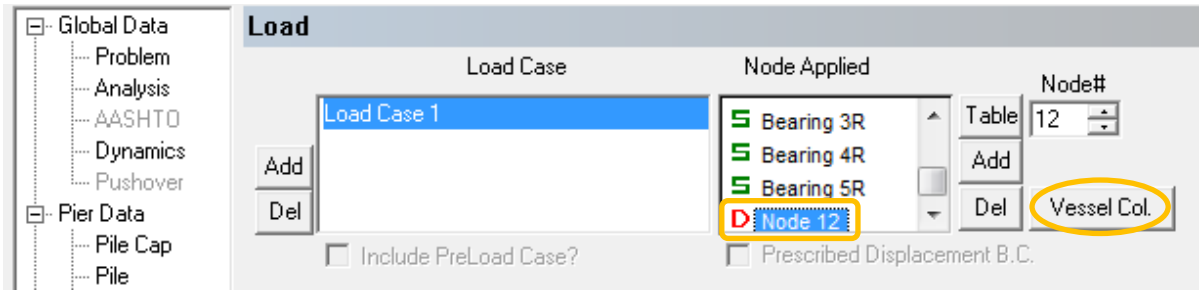

Figure 2.8 Defining the impacted node in the Load page

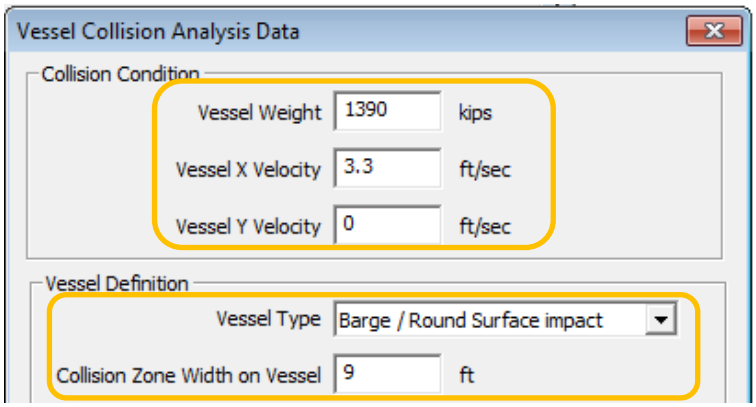

Figure 2.9 Top portion of Vessel Collision Analysis Data dialog

3. FORMATION OF OPTS MODEL

Results obtained from time-history (CVIA) analysis of the full-bridge can be obtained much more quickly for the pier of interest (Pier 2) by forming an OPTS model. The pier, soil, and span

of the OPTS model are readily formed (extracted) from the full-bridge static model by selecting the "One Pier, Two Span" problem type from within the "Problem" page (Fig. 3.1). The model created by following this process is shown in Fig. 3.2.

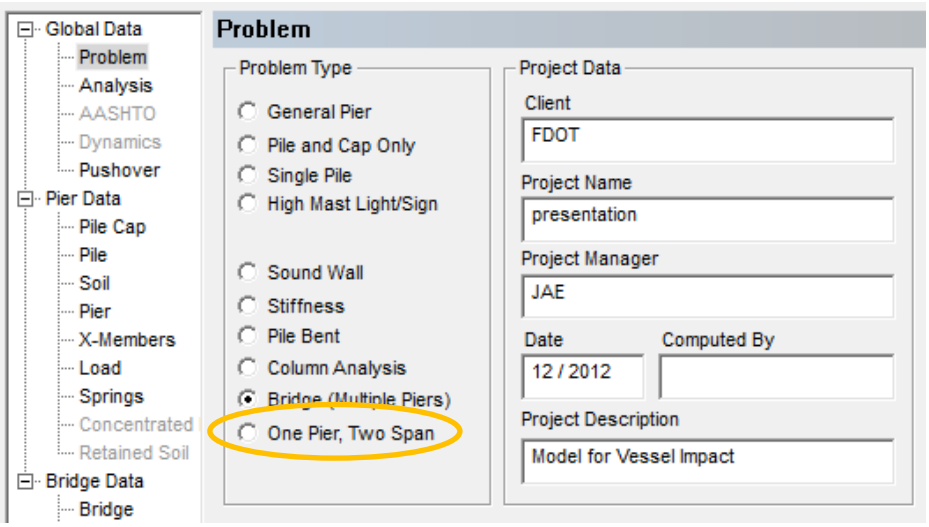

Figure 3.1 Selection of One Pier, Two Span (OPTS) Problem Type

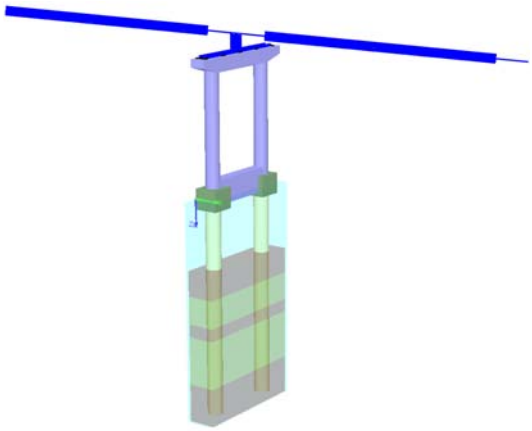

Figure 3.2 Initial formation of OPTS static model from Pier 2 of full-bridge model

FORMATION OF OPTS SPRINGS

As detailed in this section, the full-bridge model, the static estimate of impact load, and the OPTS static model are used in a chain of FBMP static analyses to iteratively calculate the OPTS model span-end stiffnesses and lumped masses. This iterative process requires as a pre-requisite that a datum of full-bridge model static response be established by subjecting the full-

bridge model to static lateral loading. Subsequently, iterations are carried out in two stages. First, estimates of the OPTS spring stiffnesses and lumped masses are calculated. The second stage of each iteration is enacted by fitting the OPTS static model with the current iteration span-springs and lumped masses, and then subjecting the OPTS model to the same static lateral loading as that employed previously in establishing the datum of response. If the OPTS model lateral-load response shows good agreement with the full-bridge model response, then the iterative procedure is considered to be complete. Otherwise, the next iteration is undertaken, and the full-bridge model static span loads supplied during the first stage of the previous iteration are modified to make better estimates in forming the OPTS springs. To illustrate this process, one full iteration is stepped through below.

DATUM ESTABLISHMENT FOR OPTS MODEL RESPONSE

First, a static lateral load is applied at node 12 in Pier 2 of the full-bridge model (for this case, the load equals 900 kips). To do this, first select Pier 2 using the Pier drop down in the toolbar (Fig. 3.3). Then on the “Load” page, select node 12 in the “Node Applied” list box, and input 900 in the “Xp Load, kips” edit box (Fig. 3.4). Vessel data is input by clicking the “Vessel Col.” button in the “Load” page (Fig. 2.8). Shown in Fig. 3.5 is the deformed shape of Pier 2 with particular annotated displacements at the laterally loaded node (i.e., the impact location), and the top of the pier column (node 97). The displacements predicted to occur at these two locations are used in the subsequent (iterative) OPTS spring formation procedure.

ITERATION 1: LOADING OF SPAN-END LOCATIONS IN THE FULL-BRIDGE MODEL

The first iteration of determining the OPTS span spring stiffnesses is initiated by loading the full-bridge static model and accessing the “Table” dialog in the “Load” page (Fig. 3.6). After the “Table” dialog appears, the “Calculation of OPTS Springs and Masses” check box is selected (Fig. 3.7), and the “Loading for OPTS Spring Formation” dialog appears (Fig. 3.8). Here, the loads applied at the individual DOFs are supplied to the span locations in the full-bridge model, i.e., a value of 360 is input in each of the “Force X” edit boxes, a value of 100 is input in each of the “Force Y” edit boxes, etc. Note that the influence of the pier of interest (Pier 2) and the directly attached spans (span 1 and span 2) are removed from the model for this special analysis case. After the span loads have been defined and a static analysis has been carried out, the first iteration estimates for the OPTS span spring stiffnesses and lumped masses are printed to the bottom of the corresponding output file (Fig. 3.11).

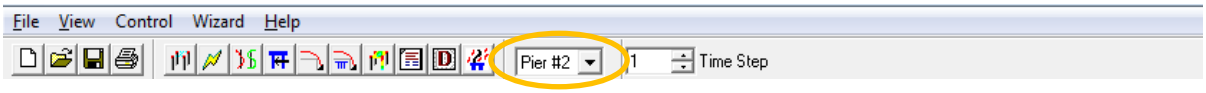

Figure 3.3 Selecting a pier in the toolbar

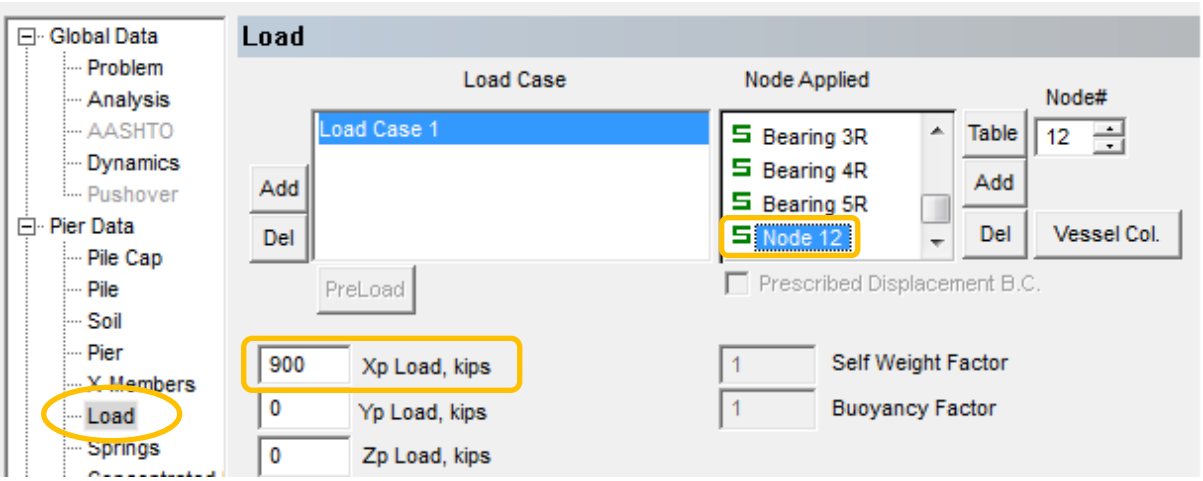

Figure 3.4 Defining the lateral load on Pier 2 on the Load page

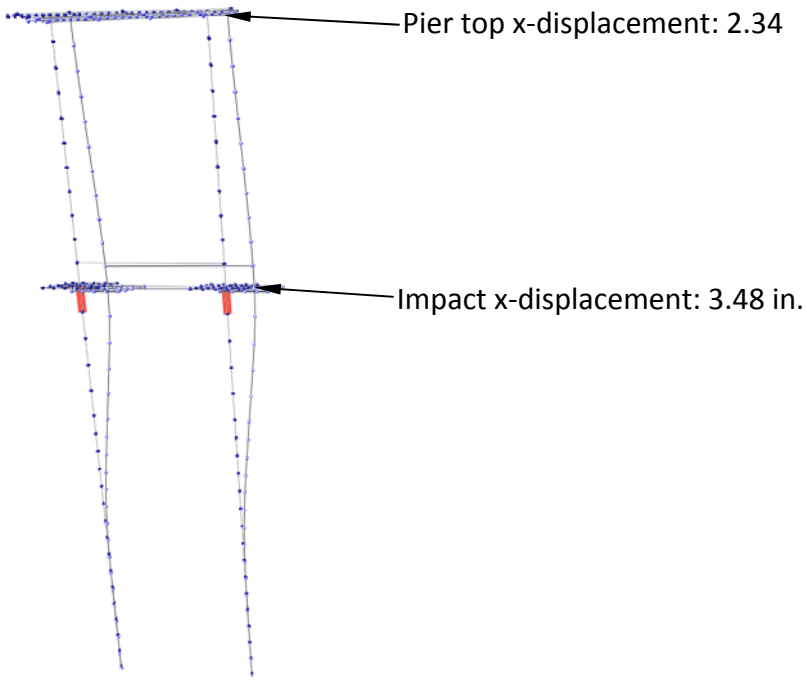

Figure 3.5 Deformed Pier 2

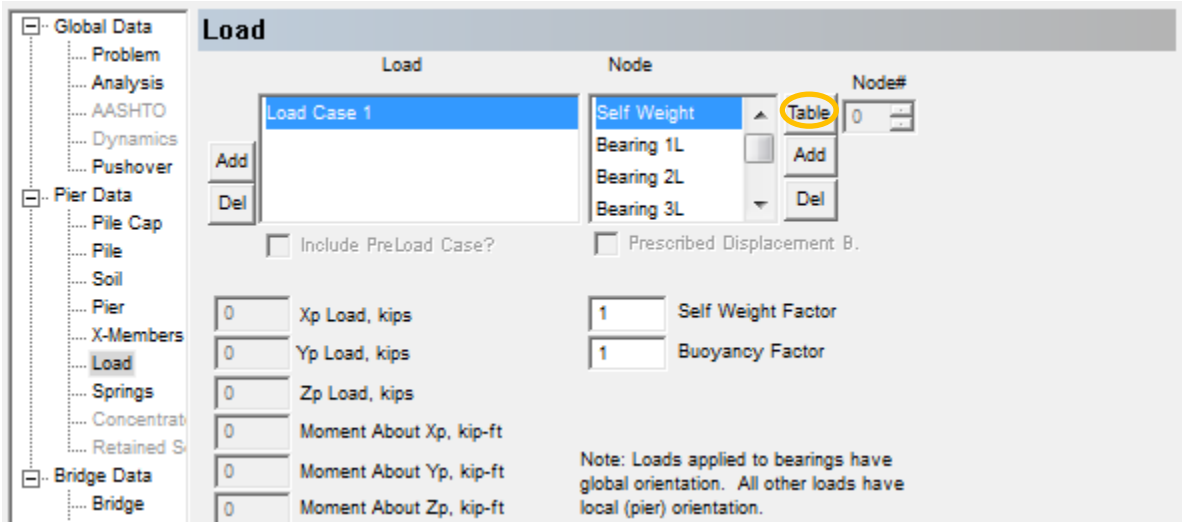

Figure 3.6 Access to OPTS Spring Formation dialog

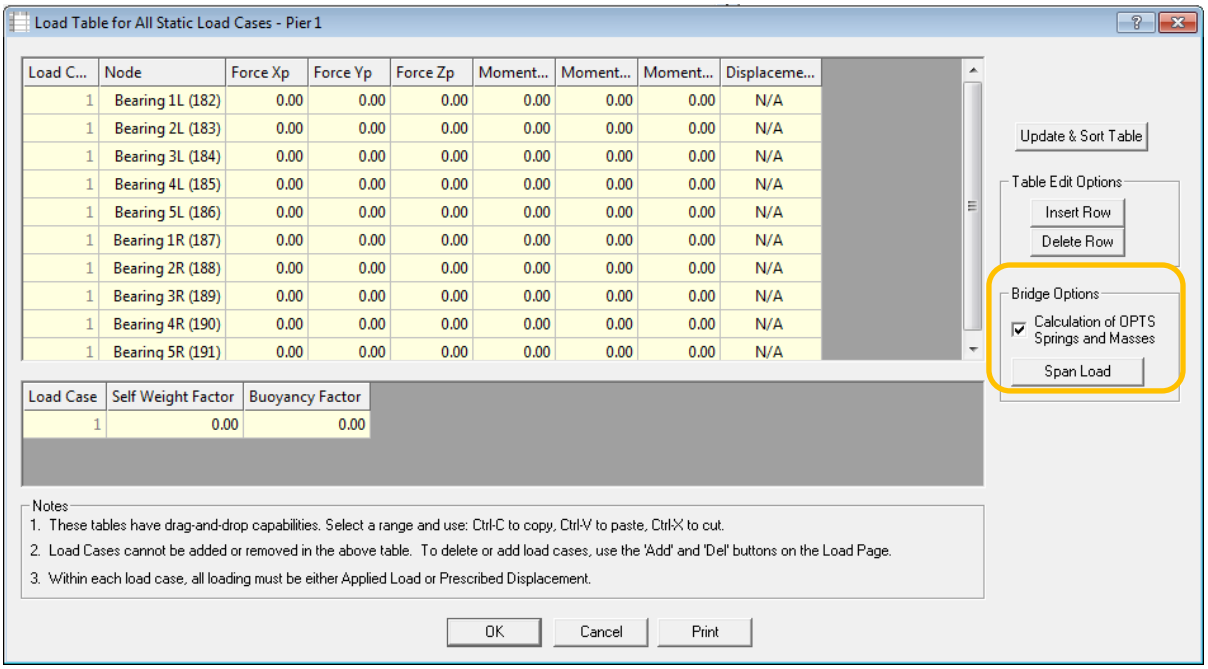

Figure 3.7 Selecting the OPTS Spring Formation option

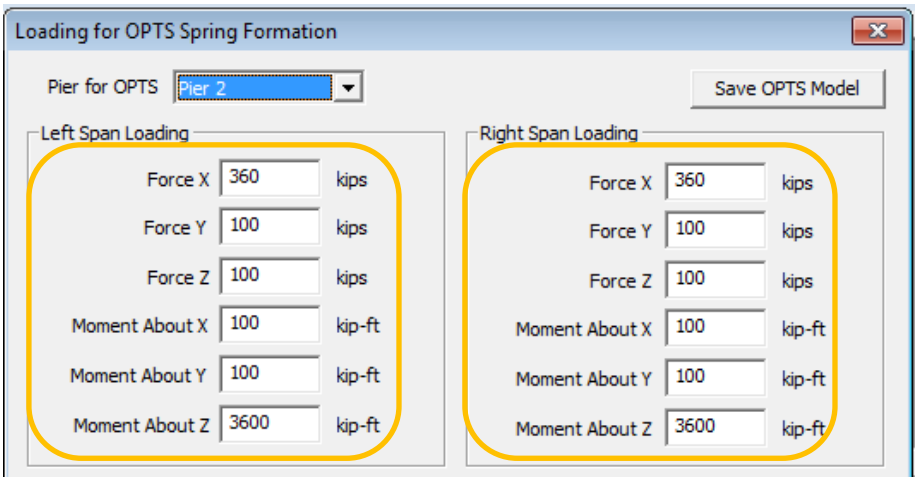

Figure 3.8 Iteration 1 stage 1 span loads

ITERATION 1: ASSESSMENT OF OPTS STATIC MODEL

The base OPTS static model can now be fitted with the iteration 1 OPTS span spring stiffnesses and lumped masses (Fig. 3.9), where the fitting process is facilitated by accessing the OPTS "Edit" button in the "Bridge" page (Fig. 3.10). The "OPTS data" dialog (Fig. 3.12) is then populated with the span springs and lumped masses determined in stage 1 (Fig. 3.11) by selecting the "Import Spring/Mass Data" button and locating the full-bridge span loading output file.

Once fitted with springs and lumped masses, the OPTS static model is used to assess the lateral load response of the static OPTS model, and compare the response to that of the full-bridge model. In particular, all dead loads and the lateral load of 900 kips are applied to the OPTS static model, and a static analysis is carried out (Fig. 3.13). Given the observed agreement in static response between the OPTS model and the full-bridge, the OPTS span spring stiffnesses are considered to have been converged upon. The OPTS model can then be subjected to modal analysis to determine the Rayleigh damping coefficients, and subsequently, used in a time-history (CVIA-OPTS) analysis to rapidly obtain the Pier 2 vessel collision response.

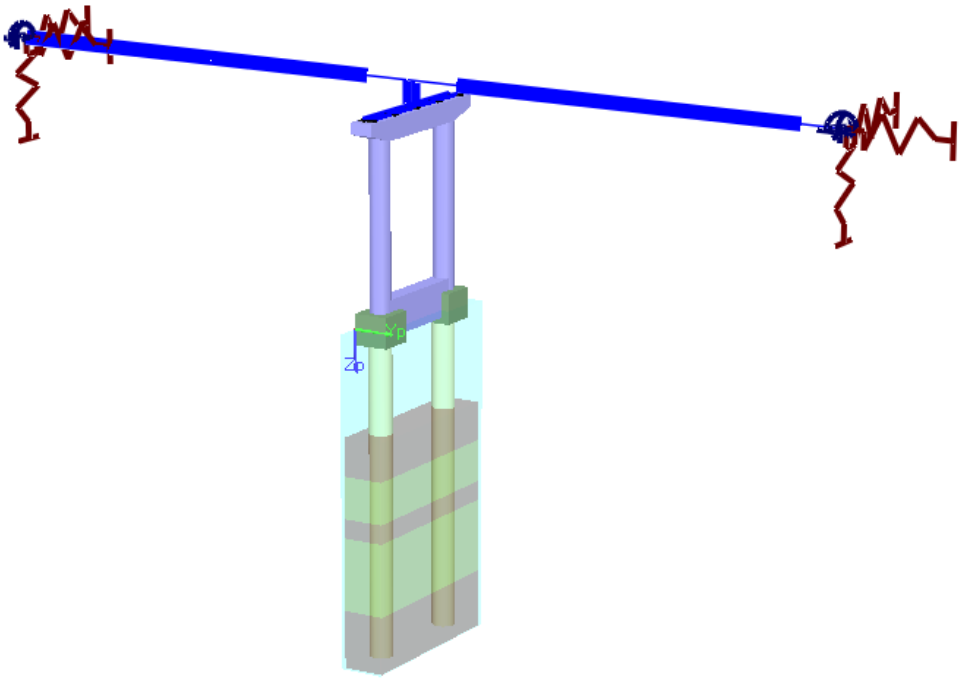

Figure 3.9 Superstructure springs and lumped masses in the Pier 2 OPTS model

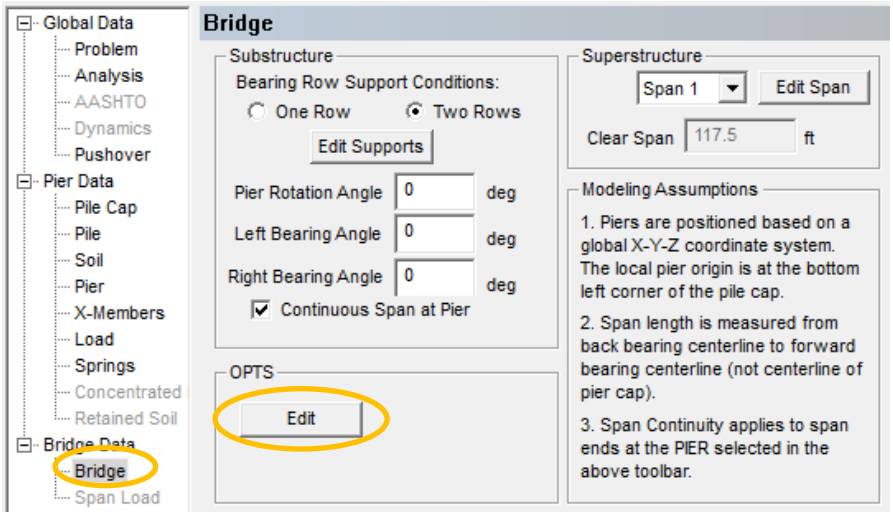

Figure 3.10 Editing of OPTS data from within the Bridge page

```
************************************************
*         OPTS SPAN-END SPRING STIFFNESSES      *
************************************************

Units are: kip/in for translational stiffnesses
           kip-ft/rad for rotational stiffnesses

_____________________________________________________
Span  1 spring stiffnesses:
X-Translation = 0.245142E+03
Y-Translation = 0.425491E+01
Z-Translation = 0.276339E+04
X-Rotation    = 0.252993E+05
Y-Rotation    = 0.804090E+07
Z-Rotation    = 0.163551E+06

_____________________________________________________
Span  2 spring stiffnesses:
X-Translation = 0.820205E+02
Y-Translation = 0.300163E+02
Z-Translation = 0.167303E+04
X-Rotation    = 0.640000E+06
Y-Rotation    = 0.157000E+07
Z-Rotation    = 0.131000E+08


************************************************
*               OPTS SPAN-END MASSES            *
************************************************

Units are: kip-sec^2/in

_____________________________________________________
Span  1 tip mass: 0.000000E+00

_____________________________________________________
Span  2 tip mass: 0.193373E+01
```

Figure 3.11 OPTS span-end spring stiffnesses and masses in output file

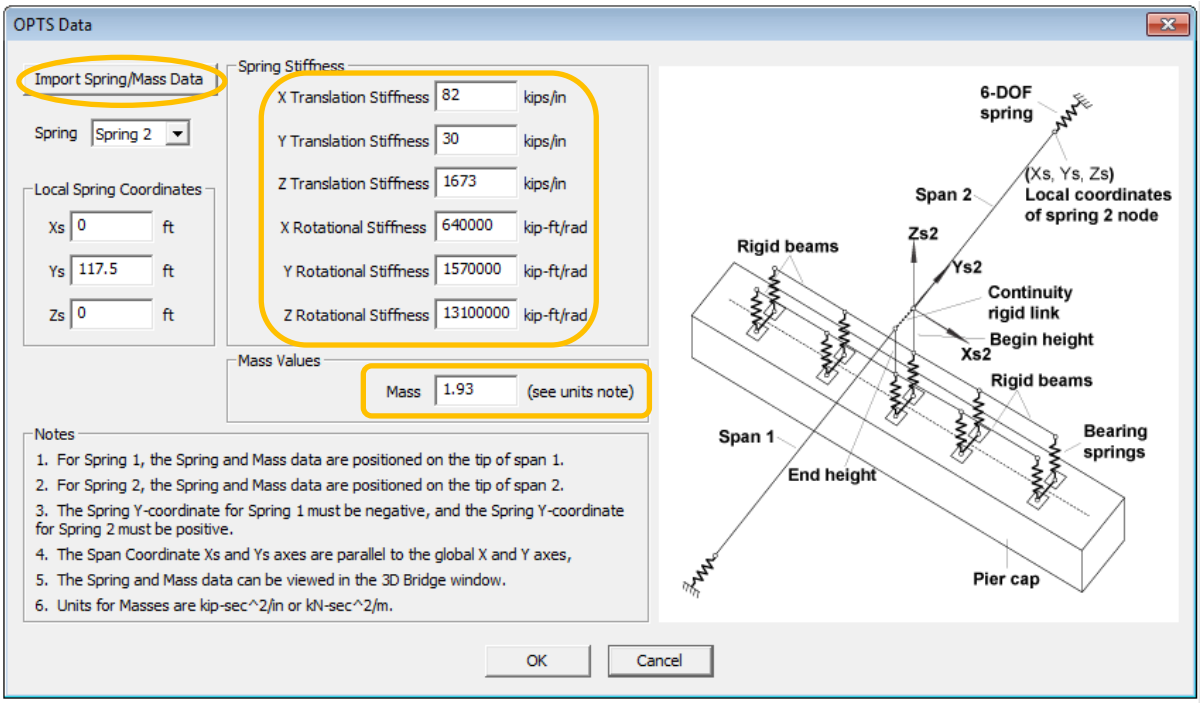

Figure 3.12 Iteration 1 OPTS spring stiffnesses and mass

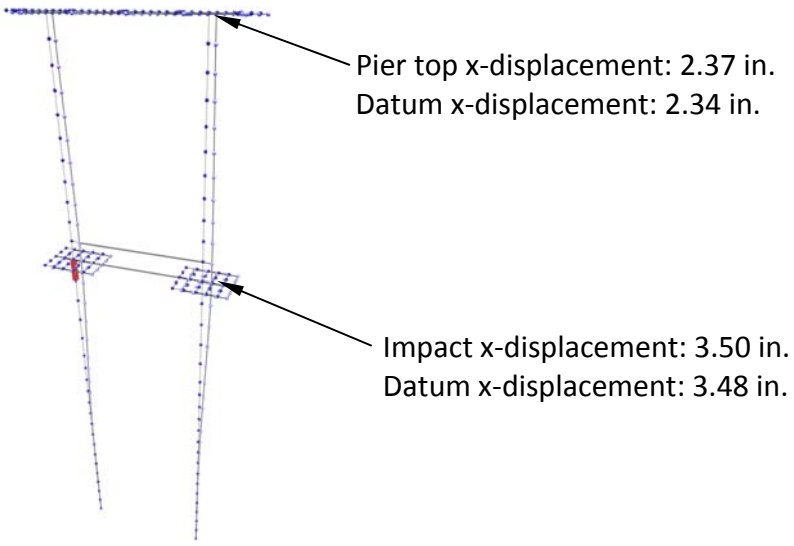

Figure 3.33 Comparison between iteration 1 OPTS response and datum of bridge response

4. DETERMINATION OF STRUCTURAL DEMANDS FROM DYNAMIC VESSEL COLLISION ANALYSIS

The efficacy found in employing the OPTS modeling approach is demonstrated by comparing select CVIA-OPTS time-histories of response to those obtained from the full-bridge CVIA results. As is shown below, excellent agreement is observed between the predictions of impact force (Fig. 4.1), and additionally the internal forces throughout Pier 2 (e.g., the internal moment at the top of the pier column, Fig. 4.2). Note that the OPTS model analysis requires less than 1 minute of wall-clock computation time on an ordinary desktop PC.

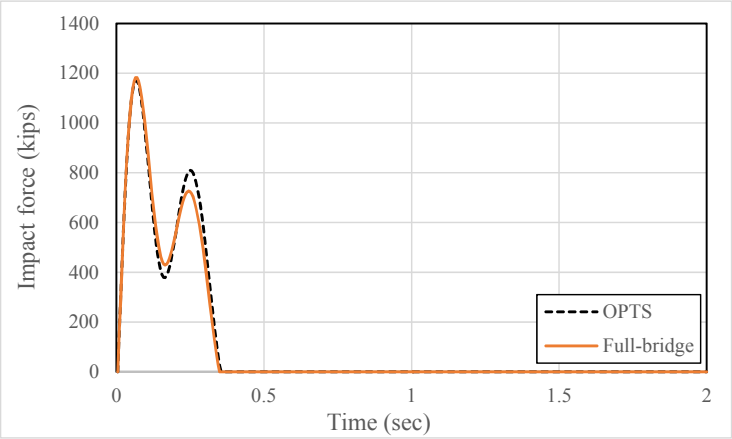

Figure 4.1 Time-histories of impact load

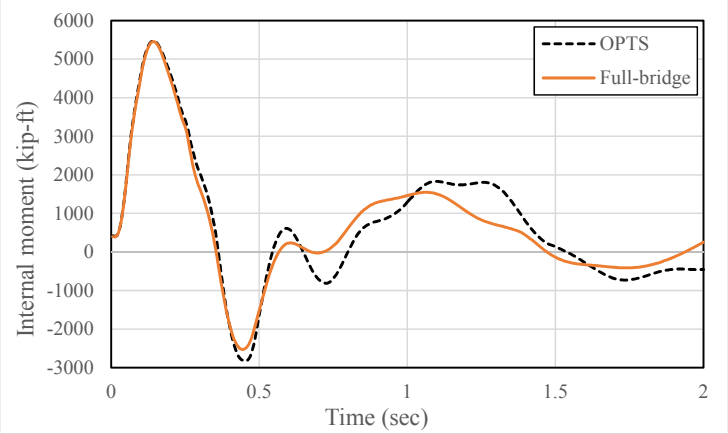

Figure 4.2 Time-histories of internal moment the top of the pier column (node 97) above the impacted node

DESIGN LOAD TABLES

Even though the OPTS model time-history analysis output is reduced (and obtained more rapidly) than the output data associated with the full-bridge model, the process of manually

identifying maximum structural demand can still require substantial effort. Such cumbersomeness arises because a complete set of soil, pier member, and span member data; nodal displacements; and internal forces are generated for each time step of the time-history analysis. For the Pier 2 CVIA, data output consists of 400 time steps, or 400 calculations of Pier 2, Span 1, and Span 2 demands. To help facilitate identification of maximum structural demands, the "Design Tables" feature in FBMP is employed. This feature distills down the results of an analysis such that the response maxima are listed concisely in a set of tables. By making use of the design tables feature, quantities such as maximum internal forces, and demand-capacity ratios can be quickly and automatically identified from among the time-step data. As examples, the process of identifying maximum internal forces in the pier columns of Pier 2 in the OPTS model is illustrated below.

MAXIMUM INTERNAL FORCES IN THE PIER COLUMNS

The "Design Table Generator" dialog is accessed by selecting the design tables icon in the program toolbar, as shown in Fig. 4.3. The main dialog (Fig. 4.4) is then used to generate summary data for a region of interest within the analyzed structure. For example, by selecting the "Max Forces for All Column Sections" table, a PDF, TXT, or Microsoft® Excel® report file is generated (Fig. 4.4), which contains the maximum pier column demands (Fig. 4.5). The corresponding PDF report is shown in Fig. 4.5, where the maximum demands are identified with ease.

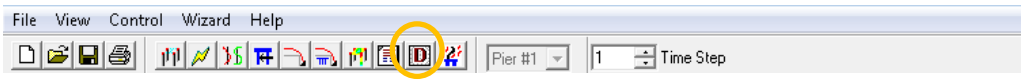

Figure 4.3 Accessing the design tables

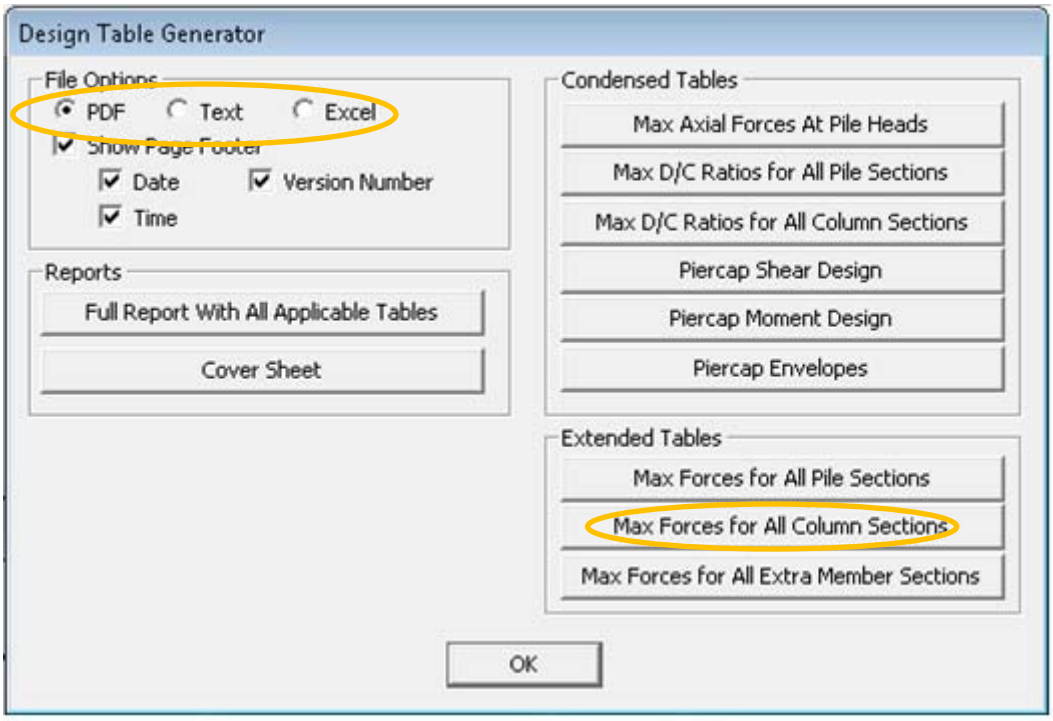

Figure 4.4 Design tables main dialog pertaining to maximum pier column demands

Maximum Forces for All Column Properties (Cross Sections)

Column Properties Data for Pier 1

PROP NO.	COLUMN NO.	ELEM NO.	NODE NO.	TIME STEP	I/J	MAX/MIN FORCE	FAX (Kips)	F22 (Kips)	F33 (Kips)	M22 (Kip-ft)	M33 (Kip-ft)	TORQUE (Kip-ft)	D/C (Ratio)
2	2	57	135	48	J	Max Axial	-214.09	-126.89	0.41	53.03	-3044.07	-94.77	0.60
2	1	9	86	26	I	Min Axial	-1780.08	-226.97	-2.72	-15.62	4129.71	-37.04	0.41
2	2	47	125	79	J	Max f22	-1354.99	177.58	-1.79	-7.68	-392.97	-12.67	0.09
2	1	9	87	13	J	Min f22	-1371.07	-398.13	-2.17	-22.30	1289.76	-5.65	0.13
2	2	47	125	121	J	Max f33	-1108.73	111.57	11.53	-69.83	516.59	246.24	0.08
2	1	9	87	120	J	Min f33	-1094.65	-28.40	-13.72	99.42	785.16	255.00	0.09
2	1	19	97	129	J	Max m22	-869.16	0.04	-5.33	212.13	-58.87	262.97	0.06
2	2	57	135	126	J	Min m22	-893.80	24.02	4.81	-210.34	703.26	267.95	0.08
2	1	10	87	28	I	Max m33	-1705.27	-188.54	-0.87	13.95	5394.24	-77.04	0.60
2	1	19	97	29	J	Min m33	-1547.54	-269.62	3.67	-47.00	-5470.53	-84.36	0.66
2	2	48	126	125	J	Max Torque	-1015.41	35.84	9.81	98.32	-325.67	269.60	0.07
2	1	10	88	187	J	Min Torque	-1078.44	-22.19	8.50	56.48	464.16	-236.23	0.08

Figure 4.5 Design tables report pertaining to maximum pier column demands

5. SUMMARY AND CONCLUSIONS

Bridges that span navigable waterways are subject to extreme event loading through vessel-bridge collision. In the event of a collision, dynamic lateral forces transmitted to the impacted bridge structure can result in the development of significant inertial forces that, in

turn, produce amplified structural demands. Collision events can, therefore, lead to severe structural damage and even catastrophic failure of the impacted bridge. In the current report, a user's guide is given for utilizing a simplified bridge modeling and numerically efficient nonlinear dynamic vessel collision analysis technique in FBMP.

The modeling and analysis procedures, as accessed from within the FBMP GUI, are showcased for a four-pier three-span demonstration case. Included in the user's guide are the steps necessary to carry out a nonlinear dynamic vessel collision analysis. Additionally, the guide details the procedure necessary to form a simplified bridge model using the multiple-pier, multiple-span bridge model, and to iteratively calculate input for spring stiffnesses and lumped masses located at the extents of the simplified bridge model. Further, dynamic input parameters necessary to account for phenomena such as damping, and characterization of the vessel collision scenario are discussed. Also, the GUI options available for entering the dynamic input are provided.

Importantly, maximum forces generated within pier members can be quickly determined by making use of the Design Table feature in FBMP, as delineated in this user's guide. Further, for the demonstration case considered in this report, it is shown that the OPTS model numerical results show good agreement with those results generated for a corresponding full-bridge analysis. As implemented in the bridge finite element analysis software FBMP, the tools constitute an easy-to-use analytical framework that facilitates rapid assessment of nonlinear dynamic vessel collision loading and bridge response. These numerical tools are put forth for use by bridge engineers in conducting accurate, efficient vessel collision analyses on bridges.

APPENDIX B
EXTENDED USER'S GUIDE FOR VESSEL COLLISION ANALYSIS AND DESIGN LOAD TABLES IN FB-MULTIPIER

Presented in the following pages is the body of an extended User's Guide that contains step-by-step instructions and contextual details that, collectively, facilitate utilization of the CVIA-OPTS features in FB-MultiPier. In addition, the step-by-step means by which design-relevant predictions of maximum structural demand can be easily extracted from the analysis results is given, specifically, through use of the Design Tables feature in FB-MultiPier. A condensed edition of the User's Guide is provided above in Appendix A.

Extended User's Guide for Vessel Collision Analysis and Design Load Tables in FB-MultiPier

Jae H. Chung, Michael Davidson, Clint Monari, Henry Bollmann, Anand Patil

Bridge Software Institute, College of Engineering, University of Florida, Gainesville FL, 32611

Contact: BSI@CE.UFL.EDU (352)392-9537 ext. 1514

1. INTRODUCTION

This document provides users with a step-by-step guide for making use of several new features that are actively being developed by the Bridge Software Institute (BSI) in the bridge finite element analysis (FEA) software FB-MultiPier (FBMP). These features are intended to facilitate designer friendly assessments of structural response for bridge piers that are subject to waterway vessel collision loading. A simplified bridge modeling procedure and a numerically-efficient dynamic vessel-collision analysis technique are the focus of this guide. Further, key analysis results are made available in a user-friendly, robust output format by making use of the Design Load Table feature in FBMP.

Dynamic (time-history) analysis of bridge structural models at any appreciable level of fidelity correlates positively with high computational cost. This correlation holds true not only with respect to hardware requirements (i.e., to maintain speed of computation), but also, with respect to the generation of cumbersomely large response datasets. Excessively large datasets, in turn, bring forth the need for extensive post-processing efforts, as pertinent response quantities are sought out (e.g., maximum through-time pier column shears). In response to this need, new numerical models are being developed in FBMP to make use of efficient response calculations. These tools are also capable of predicting impacted bridge response within reasonable margins of error. So as to contextualize the demonstration case referenced throughout this user's guide, modeling and analysis techniques that (collectively) comprise a numerically-efficient dynamic vessel-collision analysis feature are described in Sections 1.1 and 1.2, respectively. The specific areas of focus in the user's guide are subsequently established in Section 1.3.

SIMPLIFIED BRIDGE MODELING

When vessel-bridge collisions occur, stiffness and mass dependent superstructure restraint can result in significant portions of the impact load being transferred from the impacted pier to the superstructure. Hence, additional insight into impacted bridge response can be gained by

accounting for the influence of adjacent non-impacted piers and spans for vessel-bridge collision analyses. However, conducting and post-processing dynamic analyses for multiple-pier, multiple-span bridge models can rapidly become infeasible to practicing bridge engineers. Alternatively, bridge piers of interest can be analyzed in a numerically efficient manner using an equivalent one-pier two-span (OPTS) bridge model.

The OPTS model simplification procedure involves reducing a multiple-pier, multiple-span bridge model (Fig. 1.1) to an equivalent pier model with concentrated stiffnesses and masses connected at the distant ends of each of two retained spans (Fig. 1.2). The concentrated stiffnesses are formed using stiffness condensation (e.g., flexibility matrix inversion) for each of the left and right portions of the full bridge model, which are excluded from the OPTS model. The lumped masses are formed by simply lumping each of the half-span masses. A further simplification is made by negating off-diagonal stiffness terms at each condensed stiffness location, resulting in a set of independent springs and lumped masses at each end of the OPTS model (as denoted in Fig. 1.2). This simplified modeling technique has been verified to accurately predict pier structural responses relative to corresponding full-bridge structural response predictions (Consolazio et al., 2008).

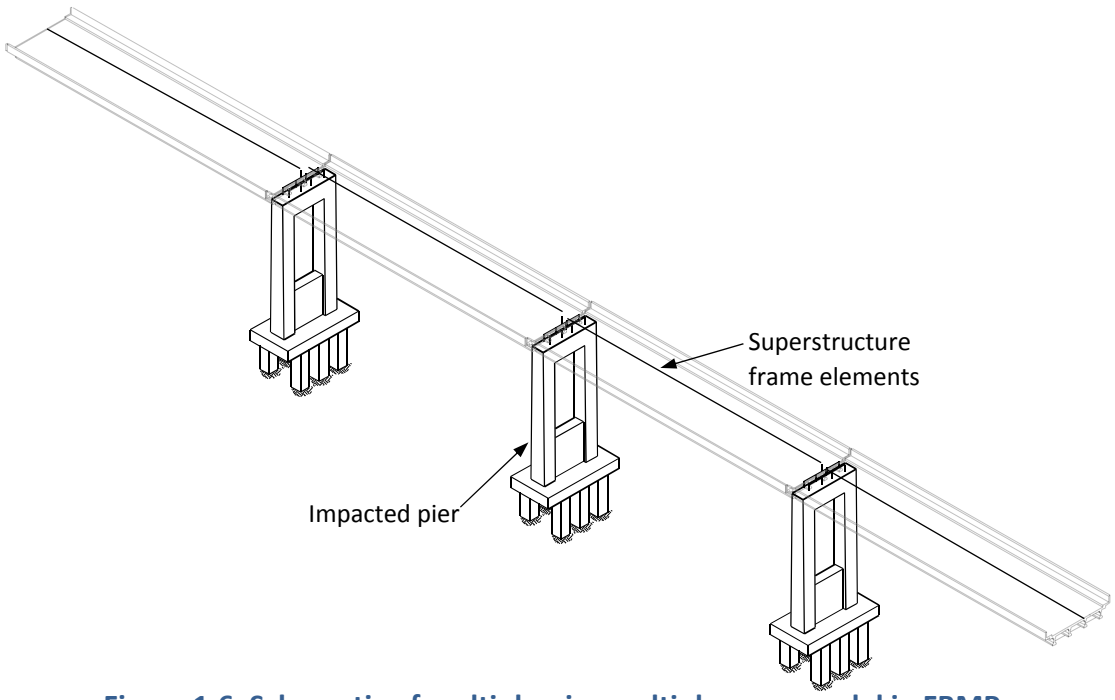

Figure 1.6. Schematic of multiple-pier multiple-span model in FBMP

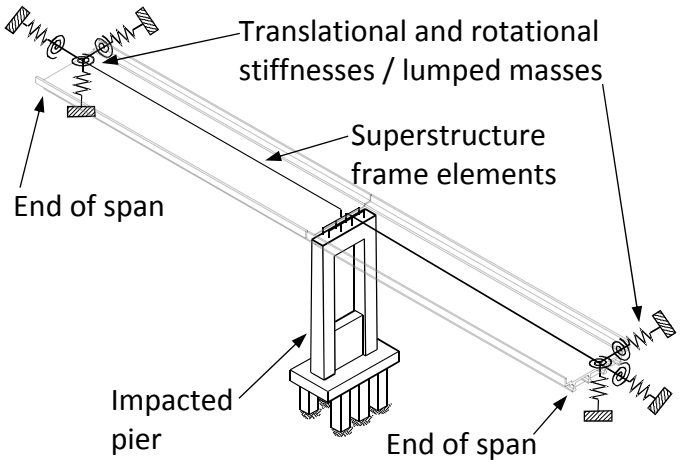

Figure 1.7. Schematic of OPTS model in FBMP

NUMERICALLY EFFICIENT NONLINEAR DYNAMIC VESSEL COLLISION ANALYSIS

Several numerical studies have been carried out to characterize force-deformation relationships for commonly piloted waterway vessels (e.g., Yuan et al., 2008; Consolazio et al., 2009). Vessel characterizations made in the numerical studies greatly facilitate the modeling of barges as single-degree-of-freedom (SDF) systems, where impact-load characteristics can account for vessel size, structural configuration, relative orientation, and the shape (i.e., the geometry) of the impacted surface (e.g., pile cap, pier column). This approach has been elected for use in the analytical framework being implemented in FBMP (BSI 2014), which significantly adds to the efficiency of dynamic barge-bridge collision analysis. Specifically, coupled vessel impact analysis (CVIA), developed previously (Consolazio and Cowan, 2005), is being implemented for designer-friendly use. In CVIA, a shared contact force, P_B, is used to computationally link a SDF vessel model—with stiffness, mass, and initial velocity—to a multiple-degree-of-freedom (MDF) bridge model (Fig. 1.3).

Upon impact, a time-varying impact force is computed, and the MDF bridge model is displaced in response. In turn, internal forces are developed throughout the bridge model. A significant advantage of employing CVIA is that the algorithm does not require *a priori* knowledge of the barge impact load-history. Also, the CVIA technique has been validated using data from selected full-scale experimental impact tests on bridge structures (Consolazio and Davidson, 2008).

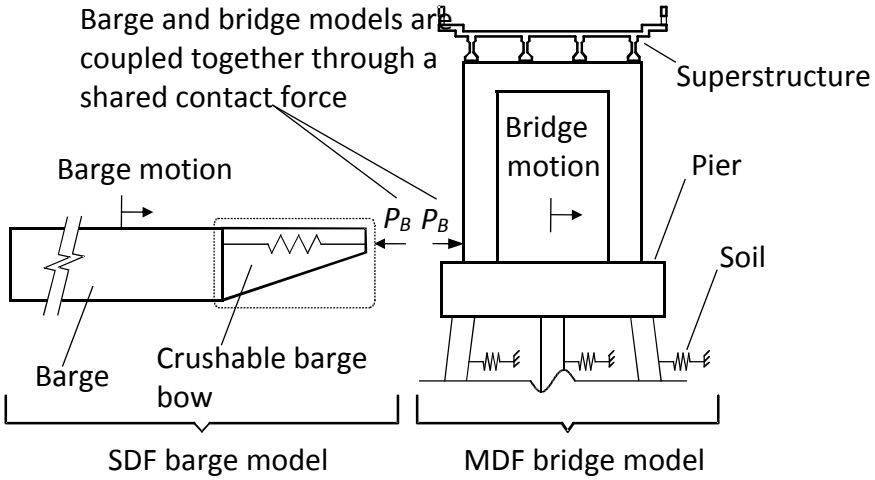

Figure 1.8. Coupling between barge and bridge in CVIA (after Consolazio and Cowan, 2005)

SCOPE OF USER'S GUIDE

The modeling and analysis techniques introduced above, as being implemented in FBMP, give bridge engineers a powerful, rapid means of carrying out nonlinear dynamic vessel collision analyses on bridge structures. The remainder of this guide is dedicated to providing step-by-step instructions for creating an OPTS model within the graphical user interface (GUI) of FBMP. Further, the OPTS model is utilized in conjunction with CVIA (via the FBMP GUI) to quickly and efficiently compute collision-induced structural demands.

More specifically, a full-bridge static analysis model is introduced and the structural configuration is briefly described. A single pier of interest, within the context of vessel collision analysis, is then identified among the piers comprising the static full-bridge model. Having identified a pier of interest, and drawing upon a reasonable set of waterway traffic characteristics, a design vessel and impact scenario are decided upon. The pier and span portions of a static OPTS model are then extracted from the full-bridge static model.

Subsequently, an iterative procedure aimed at accounting for those bridge portions located beyond the extents of the OPTS model is delineated, where span-end springs and lumped masses are used to represent the influence of the extraneous bridge structure. Upon formation of a static OPTS model that gives static responses which show good agreement with the full-

bridge static model, the process of building a dynamic OPTS model is undertaken. The dynamic model creation includes determination of Rayleigh damping coefficients and input of vessel collision characteristics. A CVIA-OPTS analysis is then carried out, and the means by which maximum response quantities can be identified is given. Finally, results obtained from utilizing CVIA-OPTS are shown to compare well with those results predicted by conducting nonlinear dynamic vessel collision analysis (i.e., CVIA) using the full-bridge model.

2. BRIDGE MODEL

This user's guide for carrying out rapid nonlinear dynamic vessel collision analysis (using CVIA-OPTS) is facilitated through examination of a bridge demonstration case. The bridge is intended to be representative of a viable physical structure, but it is not intended to represent an extant structure. In Chapter 2, the bridge demonstration case is introduced where emphases are placed on the structural configuration (Sec. 2.1). Additionally, a pier of interest is identified in Sec. 2.2 and the associated structural configuration is summarily provided. Finally, in Sec. 2.3, a vessel collision scenario is defined, and calculations are made to make a preliminary estimate of the impact load magnitudes which will be associated with the defined scenario.

STRUCTURAL CONFIGURATION

The bridge shown in Fig. 2.1 constitutes the demonstration case for this user's guide, and is intended to represent a high level approach structure leading up to the main span on a causeway-type bridge. Throughout this user's guide, the configuration shown in Fig. 2.1 is referred to as the "full-bridge model", and individual piers are referred to in order (from left to right in Fig. 2.1) as Pier 1 to Pier 4. Portions of the bridge not explicitly modeled are represented by discrete springs, as well as vertical loads (dead loads) placed along the pier caps of Pier 1 and Pier 4. Each span included in the full-bridge model is 120 ft in length. Also, each span is modeled consist with a span assembly of four constant-depth 72 in. bulb-T girders, which in turn support a cast-in-place reinforced concrete deck.

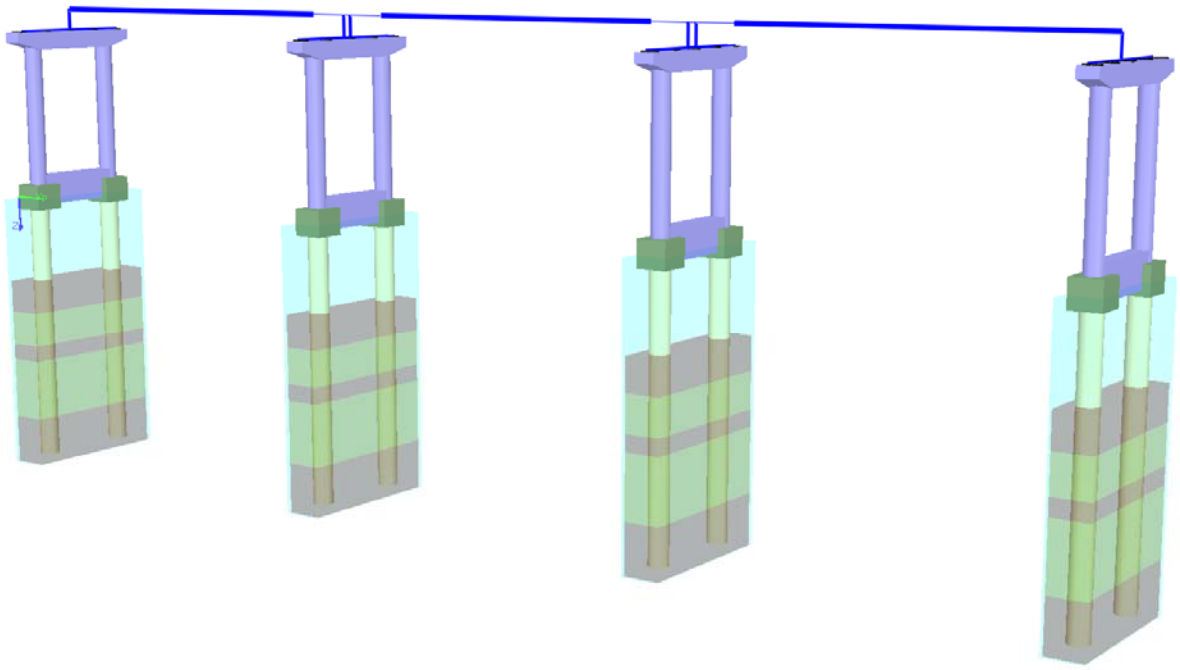

Figure 2.1. Four-pier three-span bridge model used for demonstration

For this scenario, the bridge is modeled after a configuration where the span is continuous although the underlying girder-ends may expand from pier to pier, for Pier 1 through Pier 3. To account for the continuous deck with non-continuous girders assembly, the moments of inertia of horizontal span elements are reduced for those elements located within the immediate vicinity of Pier 1 through Pier 3. Further, custom bearing force-deformation relationships and constraints are supplied in the model to facilitate uniform distributions of bearing reactions under lateral loading.

PIER OF INTEREST SELECTION

Pier 2 from the full-bridge model is selected for creation of an OPTS model (Fig. 2.2), and subsequent use of the OPTS model in performing nonlinear dynamic vessel collision analysis (CVIA). Pier 2 is comprised of a 70 in. wide by 66 in. deep, tapered reinforced concrete pier cap beam, which is supported by two 66 in. diameter round reinforced concrete pier columns. The pier columns are concentric with two 72 in. diameter drilled shaft foundation members, where a shear wall exceeding 10 ft acts to structurally tie the two pier columns and two drilled shafts. A substantial depth of water is present at the Pier 2 location, allowing for 26.5 ft of draft to waterway vessels.

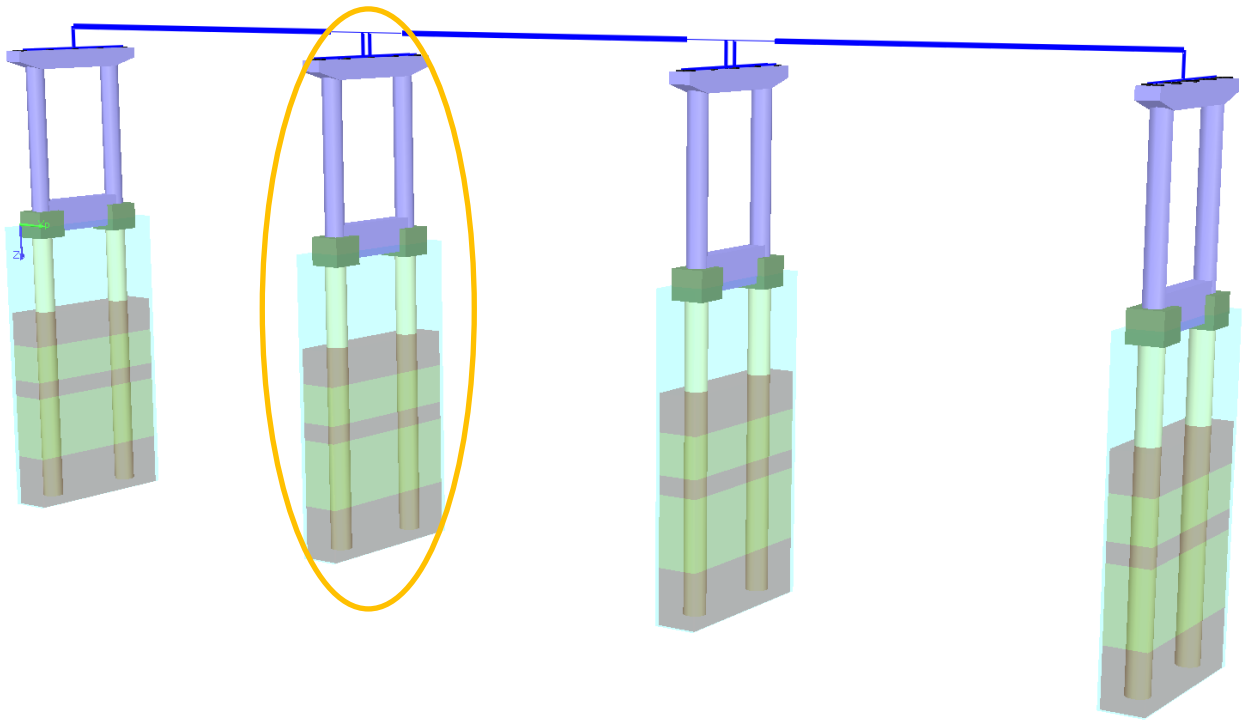

Figure 2.2. Selection of Pier 2 as the impacted pier

PRELIMINARY ESTIMATE OF IMPACT LOADING

Prior to forming an OPTS model and conducting a nonlinear dynamic vessel collision (CVIA) analysis, it is important to ascertain at least a preliminary characterization of the vessel impact load. As will be shown later in this user's guide, the preliminary load determination is instrumental in forming the span-end springs for the OPTS model. For the demonstration case considered herein, the waterway traffic is assumed to correspond to an empty oversize Tank barge (630 tonnes) acting as the design vessel. Given that Pier 2 (i.e., the pier of interest) is located outside of the channel, but well within the channel centerline offset associated with a drifting, empty barge, the design vessel initial impact velocity is taken as 2 knots (3.3 ft/sec). Making use of the empirical load determination equations given in the AASHTO specification pertaining to design for waterway vessel collision (AASHTO 2009), the impact weight and initial impact velocity can be used to make a preliminary estimate of the magnitude of impact loading that will be generated as part of subsequent vessel collision analyses. Note that other empirical approaches are also available for making this initial estimate (Consolazio et al., 2008).

Following the AASHTO provisions, the kinetic energy of the empty oversize Tank barge can be calculated as:

$$KE = \frac{C_H W V^2}{29.2} \tag{1}$$

where KE is the kinetic energy of the impacting vessel (kip-ft); C_H is the hydrodynamic mass coefficient (taken as unity for this scenario); W is the impacting vessel weight (tonnes); and V is the design speed of the vessel (ft/sec). The kinetic energy (KE) can then be empirically related to a barge bow crush deformation:

$$a_B = \left[\left(1 + \frac{KE}{5672}\right)^{1/2} - 1\right]\frac{10.2}{R_B} \tag{2}$$

where a_B is the barge bow crush deformation (ft); and R_B is a width correction factor (taken as unity for this scenario). Finally, a preliminary estimate of the general magnitude of impact load for this case can be calculated as:

$$P_B = \begin{cases} 4112 a_B R_B & \text{if } a_B < 0.34 \\ (1349 + 110 a_B) R_B & \text{if } a_B \geq 0.34 \end{cases} \tag{1}$$

where P_B is a static barge impact load (kips). Making use of the above equations given the vessel collision scenario described above, a preliminary estimate of a static impact load can be taken as approximately 900 kips.

3. FORMATION OF OPTS MODEL

Having selected a pier of interest, and having calculated an estimate for the magnitude of impact loading, the additional input parameters necessary to form the OPTS model can be calculated. Discussed in Sec 3.1 is the means by which the static OPTS model are formed. In particular, navigation (via the FBMP GUI) is given for extracting the OPTS pier, soil, and span portions from the full-bridge model. An iterative procedure for calculating the OPTS model span-end spring stiffnesses and lumped masses is then detailed in Sec. 3.2, where the full-bridge static model, the static estimate of impact loading, and the OPTS static model are employed in the iterations. Finally, in Sec. 3.3, the necessary steps and guidelines for selecting dynamic input parameters are given to enable creation of an OPTS model.

INITIAL FORMATION OF OPTS STATIC MODEL

The pier, soil, and span of the OPTS model are readily formed (extracted) from the full-bridge static model into a separate file from within the FBMP GUI. This process is initiated by opening the full-bridge static model (Fig. 3.1). After opening the file, the “One Pier, Two Span” problem type is selected from within the “Problem” page (Fig. 3.2). Upon selecting the “One Pier, Two Span” problem type, an “OPTS conversion” dialog appears (Fig. 3.3), where Pier 2 is selected as the pier of interest. Upon clicking “OK”, the corresponding OPTS model automatically opens in FBMP (Fig. 3.4). The soil, pier, and span portions of the OPTS model can now be saved as a separate input file.

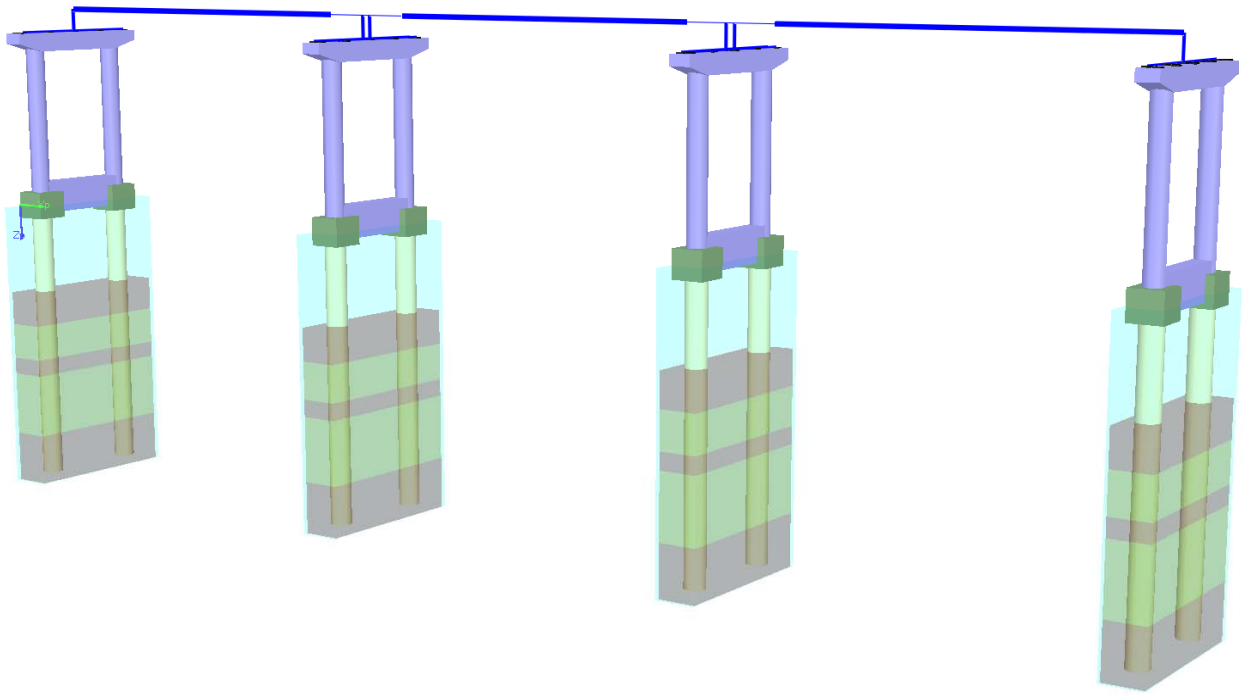

Figure 3.1 Four-pier three-span bridge model

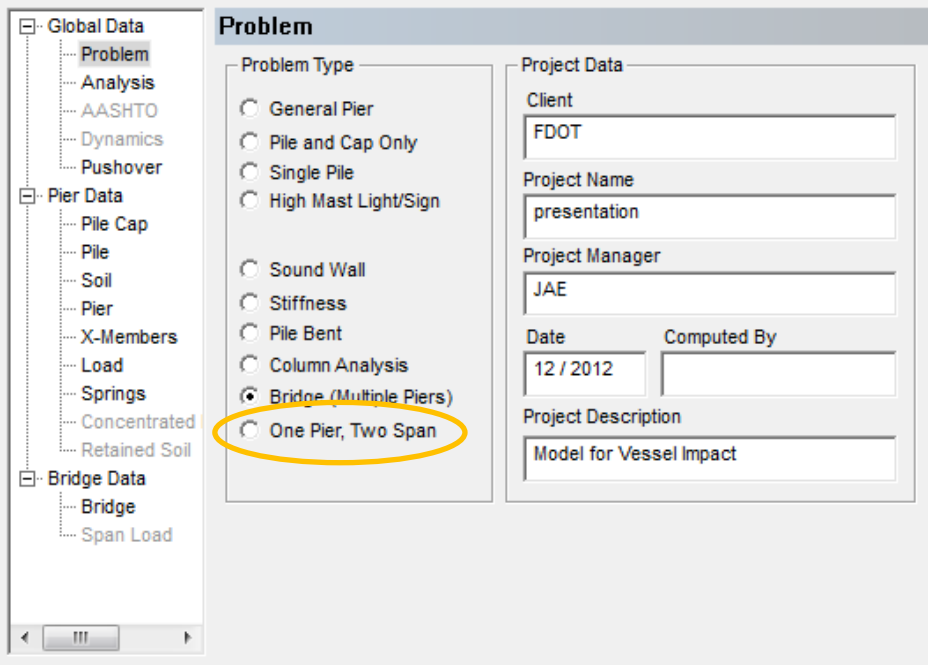

Figure 3.2 Selection of One Pier, Two Span (OPTS) Problem Type

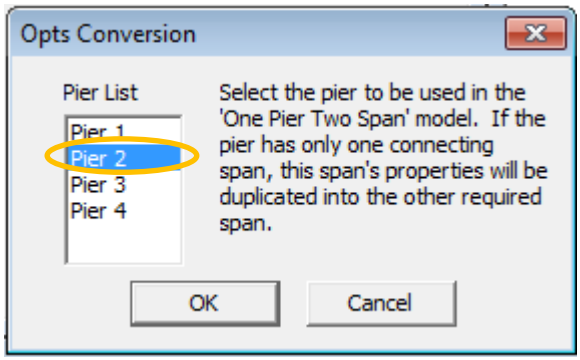

Figure 3.3 Selection of Pier 2 for OPTS Conversion

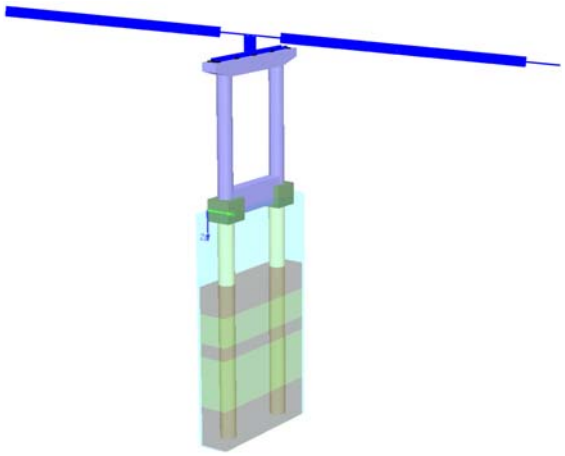

Figure 3.4 Initial formation of OPTS static model from Pier 2 of full-bridge model

FORMATION OF OPTS SPRINGS

As detailed in this section, the full-bridge model, the static estimate of impact load, and the OPTS static model are used in a chain of FBMP static analyses to iteratively calculate the OPTS model span-end stiffnesses and lumped masses. This iterative process requires as a pre-requisite that a datum of full-bridge model static response be established. Namely, the datum is established by subjecting the full-bridge model to static lateral loading (i.e., the static estimate of barge impact force), and the pier response is recorded.

Subsequently, iterations are carried out in two stages. First, estimates of the OPTS spring stiffnesses and lumped masses are calculated. Specific to the stiffness formulation, a static condensation procedure is carried out for the two locations in the full-bridge model which correspond exactly to the span-end extents of the OPTS model (Fig. 3.5a). Alternatively stated, individual static analysis load cases are defined for each degree-of-freedom (DOF) at the first horizontal span element node of Span 1, and separately, the last horizontal span element node of Span 2. For each load case, a force is applied at a given DOF, a static analysis is carried out, and the corresponding displacements at the directly loaded nodes are cataloged.

The set of six forces at each of the Span 1 start and Span 2 end nodes, and the corresponding catalog of displacements are then assembled to form two separate flexibility matrices. These matrices are inverted to form condensed stiffness matrices for each of the Span 1 and Span 2 end-nodes in the full-bridge model, which correspond exactly to the extents of the OPTS model. The diagonal terms of the condensed stiffness matrices are then supplied to the OPTS model as a collection of springs.

Lumped span mass values are also calculated at this time (Fig. 3.5b). The OPTS modeling condensed stiffness and lumped mass formation procedure is discussed in further detail in the literature (e.g., Consolazio et al., 2008).

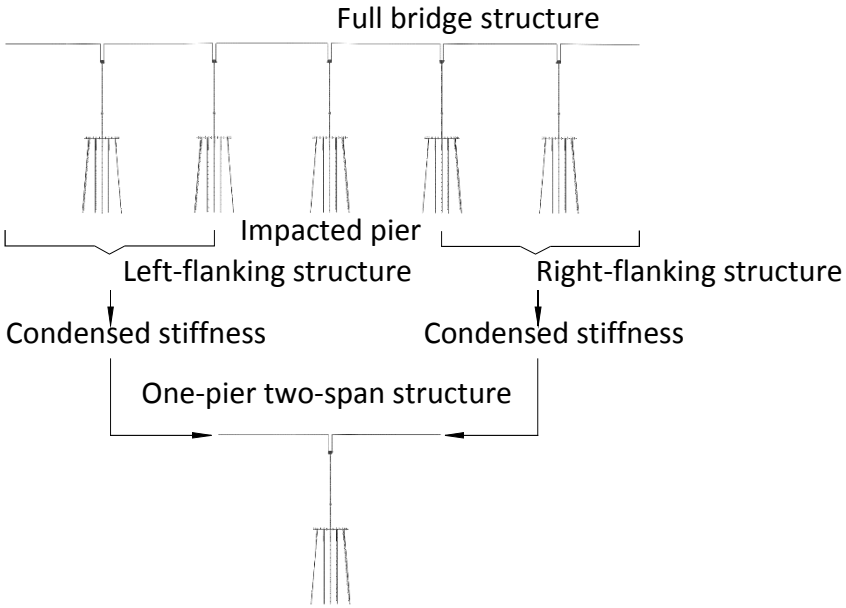

(a)

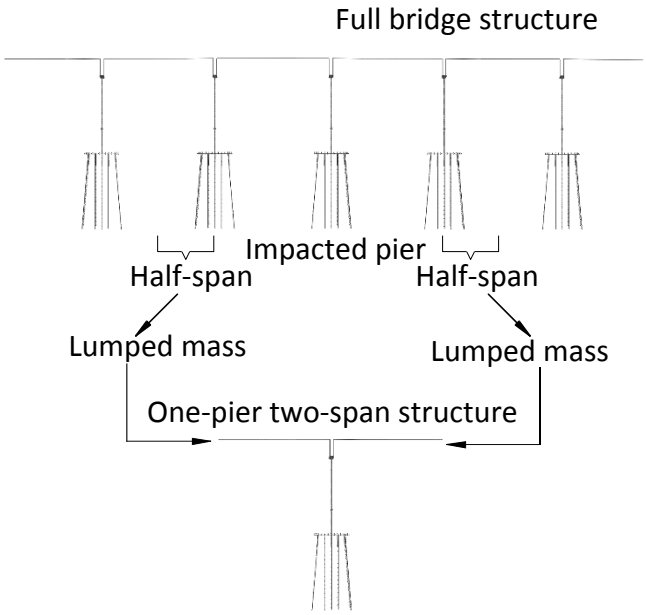

(b)

Figure 3.5 Schematics of OPTS spring and mass formation

The second stage of each iteration is enacted by fitting the OPTS static model with the current iteration span-springs and lumped masses, and then subjecting the OPTS model to the same static lateral loading as that employed previously in establishing the datum of response. If the OPTS model lateral-load response shows good agreement with the full-bridge model response, then the iterative procedure is considered to be complete. Otherwise, the next iteration is undertaken, and the full-bridge model static span loads supplied during the first stage of the previous iteration are modified to make better estimates in forming the OPTS springs. Below, each stage of the iteration process is illustrated.

DATUM ESTABLISHMENT FOR OPTS MODEL RESPONSE

To establish a datum of pier response for the pier of interest, the full bridge static model is opened (Fig. 3.6). A static lateral load of 900 kips is then applied at the MHW elevation (i.e., node 12) to Pier 2 of the full-bridge model. To accomplish this, first select Pier 2 using the Pier pull-down in the toolbar (Fig. 3.7). Then on the “Load” page, select node 12 in the “Node

Applied" list box, and input 900 in the "Xp Load, kips" edit box (Fig. 3.8). This loading is shown in Fig. 3.9 (see Sec. 4.1 for discussion pertaining to selection of the impact location). A static analysis is carried out in FBMP by clicking the "Analysis" button on the toolbar (Fig. 3.10). The Pier 2 response is cataloged, as shown in Fig. 3.11. Of particular interest during the OPTS spring iteration procedure are the displacements at the laterally loaded node (i.e., the impact location), and the top of the pier, which is taken as the top of the pier column (i.e., node 97). The displacements predicted to occur at these two locations are used in the subsequent (iterative) OPTS spring formation procedure, where the two displacements constitute a datum of response for the pier included in the static OPTS model.

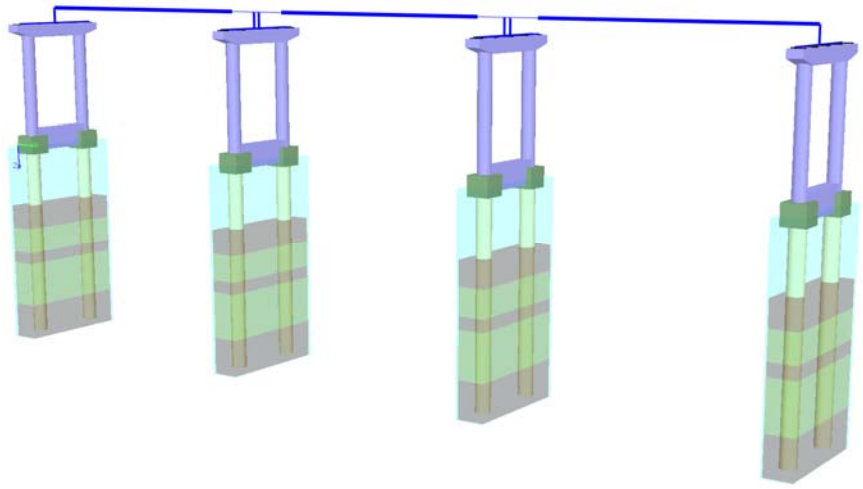

Figure 3.6 Four-pier three-span bridge model

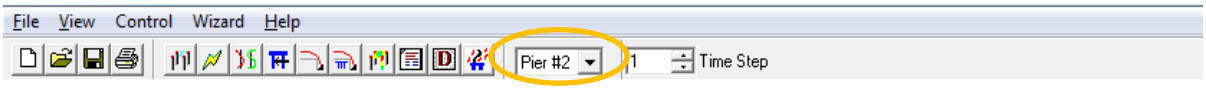

Figure 3.7 Selecting a pier in the toolbar

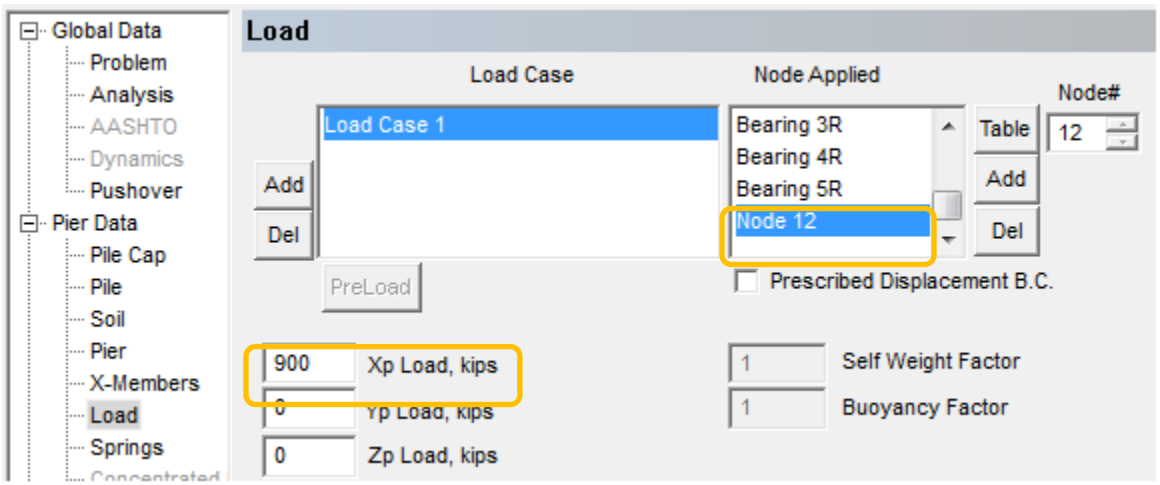

Figure 3.8 Defining load for Pier 2 at node 12 on Load page

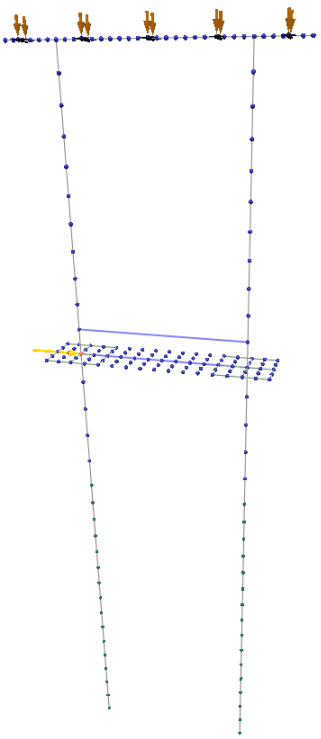

Figure 3.9 Static lateral load of 900 kips applied to Pier 2 of full-bridge model

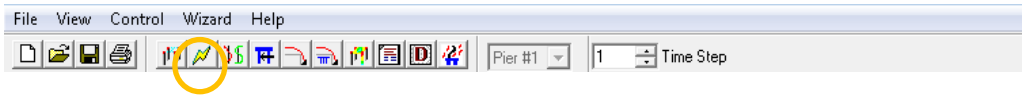

Figure 3.10 Analysis toolbar button

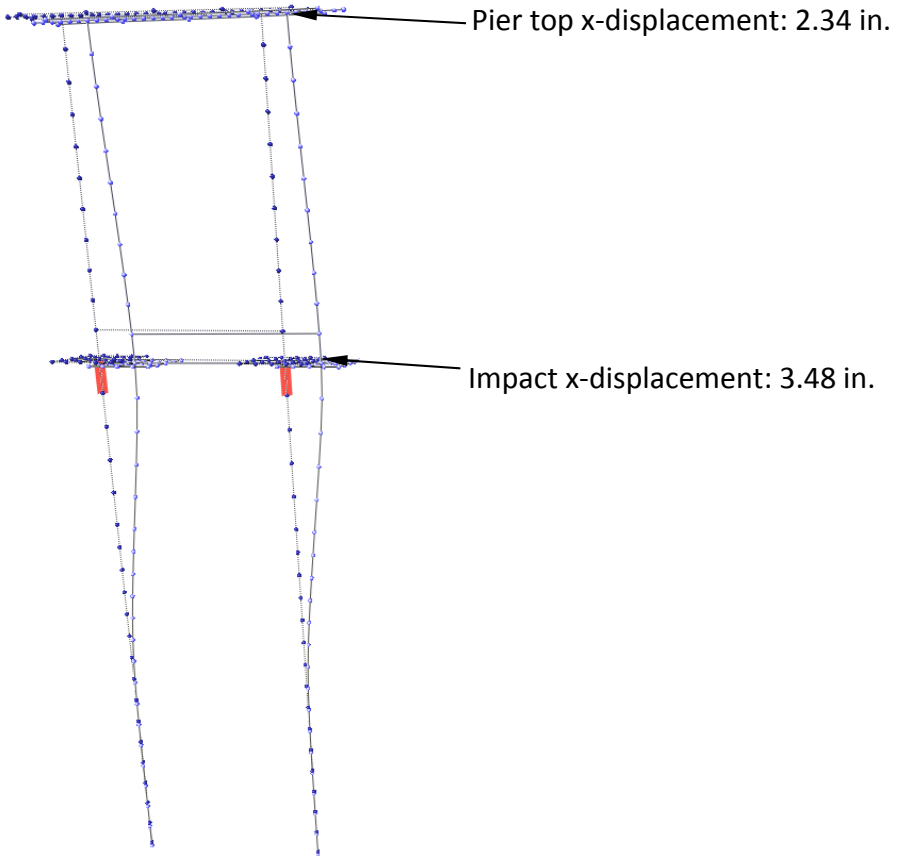

Figure 3.11 Deformed Pier 2

ITERATION 1: LOADING OF SPAN-END LOCATIONS IN THE FULL-BRIDGE MODEL

The first iteration of determining the OPTS span spring stiffnesses is initiated by opening the static full-bridge model in FBMP (Fig. 3.12). This model is used to apply static loads at each span far-end node DOF, for the spans directly attached to Pier 2 (i.e., the left end node of Span 1, and the right end node of Span 2). This process is facilitated by accessing the "Table" dialog in the "Load" page (Fig. 3.13). After the "Table" dialog appears, the "Calculation of OPTS Springs and Masses" check box is selected (Fig. 3.14), which will generate a selection confirmation

screen (Fig. 3.15). After confirming the selection, a “Loading for OPTS Spring Formation” dialog appears (Fig. 3.16). Here, the loads applied at the individual DOFs are supplied to the span locations in the full-bridge model. Note that the influence of the pier of interest (Pier 2) and the directly attached spans (span 1 and span 2) are removed from the model for this special analysis case.

As a first estimate for supplying the first iteration of static span-end loads, it is assumed that approximately one-third of the impact load will be absorbed at each span end. Therefore, given the 900 kip static estimate of impact load magnitude, 300 kips are supplied to the x-translation (i.e., “Force X”) load input boxes (Fig. 3.16). As another first estimate, a moment value equal to approximately 10 times the “Force X” load magnitude is supplied to the z-rotation (i.e., “Moment about Z”) load input boxes. The remaining load locations are filled with values of 100 kips and 100 kip-ft (corresponding to translational and rotational DOFs, respectively). It has been found that OPTS model response to vessel collision loading is relatively less sensitive to these latter DOFs (Consolazio et al., 2008), and therefore, the focus of the iteration process is primarily placed on determining spring stiffnesses in the x-translation and z-rotation DOF.

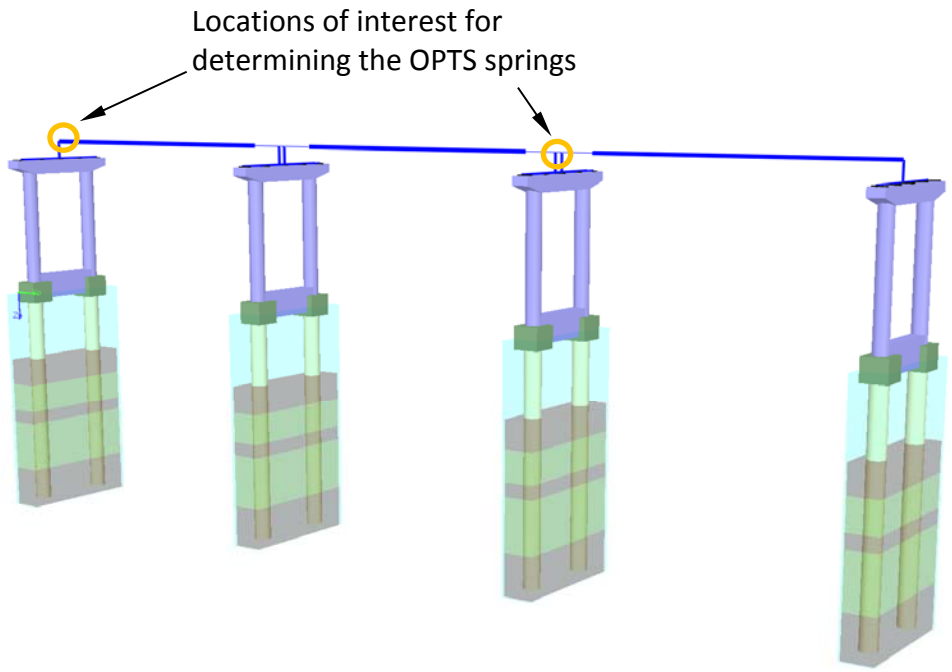

Figure 3.12 Locations of interest for forming condensed superstructure stiffness

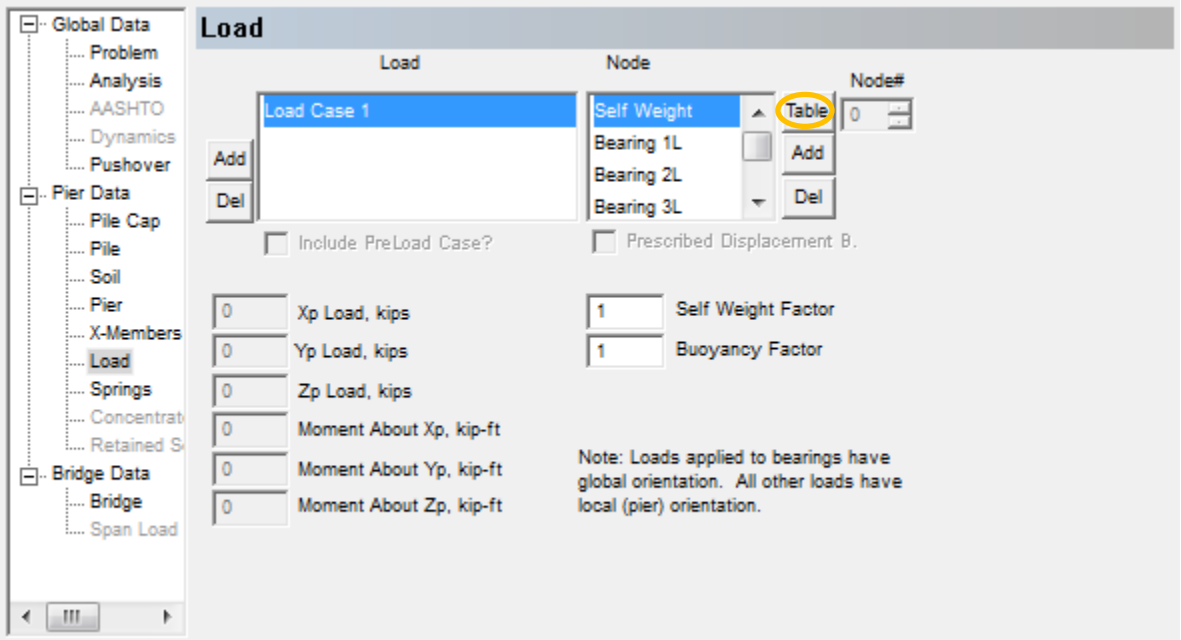

Figure 3.73 Access to OPTS Spring Formation dialog

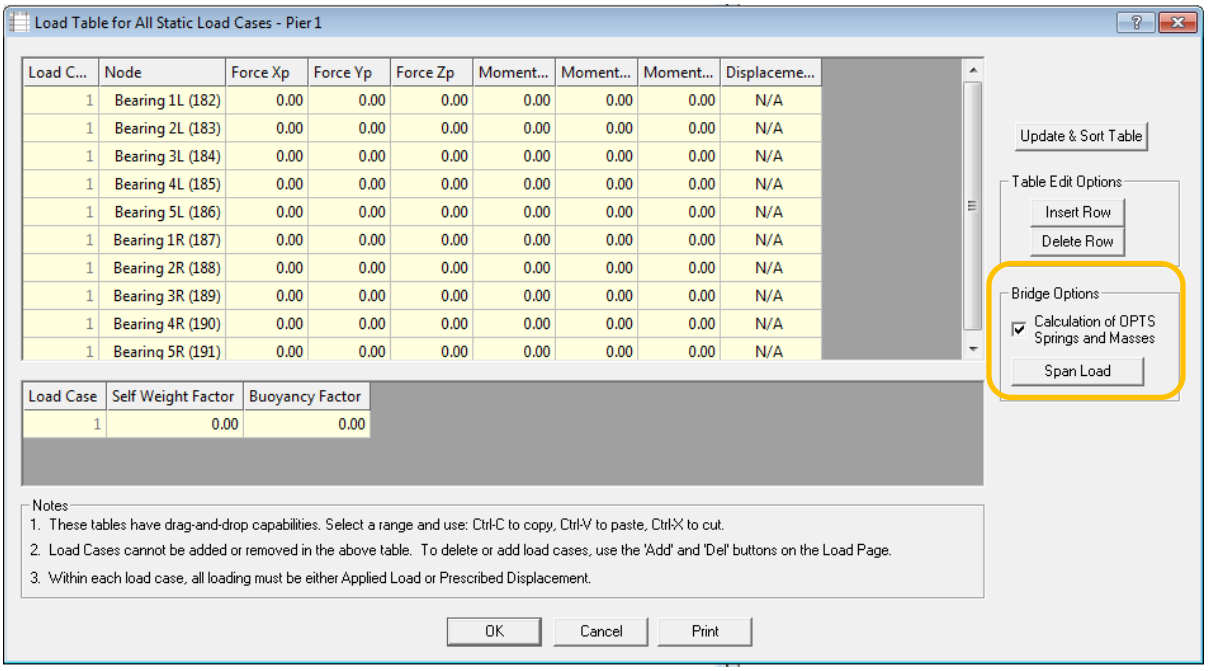

Figure 3.84 Selecting the OPTS Spring Formation option

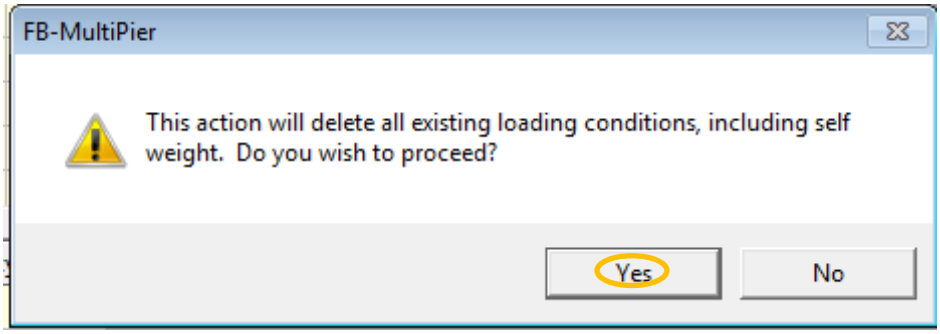

Figure 3.95 Selection confirmation

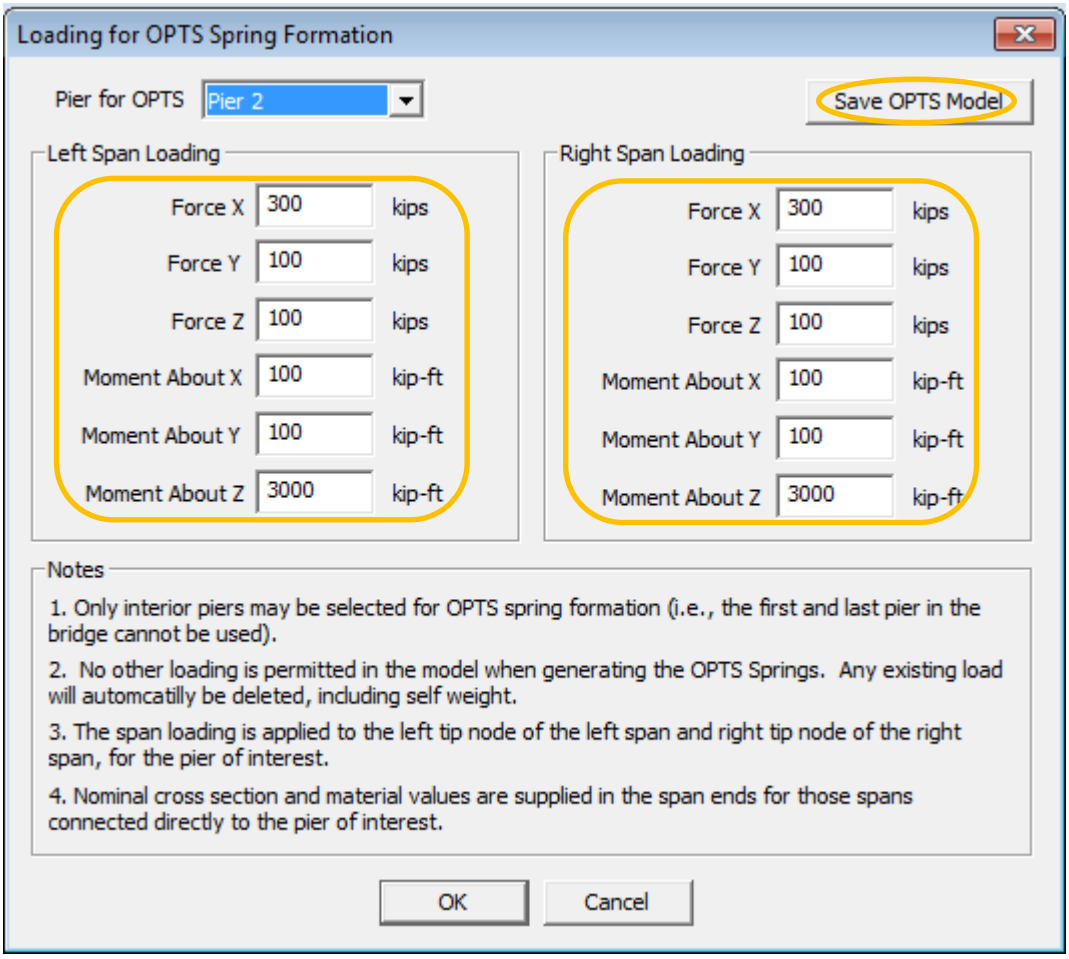

Figure 3.106 Iteration 1 stage 1 span loads

After the span loads have been defined, a static analysis is carried out by clicking the "Analysis" button on the toolbar (Fig. 3.10). The first iteration estimates for the OPTS span spring stiffnesses can then be retrieved from the bottom of the corresponding output file (Fig. 3.17). Similarly, the OPTS lumped span masses are calculated and printed to the bottom of the output file during the analysis, based on the unit weight and length of the within-range span elements. Accordingly, the lumped span masses can also be retrieved from the bottom of the output file (Fig. 3.18). Note that there is no need to iterate on the span mass values, as it has been found that lumped mass magnitudes equal to approximately one-half of the extraneous span masses suitably correspond to OPTS responses which are in-line with respective full-bridge responses (Consolazio et al., 2008). Additionally, note that the calculated Span 1 tip mass (Fig. 3.18) magnitude is calculated as 0 kip-sec^2/in. This is because the full-bridge model does not contain any spans beyond (i.e., preceding) Span 1. Therefore, the half-span mass must be manually calculated, is taken as 1.8 kip-sec^2/in, and is accounted for in both the full-bridge model and the OPTS model. In this way, both the stiffness and mass are consistent between the full-bridge model and the OPTS model.

```
************************************************
*        OPTS SPAN-END SPRING STIFFNESSES      *
************************************************

Units are: kip/in for translational stiffnesses
           kip-ft/rad for rotational stiffnessses

_____________________________________________________
Span  1 spring stiffnesses:
X-Translation = 0.237550E+03
Y-Translation = 0.385107E+01
Z-Translation = 0.276705E+04
X-Rotation    = 0.248597E+05
Y-Rotation    = 0.797984E+07
Z-Rotation    = 0.163208E+06

_____________________________________________________
Span  2 spring stiffnesses:
X-Translation = 0.107922E+03
Y-Translation = 0.298947E+02
Z-Translation = 0.167189E+04
X-Rotation    = 0.639274E+06
Y-Rotation    = 0.156367E+07
Z-Rotation    = 0.131448E+08
```

Figure 3.117 Iteration 1 OPTS spring stiffnesses (from the output file)

```
************************************************
*              OPTS SPAN-END MASSES            *
************************************************

Units are: kip-sec^2/in

_____________________________________________
Span  1 tip mass: 0.000000E+00

_____________________________________________
Span  2 tip mass: 0.193373E+01
```

Figure 3.128 Iteration 1 OPTS masses (from the output file)

ITERATION 1: ASSESSMENT OF OPTS STATIC MODEL

The base OPTS static model (recall Fig. 3.4) can now be fitted with the iteration 1 OPTS span spring stiffnesses and lumped masses, where the fitted OPTS model is shown in Fig. 3.19. The spring and mass fitting process is facilitated by making use of the FB-MultiPier GUI. As shown in Fig. 3.20, a dialog dedicated to OPTS parameter input is accessed by clicking the associated "Edit" button in the "Bridge" page. The "OPTS data" dialog (Fig. 3.21) is then populated with the iteration 1 span springs and lumped masses. Spring stiffness and mass input can be entered manually (recall Fig. 3.17 and Fig. 3.18), or it can be imported using the FBMP GUI. Specifically, automated population of the iteration 1 spring and mass data is enacted by selecting the "Import Spring/Mass Data" button shown in Fig. 3.21, and then browsing to (and selecting) the output file which contains the iteration 1 span spring stiffnesses and lumped mass values.

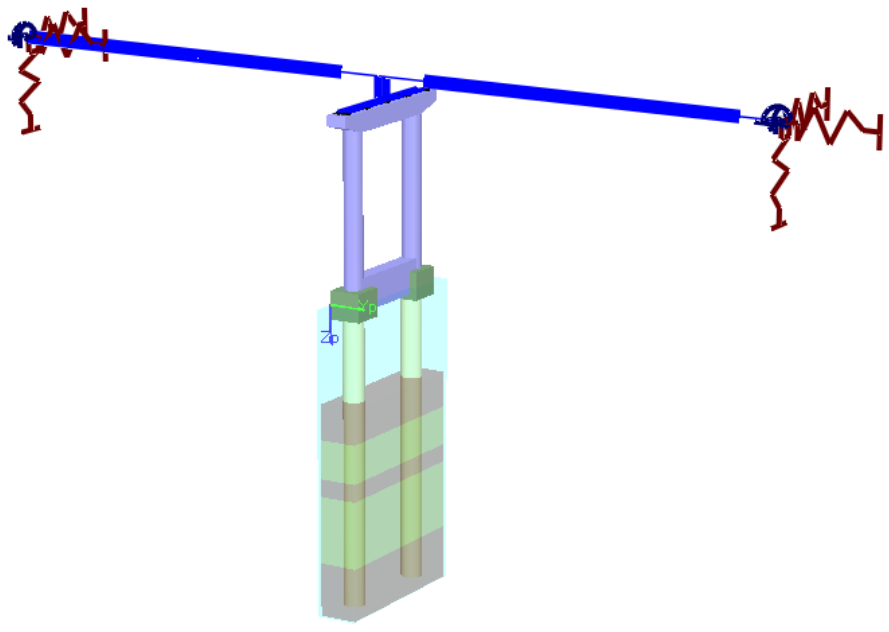

Figure 3.139 Superstructure springs and lumped masses in the Pier 2 OPTS model

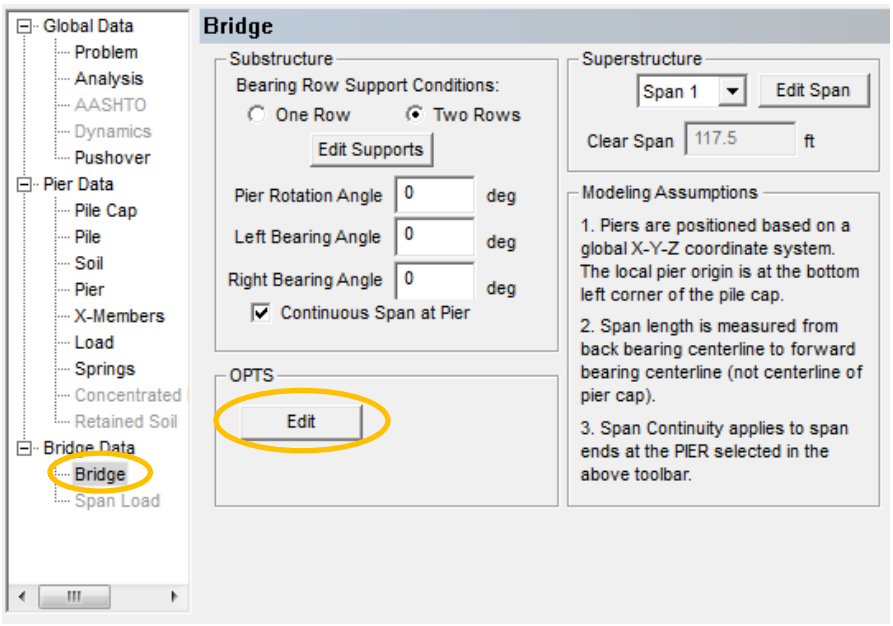

Figure 3.20 Editing of OPTS data from within the Bridge page

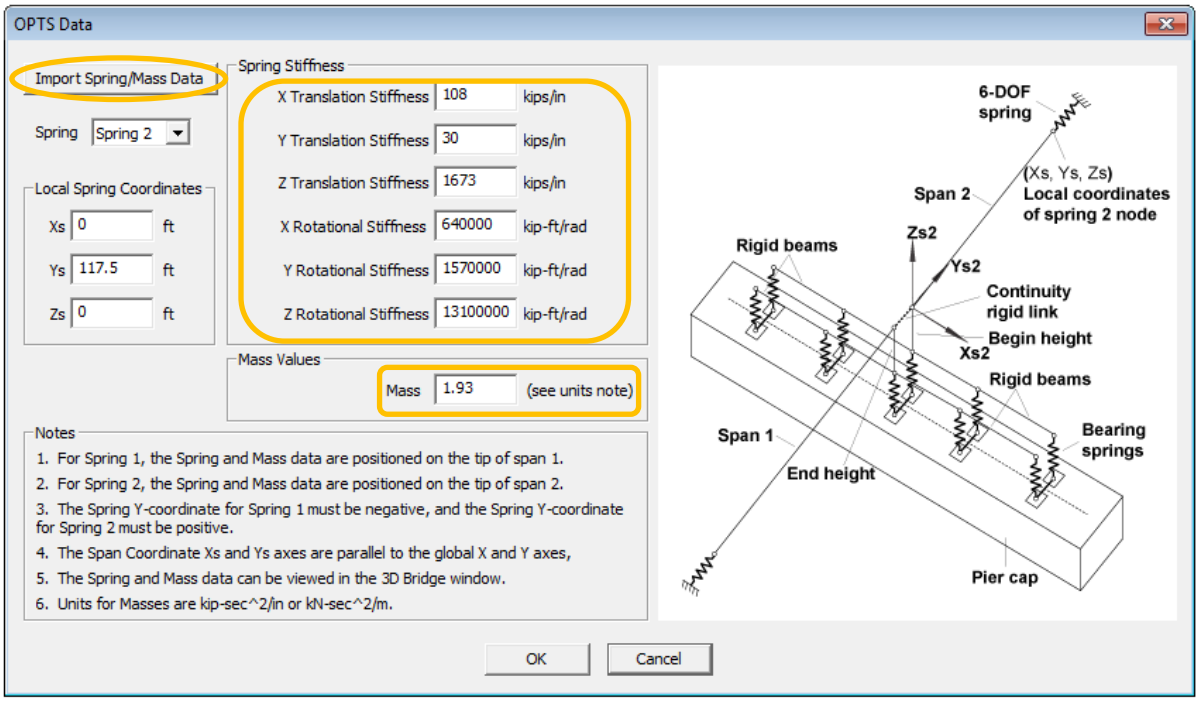

Figure 3.21 Iteration 1 OPTS spring stiffnesses and mass

Once fitted with springs and lumped masses, the OPTS static model is used to assess the lateral load response of the static OPTS model, and compare the response to that of the full-bridge model. In particular, all dead loads and the lateral load of 900 kips are applied to the OPTS static model, and a static analysis is carried out (Fig. 3.22). Displacements at the impact location (i.e., node 12) and the top of the pier column, as obtained from the iteration 1 OPTS static analysis, are compared to those of the full-bridge model (Fig. 3.23). For this first iteration, the OPTS model response is too stiff: the impact location displacement is 0.14 in. less than that of the datum response; and the pier top displacement is 0.52 in. less than that of the datum response. So as to bring the OPTS model response in-line with the datum (i.e., full-bridge) response, the span loads used in stage 1 of the iteration process will need to be increased, where the second iteration is discussed below.

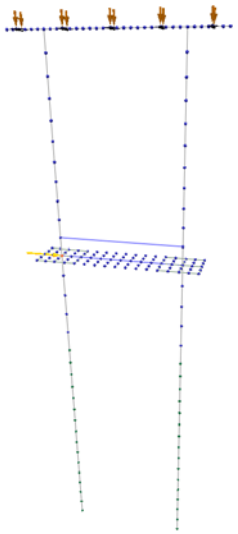

Figure 3.22 Pier 2 in OPTS model subjected to static 900 kip lateral loading

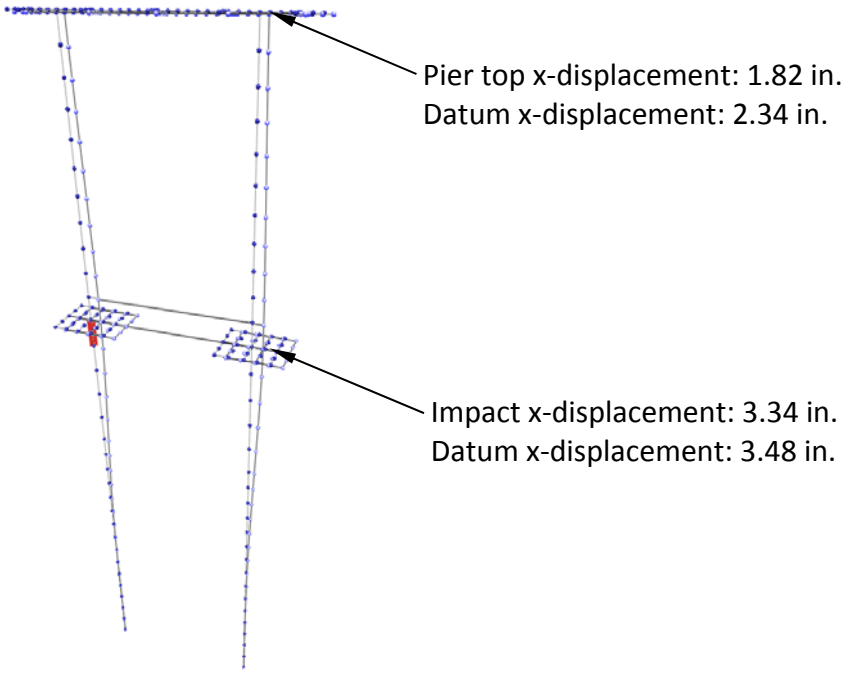

Figure 3.143 Comparison between iteration 1 OPTS response and datum of bridge response

ITERATION 2: LOADING OF SPAN-END LOCATIONS IN FULL-BRIDGE MODEL

Iteration 2 is initiated by re-opening the full-bridge model (Fig. 3.24), and applying span-end loads which are increased relative to those loads supplied in stage 1 of the first iteration. For this demonstration case, a load increase of 20% was elected. As shown in Fig. 3.25, force magnitudes of 360 kips are supplied to the "X Force" input boxes, and moment magnitudes of 3,600 kip-ft are supplied to the "Moment about Z" input boxes. Calculated spring stiffnesses and lumped mass values associated with iteration 2, as printed to the bottom of the output file, are shown in Fig. 3.26 and Fig. 3.27, respectively. Note again that the calculated masses do not need to be iterated upon.

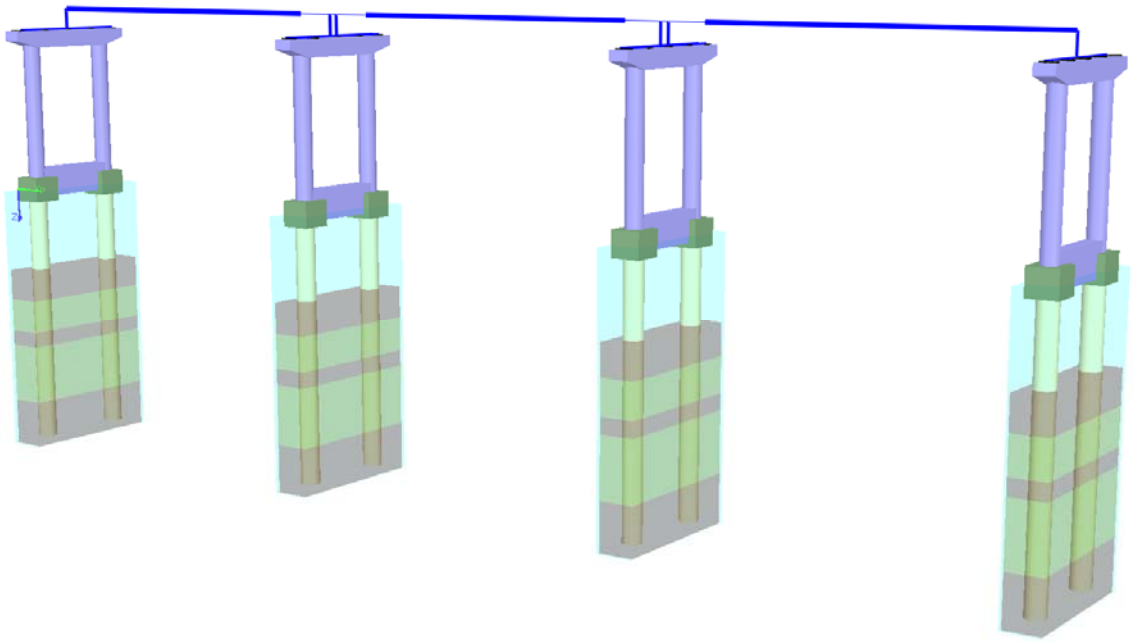

Figure 3.154 Four-pier three-span model

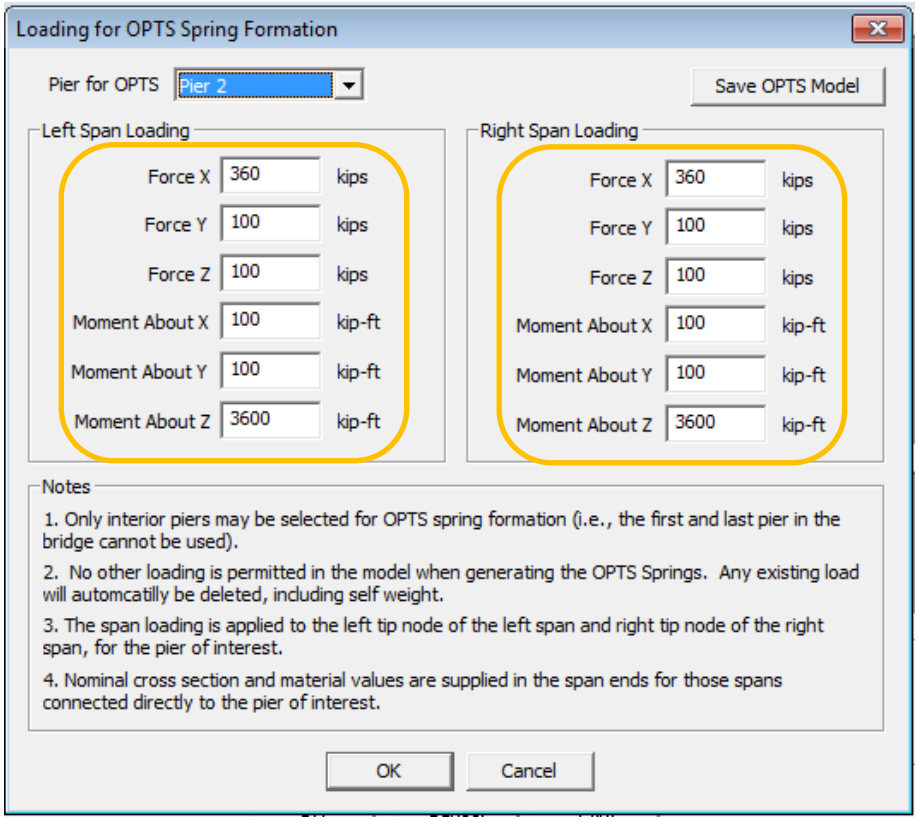

Figure 3.165 Iteration 2 stage 1 span loads

```
*************************************************
*        OPTS SPAN-END SPRING STIFFNESSES       *
*************************************************

Units are: kip/in for translational stiffnesses
           kip-ft/rad for rotational stiffnesses

_________________________________________________
Span  1 spring stiffnesses:
X-Translation = 0.230076E+03
Y-Translation = 0.385110E+01
Z-Translation = 0.276712E+04
X-Rotation    = 0.248597E+05
Y-Rotation    = 0.795565E+07
Z-Rotation    = 0.162649E+06

_________________________________________________
Span  2 spring stiffnesses:
X-Translation = 0.820501E+02
Y-Translation = 0.298948E+02
Z-Translation = 0.167225E+04
X-Rotation    = 0.639282E+06
Y-Rotation    = 0.155429E+07
Z-Rotation    = 0.130675E+08
```

Figure 3.176 Iteration 2 OPTS spring stiffnesses (from the output file)

```
*************************************************
*              OPTS SPAN-END MASSES             *
*************************************************

Units are: kip-sec^2/in

_________________________________________________
Span  1 tip mass: 0.000000E+00

_________________________________________________
Span  2 tip mass: 0.193373E+01
```

Figure 3.187 Iteration 2 OPTS span masses (from the output file)

ITERATION 2: ASSESSMENT OF OPTS STATIC MODEL

For the second stage of iteration 2, the OPTS static model is again fitted with springs and lumped masses (Fig. 3.28), where the fitting procedure is carried out in the same manner as that used during iteration 1. More specifically, the values shown in Fig. 3.26 and Fig. 3.27 can be entered manually, or the importing capabilities of the FBMP GUI can be utilized (Fig. 3.29).

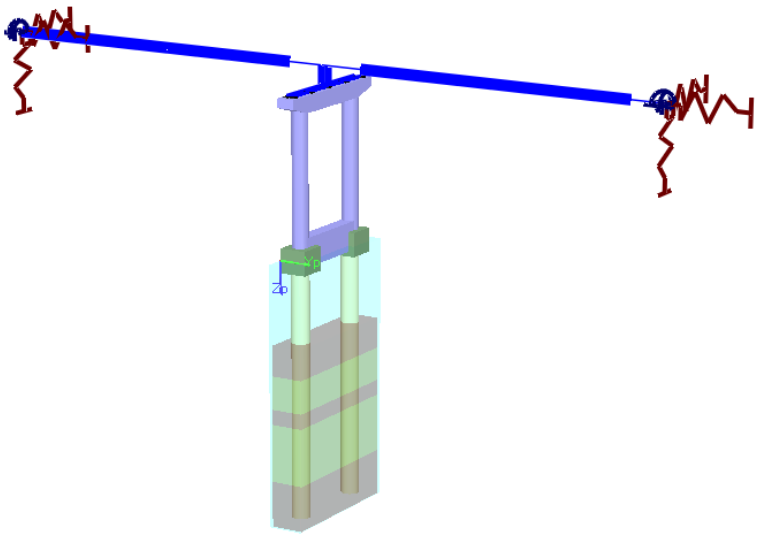

Figure 3.198 Superstructure springs and lumped masses in the Pier 2 OPTS model

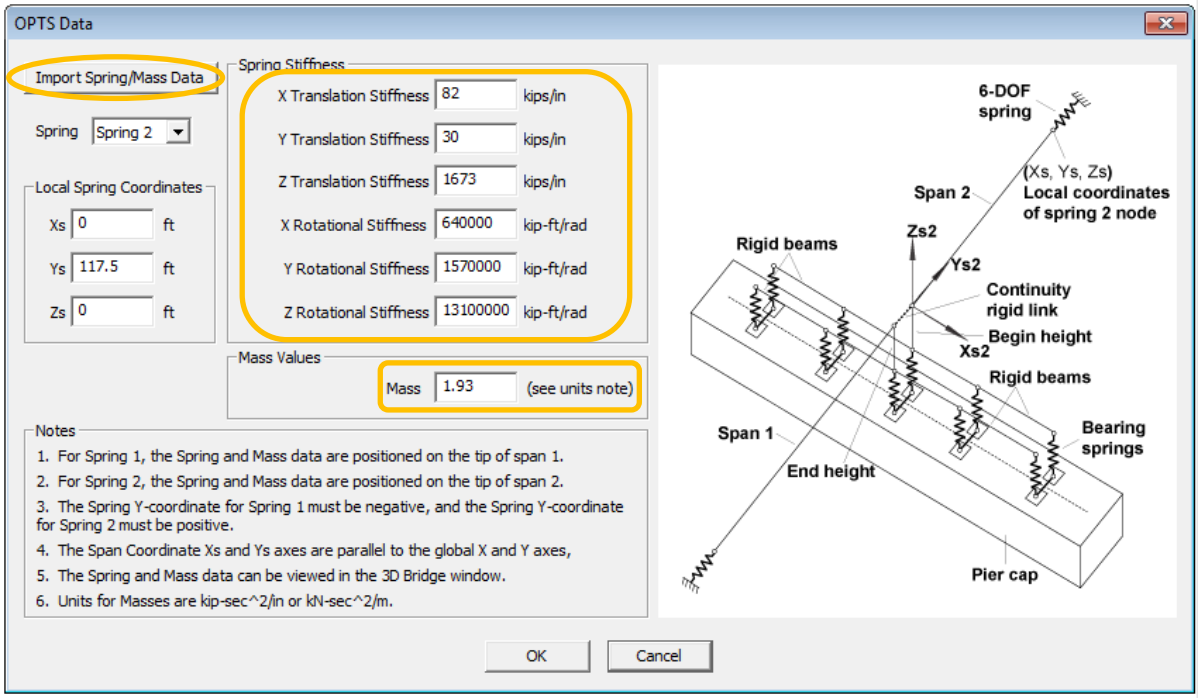

Figure 3.209 Iteration 2 OPTS spring stiffnesses and mass

Once fitted with the iteration 2 springs and lumped masses, the OPTS static model is again used to assess the lateral load response of the static OPTS model, and the response is again compared to that of the full-bridge model. Note that again, all dead loads and the lateral load

of 900 kips are applied to the OPTS static model, and a static analysis is carried out (Fig. 3.30). The displacements predicted for the iteration 2 OPTS static model show good agreement with those of the datum (i.e., full-bridge model). Namely, the OPTS model displacement at the impact location (3.50 in.) is less than 1% greater than the respective datum response displacement (3.48 in.). Likewise, the OPTS model pier-top displacement (2.37 in.) is approximately 1% greater than that of the datum pier-top response. Given the agreement in static response between the OPTS model and the full-bridge, the OPTS span spring stiffnesses are considered to have been converged upon.

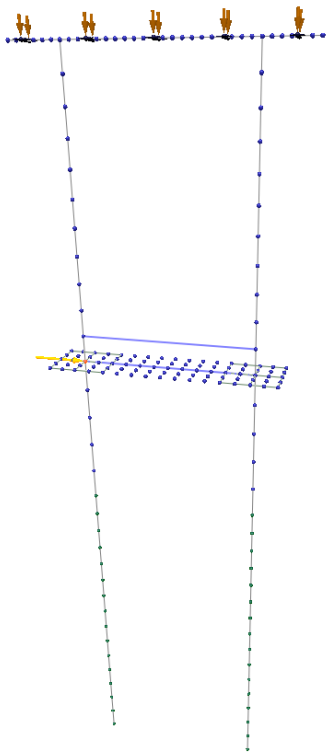

Figure 3.30. Pier 2 in OPTS model subjected to static 900 kip lateral loading

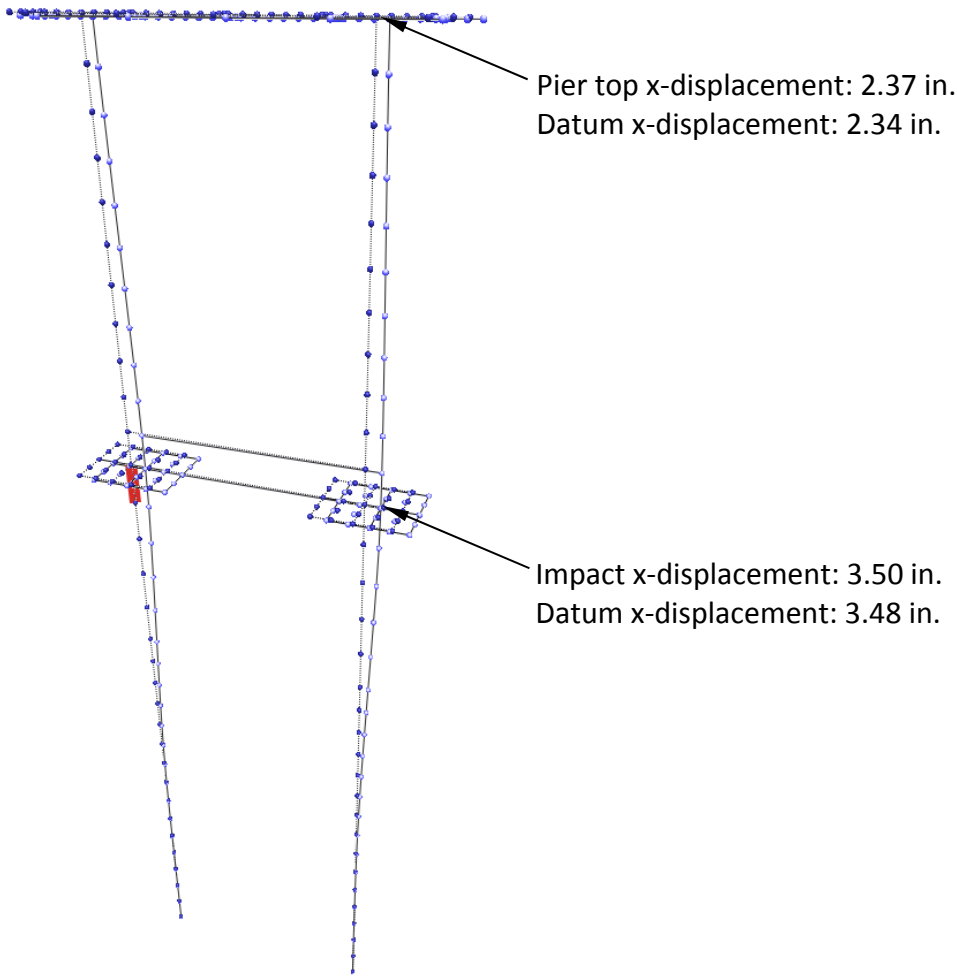

Figure 3.31. Comparison between iteration 2 OPTS response and datum of bridge response

FORMATION OF OPTS DYNAMIC MODEL

DETERMINATION OF RAYLEIGH DAMPING COEFFICIENTS

In dynamic analysis, it is important to include damping so that energy dissipation is taken into account. For time-step integration (i.e., transient, or time-history) analyses carried out in FBMP, Rayleigh damping is employed (BSI 2014). When Rayleigh damping is employed, the system damping matrix is constructed so as to be proportional to the mass and stiffness system matrices. In this way, a desired level of critical damping can be achieved over an approximate range of system vibration frequencies (see Tedesco et al., 1998 for additional details).

Relevant to short and medium span bridges, Paultre et al. (1992) carried out a research synthesis, in part, to ascertain representative values of structural damping in bridges. Their findings are consistent with the approach of damping the first five modes of vibration at a level commensurate to approximately 5% of critical damping. Accordingly, the approach of introducing 5% (of critical) damping over the first five vibration modes when conducting dynamic analyses is employed in this demonstration case.

To facilitate specification of damping properties for the OPTS model (which is fitted with the iteration 2 springs and lumped masses, Fig. 3.32), a modal analysis is carried out. Note that the modal analysis is carried out specifically to determine the system Rayleigh damping coefficients, which in turn, will produce 5% of critical damping over the first five modes of vibration during all subsequent time-history analyses. First, in this process, the OPTS static model is transformed into a dynamic analysis model. This transformation is undertaken by selecting the “Dynamic” analysis type in the “Analysis” page (Fig. 3.33).

After confirming that a dynamic analysis type is selected (Fig. 3.31), the modal response input is entered in the “Dynamics” page (Fig. 3.35). In particular, the “Modal Response” option should be selected in the “Analysis Type” section, and the “# Modes” should be set to 5 or greater. Additionally, both the “Stop Analysis after Eigenvector Results” and “Calculate Rayleigh Damping Factors” check boxes should be checked. After completing the modal analysis input, a dynamic (frequency-based, or modal) analysis is carried out, and the associated Rayleigh damping coefficients (factors) are calculated. These factors are printed to the bottom of the corresponding output file (Fig. 3.36).

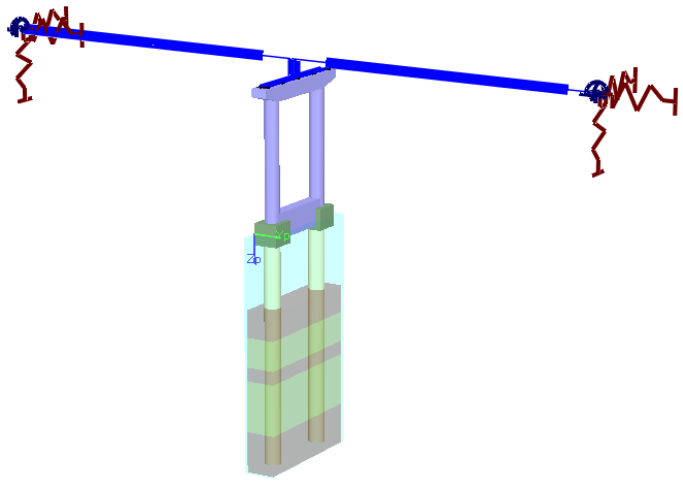

Figure 3.32 OPTS model

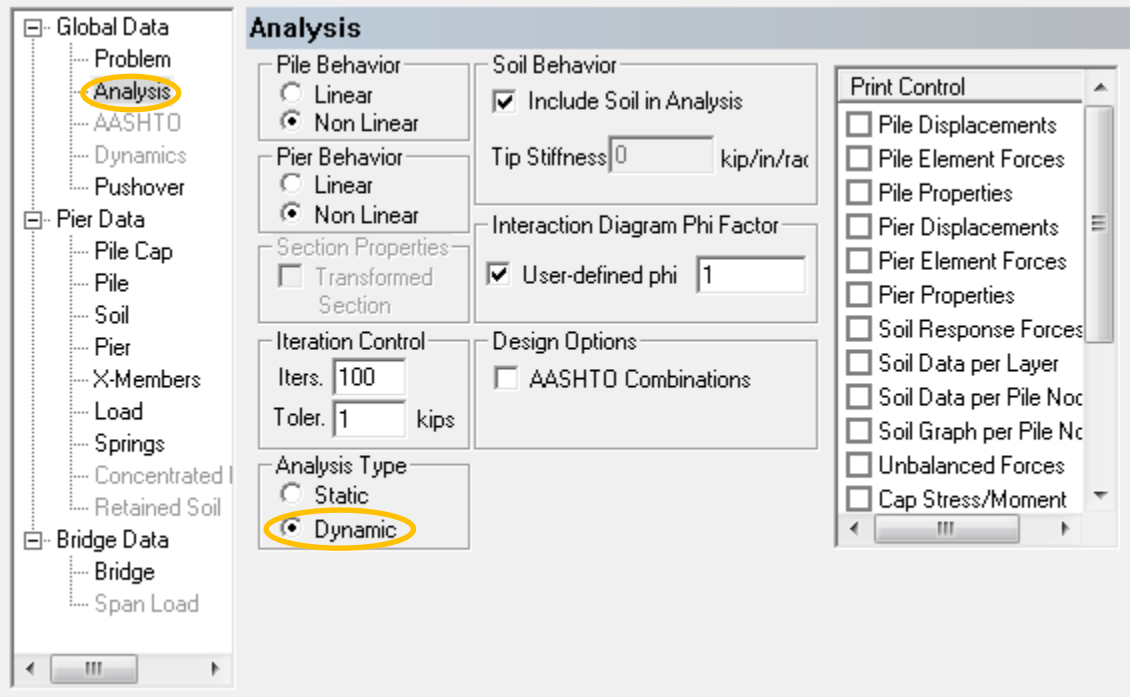

Figure 3.213 Selection of dynamic analysis in the Analysis page

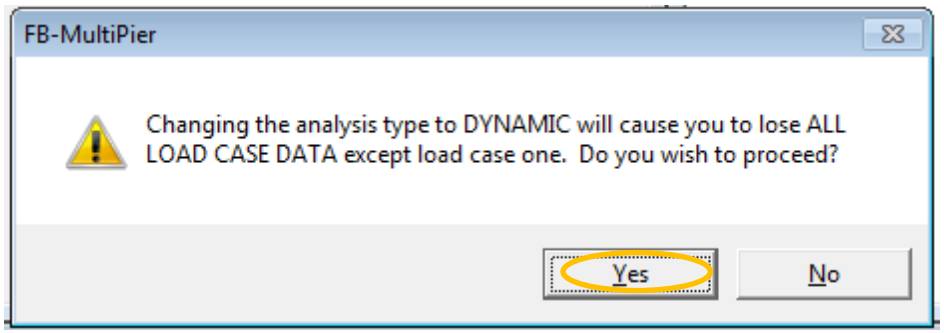

Figure 3.224 Selection confirmation

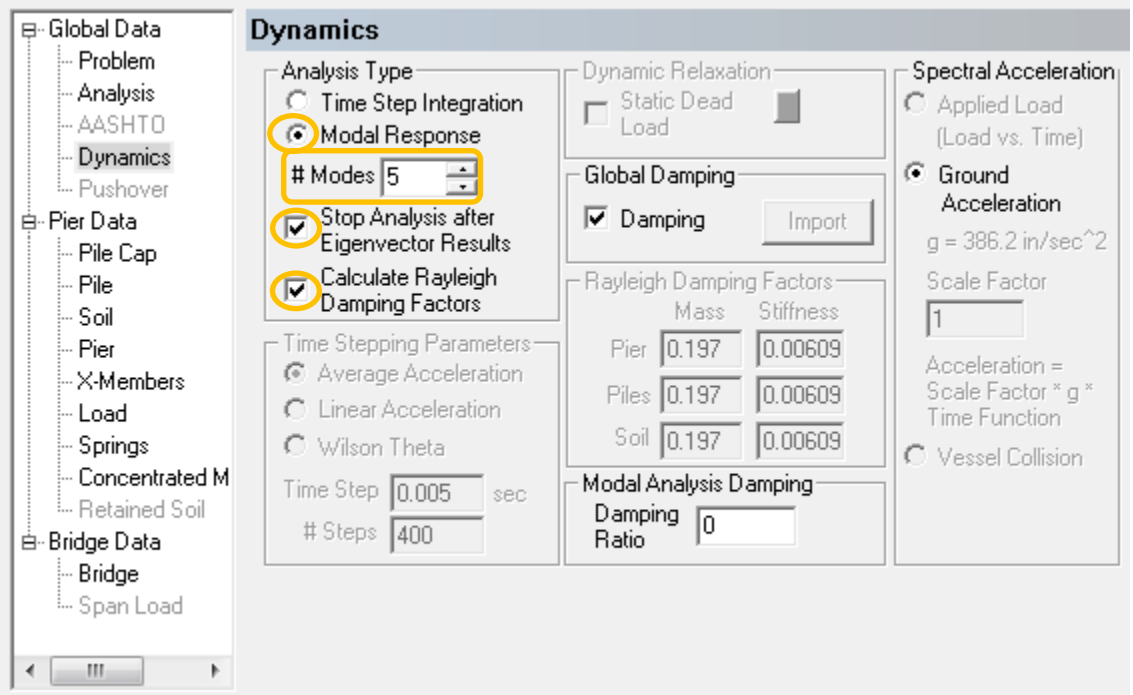

Figure 3.235. Selection of Modal Analysis (in order to determine Rayleigh damping coefficients)

```
 156    0.5907E-05    0.8092E-04   -0.5296E-03   -0.7068E-05    0.1323E-06    0.2971E-05
 157    0.1290E-04    0.4783E-03   -0.5254E-03   -0.5733E-05    0.9626E-07    0.2852E-05
 158    0.4418E-02    0.2522E+00    0.1419E-02    0.7162E-03   -0.8225E-05    0.2753E-06
 159    0.3812E-02    0.2071E+00    0.1395E-02    0.6963E-03   -0.1065E-04    0.2556E-06
 160    0.3085E-02    0.1638E+00    0.1372E-02    0.6595E-03   -0.1204E-04    0.2359E-06
 161    0.2303E-02    0.1235E+00    0.1349E-02    0.6048E-03   -0.1237E-04    0.2163E-06
 162    0.1534E-02    0.8717E-01    0.1325E-02    0.5316E-03   -0.1161E-04    0.1968E-06
 163    0.8487E-03    0.5614E-01    0.1301E-02    0.4395E-03   -0.9748E-05    0.1773E-06
 164    0.3174E-03    0.3160E-01    0.1278E-02    0.3280E-03   -0.6778E-05    0.1579E-06
 165   -0.1237E-04    0.1435E-01    0.1255E-02    0.2152E-03   -0.3674E-05    0.1415E-06
 166   -0.1711E-03    0.3674E-02    0.1233E-02    0.1227E-03   -0.1412E-05    0.1264E-06
 167   -0.2117E-03   -0.1864E-02    0.1214E-02    0.5419E-04    0.4099E-07    0.1117E-06
 168   -0.1833E-03   -0.3820E-02    0.1196E-02    0.1018E-04    0.7650E-06    0.9717E-07
 169   -0.1276E-03   -0.3676E-02    0.1180E-02   -0.1232E-04    0.9303E-06    0.8390E-07
 170   -0.7233E-04   -0.2620E-02    0.1165E-02   -0.1929E-04    0.7778E-06    0.7183E-07
 171   -0.3109E-04   -0.1432E-02    0.1153E-02   -0.1727E-04    0.5128E-06    0.6089E-07
 172   -0.6391E-05   -0.5034E-03    0.1142E-02   -0.1167E-04    0.2711E-06    0.5100E-07
 173    0.5921E-05    0.8292E-04    0.1133E-02   -0.7169E-05    0.1320E-06    0.4537E-07

***********************************************
*         RAYLEIGH DAMPING COEFFICIENTS       *
***********************************************

Values correspond to 5% critical damping over the
first five modes of vibration.

Alpha =    0.197100
Beta  =    0.006090
```

Figure 3.246 Rayleigh damping coefficients (from the Output file)

DYNAMIC ANALYSIS PARAMETER INPUT

Having calculated the Rayleigh damping coefficients (recall Fig. 3.36), the Rayleigh alpha (i.e., mass-proportional) and beta (i.e., stiffness proportional) parameters are supplied to the OPTS dynamic model as part of setting up the CVIA-OPTS (dynamic) analysis. Input of the Rayleigh damping coefficients, and other dynamic input parameters, is facilitated by making use of the FBMP GUI. Namely, the dynamic parameter input process is initiated by opening the OPTS dynamic model (Fig. 3.37).

In the "Dynamics" page, the analysis type is set to "Time Step Integration" (Fig. 3.38), where a confirmation selection dialog appears (Fig. 3.39). After confirming the selection, the "Dynamic Relaxation" option is selected by checking the "Static Dead Load" check box. Dynamic relaxation enables all permanent loads (e.g., dead load) to be incorporated into the dynamic analysis without artificially exciting the inertia of the system (see Davidson 2010 for a detailed discussion). Rayleigh damping input parameters can be manually input (recall Fig. 3.36), or imported by selecting the "Import" button, after checking the "Damping" checkbox (Fig. 3.38). For the purposes of this demonstration case, the "Vessel Collision" time function type is selected, and the time step information is supplied. Generally, the engineer should verify that the time step size is sufficiently small so that it does not distort the dynamic analysis output (see Tedesco et al., 1998 for detailed guidance).

Regarding the size of time steps for conducting CVIA in FBMP, the range of 0.0025 sec to 0.01 sec has been used (see Consolazio and Cowan, 2005 for details). For this demonstration case, a time step size of 0.005 sec is employed (Fig. 3.38). Regarding the duration of analysis, the engineer should verify that the number of time steps considered be sufficiently large to ensure that the bridge is no longer being subjected to impact load (i.e., permanent separation between the bridge and impacting vessel has occurred), and further, that the bridge maximum response has been captured. For this demonstration case, an analysis duration of 2 sec. (i.e., 400 time steps) is selected (Fig. 3.38). As will be shown later, the selected analysis duration captures the full impact duration (for the scenario considered) as well as the maximum pier response.

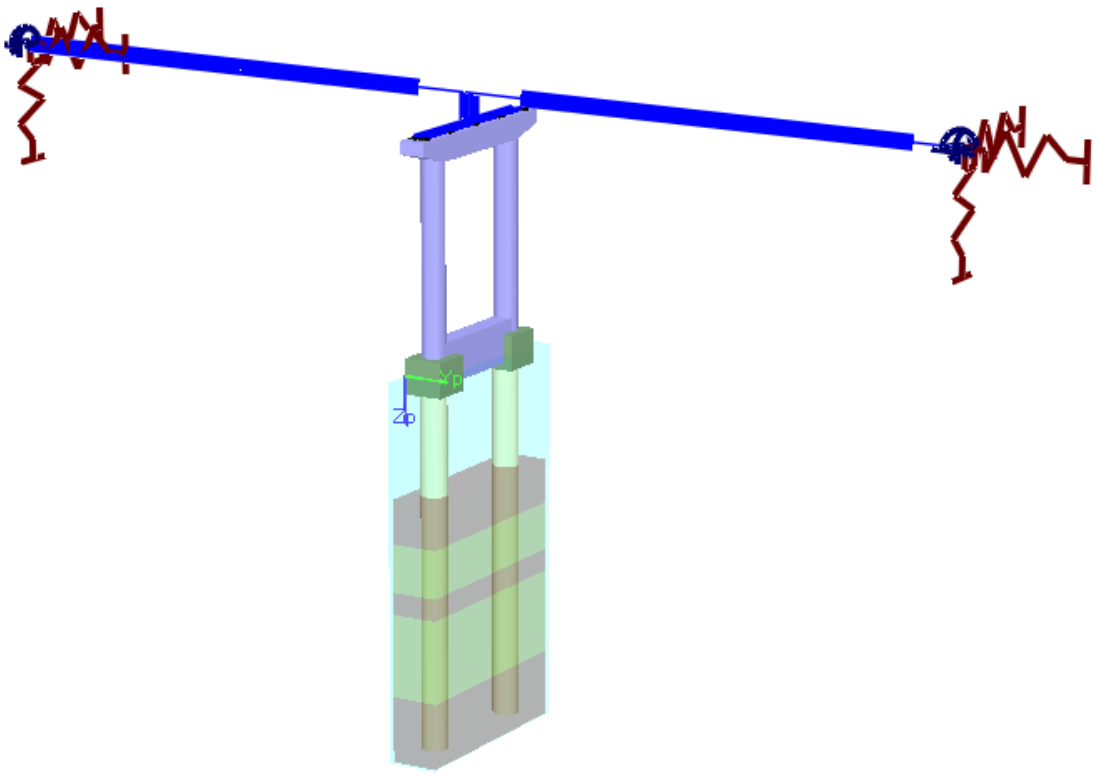

Figure 3.257 OPTS model for modal analysis

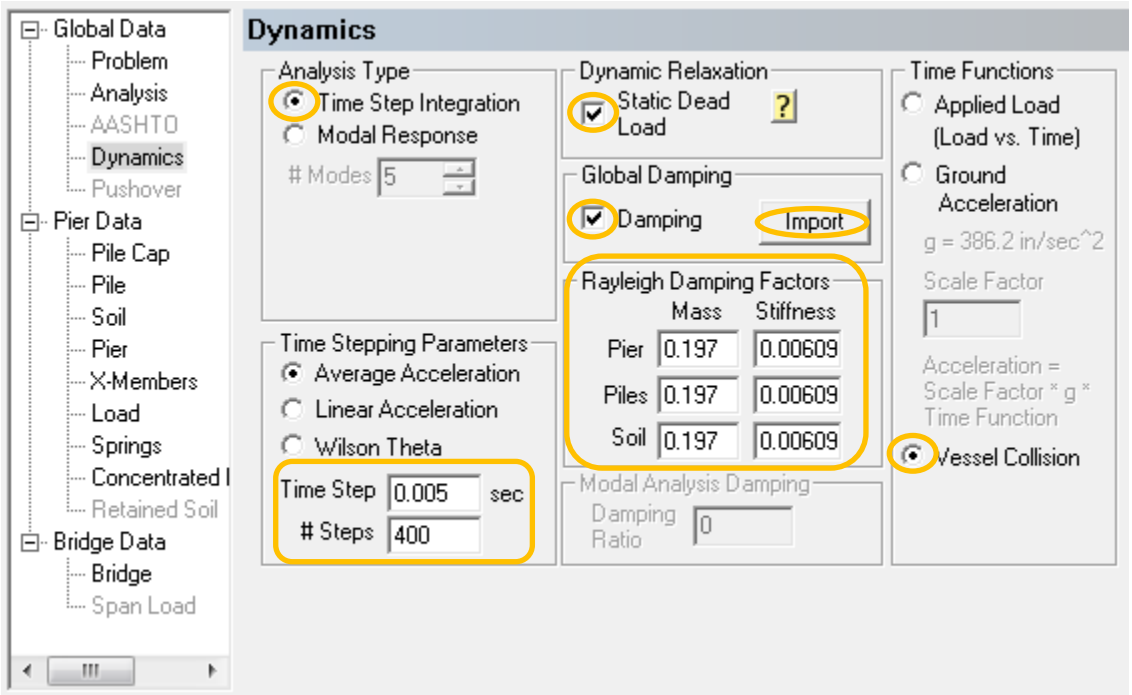

Figure 3.268 Selection of dynamic analysis in the Dynamics page

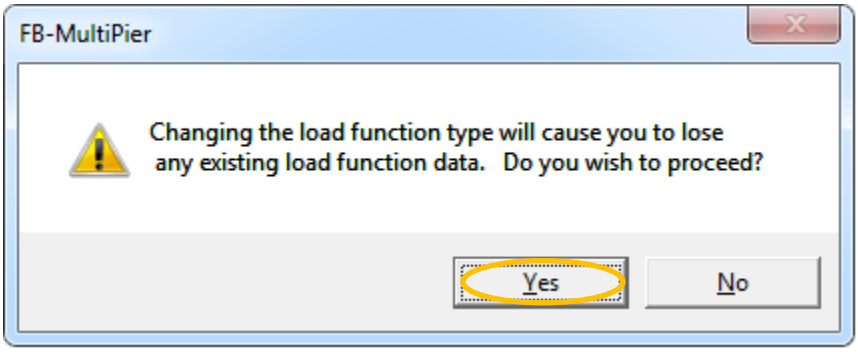

Figure 3.279 Selection confirmation

4. NONLINEAR DYNAMIC VESSEL COLLISION ANALYSIS OF OPTS MODEL

The final step in preparing the OPTS model for the nonlinear dynamic vessel collision analysis (i.e., CVIA) is supplying input to characterize the vessel collision loading. In Sec. 4.1, the selection of the impact location is discussed. Based on the impact location and collision scenario, the vessel loading is characterized, as discussed in Sec. 4.2. This final preparation step is initiated by opening the fitted dynamics OPTS model, where time step integration input (recall Chapter 3) has previously been entered (Fig. 4.1).

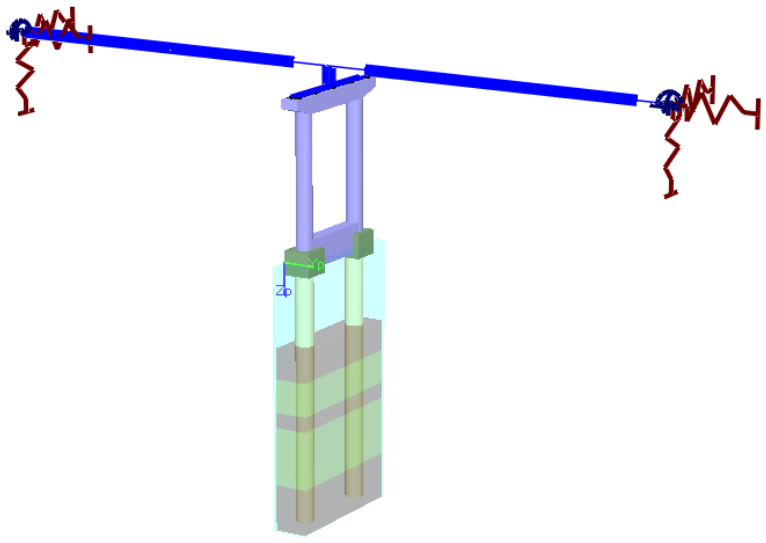

Figure 4.1 Dynamic OPTS analysis model

SELECTION OF IMPACT LOCATION

The impact location is specified by identifying a node of initial contact between the pier and impacting vessel. The impact location should be selected based on the MHW elevation, and the

draft characteristics of the design vessel. For the demonstration case, the impact location is taken at the MHW elevation (i.e., node 12, as indicated in Fig. 4.2). Accordingly, a dynamic impact load is defined at node 12.

Note that FBMP permits either head-on impacts or angled impacts to be taken into consideration. The direction of the impacting vessel (relative to the impacted pier) is defined by specifying values of non-zero initial velocities for the impacting vessel (discussed in Sec. 4.2). For the demonstration case, a head-on impact scenario is considered, and so only the "Xp dir" loading DOF is activated at node 12.

An advantage of using the FBMP CVIA-OPTS features is that the relative geometry of the pier and impacting vessel can be taken into account as part of the analysis. For the selected impact location (node 12), the impacted pier structure component is a round, 9 ft diameter shear wall surface.

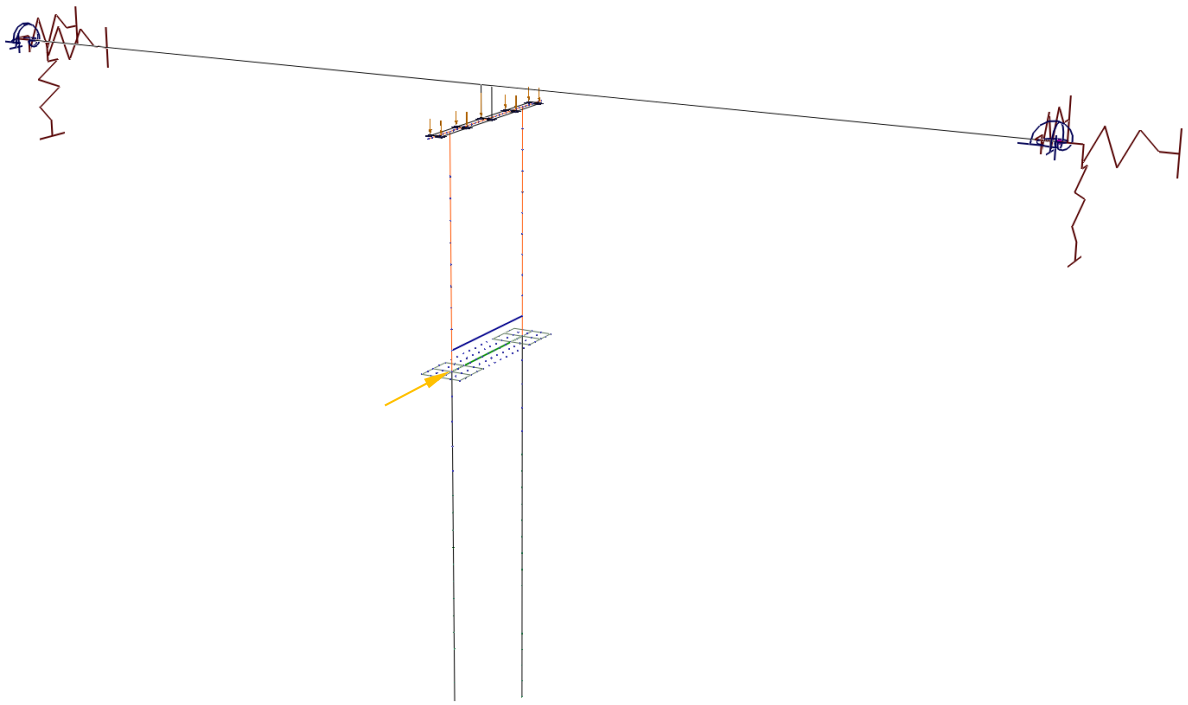

Figure 4.2 Impacted node (node 12)

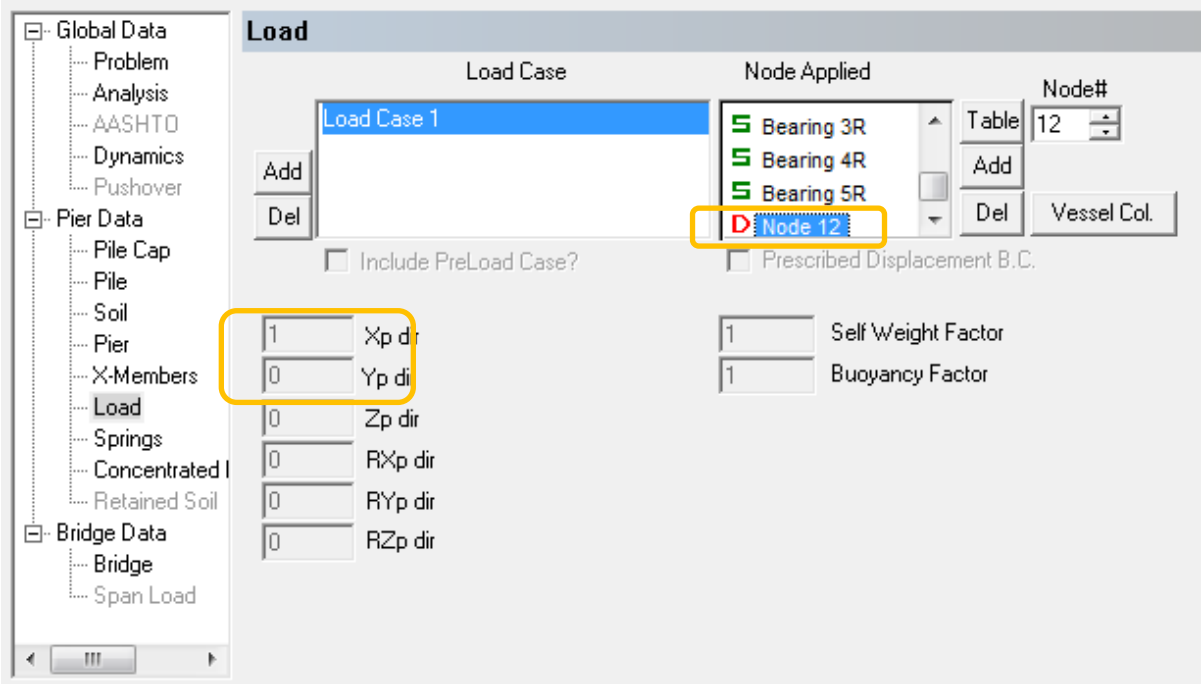

Figure 4.3 Defining the impacted node in the Load page

INPUT FOR VESSEL COLLISION SCENARIO

Having selected an impact location (node 12) in the OPTS dynamic model, the remaining input necessary to characterizing the vessel collision scenario is entered. The characterization input is accessed by clicking the "Vessel Col." Button in the "Load" page (Fig. 4.4). More specifically, in the "Vessel Collision Analysis Data" dialog (Fig. 4.5), the impacting vessel weight, initial x-velocity, and initial y-velocity (if non-zero) can be input directly. For the demonstration case, a vessel weight of 1,390 kips and a head-on (i.e., x-velocity) of 3.3 ft/sec are entered (Fig. 4.5). In addition, the vessel type is selected from the pull-down menu, where for this demonstration case, impact occurs between a barge and a round 9 ft diameter surface. The corresponding vessel bow force-deformation curve is shown at the bottom of Fig. 4.5. Note that other vessel definition options exist, which can be accessed via the "Vessel Type" pull-down menu, including:

- Barge impact on a flat (rectangular) surface;
- General elastic-plastic force-deformation; and
- General force-deformation input.

After completing the vessel collision analysis input, rapid nonlinear dynamic vessel collision analysis (CVIA-OPTS) is carried out by submitting the model for analysis.

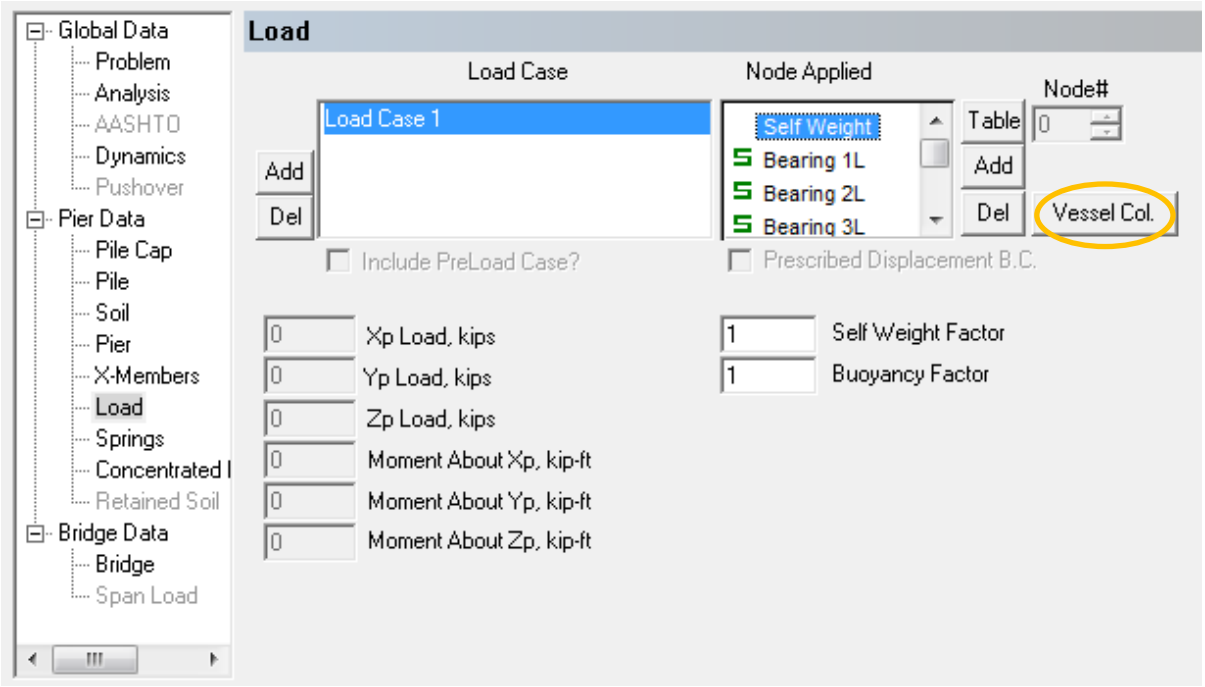

Figure 4.4 Accessing the Vessel Collision Analysis Data dialog from the Load page

.

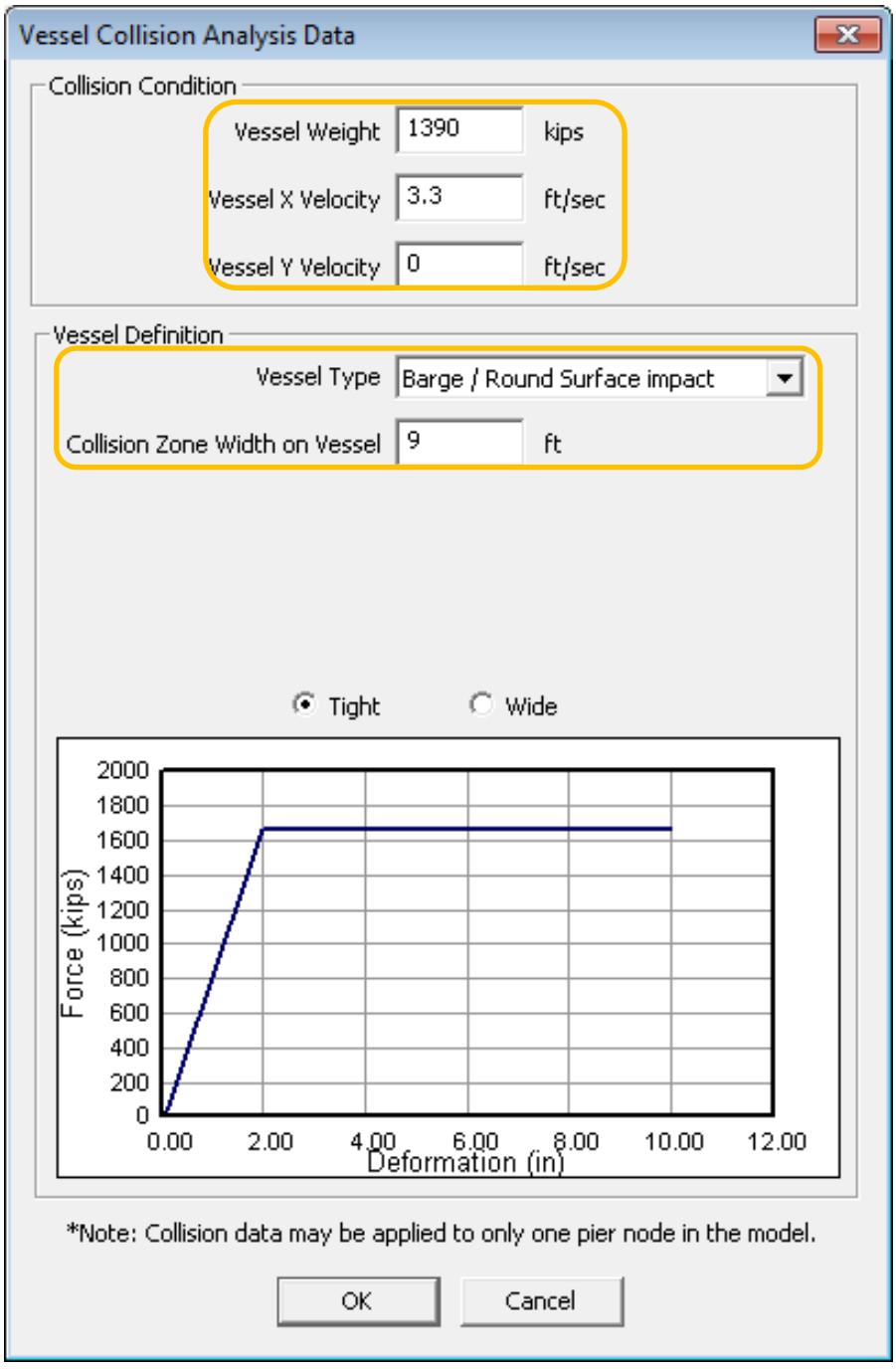

Figure 4.5 Input of vessel collision parameters

5. DETERMINATION OF STRUCTURAL DEMANDS FROM DYNAMIC VESSEL COLLISION ANALYSIS

Having carried out a CVIA-OPTS analysis for Pier 2 of the 4-pier 3-span bridge case, the response of the simplified bridge model (recall Fig. 4.1) is quantified. As a supplement to the user's guide, and as further demonstration of the efficacy found in employing the OPTS modeling approach, Sec. 5.1 is dedicated to comparing select CVIA-OPTS time-histories of response to those obtained from subjecting a dynamic version of the full-bridge (recall Fig. 2.1) model to the vessel collision conditions defined in Chapter 4. As is shown in Sec. 5.1, agreement is observed between the predictions of structural response. Further, such agreement is observed despite the considerable savings in time when making use of the OPTS model.

Even though the OPTS model output is reduced (and obtained more rapidly) than the output data that is obtained from time-history analysis of the full-bridge model, the process of identifying maximum structural demand can still require more effort relative to a static analysis. Such cumbersomeness arises because a complete set of soil, pier member, and span member data; nodal displacements; and internal forces are generated for each time step of the time-history analysis. For the Pier 2 OPTS model vessel collision scenario considered, data output consists of 400 time steps, or 400 calculations of Pier 2, Span 1, and Span 2 demands. To help facilitate identification of maximum structural demands, the "Design Tables" feature in FBMP is employed, as presented in Sec. 5.2. This feature distills down the results of an analysis such that the response maxima are listed concisely in a set of tables. By making use of the design tables feature, quantities such as maximum internal forces, and demand-capacity ratios can be quickly and automatically identified from among the time-step data.

COMPARISON OF OPTS VERSUS FULL-BRIDGE MODEL RESPONSES TO VESSEL COLLISION LOADING

As a supplement to the user's guide, it is demonstrated in this section that the OPTS modeling approach is capable of leading to structural response predictions that are in-line with those responses that would be predicted for analysis of the full-bridge model. For verification purposes, a CVIA analysis has been carried out using the full-bridge model (recall Fig. 2.1), where the vessel collision scenario defined in Chapter 4 is incorporated into the model input. Importantly, note that the computation time required to carry out multiple-second vessel collision analyses can require tens of minutes to several hours when full-bridge models are employed. In contrast, comparable results for a pier of interest can be obtained in approximately 5 min. or less when OPTS models are employed. In Sec. 5.2.1, the impact force-histories obtained from the Pier 2 CVIA-OPTS analysis output, and the corresponding full-bridge CVIA analysis output, are compared. Similarly, the OPTS and full-bridge predictions of select

time-histories of demand are compared in Sec. 5.2.2. Note that an entire catalog of OPTS versus full-bridge model dynamic response comparisons are given in Consolazio et al. (2008).

COMPARISON OF IMPACT FORCE-HISTORIES

Impact force-histories obtained from the CVIA-OPTS analysis and full-bridge CVIA analysis, where a 1,390 kip vessel traveling at 3.3 ft/sec impacts a 9 ft round diameter surface, are plotted in Fig. 5.1. Note that the duration of load-histories, and times at which the local maxima occur are in good agreement. Additionally, the peak force generated from the CVIA-OPTS analysis is 1,170 kips, which is less than 1% different from the peak impact force generated as part of the full-bridge CVIA results (1,180 kips).

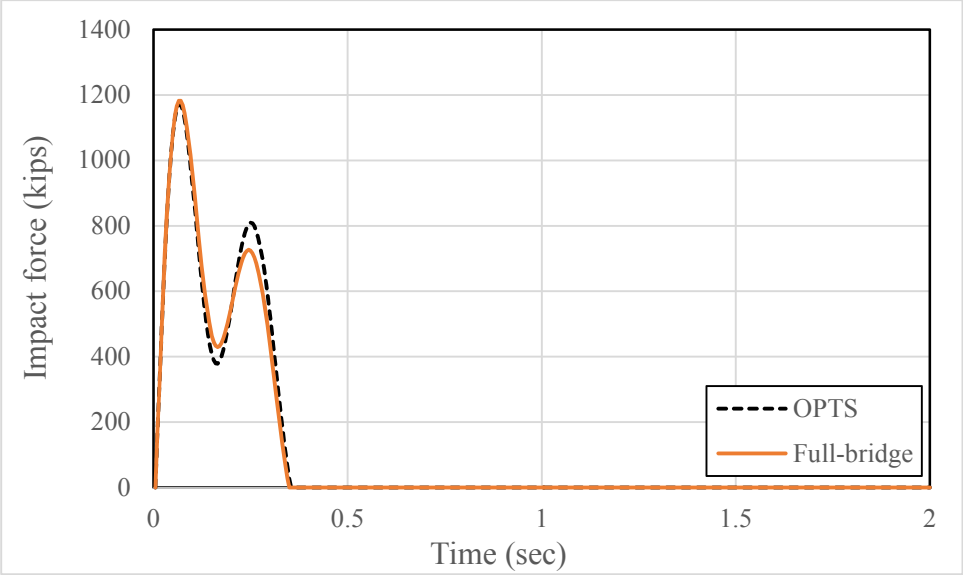

Figure 5.1 Time-histories of impact load

COMPARISON OF MEMBER INTERNAL FORCE-HISTORIES

Critical to the effectiveness of the OPTS modeling approach is the ability to predict not only impact force-histories which are in-line with full-bridge predictions, but also, the ability to predict in-line impacted pier response quantities. Shown below are selected internal force-histories along the impacted pier. Specifically, OPTS model and full-bridge internal displacement, shear, and moment time-histories generated at the base of the left pier column (i.e., directly above the impacted shear wall face) are plotted in Fig. 5.2 through Fig. 5.4, respectively. Excellent agreement is observed between the response-histories with respect to times-to-peak and maximum magnitudes. For example, the peak moment magnitudes (Fig. 5.4)

are 4,630 kip-ft and 4,600 kip-ft for the CVIA-OPTS results and full-bridge results, respectively. This difference is less than 1%.

Similar levels of agreement are observed throughout the pier. For example, the displacement, shear, and moment time-history plots obtained from the CVIA-OPTS and full-bridge CVIA are shown for the top of the pier column (above the impact location) in Fig. 5.5 through Fig. 5.7. The maximum force magnitudes occur within close proximity and differ by less than 1% for each demand type.

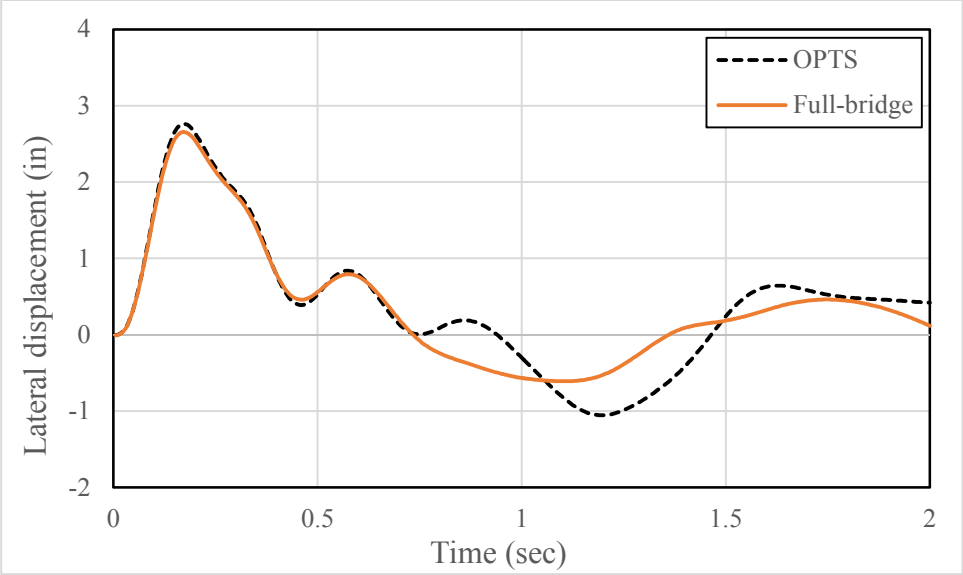

Figure 5.2 Time-histories of displacement in the pier column immediately above the impacted node

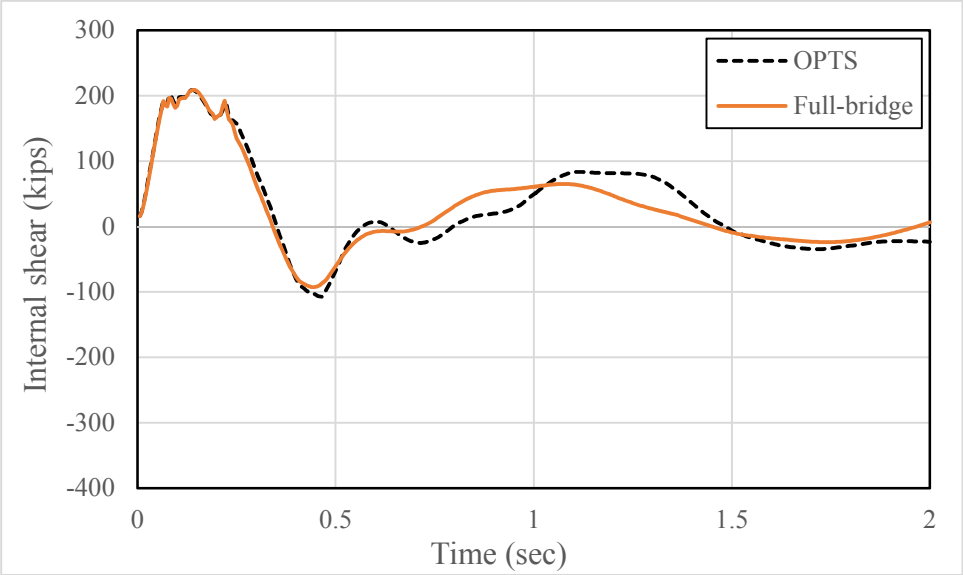

Figure 5.3 Time-histories of internal shear in the pier column immediately above the impacted node

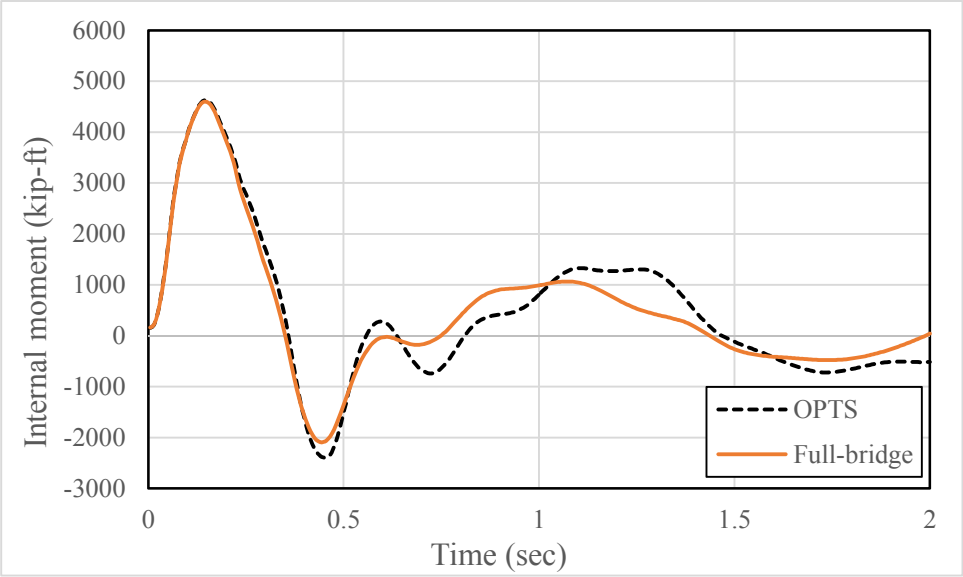

Figure 5.4 Time-histories of internal moment in the pier column immediately above the impact location

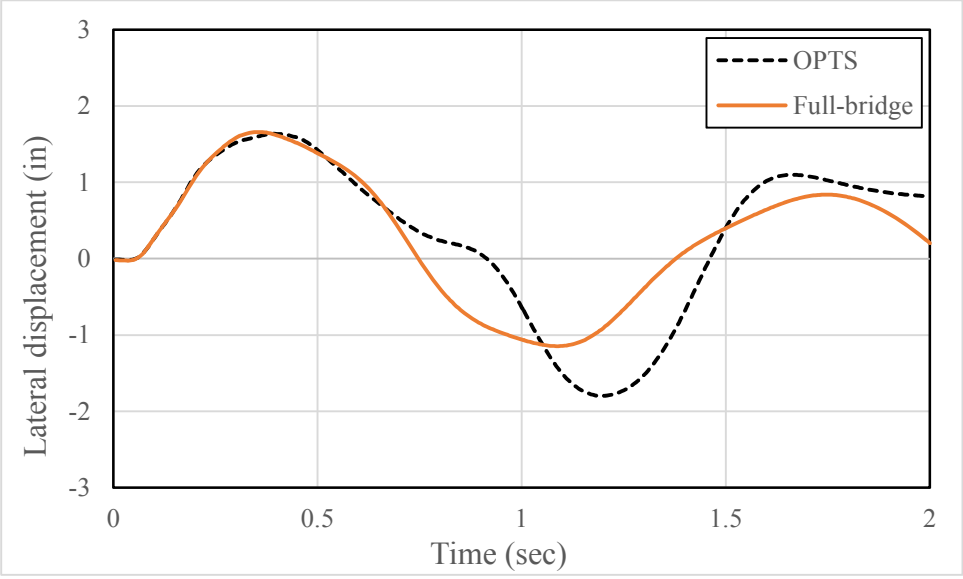

Figure 5.5 Time-histories of displacement in the top of the pier column above the impacted node

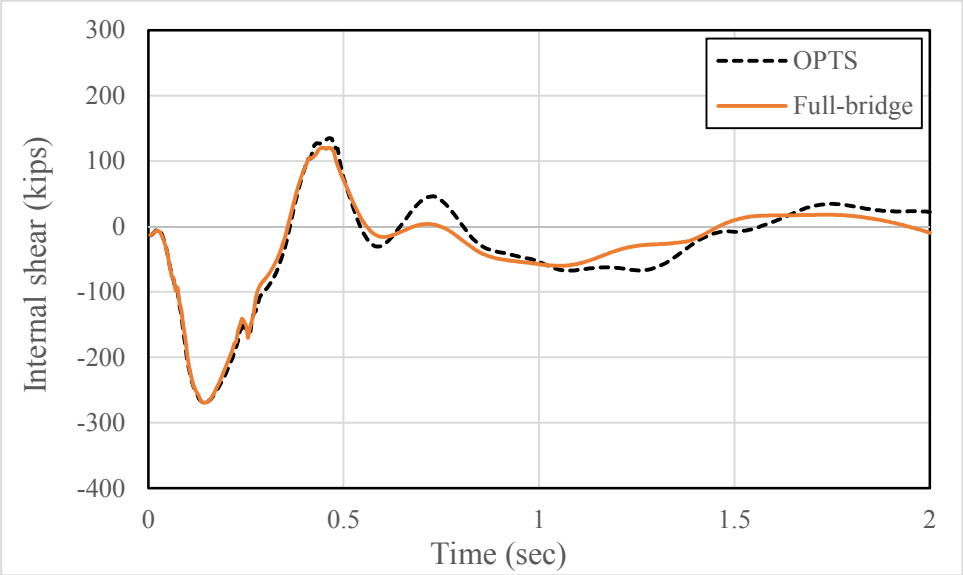

Figure 5.6 Time-histories of internal shear in the top of the pier column above the impacted node

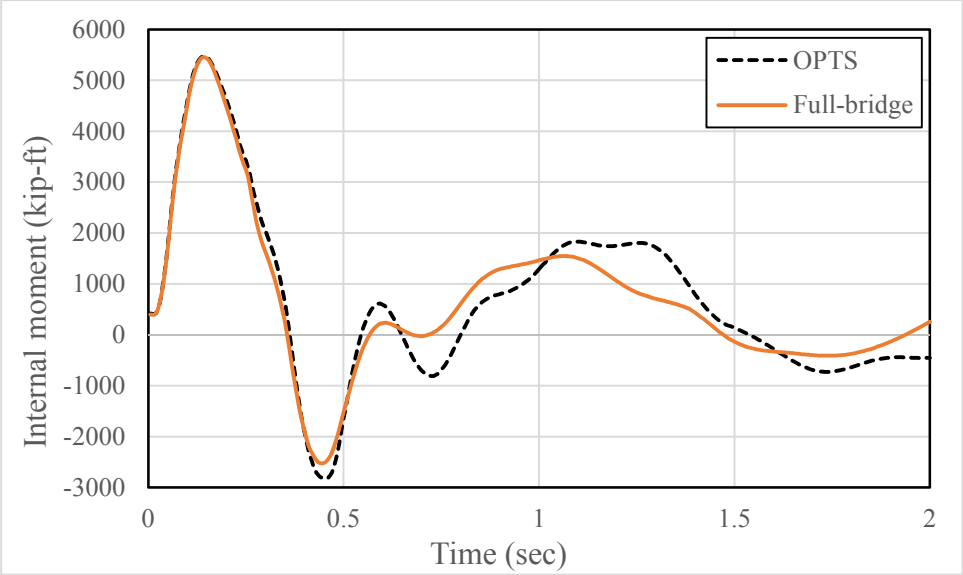

Figure 5.7 Time-histories of internal moment the top of the pier column above the impacted node

DESIGN LOAD TABLES

After completing the CVIA-OPTS analysis, maximum structural demands (through time) can be quickly identified from within the FBMP GUI. As examples, the process of identifying

maximum internal forces in the pier columns of Pier 2 in the OPTS model is illustrated in Sec. 5.1.1; and the process of identifying maximum internal forces in the drilled shafts is illustrated in Sec. 5.1.2.

MAXIMUM INTERNAL FORCES IN THE PIER COLUMNS

The "Design Table Generator" dialog is accessed by selecting the design tables icon, as shown in Fig. 5.1. The main dialog (Fig.5.8) is then used to generate summary data for a region of interest within the analyzed structure. For example, by selecting the "Max Forces for All Column Sections" table, a PDF, TXT, or Microsoft® Excel® report file is generated, which contains the maximum pier column demands (Fig. 5.9). The corresponding PDF report is shown in Fig. 5.10, where the maximum demands are identified with ease.

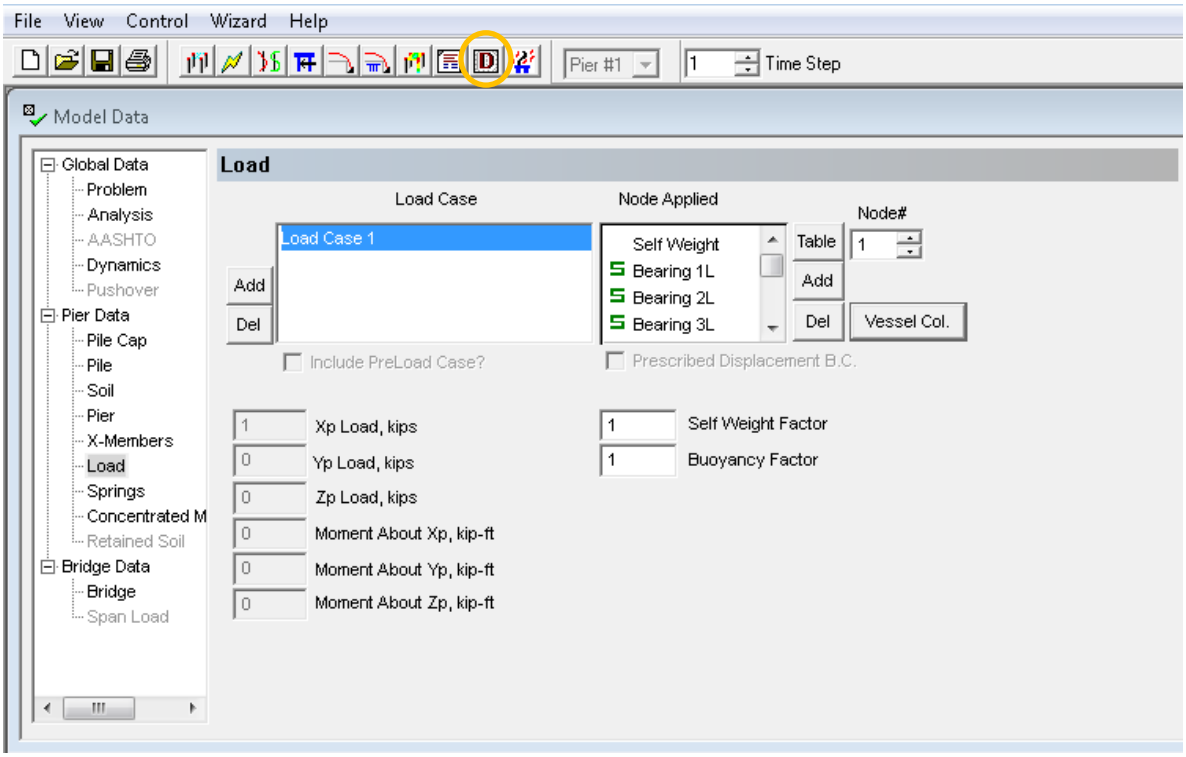

Figure 5.8 Accessing the design tables

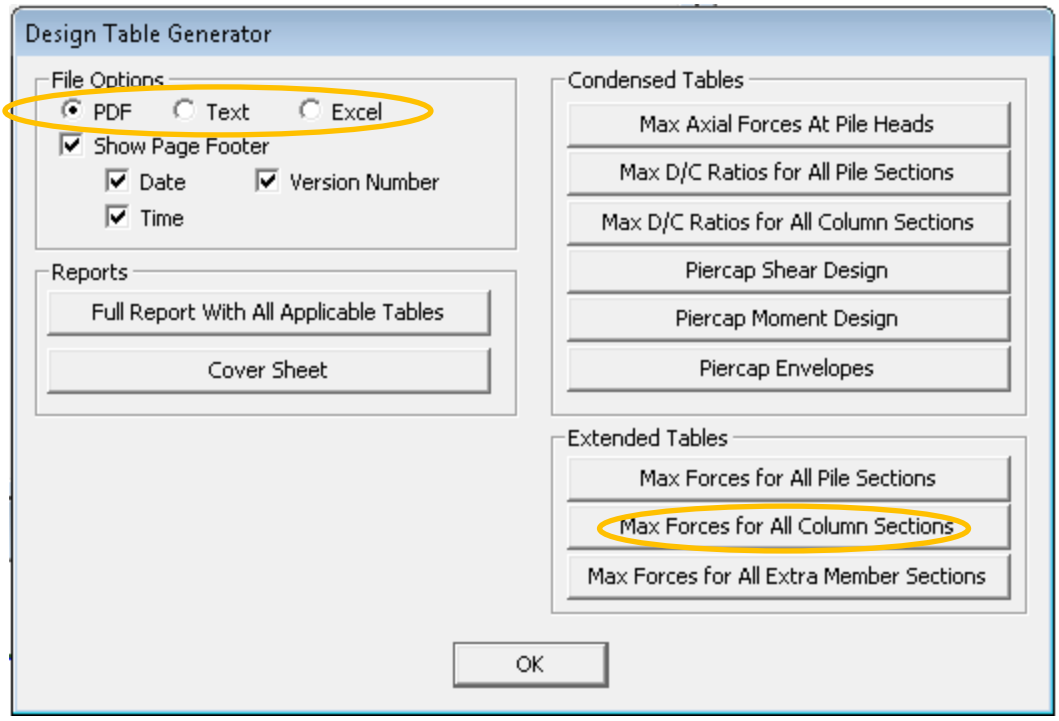

Figure 5.9 Design tables main dialog pertaining to maximum pier column demands

Maximum Forces for All Column Properties (Cross Sections)

Column Properties Data for Pier 1

PROP NO.	COLUMN NO.	ELEM NO.	NODE NO.	TIME STEP	I/J	MAX/MIN FORCE	FAX (Kips)	F22 (Kips)	F33 (Kips)	M22 (Kip-ft)	M33 (Kip-ft)	TORQUE (Kip-ft)	D/C (Ratio)
2	2	57	135	48	J	Max Axial	-214.09	-126.89	0.41	53.03	-3044.07	-94.77	0.60
2	1	9	86	26	I	Min Axial	-1780.08	-226.97	-2.72	-15.62	4129.71	-37.04	0.41
2	2	47	125	79	J	Max f22	-1354.99	177.58	-1.79	-7.68	-392.97	-12.67	0.09
2	1	9	87	13	J	Min f22	-1371.07	-398.13	-2.17	-22.30	1289.76	-5.65	0.13
2	2	47	125	121	J	Max f33	-1108.73	111.57	11.53	-69.83	516.59	246.24	0.08
2	1	9	87	120	J	Min f33	-1094.65	-28.40	-13.72	99.42	785.16	255.00	0.09
2	1	19	97	129	J	Max m22	-869.16	0.04	-5.33	212.13	-58.87	262.97	0.06
2	2	57	135	126	J	Min m22	-893.80	24.02	4.81	-210.34	703.26	267.95	0.08
2	1	10	87	28	I	Max m33	-1705.27	-188.54	-0.87	13.95	5394.24	-77.04	0.60
2	1	19	97	29	J	Min m33	-1547.54	-269.62	3.67	-47.00	-5470.53	-84.36	0.66
2	2	48	126	125	J	Max Torque	-1015.41	35.84	9.81	98.32	-325.67	269.60	0.07
2	1	10	88	187	J	Min Torque	-1078.44	-22.19	8.50	56.48	464.16	-236.23	0.08

Figure 5.10 Design tables report pertaining to maximum pier column demands

MAXIMUM INTERNAL FORCES IN THE DRILLED SHAFTS

The “Design Table Generator” dialog can be accessed again (recall Fig. 5.9) at any desired time to generate additional design-friendly reports. For example, if maximum demands in the

drilled shafts are of interest, then the associated report is generated by selecting “Max Forces for All Pile Sections” (Fig. 5.11). An excerpt of the report pertaining to the drilled shafts for the CVIA-OPTS analysis is shown in Fig. 5.12.

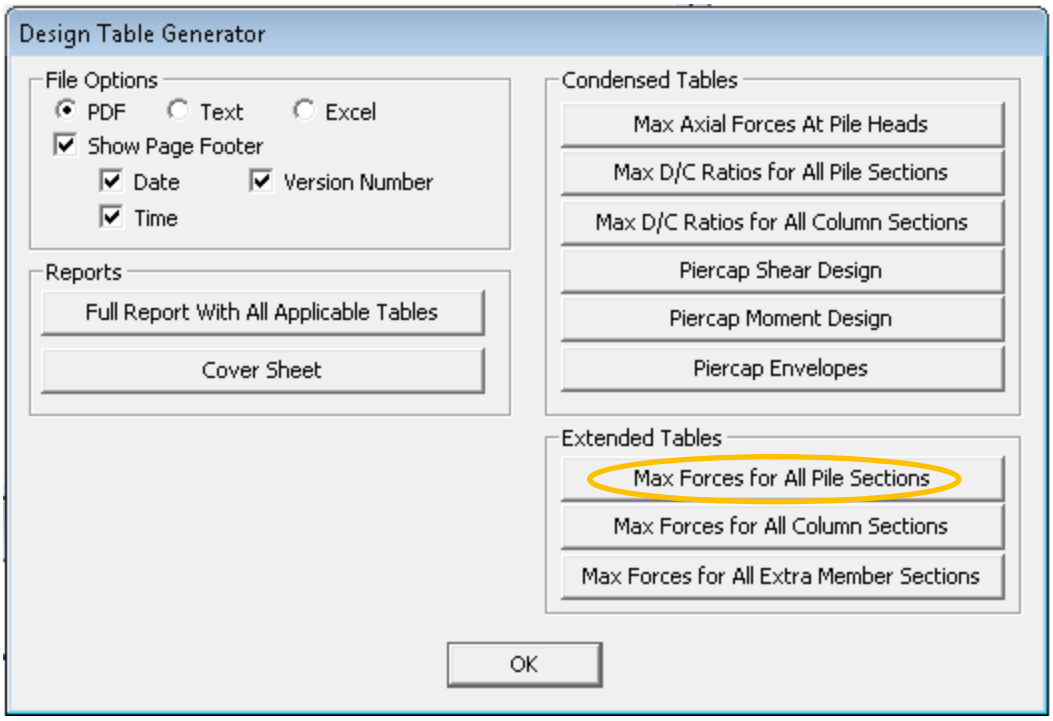

Figure 5.11 Design tables main dialog pertaining to maximum drilled shaft demands

Maximum Forces for All Pile Properties (Cross Sections)

Pile Properties Data for Pier 1

PROP NO.	PILE NO.	ELEM NO.	NODE NO.	TIME STEP	I/J	MAX/MIN FORCE	FAX (Kips)	F22 (Kips)	F33 (Kips)	M22 (Kip-ft)	M33 (Kip-ft)	TORQUE (Kip-ft)	D/C (Ratio)
1	1	66	1	76	J	Max Axial	-153.87	124.64	-1.14	-5.36	3153.08	12.79	0.59
1	1	66	142	25	I	Min Axial	-2083.35	289.41	-0.21	-25.05	5643.85	-0.25	0.59
1	1	71	146	30	J	Max f22	-1611.30	412.59	0.87	-7.03	-1124.14	14.36	0.15
1	1	76	151	35	J	Min f22	-1165.92	-248.76	-0.95	2.85	-3941.82	27.69	0.44
1	1	71	146	191	J	Max f33	-1290.40	-2.23	15.71	122.10	103.88	221.04	0.10
1	1	71	146	119	J	Min f33	-1101.72	137.35	-20.52	-232.31	-452.59	-240.06	0.09
1	1	66	1	120	J	Max m22	-1012.92	99.47	-17.06	266.24	2648.83	-240.59	0.27
1	1	72	148	119	I	Min m22	-1092.86	109.44	-4.63	-368.52	-1780.68	207.23	0.17
1	1	66	1	34	J	Max m33	-1803.19	288.70	4.63	-63.65	7672.74	35.15	0.96
1	1	74	149	31	J	Min m33	-1559.23	-105.82	0.30	-1.08	-5332.80	14.24	0.60
1	1	67	143	119	I	Max Torque	-1058.42	106.69	-17.71	80.01	1548.73	241.13	0.15
1	1	67	142	119	J	Min Torque	-1045.27	106.69	-17.71	175.81	2121.96	-241.13	0.20

Figure 5.12 Design tables report pertaining to maximum drilled shaft demands

6. SUMMARY AND CONCLUSIONS

Bridges that span navigable waterways are subject to extreme event loading through vessel-bridge collision. In the event of a collision, dynamic lateral forces transmitted to the impacted bridge structure can result in the development of significant inertial forces that, in turn, produce amplified structural demands. Collision events can, therefore, lead to severe structural damage and even catastrophic failure of the impacted bridge. In the current report, a user's guide is given for utilizing a simplified bridge modeling and numerically efficient nonlinear dynamic vessel collision analysis technique in FBMP.

The modeling and analysis procedures, as accessed from within the FBMP GUI, are showcased for a four-pier three-span demonstration case. Included in the user's guide are the guidelines and steps necessary to form a simplified bridge model using the multiple-pier, multiple-span bridge model, and to iteratively calculate input for spring stiffnesses and lumped masses located at the extents of the simplified bridge model. Further, dynamic input parameters necessary to account for phenomena such as damping, and characterization of the vessel collision scenario are discussed. Also, the GUI options available for entering the dynamic input are provided.

Importantly, maximum forces generated within pier members can be quickly determined by making use of the Design Table feature in FBMP, as delineated in this user's guide. Further, for the demonstration case considered in this report, it is shown that the OPTS model numerical results show good agreement with those results generated for a corresponding full-bridge analysis. As implemented in the bridge finite element analysis software FBMP, the tools constitute an easy-to-use analytical framework that facilitates rapid assessment of nonlinear dynamic vessel collision loading and bridge response. These numerical tools are put forth for use by bridge engineers in conducting accurate, efficient vessel collision analyses on bridges.

7. REFERENCE

AASHTO. 2009. *Guide specification and commentary for vessel collision design of highway bridges, 2nd Edition*, Washington D.C.

Bridge Software Institute (BSI). 2014. *FBMP User's Manual*. BSI, University of Florida, Gainesville, Fla.

Consolazio, G. R., and Cowan, D. R. 2005. "Numerically efficient dynamic analysis of barge collisions with bridge piers." *Journal of Structural Engineering*. 131(8), 1256–1266.

Consolazio, G. R., and Davidson, M. T. 2008. "Simplified dynamic barge collision analysis for bridge design." *Transportation Research Record. 2050*, Transportation Research Board, Washington, D.C., 13–25.

Consolazio, G. R., Davidson, M. T., and Cowan, D. R. 2009. "Barge bow force-deformation relationships for barge-bridge collision analysis." *Transportation Research Record. 2131*, Transportation Research Board, Washington, D.C., 3–14.

Consolazio, G. R., McVay, M. C., Cowan, D. R., Davidson, M. T., and Getter, D. J. 2008. "Development of improved bridge design provisions for barge impact loading." *Structures Research Report No. 51117*, Engineering and Industrial Experiment Station, University of Florida, Gainesville, Fla., April.

Davidson, M. T. 2010. "*Probability Assessment of Bridge Collapse Under Barge Collision Loading*." Dissertation, Advisor: Gary Consolazio, University of Florida, Gainesville, Florida, USA.

Davidson, M. T., and Consolazio, G. R. (2008). "Simplified dynamic head-on barge collision analysis for bridge design." *Proceedings, 25th International Bridge Conference* Transportation Research Board, Pittsburgh, Penn.

Paultre, P., Chaallal, O., and Proulx, J. 1992. "Bridge Dynamics and Dynamics Amplification Factors – a Review of Analytical and Experimental Findings." *Canadian Journal of Civil Engineering*, 19, 260-278.

Tedesco, J. W., McDougal, W. G., and Ross, A. C. 1998. *Structural Dynamics: Theory and Applications*, 1st Edition, Prentice Hall.

Yuan, P., Harik, I. E., and Davidson, M. T. 2008. “Multi-barge flotilla impact forces on bridges.” *Kentucky Transportation Center Research Report No. KTC-05/SPR261-03-1F*, University of Kentucky, Lexington, Ky.